12-2021

Design, Synthesis, and Catalytic Application of Crystalline Porous Nanomaterials

Zainab Abdullah Almansaf
University of Arkansas, Fayetteville

Design, Synthesis, and Catalytic Application of Crystalline Porous Nanomaterials

A dissertation submitted in partial fulfillment
of the requirements for the degree of
Doctor of Philosophy in Chemistry

by

Zainab Almansaf
University of Dammam
Bachelor of Science in Chemistry, 2011
University of Arkansas
Master of Science in Chemistry, 2016

December 2021
University of Arkansas

This dissertation is approved for recommendation to the Graduate Council.

Hudson Beyzavi, Ph.D.
Dissertation Director

Chenguang Fan, Ph.D.
Committee Member

Neil Allison, Ph.D.
Committee Member

David Paul, Ph.D.
Committee Member

Lauren Greenlee, Ph.D.
Committee Member

Abstract

Chapter 1: COFs (covalent organic frameworks) are a new type of microporous crystalline polymer connected by organic units via strong covalent bonds. Due to their well-defined crystalline structures and excellent chemical and thermal stabilities, COF materials are considered promising candidates in applications such as gas adsorption, catalysis, and energy storage.

Chapter 2: A new covalent organic framework (COF) based on imine bonds was assembled from 2-(4-formylphenyl)-5-formylpyridine and 1,3,6,8-tetrakis(4-aminophenyl)pyrene, which showed an interesting dual-pore structure with high crystallinity. Postmetallation of the COF with Pt occurred selectively at the N donor (imine and pyridyl) in the larger pores. The metalated COF served as an excellent recyclable heterogeneous photocatalyst for decarboxylative difluoroalkylation and oxidative cyclization reactions.

Chapter 3: We describe the design and synthesis of highly stable and irreversible amine-linked COFs. The proposed amine linkage is prepared via irreversible nucleophilic aromatic substitution reactions (S_NAr) of 5,10,15,20-tetrakis(perfluorophenyl)porphyrin (**$TPPF_{20}$**) **L1** with ethane-1,2-diamine **L2**,1,4-phenylenedimethanamine **L3,** or cta(3-aminopropyl) silsesquioxanehydrochloride (OAS-POSS) **L4** to form **COF-21**, **XYCOF**, and **SiCOF**, respectively. Post-metalation of COF-21 with iron led to FeClCOF-21, in which its model **K**1 displayed excellent catalytic performance towards a tandem catalytic synthesis of 2-phenyl-1H-benzo[d]imidazole.

Acknowledgements

I owe my deepest gratitude to God for his blessings and aid in overcoming all the difficulties and challenges that I have faced in pursuing my goals. It is a pleasure to thank all the people and institutions who have contributed to the success of this work. I am greatly indebted to my advisor, professor Beyzavi, for his support, guidance and for giving me this golden opportunity to work on this project. I am thankful to Dr. Reza and Dr. Hu, and I really appreciate the time, effort, and resources that they invested in me to become a better scientist.

I also express my gratitude to my committee members Dr. Paul, Dr. Allison, Dr. Fan, and Dr. Greenlee. I am grateful to the Department of Chemistry and Biochemistry at the University of Arkansas for the support and for giving me the opportunity to engage in research. It is an honor for me to thank King Abdullah Scholarship Program for their financial resources, without which this work would not have been possible. I am also grateful to my undergrad, Benjamin, for his help. I am thankful to all my friends, especially Sefat Alwarsh, and my family, my mom, my sister, and my kids, for their support and prayers. Lastly, I am also thankful to my dad who supported me, encouraged me, and wished to see this moment of my success, but he passed away while I was pursuing my Ph.D. degree.

Dedication

This work is dedicated to Imam Almahdi and to the family of the prophet Muhammad, peace and blessings of Allah be upon them.

Table of Contents

Table Figures

Table of Schemes

List of Tables

List of Publications

Chapter 2

Z. Almansaf, J. Hu, F. Zanca, H. R. Shahsavari, B. Kampmeyer, M. Tsuji, K. Maity, V. Lomonte, Y. Ha, P. Mastrorilli, S. Todisco, M. Benamara, R. Oktavian, A. Mirjafari, P. Z. Moghadam, A. R. Khosropour, and H. Beyzavi "Pt(II)-Decorated Covalent Organic Framework for Photocatalytic Difluoroalkylation and Oxidative Cyclization Reactions" *ACS Applied Materials & Interfaces* **2021**, *13*, 6349–6358.

Chapter 1. Introduction to Covalent Organic Frameworks (COFs)

1.1 Research Background

Over the past century, distinct types of nanoporous materials have been successfully developed and characterized by general trends in structural evolution: from inorganic to organic components, from small to large pores, from rigid frameworks to soft dynamic skeletons, and from 2D to 3D architectures. Nanoporous materials have attracted a lot of attention in recent years due to their unique properties, including persistent porosity and high and accessible interior surface areas.[1, 2] Most conventional nanoporous materials that have been widely used as adsorbents, heterogeneous catalysts, and catalyst supports, such as zeolites and activated carbon, are based on inorganic building units. However, research interest in developing nanoporous materials containing organic components has expanded rapidly. Organic components provide for exquisite structural and functional control allowing a material to be specifically designed for a unique application.[5] Some examples of nanoporous organic polymers that have been successfully developed recently include polymers of intrinsic microporosity (PIMs)[3], porous polymer networks (PPNs)[4], and conjugated microporous polymers (CMPs).[5] These materials are completely amorphous and consist of multifunctional building blocks bonded together by covalent bonds. Various studies provide synthetic methods and utility for these materials.[6] Unfortunately, the amorphous nature of these materials can result in significant pore size dispersions, preventing them from being used in some applications such as size- and shape-based gas separation and storage. Metal-organic frameworks (MOFs) are also one type of crystalline nanoporous material that has received a lot of attention. MOFs' structures are composed of metal ions or clusters connected together by organic ligands via coordination bonds. MOFs exhibit some unique features such as the chemical and

structural tunability of the organic ligands, the coordination possibilities of various metal ions, and the uniform porosity and high surface area of a crystalline nanoporous material.[7] Examples of this class of materials must contain large quantities of potentially toxic or reactive metal centers. In addition, their relatively weak coordination bonds display various stability under high humidity and temperature: conditions commonly found in industrial processes.[8] The remarkable synthesis of covalent organic frameworks (COFs) by Yaghi and co-workers in 2005 was an exciting advancement in this field.[9] Compared to the amorphous nanoporous polymers and MOFs mentioned above, COFs provide a unique combination of chemical modularity and structural diversity along with tunable pore size, high surface area, low density, thermal stability, and crystallinity.[10]

COFs are a new class of crystalline porous polymer that allows organic building units to be precisely integrated into extended 2D or 3D structures with periodic skeletons and ordered nanopores.[11, 12] COFs' structures are composed of lightweight elements such as N, O, S, Si, C, and B held together by strong covalent bonds. These strong covalent bonds are formed via reversible condensation reactions to create various linkages such as boronate, triazine, imine, and hydrazone, as shown in **Scheme 1.1**.[12]

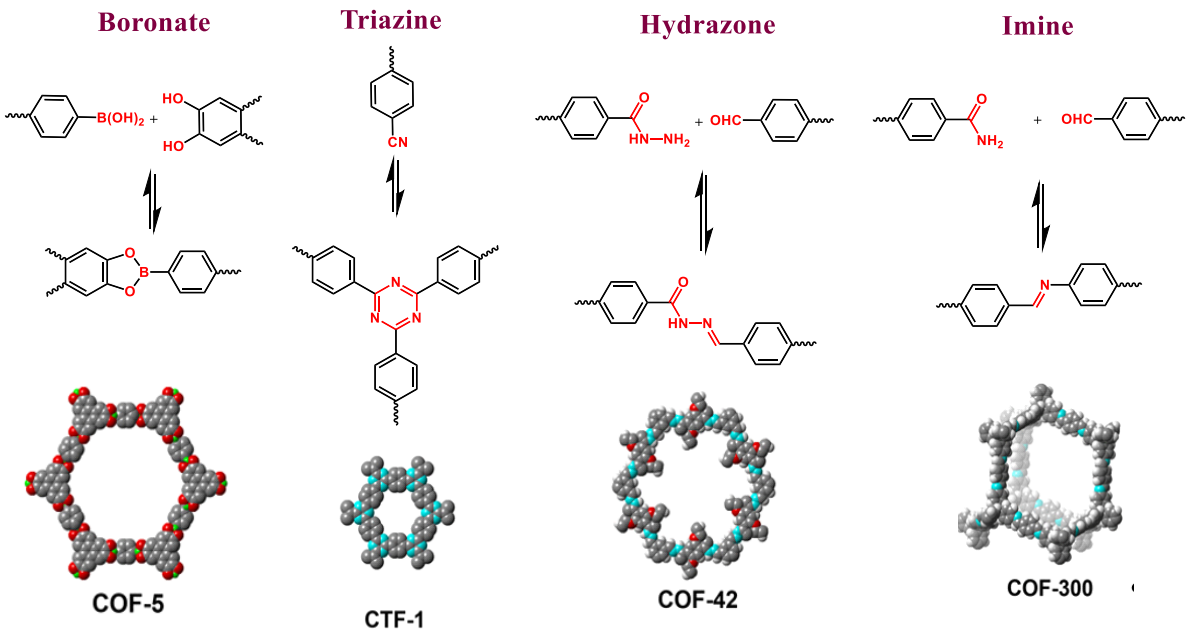

Scheme 1. 1. Diversity of linkages for the formation of COFs, adapted from ref 12, Copyright 2017 The American Association for the Advancement of Science.

1.2 Design Principle

A framework, whether a COF or another type of covalent extended structure, is built on a foundation of two main components: linkers (building blocks) and linkages (bonds linked units upon reticulation). The organic synthesis of the framework begins with the synthesis of the building blocks. It ends with the reticulation of these building blocks into an extended framework by stitching them together in a planned manner. COF skeletons and pores can be designed, using a topology diagram, based on building block geometry matching to direct the formation of polygon skeletons. Polygons are typically composed of knot and linker units with geometries that determine the shape of the polygon and dimensions that control the pore size.[11, 13,14]

Various COF polygon shapes have already been designed and reported, including hexagonal, tetragonal, and trigonal structures.[11, 13]The building units are classified as C_2-, C_3-, C_4- and C_6-symmetric units based on the directional symmetry of the reactive groups. Hexagonal COFs can be formed by combining C_3-symmetric vertices and C_2- or C_3-symmetric units or by a self-condensation of C_3-symmetric units. In addition, the hexagonal COFs can also be constructed by using a three-component double-stage system, including one C_2-symmetric linker and two C_3-symmetric knots. In contrast to hexagonal homologs, tetragonal COFs formed by C_4-symmetric knots and C_2-symmetric linkers display extended π conjugation. Trigonal COFs based on $C_6 + C_2$ topology diagram provide high π-unit density. The block model is shown in **Scheme 1.2** can be used to simplify and explain this design principle.[14]

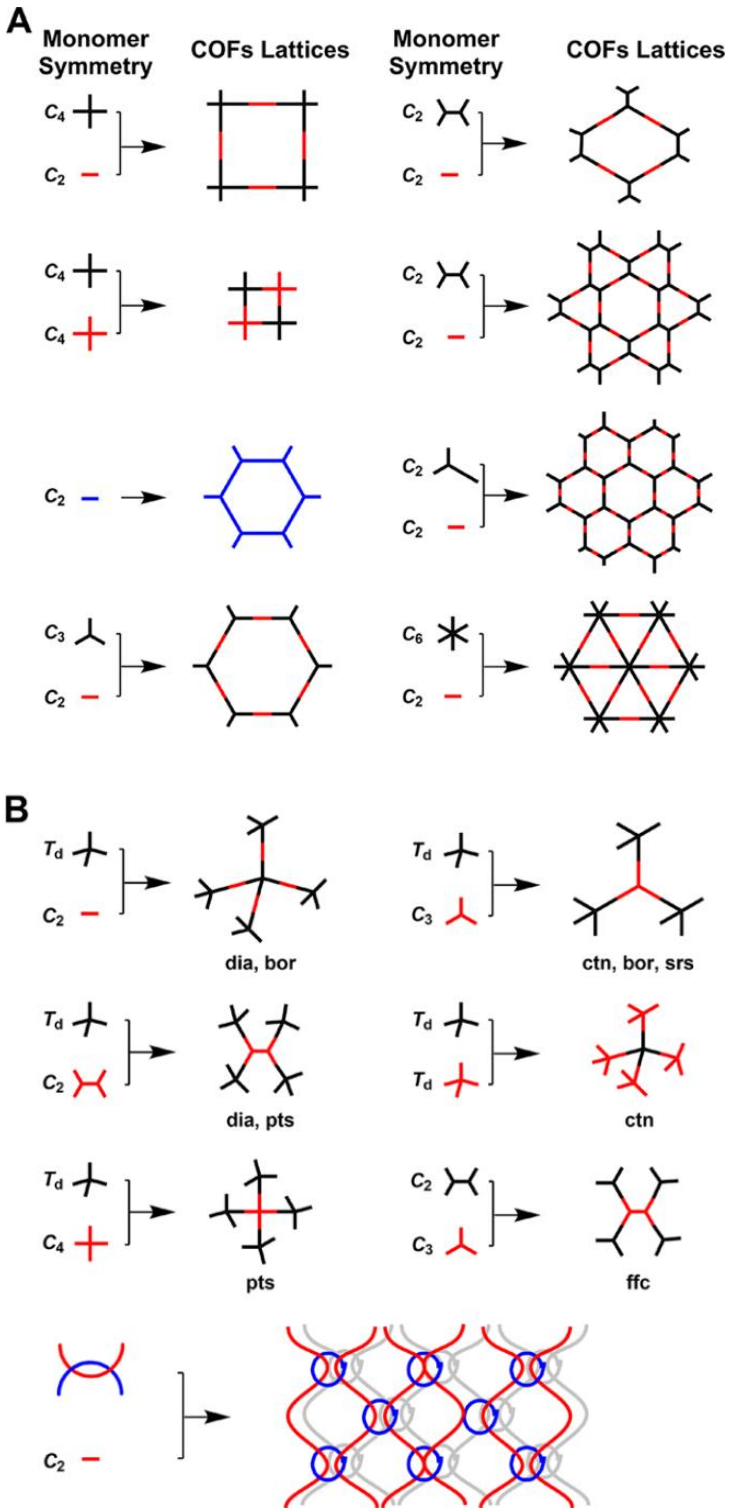

Scheme 1. 2. Topology diagrams represent the polygon of covalent organic frameworks; (A). 2D COFs and (B). 3D COFs, reprinted with permission from ref 14, Copyright 2020 American Chemical Society.

1.3. Classifications of COFs

COFs can be classified as two-dimensional (2D), or three-dimensional (3D) frameworks based on the dimensionality of the covalent connectivity. The organic ligands for 2D COFs are assembled on stacked 2D planes to form a layered eclipsed structure. This high-ordered structure has the potential to improve charge carrier mobility in the stack direction. Therefore, 2D COFs have a high potential in fluorescence and photovoltaic applications. In comparison to 2D COFs, 3D COFs are extended into three-dimensional space by the presence of an sp^3 carbon or silane atom. As a result, this structure has distinct properties such as a high surface area, low density, and multiple open sites in the framework. These properties make 3D COFs ideal for molecular capture or gas storage.[15]

COFs can also be classified into three main classes based on the type of linkages: boron-containing COFs, triazine-based COFs, and imine-based COFs.[16]

1.3.1. Boron-containing COFs

The first examples of COFs are boron-containing COFs (COF-1 and COF-5) reported by Yaghi et al. in 2005. Both COFs have been synthesized through the formation of boroxine or boronate ester, respectively. According to the synthetic strategies, boron-containing COFs can be divided into two categories. One category is synthesized by the self-condensation of single boronic acid building blocks with boroxine linkages. COF-1, connected through boroxine linkages, was successfully synthesized under solvothermal conditions through the acid-catalyzed trimerization reaction of 1,4-benzenediboronic acid (BDBA) (**Scheme 1.3 A**).[17]

The other category of boron-containing COFs is the co-condensation of two or more different building units. A variety of COFs via the co-condensation has been synthesized by selecting different building units. The most common COF researched by Yaghi and the co-workers is COF-

5, prepared by 1,4-benzenediboronic acid (BDBA)d and hexahydroxytriphenylene (HHTP) (**Scheme 1.3 C**). [17]

Powder x-ray diffraction (PXRD) showed strong signals in the low angle range, confirming the crystal structures of both COF-1 and COF-5. Gas adsorption studies showed that both COF-1 and COF-5 have permanent porosity with BET(Brunauer, Emmett and Teller) surface areas up to 1670 $m^2 g^{-1}$**.** The only issue with most of the boron-containing COFs is their instability in water or humid air.[18, 19]

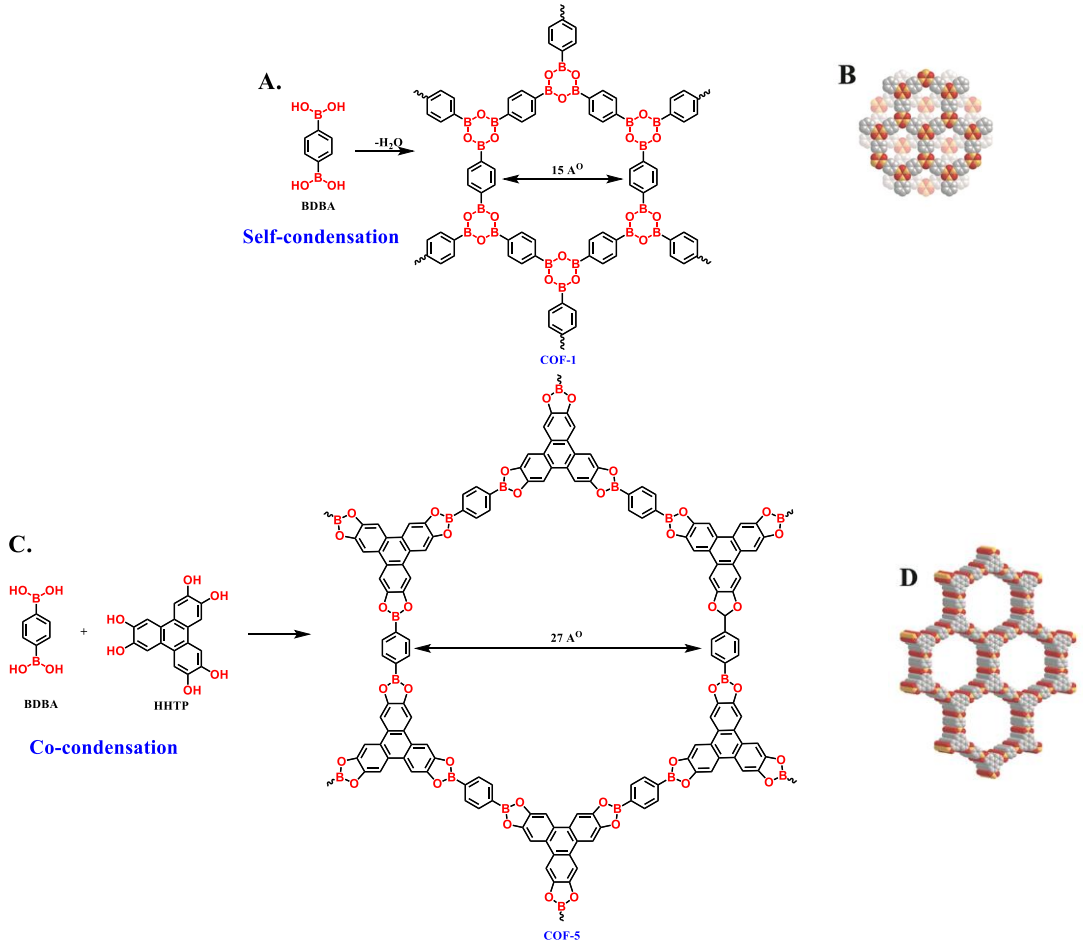

Scheme 1. 3. (A). Self-condensation of BDBA to synthesize COF-1, (B). the proposed crystalline structure of COF-1, (C). Co-condensation of BDBA and HHTP to produce COF-5 and (D). the proposed crystalline structure, adapted with permission from ref 17 , Copyright 2009 American Chemical Society.

1.3.2. Triazine-based COFs (CTFs)

Triazine-based COFs are constructed by cyclotrimerization of nitrile building blocks. Thomas and co-workers synthesized the first CTF in 2008 by cyclotrimerization of the nitrile monomer 1,4-dicyanobenzene (DCB)(**Scheme 1.4**).[20] CTF-1 exhibits poor crystallinity and low porosity due to the harsh preparation conditions such as purification in acid solution and high reaction temperature.

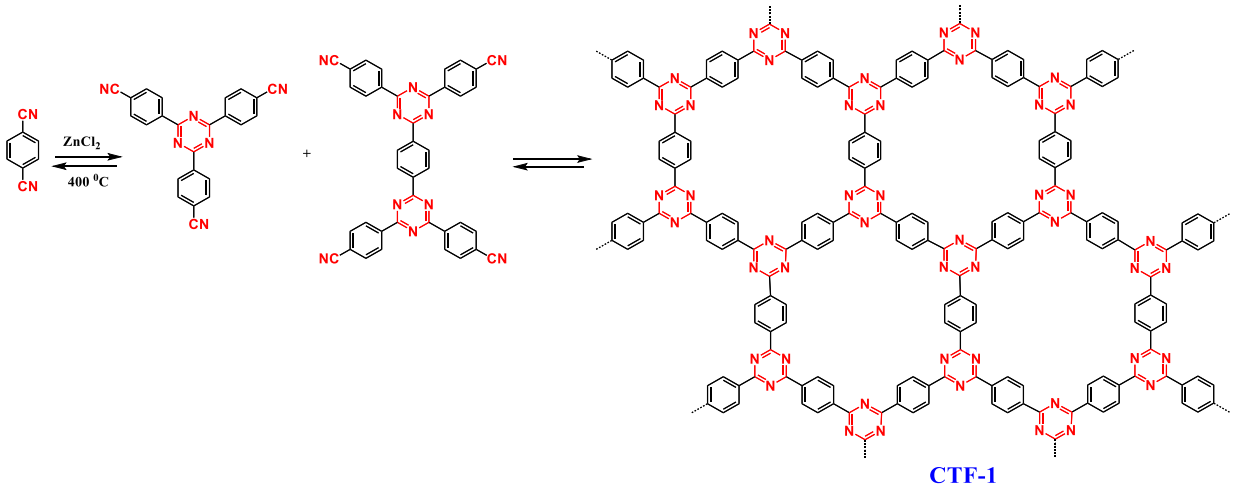

Scheme 1. 4. Trimerization of dicyanobenzene in molten $ZnCl_2$ to trimers and oligomers and then to a covalent triazine-based framework (CTF-1), adapted from ref 20 , Copyright 2008 Angewandte Chemie International Edition.

The major issue with the synthesis of CTFs is the difficulty of finding building units that can tolerate the harsh reaction temperature.[21] To overcome this limitation, Tan's group developed a new low-temperature polycondensation method for synthesizing CTFs under milder conditions.[22] CTFs were synthesized by the condensation reaction of amidines and aldehydes as shown in **scheme 1.5**.[22] These CTFs have shown good performance in the fields of gas adsorption, photocatalysis, and sodium-ion batteries.

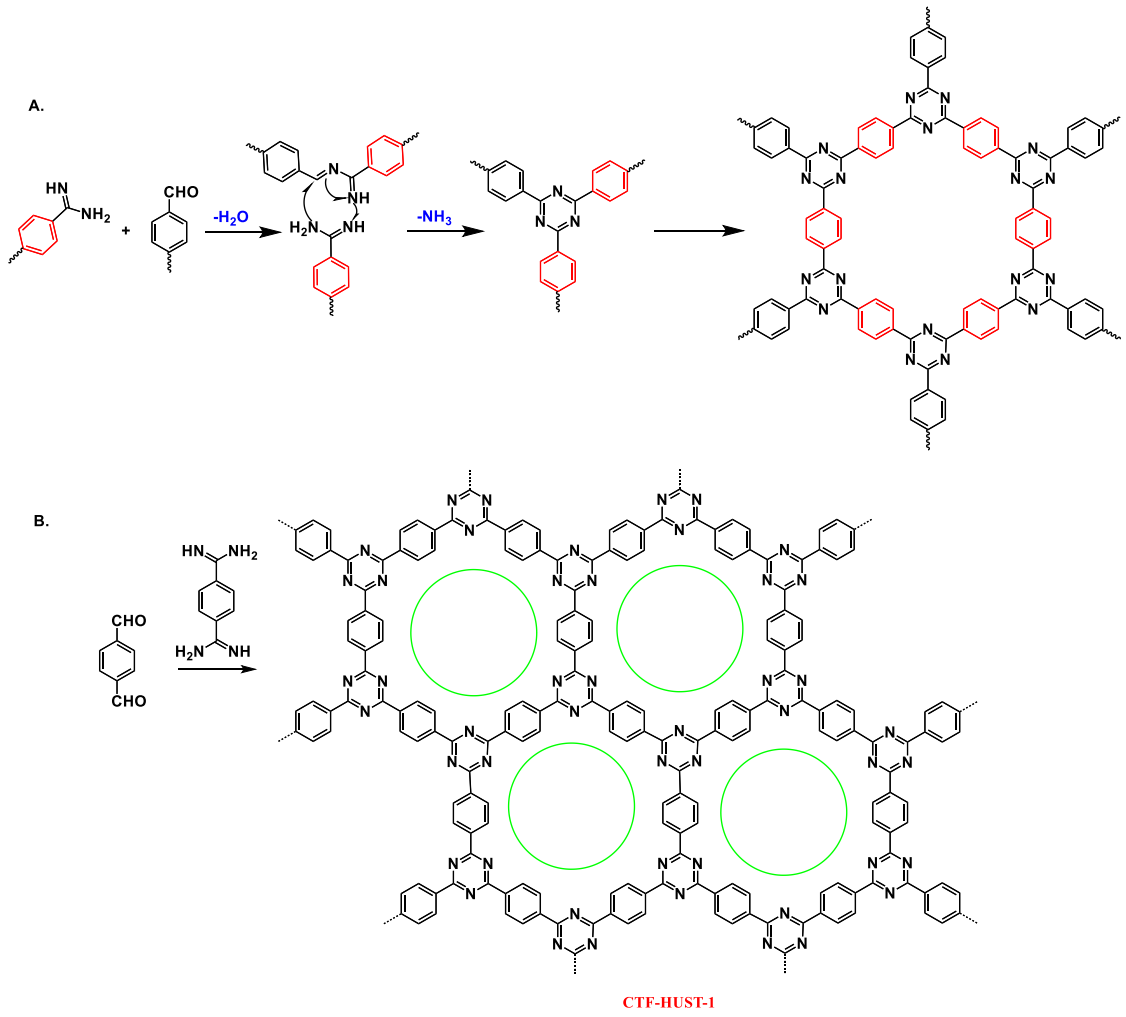

Scheme 1. 5. Representation of the reaction mechanism for CTF-HUST synthesis. (A). Reaction mechanism for triazine formation in the synthesis of CTF-HUST; (B). representative structures of CTF-HUST-1. [22]

1.3.3. Imine-based COFs

The imine-based COFs are another representative category of COFs synthesized via a reversible imine condensation reaction.[23] The first imine-based COF (COF-300) was reported in 2009 by Yaghi and co-workers through the co-condensation of aldehydes and amines.[24] The imine-based COFs are divided into two categories based on the covalent formation of –C=N– bonds. The first class is constructed through the co-condensation of amines and aldehydes, called the “Schiff base”

type (**Scheme 1.6 A)**.[24] The other class, called the "hydrazine" type, is synthesized via the co-condensation reaction of hydrazides and aldehydes (**Scheme 1.6 B**).[25]

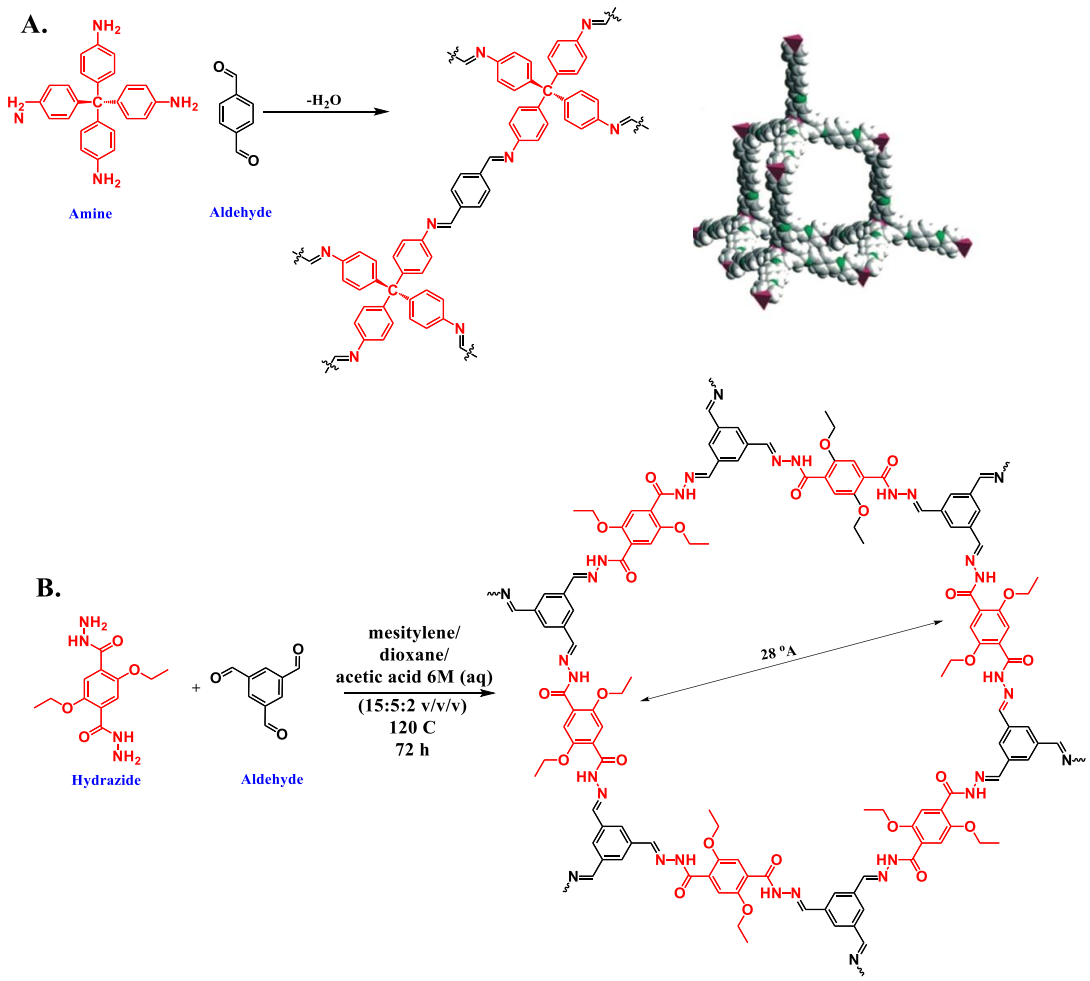

Scheme 1. 6. (A). Co-condensation of aldehyde and amine to synthesize the "Schiff base" COF, adopted with permission from ref 24, Copyright 2009 American Chemical Society. (B). Co-condensation of aldehyde and hydrazide to synthesize the "hydrazine" COF, adopted with permission from ref 25, Copyright 2011 American Chemical Society.

Now with the rapid development of COFs, imine-based COFs have attracted major interest in the area of COFs for several reasons. First, imine-based COFs have shown much better crystallinity and structure regularity compared to triazine-based COFs.[24] Second, in contrast with boron-containing COFs,[26] imine-based COFs possess better chemical stability in water and most organic

solvents. Third, nitrogen atoms in imine-based COFs are able to coordinate with multiple metal ions, increasing their potential for diverse applications.[27, 28]

1.4. Synthesis Methods

In the synthesis of polymeric materials, irreversible reactions usually result in an amorphous structure; Reversible reactions typically result in a well-defined crystalline structure due to bond conversion during the reaction. The reversible covalent bond formation reactions can generate stable products that form self-healing structures. The self-healing process is crucial for the reaction containing different reactive sites to attain a final structure without defects. In the case of COFs, the topology diagram requires the organic units to be covalently connected in an ordered and predesigned manner.[29] In addition, the chemical reactions involved in the construction of COFs should have a certain level of reversibility in order to ensure the growth of lattice structures. Although a large number of COFs have been synthesized through reversible reactions, the synthesis of COFs through irreversible nucleophilic aromatic substitution reactions have also been reported, including phanazine linkage and dioxin linkage.[30]

Despite the fact that COFs can be designed by carefully selecting monomers and synthetic routes, other important factors should be considered for COF synthesis including temperature, pressure, reaction time, and the presence of a catalyst. COFs with chemical stability, excellent porosity, and high crystallinity can be obtained by adopting suitable synthetic conditions. Furthermore, the appropriate synthetic method will significantly reduce the time of the reaction and increase product yield. In general, COF preparation methods can be divided into four categories: solvothermal, microwave, interfacial, and under ambient condition synthesis.

1.4.1. Solvothermal Synthesis

A solvothermal synthesis is the most common approach used for COF synthesis. In this method, the reversibility of the reaction along with the reactivity and solubility of the building blocks are all highly dependent on the reaction conditions. The sealed system is essential to maintain the reaction's reversibility because it preserves the produced water molecules. The reaction time, catalyst, concentration, temperature, and solvent selection are all factors to consider when constructing crystalline porous COFs. As a general synthetic protocol, a mixture of starting materials is combined with a catalyst and a solvent or a mixture of solvents in a Pyrex tube with suitable volume. The reaction mixture is then sonicated before being degassed three times in freeze-pump-thaw cycles. The Pyrex tube containing the reaction mixture is then sealed with a propane torch and kept at a suitable temperature for a specific period of time. The classical solvothermal approach usually requires heating (80-120 °C) and takes 2-9 days. After reaction completion, the tube is left to cool down to room temperature. The precipitate formed is then collected by filtration or centrifugation and washed with a suitable solvent at room temperature or by Soxhlet extraction to remove remaining oligomers or to exchange high-boiling point solvents.[31] Finally, the residue is dried under vacuum at 80−120 °C and kept under argon or nitrogen. This method has been used to synthesize COFs on a large scale. For example, TPT-COF-1 is easily prepared from 2,4,6-tris(4-aminophenoxy)-1,3,5- triazine (TPT-NH_2) and 2,4,6-tris(4-formylphenoxy)-1,3,5- triazine (TPT-CHO) on a gram scale. The obtained TPT-COF-1 exhibits high crystallinity along with a BET surface area of 1589 m^2g^{-1}.[31]

1.4.2. Microwave Synthesis

When compared to solvothermal synthesis, a microwave-assisted heating method has multiple advantages.[32] (1) The reaction time for synthesizing COFs can be significantly reduced, allowing

for large-scale synthesis for industrial production. (2) The microwave method eliminates the need for solvothermal synthesis preparations such as freeze–pump–thaw degassing and a flame-sealed vessel. (3) It is a highly efficient method that saves a significant amount of energy. (4) It is more environmentally friendly than traditional heating methods. Furthermore, microwave-assisted synthesis reduces the need for solvents. In conclusion, a microwave assisted heating method opens new opportunities for further applications in industrialization, presenting more efficient and cleaner methods for COF synthesis. Various COFs including COF-102,[32, 33] boronate-ester-linked COF-5, and imine- linked TpPa-COF[34] have been successfully synthesized using the microwave method.

1.4.3. Interfacial Synthesis

The interfacial synthetic approach is a novel and effective strategy for synthesizing COF thin films while keeping their thickness under control.[35] For example, 2DCCOF1 and 2DCCOF2 with C−C linkages have been synthesized in the interface of two solvents through the Suzuki coupling reaction. The monomers were dissolved in toluene with the catalyst $Pd(PPh_3)_4$ and added on the top of an aqueous solution of K_2CO_3. These two-phase systems were kept in a refrigerator at 2 °C under an argon atmosphere. After a month, large and stable sheets of AB-staggered COFs were formed at both interfaces. Under UV light, the 2DCCOF1 film exhibits strong blue fluorescence, indicating the formation of a large conjugated system (**Figure 1.1**).[36]

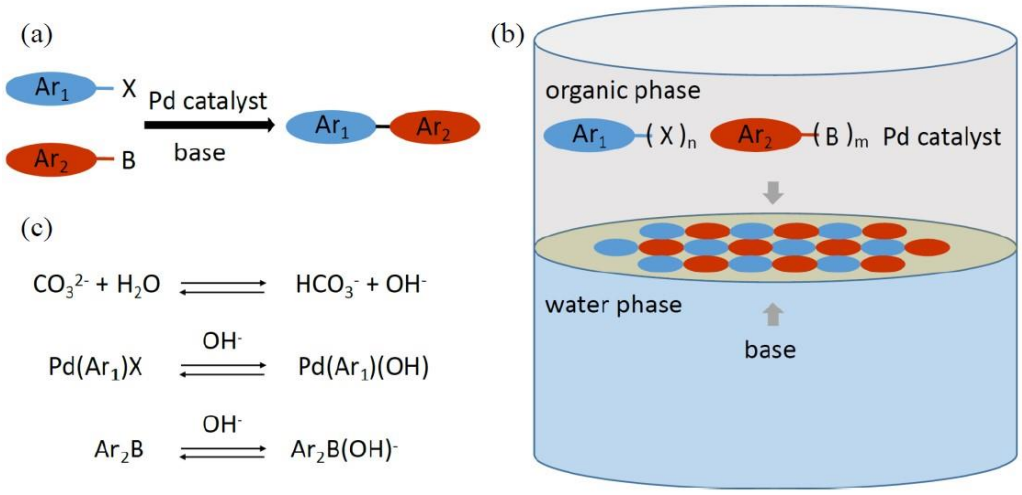

Figure 1. 1 (a) Suzuki reaction between aryl groups; (b) Preparing 2D-COF on the interface via Suzuki polymerization (**Ar** represents aryl group; **X** represents halide atom; **B** represents boronic group; m, n≥2 and at least one ≥3); (c) Reversible hydroxide/halogen exchange or hydroxylation of the boronic group in the transmetalation step (OH^- was generated by the reversible hydrolysis of CO_3^{2-}), reprinted from ref 36, Copyright 2019 Angewandte Chemie International Edition.

1.4.4 Synthesis under Ambient Conditions

Previously, COF reactions had to be carried out at high temperatures in order to promote monomer condensation. A method for an aerobic synthesis at room temperature is a promising potential topic for large-scale COF production. In general, two approaches for room temperature COF synthesis have been reported: mechanochemical grinding and rapid solution-phase synthesis.

Mechanochemical grinding has received a lot of attention as a simple method for synthesizing COFs due to its quick process and environmentally friendly reaction conditions when compared to traditional solution-based synthesis methods such as solvothermal and microwave synthesis. The bonds are constructed in a simple, economical, and environmentally benign way. In this method, COFs are generated by grinding monomers with a mortar and pestle at room temperature. Biswal et al. synthesized the beta-ketonamine COFs TpPa-1, TpPa-2, and TpBD by simply grinding precursors in a mortar for almost an hour (**Scheme 1.7**).[37] Many COFs have been

successfully synthesized by this approach including TpPa-1, TpPa-2, TpPa-F_4, TpBD, TpBD-$(NO_2)_2$, TpBD-Me_2, TpPa-NO_2, and TpBD-$(OMe)_2$.[38,39] While mechanochemical synthesis has many advantages such as accelerating the reaction rate and facilitating the homogeneity of reactants, the poor crystallinity and porosity of mechanochemically synthesized COFs pose difficult research challenges.[40-42]

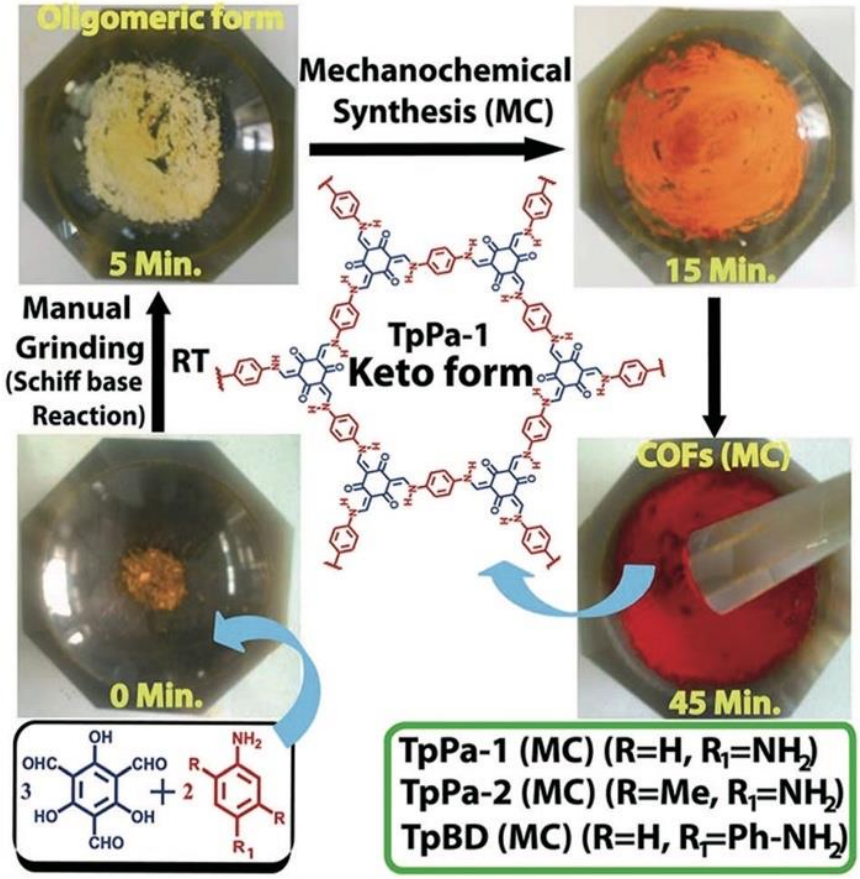

Scheme 1. 7. Schematic representation of the MC synthesis of TpPa-1 (MC), TpPa-2 (MC), and TpBD (MC) through simple Schiff base reactions performed via MC grinding using a mortar and pestle, reprinted with permission from ref [37], Copyright 2013 American Chemical Society.

Zamora and colleagues successfully synthesized RT-COF-1 (from TAPB and TFB) in 2015 using a microfluidic system. The COF obtained under continuous flow conditions was crystalline and chemically stable. At the same time, Yang et al.[43]developed COF-TpBD via a simple and

straightforward solution-phase synthesis at room temperature. Soon after, Zhao's group used a continuous flow system to synthesize COF-LZU-1 with higher crystallinity and porosity when compared to the same type of COF synthesized using the traditional solvothermal method.[44] The microfluidic synthesis of LZU-1 is claimed to have a production rate of 41 mg per hour at an extremely high space-time yield of 703 kg m^{-3} per day, indicating a promising future for large-scale COF synthesis. Later, in 2017, Dichtel and colleagues used metal triflates to superiorly catalyze the formation of the imine-linked COFs TAPB-PDA, TAPB-BPDA, and TAPB-TIDA in just 10 minutes at room temperature.[45] Not only is the reaction temperature and duration optimized, but the products also have an outstanding porous structure with a high BET surface area when compared to those obtained through a traditional solvothermal synthesis. Despite the fact that these cases point in a promising direction for the future of COF synthesis, only a few COFs have been synthesized using the rapid solution-phase method. The most extensive method for producing COFs is still solvothermal synthesis.

1.5. Characterization of COFs

COFs are characterized by various methods,[6] one of which is powder X-ray diffraction (PXRD). PXRD is a technique used to determine the crystallographic structure of a material. It is frequently used for structural analysis on COF samples, to determine the orientation of a single crystal, to find the crystal structure of an unknown material, and to measure the size, shape, and internal stress of small crystalline regions. Computational simulation with software such as Material Studio provides for a more accurate interpretation of the obtained analysis. Solid-state NMR spectroscopy is the most effective technique utilized to determine the structural regularity and atomic connectivity in COF materials, especially the formation of new covalent bonds. Solid-state NMR spectroscopy is without a doubt the most powerful technique that has been used to characterize a

variety of solid materials including zeolites, organic polymers, and MOFs. Many atoms in the COF frameworks, such as ^{1}H, ^{13}C, ^{11}B, ^{15}N, ^{29}Si, and ^{17}O are NMR active due to their nuclear spin *I*. The morphology of COF materials is studied using scanning electron microscopy (SEM), whereas the state of metal ions incorporated into COF materials can be studied using X-ray photoelectron spectroscopy (XPS). Gas adsorption-desorption measurements (nitrogen or argon) are widely used to determine the porosity and surface areas of COF materials. Meanwhile, other characterization techniques, such as infrared and UV-Vis spectroscopies, have been used to provide additional information on COF materials.[6]

1.6. Post Synthetic Modification (PSM)

Post-synthetic modification (PSM) is a powerful strategy that involves introducing functional moieties into the COF backbone through chemical transformations or modifications while retaining the original framework.[46] The suitable selection of building units enables PSM linkers with pendant reactive groups or metal binding sites to be incorporated into COFs in predetermined positions (**Figure 1. 2**).[6]

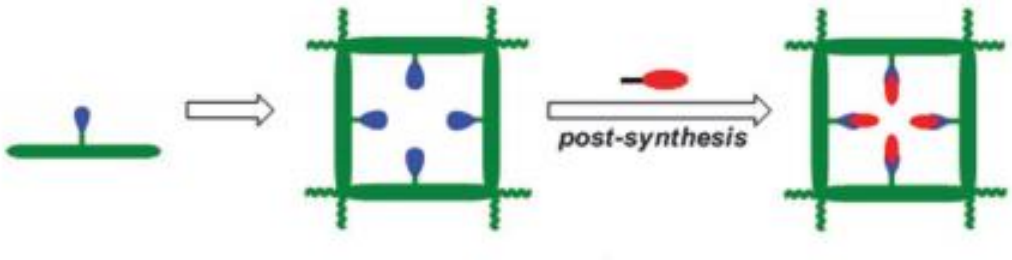

Figure 1. 2. General strategies for the designed synthesis of functional COF materials. The red ovals represent the functional moieties, reprinted with permission from ref 6, Copyright 2013 Chemical Society Reviews.

1.6.1. Covalent post-synthetic modification (covalent PSM)

Covalent PSM is the most effective strategy for COF PSM and involves functional group interconversion through various covalent reactions. It is classified into two parts: covalent PSM of linkers and covalent PSM of linkages.[46]

1.6.1.1. Covalent Post-Synthetic Modification of Linkers

The modification starts with a COF with predesigned reactive groups. Functional moieties can then be covalently bonded to the COF skeleton by reacting with linkers while retaining the original structure of the COF.[46]

I. Click Reaction

The click reaction is considered to be one of the most commonly used post-synthetic modification reactions due to its quantitative conversion yield, high specificity, and convenient synthetic protocols.[47] The first report of this strategy was by Jiang and co- workers who used a post-synthetic copper(I)-catalyzed alkyne-azide cycloaddition (CuAAC) click reaction to tailor the functionalities of a boronate ester structure with pendant alkynyl groups.[48]

The COFs can be modified with triazole moieties by reacting N_3-COF-5 with various alkynyl compounds catalyzed by CuI in anhydrous N, N-dimethylacetamide at 50 ^oC for 24 h. As a result, the density of desired functional groups in the pores has a significant impact on the gas-sorption selectivity of CO_2 over N_2 (**Scheme 1.8**).[48]

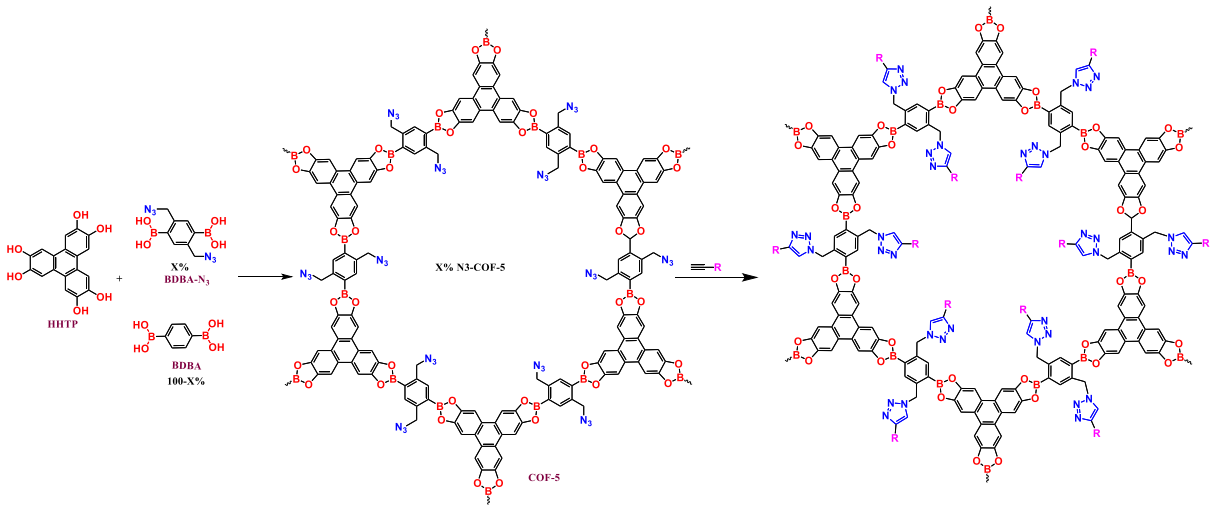

Scheme 1. 8. Post-modification of the pore surface of N_3-COF-5 via the ‘‘click’’ reaction to synthesize the functionalized COFs. The percentage (x%) of the building unit BDBA-N_3 in the original mixture could range from 5% to 100%. R represents the organic functional groups.[48]

II. Post-Synthetic Linker Exchange

Since most COFs are formed through dynamic covalent chemistry, the inherently dynamic nature of covalent bonds enables them to undergo post-synthesis linker exchange. In 2017, Zhao and colleagues successfully synthesized a benzidine-containing COF (TP-COF-BZ) capable of post-synthetic linker exchange with 1,4-diaminobenzene (**Scheme 1.9)**.[49] The featured PXRD peaks of the new COF (TP-COF-DAB) increased with increasing amounts of 1,4-diaminobenzene. That indicates the ongoing COF to COF transformation. According to time-dependent PXRD experiments, the substitution reaction of the linkers occurs in the first half-hour followed by the disassociation of TP-COF-BZ. The crystallinity of TP-COF-DAB improves significantly with extended reaction time.

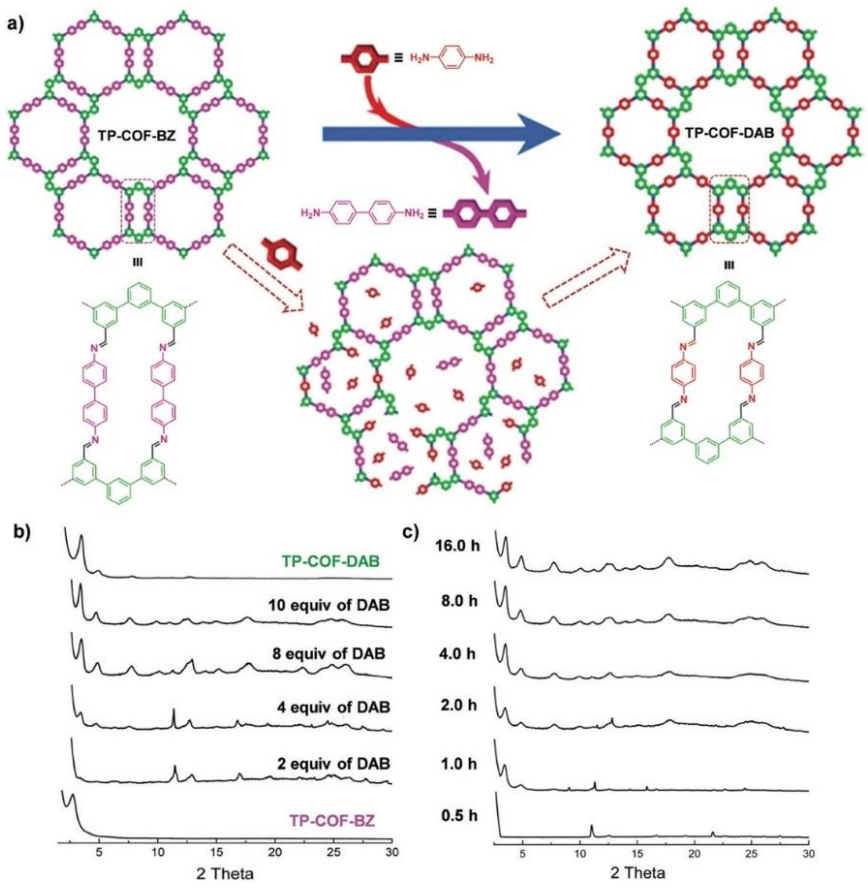

Scheme 1. 9. (a) Synthesis of TP-COF-DAB by post-synthetic linker exchange and the proposed process for the in situ transformation of TP-COF-BZ into TP-COF-DAB in the presence of 1,4-diaminobenzene. (b) The transformation from TP-COF-BZ to TP-COF-DAB in different equivalents of 1,4-diaminobenzene for 72 h at 120 1C indicated by PXRD patterns. (c) Time-dependent PXRD patterns of the samples prepared by heating a mixture of TP-COF-BZ and 1,4-diaminobenzene (10 equiv.), reprinted with permission from ref 49, Copyright 2017 American Chemical Society.

1.6.1.2. Post-Synthetic Conversion of Linkages

Both COF linkers and linkages can contribute to a PSM reaction. For example, COFs with imine linkage have been successfully converted into the corresponding modified COFs.[50] The first report of imine-linked COFs being oxidized to amine -linked COFs was in 2016 by Yaghi and co-workers (**Scheme 1.10)**.[50] While retaining the crystallinity and porosity of both COFs, the solid-state conversation of imine to amide linkages was observed to be quantitative. After treating with 12

M HCl (aq.) and 1 M NaOH (aq.), amide-linked COFs show a remarkable improvement in stability when compared to imine-linked COFs.

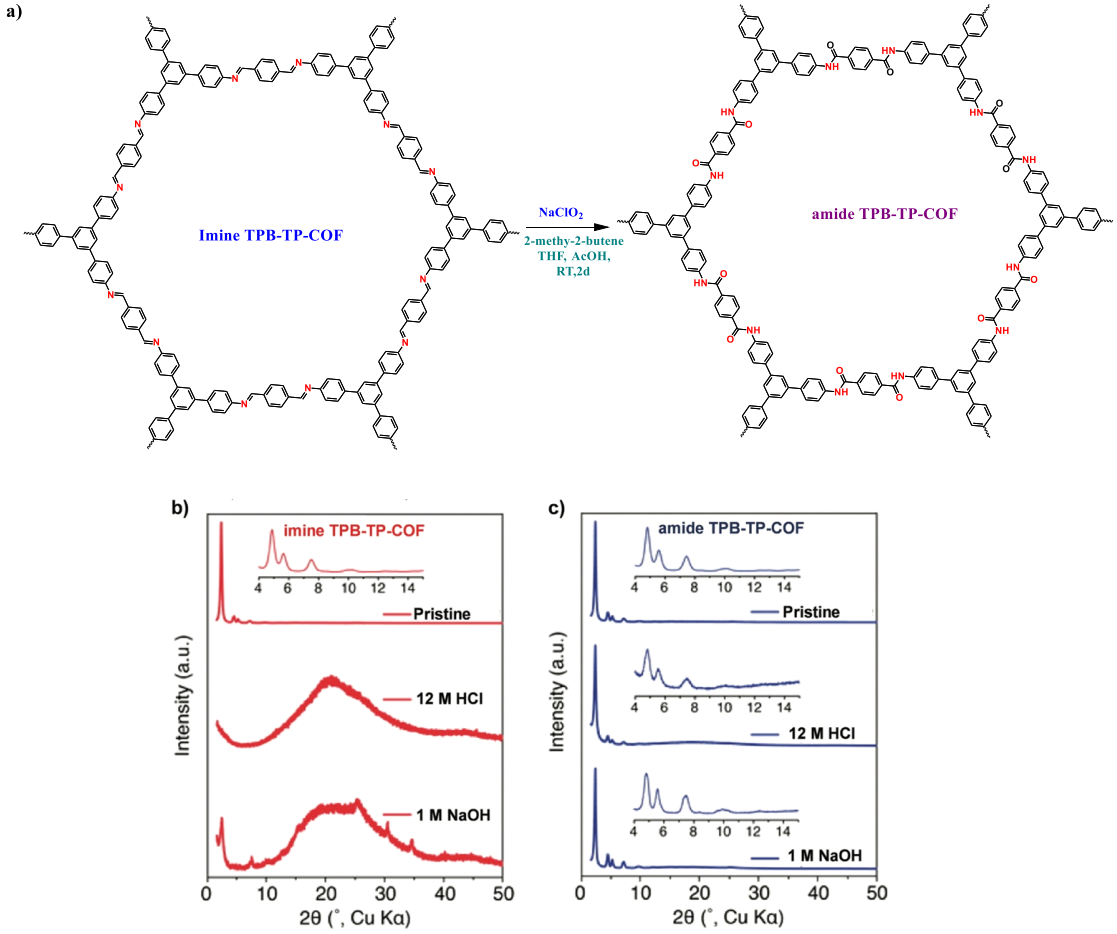

Scheme 1. 10. (a) Conversion of imine TPB-TP-COF to amide TPB-TP-COF via linkage oxidation. Comparison of diffraction patterns of imine TPB-TP-COF (b) and amide TPB-TP-COF (c) after 24 h treatment in solutions, reprinted (adapted) with permission from ref 50, Copyright 2016 American Chemical Society.

1.6.2. Post-Synthetic Metal-Functionalization

COFs are considered excellent candidates for metal-functionalization because both linkages and linkers in the COF structure are composed of anchoring sites for metal binding such as N, S, O, and others. In a general procedure, specific metal units were introduced to predesigned COFs through a coordination complexation reaction, resulting in metal-containing COFs with unique

features. The current post-synthetic metal-functionalization methods can be classified into two groups based on the various possible interactions between metal ions and COF structures: coordination with functional linker groups or linkages.

1.6.2.1. Post-Synthetic Metalation on Organic Linkers

COFs with multidentated ligands including porphyrin, bipyridine, N,N-bis(salicylidene)ethylenediamine (Salen), and others can be used as metalation matrices. Porphyrins have a unique ability to coordinate with various metal ions to form a metalloporphyrin with distinct photophysical and photochemical properties.[51-53] Wang et al. reported the successful incorporation of both Zn^{2+} and Co^{2+} into porphyrin-based COFs, resulting in different charge distribution and internal chemical environment.[54]

1.6.2.2. Post-Synthetic Metalation with Linkages

The COF linkages, including imine and hydrazine bonds, have the ability to bind to particular metal ions. In 2011, Wang et al. designed Pd/COF eclipsed and ordered π-columnar structures with palladium metals sandwiched between adjacent COF layers through coordinated imine bonds. The obtained Pd/COF-LZU1 showed excellent catalytic activity in the Suzuki–Miyaura coupling reaction (**Scheme 1.11)**.[55]

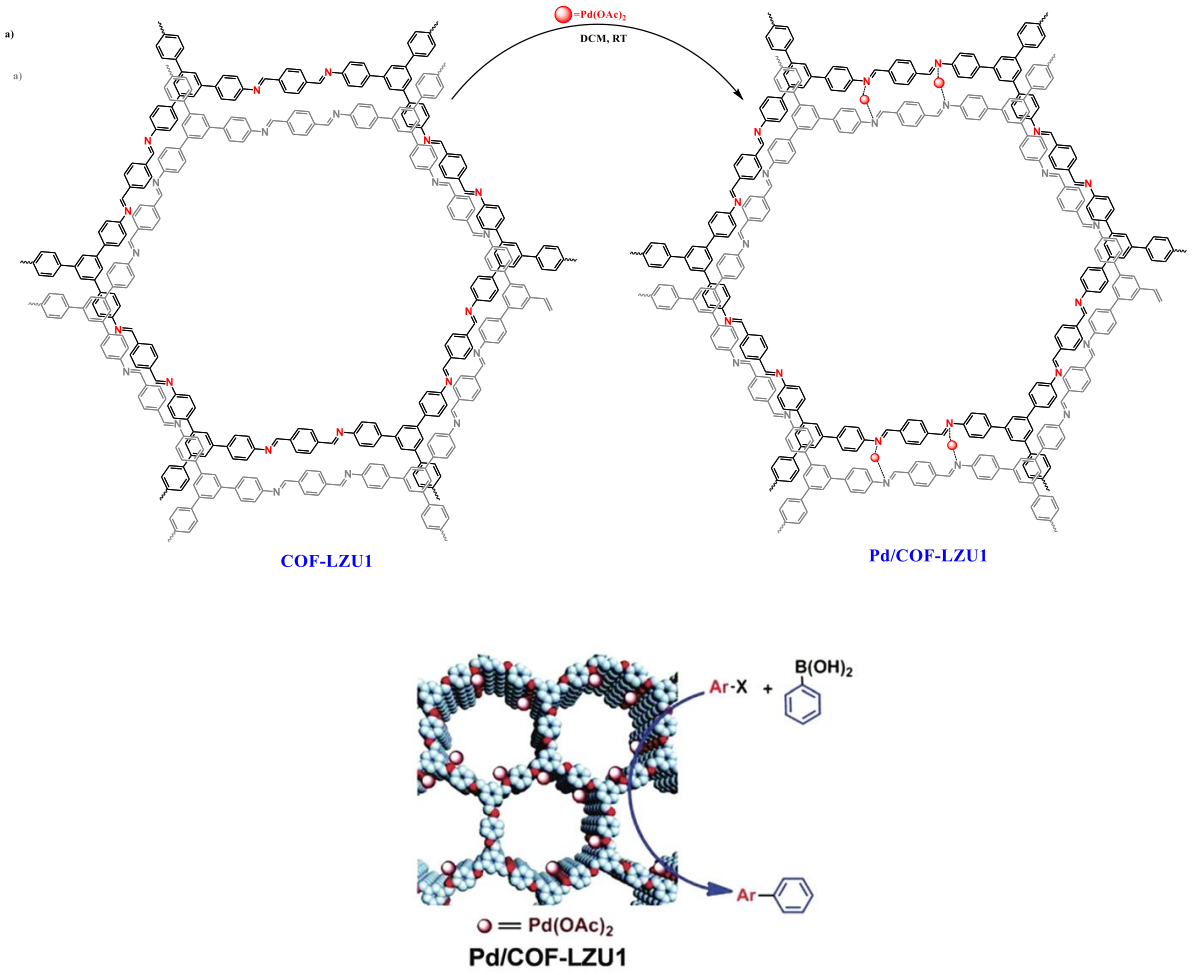

Scheme 1. 11. Post-synthetic metalation of COF-LZU1 with $Pd(OAc)_2$. The resulting Pd/COF-LZU1 was used as a catalyst in a Suzuki–Miyaura coupling reaction, reprinted (adapted) with permission from ref 55, Copyright 2011 American Chemical Society.

1.7. COFs Features

COFs exhibit numerous unique features, such as excellent crystallinity, large surface area, high flexibility, and intrinsic adaptability in structural and functional design. Indeed, the high porosity and chemical and thermal stability of COFs endow robust architectures. This allows the organic and inorganic reactions to be accomplished (executed) on these frameworks without losing any of their porosity or crystallinity. Compared to metal–organic frameworks (MOFs), the COF materials show enhanced stability above 300 °C. In addition, most of the frameworks are insoluble and maintain their linkages and stacking when exposed to solvents. COFs that have recently been developed are highly resistant to extreme pHs,[56] hydrolysis,[57] and reductive[11] and oxidative environments.[58]

1.8. Applications of COFs

Compared to other porous materials such as metal organic frameworks (MOFs), zeolitic imidazolate frameworks (ZIFs), and porous carbons, COFs are promising candidates for a wide range of applications such as gas adsorption and catalysis. COFs are also superior adsorbents used for pollutant removal and biomedical applications due to their high surface area and crystalline, large pore volume, tunable porosity, and conjugation with unique photoelectric features.[59]

1.8.1. Gas Storage

1.8.1.1. Hydrogen Storage: The need to reduce air pollution and increased energy demands have led to the necessity for new and cleaner energy sources. Because of its high chemical energy density and clean combustion, hydrogen has been studied as a potential substitute for conventional fossil fuels, especially in automotive applications. Therefore, numerous studies have focused on hydrogen storage using porous materials. The use of COF materials for hydrogen storage has

recently been investigated. A study found that COFs with large surface areas exhibit higher hydrogen uptake capacities when compared to other materials. COF-18 with a BET surface area of 1263 m^2 g^{-1} , for instance, possesses the highest hydrogen uptake (1.55 wt percent at 1 bar, 77 K) when compared to similar 2D COFs.[59]

1.8.1.2. Carbon Dioxide: Carbon dioxide emissions from the combustion of fossil fuels are found to be a major contribution to global warming. Carbon dioxide capture and storage has proved to be a major research interest. CO_2 storage has been studied extensively using a variety of porous materials, including porous carbon, silica, and MOFs.[60] COF materials have also been used as storage media. A study found that COF-102 possesses the highest CO_2 uptakes with a maximum value of 1200 mg g^{-1} at 55 bar and 298 K, proving that COFs make excellent materials for capturing carbon dioxide. Incorporation of functional moieties into COFs may become a preferable option for increasing their CO_2 storage capacity, as demonstrated in other porous materials such as ZIFs.[17]

1.8.1.3. Ammonia Storage: ammonia has a wide range of applications in industry, including the production of nitrogen fertilizers. Compressed liquid ammonia is needed for commercial transportation and application, but liquid nitrogen is difficult to handle because of its toxicity. The practical way to solve this problem is by storing ammonia in adsorbents. Yagi and co-workers found that COF-10, a boron-containing COF, possesses the highest ammonia uptake capacity when compared to other porous materials. During the adsorption cycles, the layered morphology of COF-10 was disrupted, but the atomic connectivity and periodicity were preserved. The exceptionally high uptake of ammonia by COF-10 was due to the formation of a classical ammonia-borane coordination bond (**Scheme 1. 12**).[61]

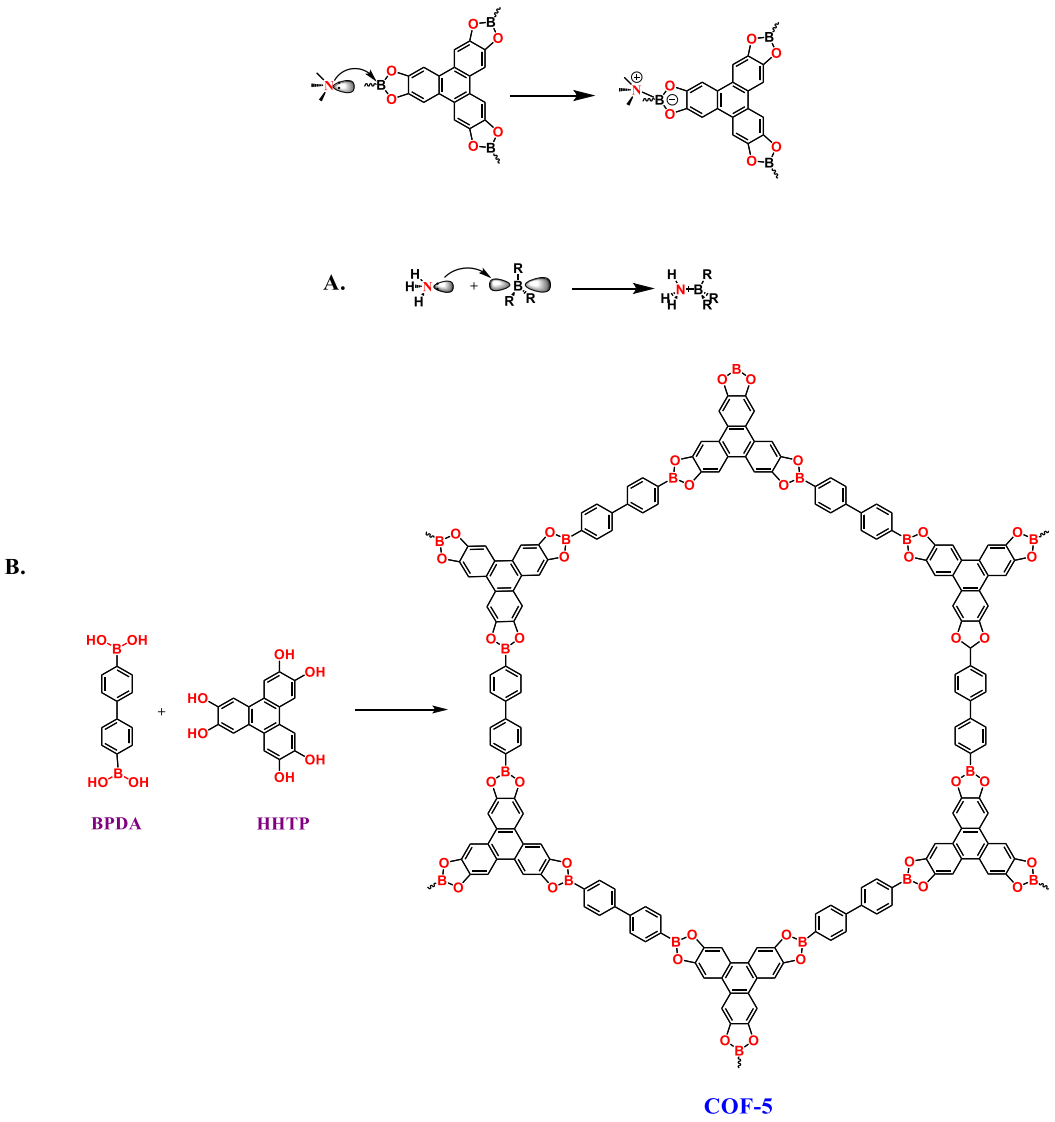

Scheme 1. 12. The proposed ammonia–boron interaction upon the adsorption of ammonia on COF-10, adapted from ref .61, Copyright 2010 Springer Nature.

1.8.2. Applications in Catalysis

COF materials contain highly reactive sites within their pores, making them efficient, robust catalysts used in a variety of organic chemical reactions.[6, 62] COFs possess unique properties such as high porosity, designable molecular skeletons, and controllable networks, which can be functionalized to introduce catalytic sites.[63, 64] When compared to traditional heterogeneous catalysts, the COF materials show better stability and recycling ability. COFs with imine or

hydrazone linkages, for example, are resistant to decomposition in air and in a variety of protic and aprotic solvents. Therefore, they have emerged as a special class of multifunctional materials with unique properties, opening up tremendous opportunities in the field of catalysis.[65, 66]

1.8.2.1. Coupling Reaction

Studies over the last decade have shown that functional porous COFs materials can be used as catalysts in cross-coupling catalytic reactions. The first example of the design, synthesis, and application of imine-linked COFs to catalyze the Suzuki-Miyaura coupling reaction was described in an early study by Wang and co-workers. For Example, COF-LZU1 is an imine-linked COF, 2D sheet layered structure, that was prepared by the co-condensation of building units 1,3,5-Triformylbenzene (TFB) and 1,4-diaminobenzene (DAB) **(Scheme 1.13).**[55] The distance between two nitrogen atoms in the adjacent layers is 3.7 A^{o}, which is ideal for the strong coordination of metal ions such as Pd (II). Pd/COF-LZU1 was tested as a catalyst for the Suzuki–Miyaura coupling reaction using a broad range of reactants. The excellent yields (96–98%) of the reaction products as well as the high stability and easy recyclability of the catalyst, all draw attention to the excellent catalytic performance of the catalyst.[55]

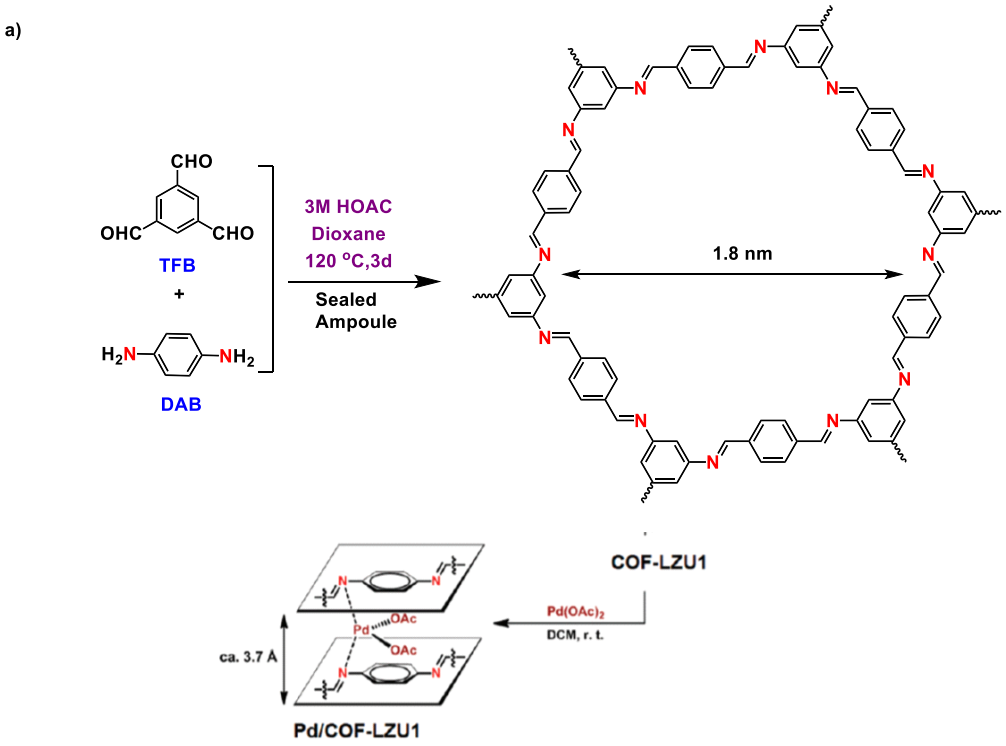

Scheme 1. 13. Construction of COF-LZU1 and Pd/COF-LZU1m reprinted (adapted) with permission from ref 55, Copyright 2011 American Chemical Society.

1.8.2.2. Oxidation Reaction

A variety of functional COF complexes has been extensively studied in selective oxidation reactions. In 2015, Chen et al.[67] reported the synthesis of novel 2D Cu-docked TAPT-DHTA-COF using 2,5-dihydroxy-terephthalaldehyde (DHTA) as vertices and 1,3,5-tris-(4-aminophenyl)triazine (TAPT) as edges. Not only did the 2D COF catalyst possess good thermal stability, but it also showed high catalytic efficiency and recyclability towards oxidation/conversion of styrene to benzaldehyde.

1.8.2.3. Addition Reaction

The addition reaction is a significant reaction for the growth of a carbon chain, making it an excellent synthetic tool for the production of essential intermediates in therapeutic drugs, herbicides, insecticides, cosmetics, and agrochemicals. COFs have also been recognized as ideal

solid organocatalysts for addition reactions such as cycloaddition and Michael addition due to their special channel structure, reusability, and functional diversity. Jiang et al. developed a series of new chiral COFs, namely [(S)-Py]-TPB-DMTP-COF, by incorporating both chiral centers and organocatalytic species into the COF skeletons, making them suitable candidates as heterogeneous catalysts for Michael reactions of cyclohexanone and β-nitrostyrene.[68] The reaction exhibited excellent catalytic activity with 100 percent conversion and 92 percent enantioselectivity achieved in just 12 hours.

1.8.3. Superior Adsorbents for Pollutants Removal

COFs are considered one of the most widely used materials in environmental pollution management due to their unique features including: high surface area, large pore size, low mass density, and high thermal stability. In contrast with traditional adsorbents, COFs possess special advantages such as 1) high chemical and thermal stability due to their strong covalent bonds; 2) porous channels that offer numerous adsorption sites and help accelerate the diffusion rate of pollutants; 3) A tunable shape and pore size providing for the separation of distinct contaminants.[69-71]

1.8.3.1. Decontamination of Water

Water contaminants have become a serious concern for public health and environmental conservation as a result of the rapid growth of industrialization. Toxic heavy metal ions (e.g., $Hg^{2+,}$ $Pb^{2+,}$ Cd^{2+}, and Cu^{2+}) in radioactive waste, as well as radionuclides (e.g., ^{128}Pd, ^{137}Cs, ^{137}Cs, ^{59}Fe, ^{57}Co, ^{65}Zn, ^{89}Sr, ^{235}U, ^{79}Se, ^{99}Tc, ^{153}Eu, and ^{129}I) and organic contaminants (e.g., rhodamine B [RhB], CR, Methyl orange [MO], Bisphenol A [BPA], methylene blue [MB], polycyclic aromatic hydrocarbons [PAHs], sulfamerazine [SMT] in industrial wastewater are considered the main

pollutants in aqueous solutions that can accumulate in living organisms and cause a serious impact on humans' health through the food chain.[72]

1.8.3.1.1. Removal of Toxic Heavy Metals

The industrial wastewater contaminated with heavy metals is typically acidic, so it requires highly stable adsorbents. COFs are highly stable in strong basic and acidic due to the strong covalent bonds connecting their building units. COFs also have regular channels and an adjustable pore size, which allow the adsorbed heavy metal ions to disperse uniformly in COFs and be effectively captured. As a result, COF-based products can effectively remove heavy metals from wastewater and have excellent adsorption performance toward different heavy metal ions.[72] The functional groups that contain N, O, or S atoms display a high adsorption capacity for heavy metal ions. Consequently, introducing specific functional groups (e.g., -COOH, $-NH_2$, -CN, -SH, $-SCH_3$, and $-SO_3H$) into the framework of COFs will significantly enhance metal ion removal efficiency. Hg^{2+} can negatively impact cell function and growth and even cause cell necrosis by impacting metabolic pathways. COFs with functional groups containing N, O, or S through stable covalent bonds are able to effectively remove this harmful metal. Therefore, COF-based materials with high O, N, or S contents are found to be effective on Hg^{2+} adsorption. Ding et al.[73] developed COF-LZU8 with thioether hydrazone bonding to remove Hg^{2+} with high sensitivity, selectivity, and adsorption capacity. The rigid π conjugation structure of COF-LZU8 serves as a fluorophore for signal detection, while the evenly and densely distributed thioether side chains serve as ion receptors for capturing Hg^{2+}.

1.8.3.1.2. Removal of Organic Dyes

More than 100,000 organic dyes have been used by the printing, leather tanning, textile, and plastic industries.[74] The majority of industrial waste effluent is released into the rivers or oceans without

proper management. Organic molecules with their complex properties and structural diversity have the potential to negatively impact the natural environment and humans' health. That is because of their esthetic consequences, toxicological characteristics, xenobiotic properties, and other health-risk factors.[75] Organic dyes can be classified into anionic, cationic, and nonionic dyes based on the charge of the chromophore groups.

I. Elimination of Cationic Dyes

Methylene Blue [MB] is one of the most widely used cationic organic dyes in paper manufacturing and cellular staining. Even though MB is not considered the most poisonous or pathogenic organic pollutant, it does cause a negative impact on humans' health, such as vomiting, an increase in heart rate and obnubilation, when ingested in low doses.[76] A study found that utilizing COFs, such as TPT-DMBD-COF, recorded good data in removing MB from water.[77] The well-fitted intraparticle diffusion model described a two-stage adsorption reaction: intraparticle diffusion and film diffusion. Moreover, electrostatic attraction of π-π stacking of aromatic rings in COF structure and the pore size differences between MB and COF are the two main factors that play a significant role in the uptake of MB by COFs.

A study by Yan's group explored the use of carboxyl COF-TzDBd to uptake triphenylmethane dyes (crystal violet CV and BG brilliant green).[78] Even though the adsorption processes of CV and BG onto COF-TzDBd exhibited good resistance at 0.2 mol/L, the adsorptive capacities dramatically decreased when the concentration was increased above 0.2 mol/L, suggesting that the electrostatic interaction could be one of the removal mechanisms for triphenylmethane dye uptake. The UV-vis spectroscopy analyses display an apparent redshift of characteristic peaks, confirming the synergistic effects of π-π interaction from the conjugated aromatic structure of COF-TzDBd.

Furthermore, the molecular sizes of cationic CV and BG were preferable for the capture by TzDBd with an anionic surface and the pore size of ~40A^0.

II. Anionic Dyes

Congo red CR is a common anionic dye that is widely used in the paper-making industry, as well as an acid-base indicator and biological dye.[79] Because of its complex chemical structure, high solubility, and carcinogenicity, CR removal from the hydrosphere has received high priority in research. Numerous COF-based materials have been developed so far for CR removal purposes. A novel COF-COOH was produced via polymerization of Tp and DBA.[80] Then, modified ions (Ca^{2+}/Ni^{2+}) were incorporated to form COF-COOCa and COF-COONi, respectively. The FTIR results show new peaks at 1,574 and 1,224 cm^{-1}, which correspond to C=C and C-N bonds. That indicates the formation of a keto structure in COF-COOH. The π -conjugated structure as well as the numerous hydrogen bonding sites of COF-COOH, contributed to the high capture efficiency for CR. The adsorption capacities of CR on COF-COOCa and COF-COONi were determined to be 704.2 and 781.3 mg. g^{-1} respectively. That was due to the increase of electrostatic interaction of metal ion sites with CR.

Overall, in adsorptive applications of COFs, the molecular size of organic contaminants and predesigned pore diameter are extremely significant. Furthermore, introducing additives to COF-based materials could improve the electrostatic interaction between COFs and contaminants, resulting in enhancing the removal efficiency of COF-based materials.[72]

1.8.4. COFs for Biomedical Applications

COFs have been explored in biomedical applications, such as drug delivery, photodynamic therapy, and bioimaging because of their great potential and unique features in diagnosis and treatment.

1.8.4.1. Drug delivery

One example of applying COFs to drug delivery was reported by Banerjee and co-workers who did a series of explorations on imine-based COFs for drug loading and release. They observed that the capacity of drug loading was only 0.35 mg/g for Doxorubicin (DOX), calculated by UV-Vis absorbance spectra. Indeed, the rate of the release was slow, and about 50% remained in pH 5 phosphate buffer after 7 days. Then, they designed self-standing porous COF membranes in order to obtain larger molecules with more than 1 nm, such as tetracycline. They found only about 5% of the administrated nanoparticle reached the target tumor. One possible way to improve the use of nanocarriers is to modify them with target groups. Banerjee and co-workers made a modification on covalent organic nanosheets with folic acid, called TpASH-FA, via the post-synthetic modification method using 5-FU as a model drug. Even though these nanosheets show the loading efficiency to be only 12%, which is lower than other COFs, the anticancer activity exhibited by these nanosheets was very good. In addition, only 14% of MDA-MB-231 cells survived at a dosage of 50 µg/ml (**Scheme 1.14**).[81]

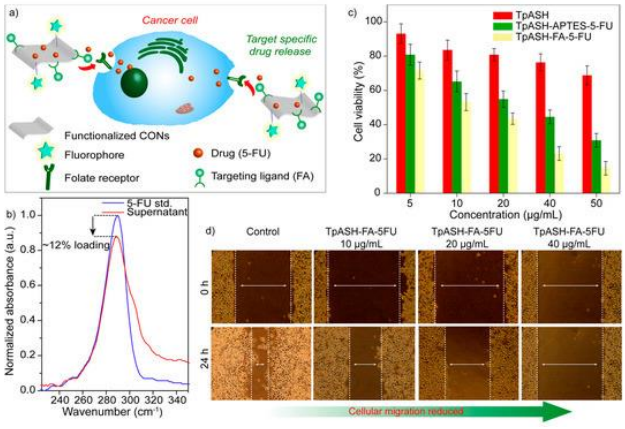

Scheme 1. 14. (a) Representation of targeted drug delivery by CONs (sheet-like material denotes CONs here); (b) Drug loading study of 5-FU by UV−vis; (c) MTT assay on MDA-MB-231 cell lines showing cellular viability, and (d) Comparison of cellular migration study between control and TpASH-FA-5-FU treated sets, reprinted with permission from ref 82 , Copyright 2017 American Chemical Society.

1.8.4.2. Photothermal and Photodynamic Therapy

COFs can be used for photothermal therapy (PTT) and photodynamic therapy (PDT) in addition to chemotherapy. Porphyrin, a large, planar macrocyclic compound with an 18-electron π system, and its derivatives have been widely studied as photosensitizers for PDT to generate singlet oxygen ($^1O_2$) under photoirradiation. In aqueous media, substituted protoporphyrins and amphiphilic tetraphenylporphyrins aggregate to form fibers, tubules, helical ribbons, and sheets. Using porphyrin derivatives as building blocks to form photosensitive COFs is a promising way to prevent the aggregation of porphyrin macrocycles in aqueous media and to improve their efficiency in vivo. Wang and co-workers synthesized 3D porphyrin-based COFs exhibiting excellent photosensitivity that was used to generate reactive singlet oxygen under photoirradiation. They also discovered that the photosensitive characteristics could be optimized by incorporating metal ions into porphyrin macrocycles.[53]

1.9. References

1. Zhang, P.; Chen, S.; Zhu, C.; Hou, L.; Xian, W.; Zuo, X.; Zhang, Q.; Zhang, L.; Ma, S.;Sun, Q., Covalent organic framework nanofluidic membrane as a platform for highly sensitive bionic thermosensation. *Nat. Commun.* **2021**, *12*.

2. Dogru, M.;Bein, T., On the road towards electroactive covalent organic frameworks. *Chemical Communications* **2014**, *50*, 5531-5546.

3. McKeown, N. B.;Budd, P. M., Polymers of intrinsic microporosity (PIMs): organic materials for membrane separations, heterogeneous catalysis and hydrogen storage. *Chem. Soc. Rev.* **2006**, *35*, 675-683.

4. Yuan, D.; Lu, W.; Zhao, D.;Zhou, H. C., Highly stable porous polymer networks with exceptionally high gas-uptake capacities. *Advanced materials (Deerfield Beach, Fla.)* **2011**, *23*, 3723-5.

5. Jiang, J. X.; Su, F.; Trewin, A.; Wood, C. D.; Campbell, N. L.; Niu, H.; Dickinson, C.; Ganin, A. Y.; Rosseinsky, M. J.; Khimyak, Y. Z.;Cooper, A. I., Conjugated microporous poly(aryleneethynylene) networks. *Angewandte Chemie (International ed. in English)* **2007**, *46*, 8574-8.

6. Ding, S.-Y.;Wang, W., Covalent organic frameworks (COFs): from design to applications. *Chem. Soc. Rev.* **2013**, *42*, 548-568.

7. Zhou, H. C.; Long, J. R.;Yaghi, O. M., Introduction to metal-organic frameworks. *Chem Rev* **2012**, *112*, 673-4.

8. Zhu, Y.; Long, H.;Zhang, W., Imine-linked porous polymer frameworks with high small gas (H2, CO2, CH4, C2H2) uptake and CO 2/N2 selectivity. *Chem Mater* **2013**, *25*, 1630.

9. Singh, H.; Tomer, V. K.; Jena, N.; Bala, I.; Sharma, N.; Nepak, D.; De Sarkar, A.; Kailasam, K.;Pal, S. K., A porous, crystalline truxene-based covalent organic framework and its application in humidity sensing. *J Mater Chem A* **2017**, *5*, 21820-21827.

10. Zhao, W.; Xia, L.;Liu, X., Covalent Organic Frameworks (COFs): Perspectives of Industrialization. *CrystEngComm* **2018**, *20*.

11. Bisbey, R. P.;Dichtel, W. R., Covalent Organic Frameworks as a Platform for Multidimensional Polymerization. *ACS Central Science* **2017**, *3*, 533-543.

12. Diercks, C. S.;Yaghi, O. M., The atom, the molecule, and the covalent organic framework. *Science* **2017**, *355*.

13. Guo, J.;Jiang, D., Covalent Organic Frameworks for Heterogeneous Catalysis: Principle, Current Status, and Challenges. *ACS Central Science* **2020**, *6*, 869-879.

14. Geng, K.; He, T.; Liu, R.; Dalapati, S.; Tan, K. T.; Li, Z.; Tao, S.; Gong, Y.; Jiang, Q.;Jiang, D., Covalent Organic Frameworks: Design, Synthesis, and Functions. *Chem. Rev.* **2020**, *120*, 8814-8933.

15. Feng, X.; Ding, X.;Jiang, D., Covalent organic frameworks. *Chem. Soc. Rev.* **2012**, *41*, 6010-6022.

16. Zhao, W.; Xia, L.;Liu, X., Covalent organic frameworks (COFs): perspectives of industrialization. *CrystEngComm* **2018**, *20*, 1613-1634.

17. Furukawa, H.;Yaghi, O. M., Storage of Hydrogen, Methane, and Carbon Dioxide in Highly Porous Covalent Organic Frameworks for Clean Energy Applications. *J. Am. Chem. Soc.* **2009**, *131*, 8875-8883.

18. Côté, A. P.; Benin, A. I.; Ockwig, N. W.; O'Keeffe, M.; Matzger, A. J.;Yaghi, O. M., Porous, crystalline, covalent organic frameworks. *Science* **2005**, *310*, 1166-70.

19. Lanni, L. M.; Tilford, R. W.; Bharathy, M.;Lavigne, J. J., Enhanced Hydrolytic Stability of Self-Assembling Alkylated Two-Dimensional Covalent Organic Frameworks. *J. Am. Chem. Soc.* **2011**, *133*, 13975-13983.

20. Kuhn, P.; Antonietti, M.;Thomas, A., Porous, covalent triazine-based frameworks prepared by ionothermal synthesis. *Angewandte Chemie (International ed. in English)* **2008**, *47*, 3450-3.

21. Chan-Thaw, C. E.; Villa, A.; Katekomol, P.; Su, D.; Thomas, A.;Prati, L., Covalent Triazine Framework as Catalytic Support for Liquid Phase Reaction. *Nano Letters* **2010**, *10*, 537-541.

22. Wang, K.; Yang, L.-M.; Wang, X.; Guo, L.; Cheng, G.; Zhang, C.; Jin, S.; Tan, B.;Cooper, A., Covalent Triazine Frameworks via a Low-Temperature Polycondensation Approach. *Angew. Chem. Int. Ed.* **2017**, *56*, 14149-14153.

23. Luo, W.; Zhu, Y.; Zhang, J.; He, J.; Chi, Z.; Miller, P. W.; Chen, L.;Su, C.-Y., A dynamic covalent imine gel as a luminescent sensor. *Chemical Communications* **2014**, *50*, 11942-11945.

24. Uribe-Romo, F. J.; Hunt, J. R.; Furukawa, H.; Klöck, C.; O'Keeffe, M.;Yaghi, O. M., A Crystalline Imine-Linked 3-D Porous Covalent Organic Framework. *J. Am. Chem. Soc.* **2009**, *131*, 4570-4571.

25. Uribe-Romo, F. J.; Doonan, C. J.; Furukawa, H.; Oisaki, K.;Yaghi, O. M., Crystalline covalent organic frameworks with hydrazone linkages. *J Am Chem Soc* **2011**, *133*, 11478-81.

26. Du, Y.; Calabro, D.; Wooler, B.; Kortunov, P.; Li, Q.; Cundy, S.;Mao, K., One Step Facile Synthesis of Amine-Functionalized COF-1 with Enhanced Hydrostability. *Chem Mater* **2015**, *27*, 1445-1447.

27. Fang, Q.; Gu, S.; Zheng, J.; Zhuang, Z.; Qiu, S.;Yan, Y., 3D Microporous Base-Functionalized Covalent Organic Frameworks for Size-Selective Catalysis. *Angew. Chem. Int. Ed.* **2014**, *53*, 2878-2882.

28. Das, G.; Biswal, B. P.; Kandambeth, S.; Venkatesh, V.; Kaur, G.; Addicoat, M.; Heine, T.; Verma, S.;Banerjee, R., Chemical sensing in two dimensional porous covalent organic nanosheets. *Chem. Sci.* **2015**, *6*, 3931-3939.

29. Jin, Y.; Yu, C.; Denman, R. J.;Zhang, W., Recent advances in dynamic covalent chemistry. *Chem. Soc. Rev.* **2013**, *42*, 6634-6654.

30. Zhang, B.; Wei, M.; Mao, H.; Pei, X.; Alshmimri, S. A.; Reimer, J. A.;Yaghi, O. M., Crystalline Dioxin-Linked Covalent Organic Frameworks from Irreversible Reactions. *J. Am. Chem. Soc.* **2018**, *140*, 12715-12719.

31. Xu, L.; Ding, S.-Y.; Liu, J.; Sun, J.; Wang, W.;Zheng, Q.-Y., Highly crystalline covalent organic frameworks from flexible building blocks. *Chemical Communications* **2016**, *52*, 4706-4709.

32. Campbell, N. L.; Clowes, R.; Ritchie, L. K.;Cooper, A. I., Rapid Microwave Synthesis and Purification of Porous Covalent Organic Frameworks. *Chem Mater* **2009**, *21*, 204-206.

33. Ritchie, L. K.; Trewin, A.; Reguera-Galan, A.; Hasell, T.;Cooper, A. I., Synthesis of COF-5 using microwave irradiation and conventional solvothermal routes. *Microporous and Mesoporous Materials* **2010**, *132*, 132-136.

34. Wei, H.; Chai, S.; Hu, N.; Yang, Z.; Wei, L.;Wang, L., The microwave-assisted solvothermal synthesis of a crystalline two-dimensional covalent organic framework with high CO2 capacity. *Chemical Communications* **2015**, *51*, 12178-12181.

35. Dey, K.; Pal, M.; Rout, K. C.; Kunjattu H, S.; Das, A.; Mukherjee, R.; Kharul, U. K.;Banerjee, R., Selective Molecular Separation by Interfacially Crystallized Covalent Organic Framework Thin Films. *J. Am. Chem. Soc.* **2017**, *139*, 13083-13091.

36. Zhou, D.; Tan, X.; Wu, H.; Tian, L.;Li, M., Synthesis of C-C Bonded Two-Dimensional Conjugated Covalent Organic Framework Films by Suzuki Polymerization on a Liquid-Liquid Interface. *Angewandte Chemie (International ed. in English)* **2019**, *58*, 1376-1381.

37. Biswal, B. P.; Chandra, S.; Kandambeth, S.; Lukose, B.; Heine, T.;Banerjee, R., Mechanochemical Synthesis of Chemically Stable Isoreticular Covalent Organic Frameworks. *J. Am. Chem. Soc.* **2013**, *135*, 5328-5331.

38. Chandra, S.; Kandambeth, S.; Biswal, B. P.; Lukose, B.; Kunjir, S. M.; Chaudhary, M.; Babarao, R.; Heine, T.;Banerjee, R., Chemically Stable Multilayered Covalent Organic Nanosheets from Covalent Organic Frameworks via Mechanical Delamination. *J. Am. Chem. Soc.* **2013**, *135*, 17853-17861.

39. Biswal, B. P.; Chandra, S.; Kandambeth, S.; Lukose, B.; Heine, T.;Banerjee, R., Mechanochemical synthesis of chemically stable isoreticular covalent organic frameworks. *J Am Chem Soc* **2013**, *135*, 5328-31.

40. Shinde, D. B.; Aiyappa, H. B.; Bhadra, M.; Biswal, B. P.; Wadge, P.; Kandambeth, S.; Garai, B.; Kundu, T.; Kurungot, S.;Banerjee, R., A mechanochemically synthesized covalent organic framework as a proton-conducting solid electrolyte. *J Mater Chem A* **2016**, *4*, 2682-2690.

41. Peng, Y.; Xu, G.; Hu, Z.; Cheng, Y.; Chi, C.; Yuan, D.; Cheng, H.;Zhao, D., Mechanoassisted Synthesis of Sulfonated Covalent Organic Frameworks with High Intrinsic Proton Conductivity. *Acs Appl Mater Inter* **2016**, *8*, 18505-18512.

42. Das, G.; Balaji Shinde, D.; Kandambeth, S.; Biswal, B. P.;Banerjee, R., Mechanosynthesis of imine, β-ketoenamine, and hydrogen-bonded imine-linked covalent organic frameworks using liquid-assisted grinding. *Chemical Communications* **2014**, *50*, 12615-12618.

43. Yang, C.-X.; Liu, C.; Cao, Y.-M.;Yan, X.-P. J. C. c., Facile room-temperature solution-phase synthesis of a spherical covalent organic framework for high-resolution chromatographic separation. **2015**, *51 61*, 12254-7.

44. Peng, Y.; Wong, W. K.; Hu, Z.; Cheng, Y.; Yuan, D.; Khan, S. A.;Zhao, D. J. C. o. M., Room Temperature Batch and Continuous Flow Synthesis of Water-Stable Covalent Organic Frameworks (COFs). **2016**, *28*, 5095-5101.

45. Matsumoto, M.; Dasari, R. R.; Ji, W.; Feriante, C. H.; Parker, T. C.; Marder, S. R.;Dichtel, W. R., Rapid, Low Temperature Formation of Imine-Linked Covalent Organic Frameworks Catalyzed by Metal Triflates. *J Am Chem Soc* **2017**, *139*, 4999-5002.

46. Ding, H.; Mal, A.;Wang, C., Tailored covalent organic frameworks by post-synthetic modification. *Mater. Chem. Front.* **2020**, *4*, 113-127.

47. Kolb, H. C.; Finn, M. G.;Sharpless, K. B., Click Chemistry: Diverse Chemical Function from a Few Good Reactions. *Angewandte Chemie (International ed. in English)* **2001**, *40*, 2004-2021.

48. Nagai, A.; Guo, Z.; Feng, X.; Jin, S.; Chen, X.; Ding, X.;Jiang, D., Pore surface engineering in covalent organic frameworks. *Nat Commun* **2011**, *2*, 536.

49. Qian, C.; Qi, Q.-Y.; Jiang, G.-F.; Cui, F.-Z.; Tian, Y.;Zhao, X., Toward Covalent Organic Frameworks Bearing Three Different Kinds of Pores: The Strategy for Construction and COF-to-COF Transformation via Heterogeneous Linker Exchange. *J. Am. Chem. Soc.* **2017**, *139*, 6736-6743.

50. Waller, P. J.; Lyle, S. J.; Osborn Popp, T. M.; Diercks, C. S.; Reimer, J. A.;Yaghi, O. M., Chemical Conversion of Linkages in Covalent Organic Frameworks. *J Am Chem Soc* **2016**, *138*, 15519-15522.

51. Suslick, K. S.; Bhyrappa, P.; Chou, J. H.; Kosal, M. E.; Nakagaki, S.; Smithenry, D. W.;Wilson, S. R., Microporous porphyrin solids. *Acc Chem Res* **2005**, *38*, 283-91.

52. Eder, G. M.; Pyles, D. A.; Wolfson, E. R.;McGrier, P. L., A ruthenium porphyrin-based porous organic polymer for the hydrosilylative reduction of CO2 to formate. *Chemical Communications* **2019**, *55*, 7195-7198.

53. Lin, G.; Ding, H.; Chen, R.; Peng, Z.; Wang, B.;Wang, C., 3D Porphyrin-Based Covalent Organic Frameworks. *J. Am. Chem. Soc.* **2017**, *139*, 8705-8709.

54. Xu, K.; Dai, Y.; Ye, B.;Wang, H., Two dimensional covalent organic framework materials for chemical fixation of carbon dioxide: excellent repeatability and high selectivity. *Dalton Trans.* **2017**, *46*, 10780-10785.

55. Ding, S.-Y.; Gao, J.; Wang, Q.; Zhang, Y.; Song, W.-G.; Su, C.-Y.;Wang, W., Construction of Covalent Organic Framework for Catalysis: Pd/COF-LZU1 in Suzuki–Miyaura Coupling Reaction. *J. Am. Chem. Soc.* **2011**, *133*, 19816-19822.

56. Kandambeth, S.; Mallick, A.; Lukose, B.; Mane, M. V.; Heine, T.;Banerjee, R., Construction of crystalline 2D covalent organic frameworks with remarkable chemical (acid/base) stability via a combined reversible and irreversible route. *J Am Chem Soc* **2012**, *134*, 19524-7.

57. Uribe-Romo, F.; Doonan, C.; Furukawa, H.; Oisaki, K.;Yaghi, O., Crystalline Covalent Organic Frameworks with Hydrazone Linkages. *J. Am. Chem. Soc.* **2011**, *133*, 11478-81.

58. Huang, N.; Wang, P.;Jiang, D., Covalent organic frameworks: a materials platform for structural and functional designs. *Nature Reviews Materials* **2016**, *1*, 16068.

59. Tilford, R. W.; Mugavero, S. J., 3rd; Pellechia, P. J.;Lavigne, J. J., Tailoring microporosity in covalent organic frameworks. *Advanced materials (Deerfield Beach, Fla.)* **2008**, *20*, 2741-6.

60. D'Alessandro, D. M.; Smit, B.;Long, J. R., Carbon dioxide capture: prospects for new materials. *Angewandte Chemie (International ed. in English)* **2010**, *49*, 6058-6082.

61. Doonan, C. J.; Tranchemontagne, D. J.; Glover, T. G.; Hunt, J. R.;Yaghi, O. M., Exceptional ammonia uptake by a covalent organic framework. *Nat Chem* **2010**, *2*, 235-8.

62. Aiyappa, H. B.; Thote, J.; Shinde, D. B.; Banerjee, R.;Kurungot, S., Cobalt-Modified Covalent Organic Framework as a Robust Water Oxidation Electrocatalyst. *Chem Mater* **2016**, *28*, 4375-4379.

63. Sun, Q.; Aguila, B.; Lan, P. C.;Ma, S., Tuning Pore Heterogeneity in Covalent Organic Frameworks for Enhanced Enzyme Accessibility and Resistance against Denaturants. *Advanced Materials* **2019**, *31*, 1900008.

64. Chen, L.;Xu, Q., Metal-Organic Framework Composites for Catalysis. *Matter* **2019**, *1*, 57-89.

65. Blunt, M. O.; Russell, J. C.; Champness, N. R.;Beton, P. H., Templating molecular adsorption using a covalent organic framework. *Chemical Communications* **2010**, *46*, 7157-7159.

66. Nagai, A.; Chen, X.; Feng, X.; Ding, X.; Guo, Z.;Jiang, D., A Squaraine-Linked Mesoporous Covalent Organic Framework. *Angew. Chem. Int. Ed.* **2013**, *52*, 3770-3774.

67. Mu, M.; Wang, Y.; Qin, Y.; Yan, X.; Li, Y.;Chen, L., Two-Dimensional Imine-Linked Covalent Organic Frameworks as a Platform for Selective Oxidation of Olefins. *ACS Appl Mater Interfaces* **2017**, *9*, 22856-22863.

68. Xu, H.; Gao, J.;Jiang, D., Stable, crystalline, porous, covalent organic frameworks as a platform for chiral organocatalysts. *Nat Chem* **2015**, *7*, 905-12.

69. Lu, Q.; Ma, Y.; Li, H.; Guan, X.; Yusran, Y.; Xue, M.; Fang, Q.; Yan, Y.; Qiu, S.;Valtchev, V., Postsynthetic Functionalization of Three-Dimensional Covalent Organic Frameworks for Selective Extraction of Lanthanide Ions. *Angewandte Chemie (International ed. in English)* **2018**, *57*, 6042-6048.

70. Liu, W.; Zhang, L.; Chen, F.; Wang, H.; Wang, Q.;Liang, K., Efficiency and mechanism of adsorption of low-concentration uranium from water by a new chitosan/aluminum sludge composite aerogel. *Dalton Trans.* **2020**, *49*, 3209-3221.

71. Wen, R.; Li, Y.; Zhang, M.; Guo, X.; Li, X.; Li, X.; Han, J.; Hu, S.; Tan, W.; Ma, L.;Li, S., Graphene-synergized 2D covalent organic framework for adsorption: A mutual promotion strategy to achieve stabilization and functionalization simultaneously. *Journal of hazardous materials* **2018**, *358*, 273-285.

72. Liu, X.; Pang, H.; Liu, X.; Li, Q.; Zhang, N.; Mao, L.; Qiu, M.; Hu, B.; Yang, H.;Wang, X., Orderly Porous Covalent Organic Frameworks-based Materials: Superior Adsorbents for Pollutants Removal from Aqueous Solutions. *The Innovation* **2021**, *2*, 100076.

73. Ding, S.-Y.; Dong, M.; Wang, Y.-W.; Chen, Y.-T.; Wang, H.-Z.; Su, C.-Y.;Wang, W., Thioether-Based Fluorescent Covalent Organic Framework for Selective Detection and Facile Removal of Mercury(II). *J. Am. Chem. Soc.* **2016**, *138*, 3031-3037.

74. Gupta, V. K.; Kumar, R.; Nayak, A.; Saleh, T. A.;Barakat, M. A., Adsorptive removal of dyes from aqueous solution onto carbon nanotubes: a review. *Advances in colloid and interface science* **2013**, *193-194*, 24-34.

75. Yagub, M. T.; Sen, T. K.; Afroze, S.;Ang, H. M., Dye and its removal from aqueous solution by adsorption: a review. *Advances in colloid and interface science* **2014**, *209*, 172-84.

76. Rafatullah, M.; Sulaiman, O.; Hashim, R.;Ahmad, A., Adsorption of methylene blue on low-cost adsorbents: A review. *Journal of hazardous materials* **2010**, *177*, 70-80.

77. Huo, J.; Luo, B.;Chen, Y., Crystalline Covalent Organic Frameworks from Triazine Nodes as Porous Adsorbents for Dye Pollutants. *ACS Omega* **2019**, *4*, 22504-22513.

78. Sharma, R. K.; Yadav, P.; Yadav, M.; Gupta, R.; Rana, P.; Srivastava, A.; Zbořil, R.; Varma, R. S.; Antonietti, M.;Gawande, M. B., Recent development of covalent organic frameworks (COFs): synthesis and catalytic (organic-electro-photo) applications. *Materials Horizons* **2020**, *7*, 411-454.

79. Raval, N. P.; Shah, P. U.;Shah, N. K., Adsorptive amputation of hazardous azo dye Congo red from wastewater: a critical review. *Environ Sci Pollut R* **2016**, *23*, 14810-14853.

80. Yue, J.-Y.; Wang, L.; Ma, Y.; Yang, P.; Zhang, Y.-Q.; Jiang, Y.;Tang, B., Metal ion-assisted carboxyl-containing covalent organic frameworks for the efficient removal of Congo red. *Dalton Trans.* **2019**, *48*, 17763-17769.

81. Zhao, F.; Liu, H.; Mathe, S. D. R.; Dong, A.;Zhang, J., Covalent Organic Frameworks: From Materials Design to Biomedical Application. *Nanomaterials (Basel)* **2017**, *8*, 15.

82. Mitra, S.; Sasmal, H. S.; Kundu, T.; Kandambeth, S.; Illath, K.; Díaz Díaz, D.;Banerjee, R., Targeted Drug Delivery in Covalent Organic Nanosheets (CONs) via Sequential Postsynthetic Modification. *J. Am. Chem. Soc.* **2017**, *139*, 4513-4520.

Chapter 2. A Pt(II) Decorated Covalent Organic Framework for Photocatalytic Difluoroalkylation and Oxidative Cyclization Reactions

This chapter is from the following publication:

Z. Almansaf, J. Hu, F. Zanca, H. R. Shahsavari, B. Kampmeyer, M. Tsuji, K. Maity, V. Lomonte, Y. Ha, P. Mastrorilli, S. Todisco, M. Benamara, R. Oktavian, A. Mirjafari, P. Z. Moghadam, A. R. Khosropour, and H. Beyzavi "Pt(II)-Decorated Covalent Organic Framework for Photocatalytic Difluoroalkylation and Oxidative Cyclization Reactions" *ACS Applied Materials & Interfaces* **2021**, *13*, 6349–6358.

Modifications have been made to the original document to adapt the content to this dissertation.

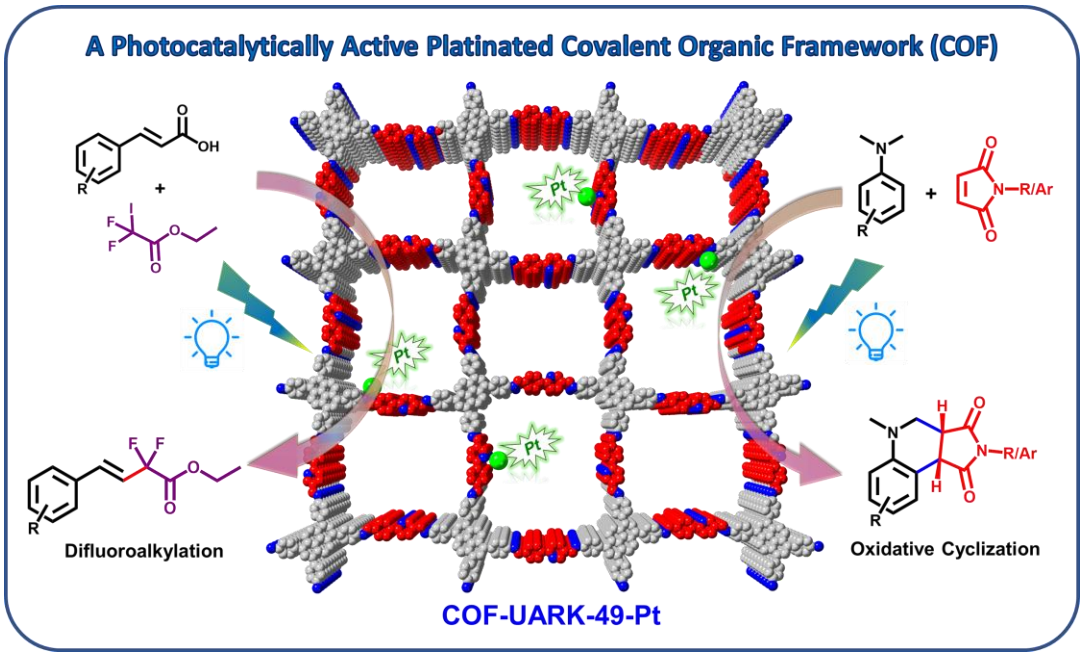

2.1. Abstract

A new covalent organic framework (COF) based on imine bonds was assembled from 2-(4-formylphenyl)-5-formylpyridine and 1,3,6,8-tetrakis(4-aminophenyl)pyrene, which showed an interesting dual-pore structure with high crystallinity. Postmetallation of the COF with Pt occurred selectively at the N donor (imine and pyridyl) in the larger pores. The metallated COF served as an excellent recyclable heterogeneous photocatalyst for decarboxylative difluoroalkylation and oxidative cyclization reactions.

2.2. Introduction

As a green synthetic route to value-added chemicals, visible light promoted organic transformations have attracted significant attention in the past years.[1-3] One of the important research topics is to develop new photocatalysts that are both highly active and stable. Heterogeneous visible light photocatalysts are particularly promising for industrial applications because of the great recyclability compared to homogeneous ones.[4] Covalent organic frameworks (COFs), an emerging class of crystalline porous polymer material, are found to be an excellent photocatalyst candidate group.[5-8] Firstly, the extended, conjugated framework of COFs provides strong absorption in the visible range. Secondly, the ordered porous structure could facilitate mass, energy, electron, and hole transfer which are critical for photocatalysis. Thirdly, the structure and function of COFs can be tailored in a controllable manner using predesigned molecular linkers enabled by reticular chemistry. These structural features make COFs more promising than inorganic semiconductors.[9-12] The superior photocatalytic performance of COFs has been demonstrated in hydrogen evolution,[13-15] CO_2 reduction,[16-22] and organic transformations.[23-27]

To improve the photocatalytic efficiency of COF photocatalysts, the engineering of the COF structure has identified some critical factors such as chemical linkage,[28-31] built in donor−acceptor

moieties,[16, 32, 33] electronic structure of linkers[13, 34], and so on. Alternatively, doping transition metal atoms into the framework can efficiently modify the photophysical properties of COFs. The *d* orbitals of transition metals offer additional charge transfer process such as ligand-to-metal charge transfer (LMCT) thus further broadening the visible light absorbance of the resulting COFs. Moreover, metal atoms are also able to facilitate electron charge transfer and inhibit electron and hole recombination.[26, 35-37]

In this work, we introduced 2-(4-formylphenyl)-5-formylpyridine (**L2**) as a COF linker for the first time, complementary to commonly used 2,2'-bipyridine[38-41], porphyrin[42-46], salen,[47-50] and catechol,[51-53] to bind metals. Phenylpyridine derivatives have versatile metal binding modes such as simple pyridine coordination and cyclometallation, which could be an ideal platform to expand the coordination chemistry of COFs. A new stable imine COF was then constructed with 1,3,6,8-tetrakis(4-aminophenyl)pyrene (**L1**) as the amine linker (COF-UARK-49). Post-metalation with platinum leaded to COF-UARK-49-Pt, which displayed excellent photocatalytic performance towards decarboxylative difluoroalkylation and oxidative cyclization reaction.

2.3. Results and Discussions

Synthesis and Characterization. COF-UARK-49 was synthesized *via* imine condensation of **L1** and **L2** in a mixture solvent of 1,4-dioxane/mesitylene/3M AcOH (1/1/0.2, v/v) at 120 ^{o}C for 3 days (**Scheme 2.1**, see Supporting Information for details). The successful formation of the imine linkage was confirmed by FT-IR spectroscopy and cross-polarization magic-angle-spinning (CP/MAS) solid-state ^{13}C NMR spectroscopy. The IR spectrum of COF-UARK-49 showed the presence of C=N stretching vibrations at 1622 cm^{-1} and the absence of characteristic N–H stretching vibration at 3323cm^{-1} and C=O stretching vibration of at 1738 cm^{-1} of the two linkers respectively (**Figure 2.5**). The solid state ^{13}C NMR spectra showed the characteristic signal for the

imine carbon at 164 ppm (**Figure 2.6**). The crystallinity of COF-UARK-49 was investigated by powder X-ray diffraction (PXRD). As shown in Figure 1A, COF-UARK-49 exhibited strong diffraction peaks at 2θ = 3.18, 4.90, 6.36, 7.90, and 9.76°, respectively.

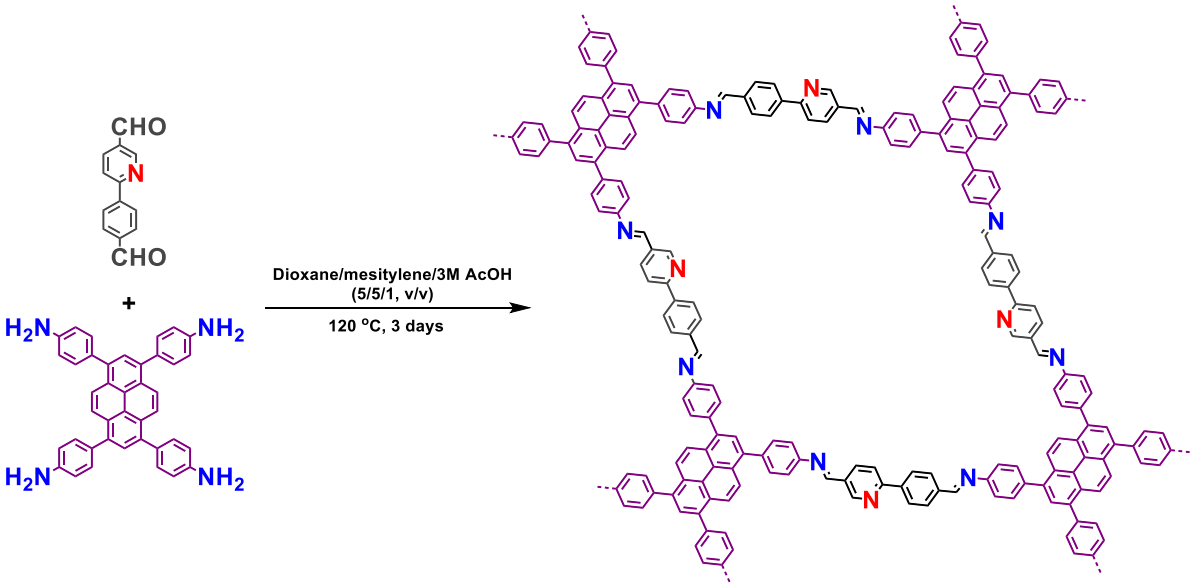

Scheme 2. 1. Synthesis of COF-UARK-49 via imine condensation.

To understand the structure of COF-UARK-49, eclipsed and staggered stacking structures which are commonly observed for 2D COFs were modelled in Materials Studio. The eclipsed structure resulted in good consistency with the experimental PXRD patterns (**Figure 2.1A**). The interlayer distance deduced from 001 diffraction peak at 2θ = 24° of 3.7 Å is also consistent with the simulated value of 3.8 Å. Interestingly, the simulated AA stacking structure of COF-UARK-49 has two kinds of concave and convex square pores as a result of *cis* orientation of the adjacent imine linkage.

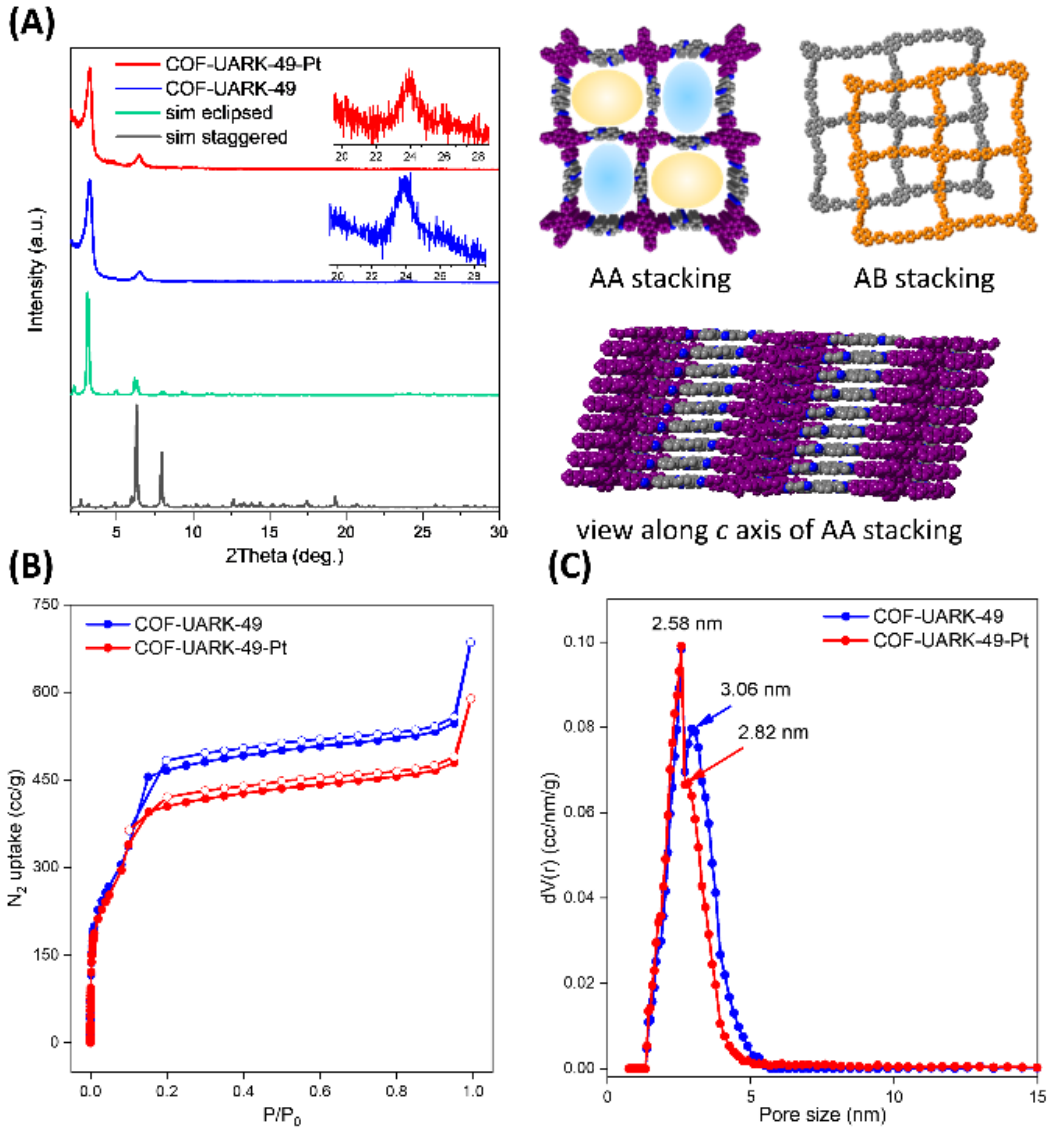

Figure 2. 1. (A) PXRD pattern of COF-UARK-49-Pt (red line), COF-UARK-49 (blue line), with the simulated patterns for eclipsed (green line) and staggered (gray line) stacking; (B) N_2 isotherms at 77K; and (C) Pore size distribution.

The dual-pore structure of COF-UARK-49 was clearly evidenced by nitrogen adsorption−desorption experiment. As shown in Figure 1B, COF-UARK-49 showed a type IV isotherm, featuring a sharp uptake below P/P_0 = 0.01 and a step between P/P_0 = 0.10−0.20, indicating sequential pore filling of two types of pores. Nonlocal density functional theory (NLDFT) calculation revealed two narrow pore size distributions at 2.58 nm and 3.06 nm,

respectively, assigned to the concave and convex square micropores, respectively (**Figure 2.1C**). We also performed grand canonical Monte Carlo (GCMC) simulations of N_2 adsorption in COF-UARK-49 (**Figure 2.1B and C**). The simulated isotherm overpredict N_2 uptake specifically in $P/P_0 > 0.1$. This effect could be due to the fact that adsorption simulations are performed on pristine crystal structure whereas in experiments structural defects, pore blockage and/or residual solvents may be present and affect adsorption properties. Importantly, the simulation accurately predicts the position of the isotherm steps at ca. $P/P_0 = 0.01$ and 0.1—indicating sequential pore filling of two types of pores. To further explore this effect, we took a few simulation snapshots from the positioning of N_2 molecules inside the pores at different pressures (**Figure 2.2**). The snapshots reveal local ordering of N_2 molecules in the corner of the small pores prior to formation of monolayer within the framework and ultimately pore filling at saturation loadings. The Brunauer−Emmett−Teller (BET) surface area and the total pore volume of COF-UARK-49 were derived to be 1430 $m^2\ g^{-1}$ and 0.897 $cm^3\ g^{-1}$, respectively. It should be noted that, the isoreticular COF built from 4,4'-biphenyldicarboxaldehyde (Py-2P COF)[54] or 2,2'-bipyridine-5,5'-dicarbaldehyde (Py-2,2'-BPyPh COF)[51] only has one type of pore at around 2.8 nm. The subtle change of the linker structure could be a potential alternative strategy to heteropore COFs[55-57]. Besides, unlike Py-2P COF that quickly lost its crystallinity upon activation due to the disrupted synchronized offset stacking by the twisted biphenyl,[54] COF-UARK-49 is highly stable because of the less twisted nature of 2-phenylpyridine motif compared to biphenyl. Thermogravimetric analysis (TGA) under N_2 proved COF-UARK-49 to be thermally stable up to 480 ºC (**Figure 2.7**).

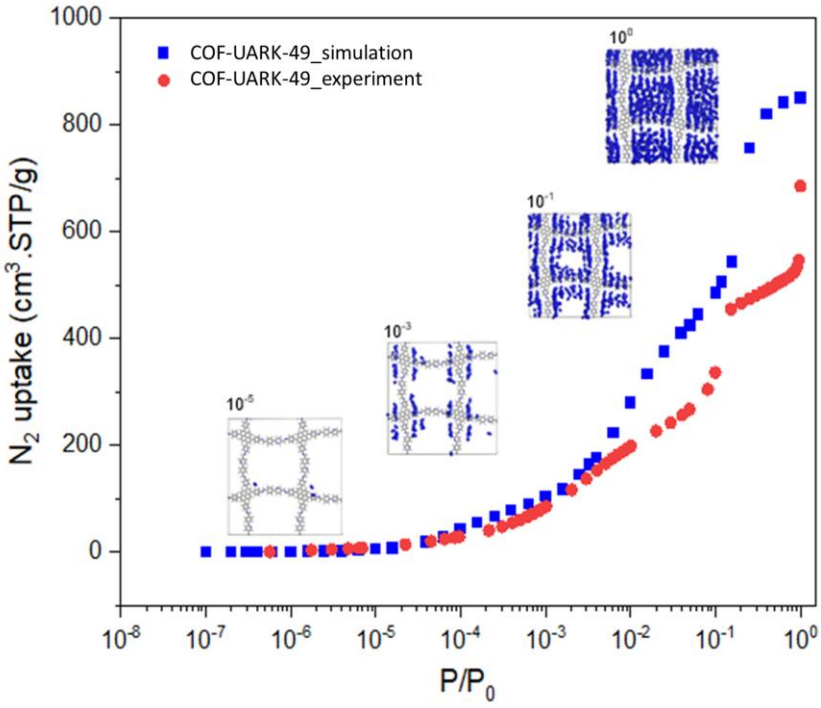

Figure 2. 2. Comparison of experimental and simulated N_2 uptake for COF-UARK-49. N_2 favorable adsorption sites at different pressures are shown in the inset. Blue spheres represent N_2 molecules. Framework atoms are shown in ball and stick representation.

2-phenylpyridine derivatives are attractive ligands for transition metals such as Ir and Pt. In particular, Pt(II) complexes are promising photocatalytic centers for both energy transfer and electron transfer process.[58, 59] We therefore firstly explored the Pt binding ability of COF-UARK-49. The platination was conducted by heating *cis*-[$PtCl_2(DMSO)_2$] and COF-UARK-49 in toluene at 50 °C overnight. The obtained COF-UARK-49-Pt showed identical PXRD pattern to that of COF-UARK-49, suggesting the preservation of crystallinity (**Figure 2.1A**). The BET surface area and total pore volume was slightly reduced to 1320 $m^2\ g^{-1}$ and 0.774 $cm^3\ g^{-1}$ respectively (**Figure 2.1B**). The Pt loading was determined to be 9.1% Pt by inductively coupled plasma mass spectrometry (ICP-MS) analysis. Due to the rich metal binding site of COF-UARK-49, various Pt coordinating modes are possible (**Scheme 2.2**). To understand the coordination environment of Pt

inside the framework, we performed both experimental and computational studies. First of all, EDX analysis revealed the relative ratio of Pt/Cl/S was close to 1/2/1 (**Figure 2.8**), thus excluding the cyclometallation modes (**Scheme 2.2C and 2.2D**) and the chelating binding modes by two nitrogen donors from adjacent COF layers (**Scheme 2.2E and 2.2F**) that have been observed for Pd(II)[60]. Thus, only one N donor from the COF (imine or pyridyl N) contributes to the Pt complexation. XPS analysis of the N 1s binding energy revealed that three sub peaks at 397.2, 398.0, 399.2 eV fitted best for COF-UARK-49-Pt, which are assigned to free imine, free pyridyl and Pt coordinated N respectively (**Figures 2.3 and 2.9**). Our attempts to study the potential competing binding by imine and pyridine nitrogen to Pt of a model compound resulted in ligand decomposition to unidentified products. We therefore used the isoreticular COF constructed from 4,4'-biphenyldicarbaldehyde, Py-2P, that only has imine nitrogen for comparison.[39, 54] Platination of Py-2P COF resulted in a Pt loading of 12.5% as determined by ICP-MS for Py-2P-Pt. Py-2P-Pt COF displayed two sub peaks in the N 1s XPS spectrum at binding energy of 398.0 eV for free imine N and 399.0 eV for Pt bonded N respectively (**Figure 2.10**). The complex $PtCl_2$(pyridine)(DMSO) showed the N 1s binding energy at 399.0 eV (**Figure 2.11**). Therefore, it is not conclusive for the Pt coordination environment clarification with XPS analysis. Moreover, DFT calculations showed that the Gibbs free energy difference of the two structures in **Scheme 2.2A and B** was less than 1 kcal/mol (**Table 2.2**). We thus believe that both coordination modes of **Scheme 2.2A and B** could be present in COF-UARK-49-Pt.

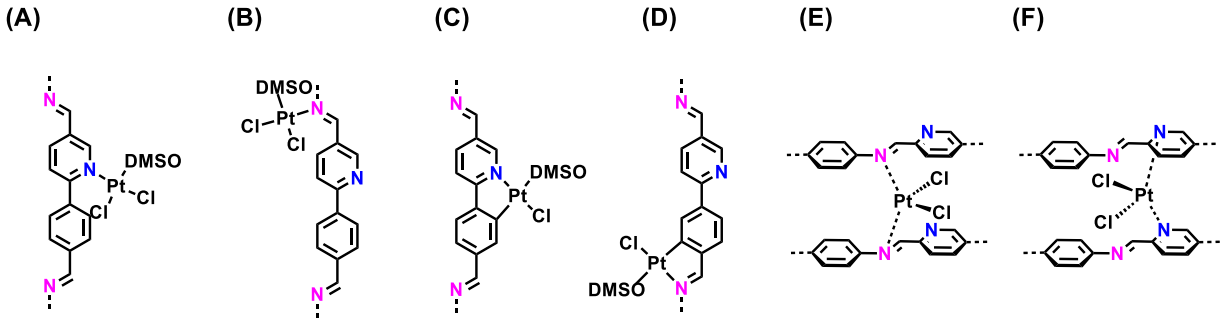

Scheme 2. 2. (A−F) Possible coordination modes of Pt in COF-UARK-49-Pt (isomers are not shown).

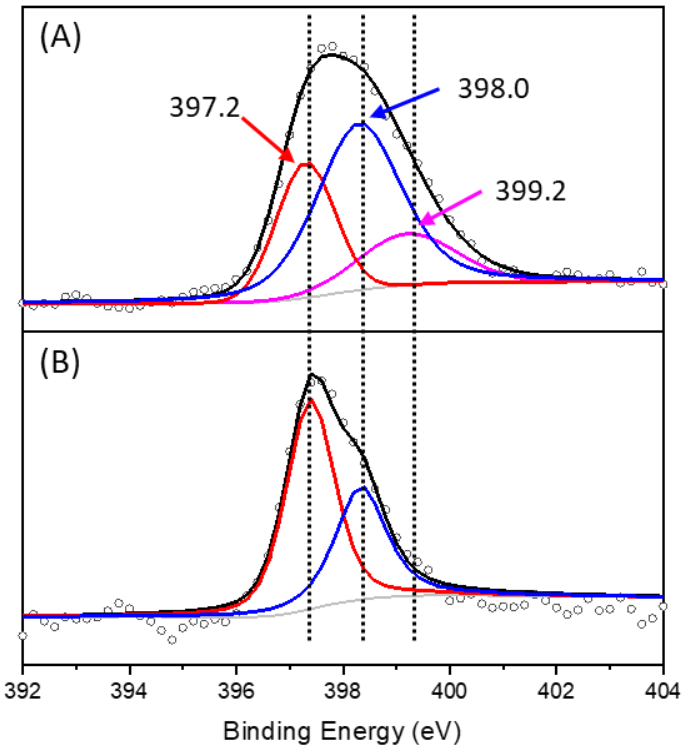

Figure 2. 3. XPS spectra of the N1s binding energy of (A) COF-UARK-49-Pt, (B) COF-UARK-49.

Pore size distribution analysis from the nitrogen isotherm revealed a pore size decrease to 2.82 nm and less population of the larger pore compared to COF-UARK-49 while leaving the small concave pore intact (Figure 2.1C). This indicates that the platination took place exclusively at the convex

pores. Based on the Pt loading amount, it is deduced that each of the convex pores is metalated with one platinum. It is also consistent with the experiment finding that using excess platinum precursor did not give higher platinum incorporation. Similar N_2 adsorption behavior was observed for COF-UARK-49-Pt. The morphology of COF-UARK-49 and COF-UARK-49-Pt was studied by scanning electron microscopy (SEM). Both COFs displayed uniform cubic-like morphology (**Figure 2.12**).

COF-UARK-49-Pt as a Photocatalyst for Organic Transformations. Pyrene based COFs have shown intriguing photophysical properties that can be used for sensing and photocatalysis. The solid-state UV-vis diffuse reflectance spectrum showed that COF-UARK-49 has a broad absorption between 200–600 nm because of increased conjugation compared to the two linkers (**Figure 2.4**). Pt incorporation further expands the absorption band to *ca*. 700 nm, covering the whole visible spectrum range, making it an excellent system for visible-light harvesting. The band gap was calculated to be 2.24 and 2.00 eV for COF-UARK-49 and COF-UARK-49-Pt respectively from the UV-vis spectra *via* the Tauc plot (**Figures 2.14**), demonstrating the key role of Pt in tuning the band gap. In addition, Pt(II) complexes with vacant axial coordination sites could provide great opportunities for both outer sphere and inner sphere interactions with substrates. We therefore set to investigate the photocatalytic activity of COF-UARK-49-Pt for the decarboxylative difluoroalkylation and oxidative cyclization reactions, both of which are believed to occur *via* electron transfer pathways.[61-64]

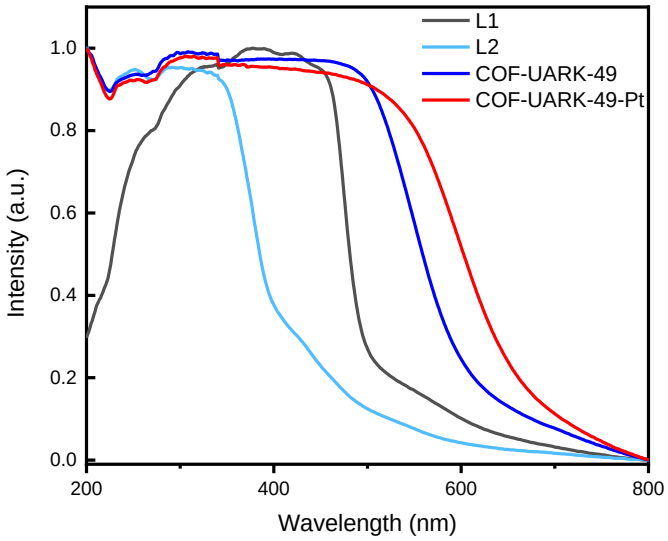

Figure 2. 4. Solid-state UV-vis absorption spectra of two linkers, COF-UARK-49 and COF-UARK-49-Pt.

Gem-difluoromethylene group is a valuable fluorinated motif widely present in pharmaceuticals and biologically active compounds, *e.g.* Maraviroc (HIV-1 therapeutic agent), Tafluprost (ocular hypertension drug), and Gemcitabine (chemotherapy drug).[65-68] However, using COFs as a (photo)catalyst for fluorination reactions remains to be explored.[69, 70] We utilized COF-UARK-49-Pt to catalyze the decarboxylative difluoroalkylation reaction, which was found to be an efficient method of synthesizing fluorinated compounds. First, we optimized the reaction conditions (**Table 2.1**). We found that under the optimized reaction conditions, the model reaction between **1a** and **2** proceeded smoothly to give **3a** in 64% yield in the presence of COF-UARK-49-Pt, illuminated with a blue LED light (**Table 2.1, entry 2**). Control reactions disclosed that both light and photocatalyst were crucial to the reaction efficiency (**Table 2.1, entries 1 and 4**). Under similar conditions, COF-UARK-49 gave a much lower yield of 23%, indicating important role of Pt in the framework (**Table 2.1, entry 3**). The COF catalyst are recyclable for at least five runs without

compromising the efficiency (**Figure 2.15**). A wide range of cinnamic acids were readily converted to the corresponding *E*-difluoroacetyl alkenes in good to excellent yields with high *E*/*Z* selectivity using COF-UARK-49-Pt as a photocatalyst (**Scheme 2.3**). Cinnamic acids bearing both electron-donating (**3d**, **3e**) and -withdrawing (**3g**-**3c**) substituents on the aromatic rings gave good to excellent yield. Halogen substitutions such as fluoro (**3g**) or chloro (**3b**) on the aromatic ring were tolerated without undesired dehalogenation. Nitro substitutions (**3c**) also remained intact during the reaction. The scope of the presented procedure also includes carbocyclic (**3a** and **3f**) and heterocyclic (**3h**) difluorinated systems.

Table 2. 1. Optimization of the reaction conditions for the photo-induced decarboxylation-difluoroalkylation.[a]

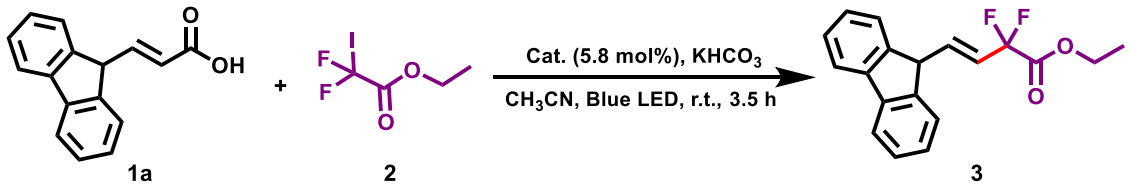

Entry	Cat.	Yield (%)
1	None	<2
2	COF-UARK-49-Pt	64
3	COF-UARK-49	23
4[b]	COF-UARK-49-Pt	0
5	$PtCl_2$(DMSO)(pyridine)	7

[a] **1a** (0.04 mmol), **2** (0.044 mmol), $KHCO_3$ (0.044 mmol), CH_3CN (1 ml) in the presence of 5 mg (5.8 mol% based on Pt) catalyst. Yields were determined by HPLC. [b] In dark.

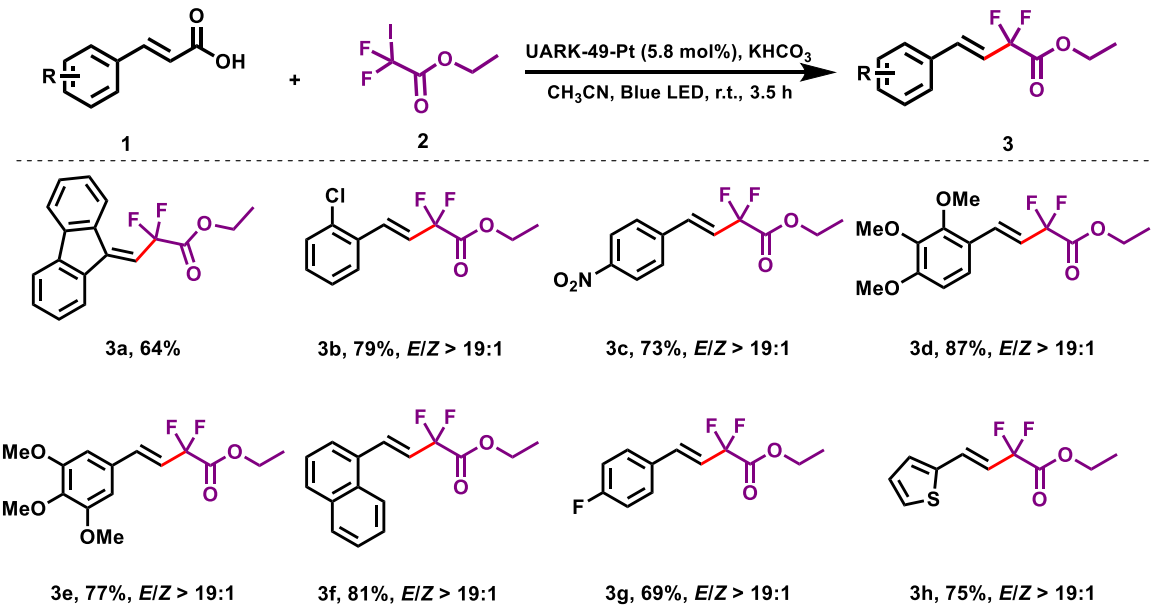

Scheme 2. 3. Substrate scope of decarboxylation-difluoroalkylation.

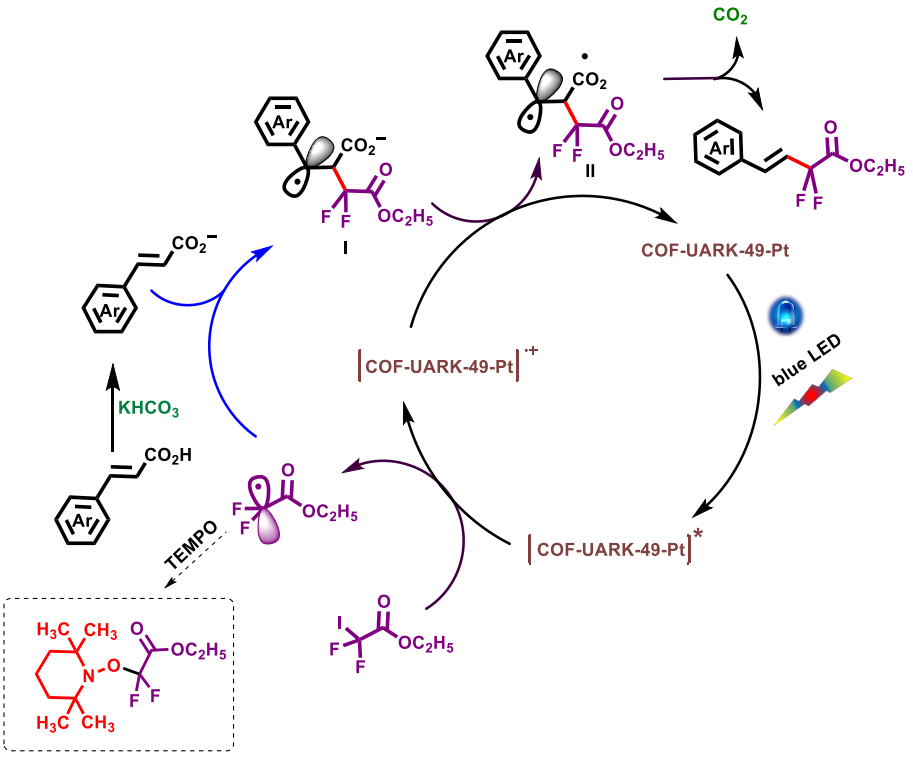

Scheme 2. 4. Proposed mechanism for the decarboxylation-difluoroalkylation reaction.

A plausible mechanism for this transformation is depicted in **Scheme 2.4** according to the literature.[61] Upon COF-UARK-49-Pt light excitation, a single electron transfer (SET) reduction of R_F-I by excited [COF-UARK-49-Pt]* generates one electron-oxidized species [COF-UARK-49-Pt]$^+$ and radical $^{\bullet}R_F$ which reacts with the deprotonated α,β-vinyl carboxylate to generate **I** as a benzylic radical species. Its subsequent oxidation by [COF-UARK-49-Pt]$^+$ generates carboxyl radical intermediate **II** which furnishes the desired product with high *E* selectivity *via* decarboxylation. The generation of $^{\bullet}R_F$ radical during the reaction was demonstrated in a trapping experiment. In the presence of TEMPO as a radical inhibitor, no difluoroacetyl alkenes product was obtained, and TEMPO-trapped difluoroacetyl product was observed instead (**Figure 2.16**).

Motivated by the successful decarboxylation-difluoroalkylation, we extended our investigation on the photo-oxidative cyclization reaction using COF-UARK-49-Pt (**Scheme 2.5**). After optimization of the reaction conditions, we were pleased to find that COF-UARK-49-Pt readily catalyzed the reaction, giving **6a** in 66% yield (**Table 2.3**). Likewise, a series of control experiments proved that COF-UARK-49-Pt was superior to COF-UARK-49, emphasizing the importance of Pt within the COF (**Table 2.3**). The involvement of O_2 in the reaction was confirmed by the low yield (7%, **Table 2.3**) when the reaction was carried out under N_2 atmosphere. As illustrated in **Scheme 2.5**, substrates with electron withdrawing groups, *i.e.*, –F (**4b**), –Br (**4c** and **4d)** are compatible with this method and the desired products were obtained in good to excellent yields (66–85%). It is worth noting that 3-fluoro-*N*,*N*-dimthylaniline provides two isomers with almost equal ratio (**Scheme 2.5, 6b**). 1-*N*,*N*-dimethylaminonaphthalene produced the corresponding product in an excellent yield (82%, **6e**). On the other hand, by using *N*-methylmaleimide instead of *N*-phenylmaleimide, the desired products were obtained in 78% and 85% (**6f** and **6g**), respectively. The recyclability of COF-UARK-49-Pt was also evaluated for

oxidative cyclization reaction. The COF catalyst can be reused for at least ten runs without any notable loss of its catalytic performance (**Figures 2.17and 2.18**).

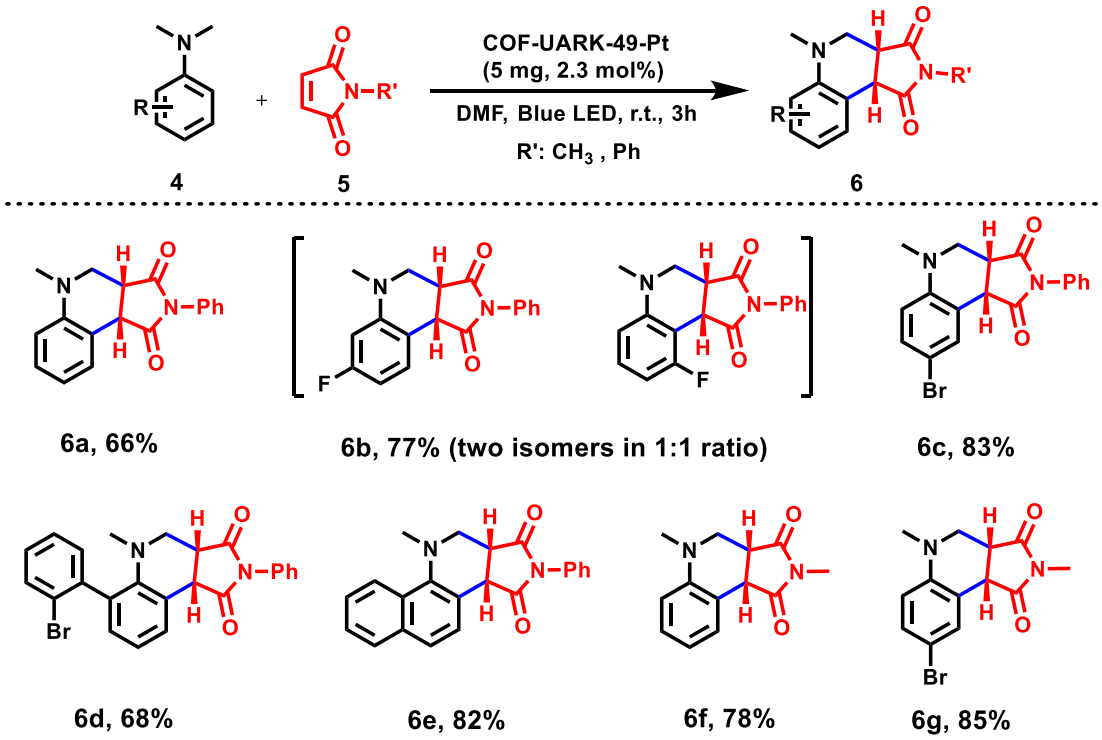

[a] A mixture of **4** (0.2 mmol) and **5** (0.1 mmol) in 1 mL DMF were illuminated with a blue LED light for 3 h in the presence of 5 mg (2.3 mol% based on Pt) of the catalyst. Yields were determined by HPLC.

Scheme 2. 5. Photo-induced oxidative cyclization reaction catalyzed by COF-UARK-49-Pt.[a]

Based on literature reports,[62-64] a plausible mechanism for the photo-induced oxidative cyclization is shown in **Scheme 2.6**. An SET from I to [COF-UARK-49-Pt]*generates the amine radical cation II, while [COF-UARK-49-Pt]* is reduced to the [COF-UARK-49-Pt]$^{-}$. In the presence of oxygen, the photoredox catalytic cycle of COF-UARK-49-Pt is finished via an SET oxidation, with the production of a superoxide radical anion $O_2^{\bullet-}$. Deprotonation of II generates α-aminoalkyl radical III. Then III reacts with IV to generate radical V, and the latter then undergoes cyclization to form intermediate VI. Proton and electron transfer from VI to $O_2^{\bullet-}$ yields the final product VII and

HOO^-. The HOO^- will be subsequently protonated to yield H_2O_2 as the by-product. The significant inhibition of the reaction in the presence of KI as a hole scavenger, $AgNO_3$ as an electron scavenger and 1,4-benzoquinone as a $O_2^{\bullet-}$ radical scavenger supports the proposed mechanism (**Table 2.3**).

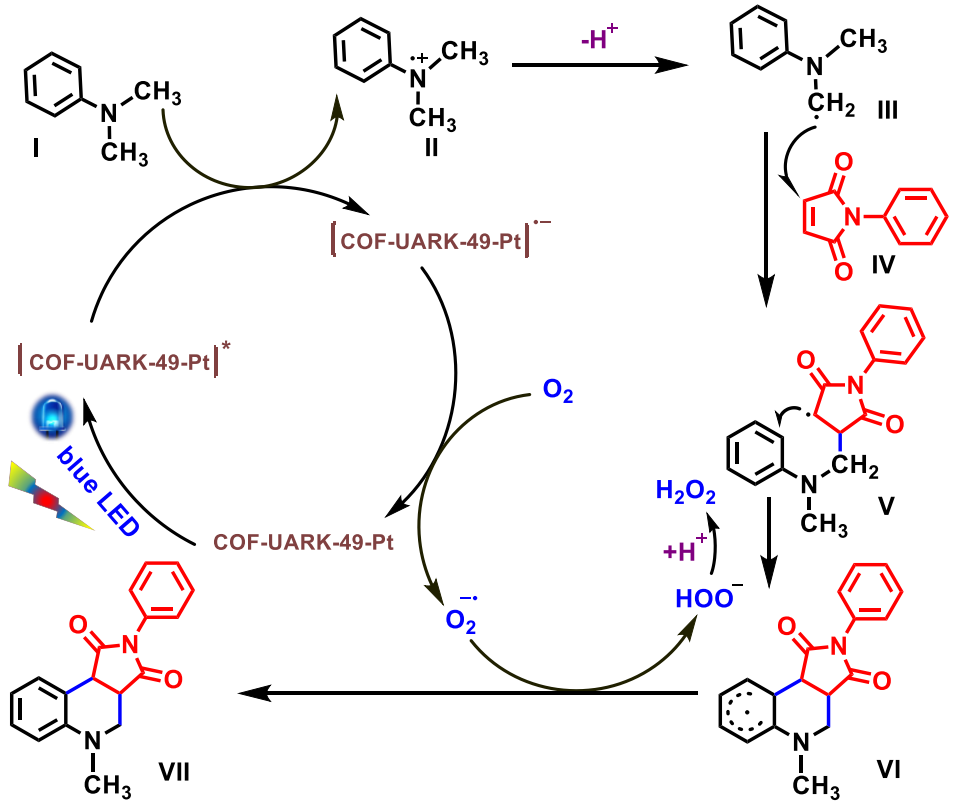

Scheme 2. 6. Proposed mechanism for the photo oxidative cyclization reaction.

2.4. Conclusion

In summary, we reported here a pyrene-based imine COF with the incorporation of 2-phenylpyridine as a new metal binding group on the pore wall. The COF-UARK-49 adopted an unprecedented hetero-pore structure that results from the cis orientation of the C=N linkages. It also showed selective metalation (Pt) of the larger pores and enhanced photocatalytic performance in decarboxylative difluoroalkylation and oxidative cyclization reactions after Pt loading. Although imine and pyridyl *N* had similar stabilization effect for Pt in this work, the well-known

cyclometallation chemistry of 2-phenylpyridine derivatives could introduce interesting metallacycles decorated COFs if other metals are used (e.g. Ir).

2.5. References

1. Marzo, L.; Pagire, S. K.; Reiser, O.;König, B., Visible-Light Photocatalysis: Does It Make a Difference in Organic Synthesis? *Angew. Chem. Int. Ed.* **2018**, *57*, 10034-10072.

2. Schultz, D. M.;Yoon, T. P., Solar Synthesis: Prospects in Visible Light Photocatalysis. *Science* **2014**, *343*, 1239176.

3. Yoon, T. P.; Ischay, M. A.;Du, J., Visible Light Photocatalysis as a Greener Approach to Photochemical Synthesis. *Nat. Chem.* **2010**, *2*, 527-532.

4. Lang, X.; Chen, X.;Zhao, J., Heterogeneous Visible Light Photocatalysis for Selective Organic Transformations. *Chem. Soc. Rev.* **2014**, *43*, 473-486.

5. Geng, K.; He, T.; Liu, R.; Tan, K. T.; Li, Z.; Tao, S.; Gong, Y.; Jiang, Q.;Jiang, D., Covalent Organic Frameworks: Design, Synthesis, and Functions. *Chem. Rev.* **2020**, *120*, 8814–8933.

6. Lohse, M. S.;Bein, T., Covalent Organic Frameworks: Structures, Synthesis, and Applications. *Adv. Funct. Mater.* **2018**, *28*, 1705553.

7. Diercks, C. S.;Yaghi, O. M., The Atom, the Molecule, and the Covalent Organic Framework. *Science* **2017**, *355*, eaal1585.

8. Tao, S.;Jiang, D., Covalent Organic Frameworks for Energy Conversions: Current Status, Challenges, and Perspectives. *CCS Chem.* **2020**, *2*, 2003–2024.

9. Li, X.; Zhang, J.; Huo, Y.; Dai, K.; Li, S.;Chen, S., Two-Dimensional Sulfur- and Chlorine-Codoped g-C_3N_4/CdSe-Amine Heterostructures Nanocomposite with Effective Interfacial Charge Transfer and Mechanism Insight. *Appl. Catal. B Environ.* **2021**, *280*, 119452.

10. Huo, Y.; Zhang, J.; Dai, K.; Li, Q.; Lv, J.; Zhu, G.;Liang, C., All-Solid-State Artificial Z-Scheme Porous g-C3N4/Sn2S3-DETA Heterostructure Photocatalyst with Enhanced Performance in Photocatalytic CO_2 Reduction. *Appl. Catal. B Environ.* **2019**, *241*, 528-538.

11. Lv, J.; Zhang, J.; Liu, J.; Li, Z.; Dai, K.;Liang, C., Bi SPR-Promoted Z-Scheme Bi2MoO6/CdS-Diethylenetriamine Composite with Effectively Enhanced Visible Light Photocatalytic Hydrogen Evolution Activity and Stability. *ACS Sustain. Chem. Eng.* **2018**, *6*, 696-706.

12. Asahi, R.; Morikawa, T.; Irie, H.;Ohwaki, T., Nitrogen-Doped Titanium Dioxide as Visible-Light-Sensitive Photocatalyst: Designs, Developments, and Prospects. *Chem. Rev.* **2014**, *114*, 9824-9852.

13. Vyas, V. S.; Haase, F.; Stegbauer, L.; Savasci, G.; Podjaski, F.; Ochsenfeld, C.;Lotsch, B. V., A Tunable Azine Covalent Organic Framework Platform for Visible Light-Induced Hydrogen Generation. *Nat. Commun.* **2015**, *6*, 8508.

14. Wang, X.; Chen, L.; Chong, S. Y.; Little, M. A.; Wu, Y.; Zhu, W.-H.; Clowes, R.; Yan, Y.; Zwijnenburg, M. A.; Sprick, R. S.;Cooper, A. I., Sulfone-Containing Covalent Organic Frameworks for Photocatalytic Hydrogen Evolution from Water. *Nat. Chem.* **2018**, *10*, 1180-1189.

15. Stegbauer, L.; Schwinghammer, K.;Lotsch, B. V., A Hydrazone-Based Covalent Organic Framework for Photocatalytic Hydrogen Production. *Chem. Sci.* **2014**, *5*, 2789-2793.

16. Jin, E.; Lan, Z.; Jiang, Q.; Geng, K.; Li, G.; Wang, X.;Jiang, D., 2D sp^2 Carbon-Conjugated Covalent Organic Frameworks for Photocatalytic Hydrogen Production from Water. *Chem* **2019**, *5*, 1632-1647.

17. Yang, S.; Hu, W.; Zhang, X.; He, P.; Pattengale, B.; Liu, C.; Cendejas, M.; Hermans, I.; Zhang, X.;Zhang, J., 2D Covalent Organic Frameworks as Intrinsic Photocatalysts for Visible Light-Driven CO_2 Reduction. *J. Am. Chem. Soc.* **2018**, *140*, 14614-14618.

18. Popov, D. A.; Luna, J. M.; Orchanian, N. M.; Haiges, R.; Downes, C. A.;Marinescu, S. C., A 2,2′-Bipyridine-Containing Covalent Organic Framework Bearing Rhenium(I) Tricarbonyl Moieties for CO_2 Reduction. *Dalton Trans.* **2018**, *47*, 17450-17460.

19. Deng, X.; Qin, Y.; Hao, M.;Li, Z., MOF-253-Supported Ru Complex for Photocatalytic CO_2 Reduction by Coupling with Semidehydrogenation of 1,2,3,4-Tetrahydroisoquinoline (THIQ). *Inorg. Chem.* **2019**, *58*, 16574-16580.

20. Deng, X.; Albero, J.; Xu, L.; García, H.;Li, Z., Construction of a Stable Ru–Re Hybrid System Based on Multifunctional MOF-253 for Efficient Photocatalytic CO_2 Reduction. *Inorg. Chem.* **2018**, *57*, 8276-8286.

21. Sun, D.; Gao, Y.; Fu, J.; Zeng, X.; Chen, Z.;Li, Z., Construction of a Supported Ru Complex on Bifunctional MOF-253 for Photocatalytic CO_2 Reduction under Visible Light. *Chem. Commun.* **2015**, *51*, 2645-2648.

22. Zhou, T.; Du, Y.; Borgna, A.; Hong, J.; Wang, Y.; Han, J.; Zhang, W.;Xu, R., Post-Synthesis Modification of a Metal–Organic Framework to Construct a Bifunctional Photocatalyst for Hydrogen Production. *Energy Environ. Sci.* **2013**, *6*, 3229-3234.

23. Zhang, T.; Xing, G.; Chen, W.;Chen, L., Porous organic polymers: a promising platform for efficient photocatalysis. *Mater. Chem. Front.* **2020**, *4*, 332-353.

24. Wang, G.-B.; Li, S.; Yan, C.-X.; Zhu, F.-C.; Lin, Q.-Q.; Xie, K.-H.; Geng, Y.;Dong, Y.-B., Covalent Organic Frameworks: Emerging High-Performance Platforms for Efficient Photocatalytic Applications. *J. Mater. Chem. A* **2020**, *8*, 6957-6983.

25. Guo, L. P.;Jin, S. B., Stable Covalent Organic Frameworks for Photochemical Applications. *ChemPhotoChem* **2019**, *3*, 973-983.

26. Wang, H.; Wang, H.; Wang, Z.; Tang, L.; Zeng, G.; Xu, P.; Chen, M.; Xiong, T.; Zhou, C.; Li, X.; Huang, D.; Zhu, Y.; Wang, Z.;Tang, J., Covalent Organic Framework Photocatalysts: Structures and Applications. *Chem. Soc. Rev.* **2020**, *49*, 4135-4165.

27. Yang, Q.; Luo, M.; Liu, K.; Cao, H.;Yan, H., Covalent Oganic Frameworks for Photocatalytic Applications. *Appl. Catal. B Environ.* **2020**, *276*, 119174.

28. Li, S.; Li, L.; Li, Y.; Dai, L.; Liu, C.; Liu, Y.; Li, J.; Lv, J.; Li, P.;Wang, B., Fully Conjugated Donor–Acceptor Covalent Organic Frameworks for Photocatalytic Oxidative Amine Coupling and Thioamide Cyclization. *ACS Catal.* **2020**, *10*, 8717-8726.

29. Chen, R.; Shi, J.-L.; Ma, Y.; Lin, G.; Lang, X.;Wang, C., Designed Synthesis of a 2D Porphyrin-Based sp^2 Carbon-Conjugated Covalent Organic Framework for Heterogeneous Photocatalysis. *Angew. Chem. Int. Ed.* **2019**, *58*, 6430-6434.

30. Mo, C.; Yang, M.; Sun, F.; Jian, J.; Zhong, L.; Fang, Z.; Feng, J.;Yu, D., Alkene-Linked Covalent Organic Frameworks Boosting Photocatalytic Hydrogen Evolution by Efficient Charge Separation and Transfer in the Presence of Sacrificial Electron Donors. *Adv. Sci.* **2020**, 1902988.

31. Wang, H.; Qian, C.; Liu, J.; Zeng, Y.; Wang, D.; Zhou, W.; Gu, L.; Wu, H.; Liu, G.;Zhao, Y., Integrating Suitable Linkage of Covalent Organic Frameworks into Covalently Bridged Inorganic/Organic Hybrids toward Efficient Photocatalysis. *J. Am. Chem. Soc.* **2020**, *142*, 4862-4871.

32. Ghosh, S.; Nakada, A.; Springer, M. A.; Kawaguchi, T.; Suzuki, K.; Kaji, H.; Baburin, I.; Kuc, A.; Heine, T.; Suzuki, H.; Abe, R.;Seki, S., Identification of Prime Factors to Maximize the Photocatalytic Hydrogen Evolution of Covalent Organic Frameworks. *J. Am. Chem. Soc.* **2020**, *142*, 9752-9762.

33. Wang, G.-B.; Li, S.; Yan, C.-X.; Lin, Q.-Q.; Zhu, F.-C.; Geng, Y.;Dong, Y.-B., A Benzothiadiazole-Based Covalent Organic Framework for Highly Efficient Visible-Light Driven Hydrogen Evolution. *Chem. Commun.* **2020**, *56*, 12612-12615.

34. Chen, W.; Wang, L.; Mo, D.; He, F.; Wen, Z.; Wu, X.; Xu, H.;Chen, L., Modulating Benzothiadiazole-Based Covalent Organic Frameworks via Halogenation for Enhanced Photocatalytic Water Splitting. *Angew. Chem. Int. Ed.* **2020**, *59*, 16902-16909.

35. Chen, J.; Tao, X.; Tao, L.; Li, H.; Li, C.; Wang, X.; Li, C.; Li, R.;Yang, Q., Novel Conjugated Organic Polymers as Candidates for Visible-Light-Driven Photocatalytic Hydrogen Production. *Appl. Catal. B Environ.* **2019**, *241*, 461-470.

36. Zhang, Y.; Hu, Y.; Zhao, J.; Park, E.; Jin, Y.; Liu, Q.;Zhang, W., Covalent Organic Framework-Supported Fe–TiO_2 Nanoparticles as Ambient-Light-Active Photocatalysts. *J. Mater. Chem. A* **2019**, *7*, 16364-16371.

37. Dong, Z.; Zhang, L.; Gong, J.;Zhao, Q., Covalent Organic Framework Nanorods Bearing Single Cu Sites for Efficient Photocatalysis. *Chem. Eng. J. 403*, 126383.

38. Sun, Q.; Aguila, B.; Perman, J.; Nguyen, N.;Ma, S., Flexibility Matters: Cooperative Active Sites in Covalent Organic Framework and Threaded Ionic Polymer. *J. Am. Chem. Soc.* **2016**, *138*, 15790-15796.

39. Leng, W.; Peng, Y.; Zhang, J.; Lu, H.; Feng, X.; Ge, R.; Dong, B.; Wang, B.; Hu, X.;Gao, Y., Sophisticated Design of Covalent Organic Frameworks with Controllable Bimetallic Docking for a Cascade Reaction. *Chem. Eur. J.* **2016**, *22*, 9087-9091.

40. Aiyappa, H. B.; Thote, J.; Shinde, D. B.; Banerjee, R.;Kurungot, S., Cobalt-Modified Covalent Organic Framework as a Robust Water Oxidation Electrocatalyst. *Chem. Mater.* **2016**, *28*, 4375-4379.

41. Zhong, W.; Sa, R.; Li, L.; He, Y.; Li, L.; Bi, J.; Zhuang, Z.; Yu, Y.;Zou, Z., A Covalent Organic Framework Bearing Single Ni Sites as a Synergistic Photocatalyst for Selective Photoreduction of CO_2 to CO. *J. Am. Chem. Soc.* **2019**, *141*, 7615-7621.

42. Lin, S.; Diercks, C. S.; Zhang, Y.-B.; Kornienko, N.; Nichols, E. M.; Zhao, Y.; Paris, A. R.; Kim, D.; Yang, P.; Yaghi, O. M.;Chang, C. J., Covalent Organic Frameworks Comprising Cobalt Porphyrins for Catalytic CO_2 Reduction in Water. *Science* **2015**, *349*, 1208-1213.

43. Chen, X.; Addicoat, M.; Jin, E.; Zhai, L.; Xu, H.; Huang, N.; Guo, Z.; Liu, L.; Irle, S.;Jiang, D., Locking Covalent Organic Frameworks with Hydrogen Bonds: General and Remarkable Effects on Crystalline Structure, Physical Properties, and Photochemical Activity. *J. Am. Chem. Soc.* **2015**, *137*, 3241-3247.

44. Wang, H.; Ding, H.; Meng, X.;Wang, C., Two-Dimensional Porphyrin- and Phthalocyanine-Based Covalent Organic Frameworks. *Chin. Chem. Lett.* **2016**, *27*, 1376-1382.

45. Lin, G.; Ding, H.; Chen, R.; Peng, Z.; Wang, B.;Wang, C., 3D Porphyrin-Based Covalent Organic Frameworks. *J. Am. Chem. Soc.* **2017**, *139*, 8705-8709.

46. Meng, Y.; Luo, Y.; Shi, J. L.; Ding, H.; Lang, X.; Chen, W.; Zheng, A.; Sun, J.;Wang, C., 2D and 3D Porphyrinic Covalent Organic Frameworks: The Influence of Dimensionality on Functionality. *Angew. Chem. Int. Ed.* **2020**, *59*, 3624-3629.

47. Li, L.-H.; Feng, X.-L.; Cui, X.-H.; Ma, Y.-X.; Ding, S.-Y.;Wang, W., Salen-Based Covalent Organic Framework. *J. Am. Chem. Soc.* **2017**, *139*, 6042-6045.

48. Han, X.; Xia, Q.; Huang, J.; Liu, Y.; Tan, C.;Cui, Y., Chiral Covalent Organic Frameworks with High Chemical Stability for Heterogeneous Asymmetric Catalysis. *J. Am. Chem. Soc.* **2017**, *139*, 8693-8697.

49. Yuan, G.; Jiang, H.; Zhang, L.; Liu, Y.;Cui, Y., Metallosalen-Based Crystalline Porous Materials: Synthesis and Property. *Coord. Chem. Rev.* **2019**, *378*, 483-499.

50. Yan, S.; Guan, X.; Li, H.; Li, D.; Xue, M.; Yan, Y.; Valtchev, V.; Qiu, S.;Fang, Q., Three-dimensional Salphen-based Covalent–Organic Frameworks as Catalytic Antioxidants. *J. Am. Chem. Soc.* **2019**, *141*, 2920-2924.

51. Chen, X.; Huang, N.; Gao, J.; Xu, H.; Xu, F.;Jiang, D., Towards Covalent Organic Frameworks with Predesignable and Aligned Open Docking Sites. *Chem. Commun.* **2014**, *50*, 6161-6163.

52. Zhang, W.; Jiang, P.; Wang, Y.; Zhang, J.; Gao, Y.;Zhang, P., Bottom-up Approach to Engineer a Molybdenum-Doped Covalent-Organic Framework Catalyst for Selective Oxidation Reaction. *RSC Adv.* **2014**, *4*, 51544-51547.

53. Vardhan, H.; Verma, G.; Ramani, S.; Nafady, A.; Al-Enizi, A. M.; Pan, Y.; Yang, Z.; Yang, H.;Ma, S., Covalent Organic Framework Decorated with Vanadium as a New Platform for Prins Reaction and Sulfide Oxidation. *ACS Appl. Mater. Interfaces* **2019**, *11*, 3070-3079.

54. Auras, F.; Ascherl, L.; Hakimioun, A. H.; Margraf, J. T.; Hanusch, F. C.; Reuter, S.; Bessinger, D.; Döblinger, M.; Hettstedt, C.; Karaghiosoff, K.; Herbert, S.; Knochel, P.; Clark, T.;Bein, T., Synchronized Offset Stacking: A Concept for Growing Large-Domain and Highly Crystalline 2D Covalent Organic Frameworks. *J. Am. Chem. Soc.* **2016**, *138*, 16703-16710.

55. Liang, R.-R.;Zhao, X., Heteropore Covalent Organic Frameworks: A New Class of Porous Organic Polymers with Well-Ordered Hierarchical Porosities. *Org. Chem. Front.* **2018**, *5*, 3341-3356.

56. Liang, R.-R.; Jiang, S.-Y.; A, R.-H.;Zhao, X., Two-Dimensional Covalent Organic Frameworks with Hierarchical Porosity. *Chem. Soc. Rev.* **2020**, *49*, 3920-3951.

57. Jin, Y.; Hu, Y.;Zhang, W., Tessellated Multiporous Two-Dimensional Covalent Organic Frameworks. *Nat. Rev. Chem.* **2017**, *1*, 0056.

58. Casado-Sánchez, A.; Gómez-Ballesteros, R.; Tato, F.; Soriano, F. J.; Pascual-Coca, G.; Cabrera, S.;Alemán, J., Pt(II) Coordination Complexes as Visible Light Photocatalysts for the Oxidation of Sulfides Using Batch and Flow Processes. *Chem. Commun.* **2016**, *52*, 9137-9140.

59. López-Magano, A.; Platero-Prats, A. E.; Cabrera, S.; Mas-Ballesté, R.;Alemán, J., Incorporation of Photocatalytic Pt(II) Complexes into Imine-Based Layered Covalent Organic Frameworks (COFs) Through Monomer Truncation Strategy. *Appl. Catal. B Environ.* **2020**, *272*, 119027.

60. Ding, S.-Y.; Gao, J.; Wang, Q.; Zhang, Y.; Song, W.-G.; Su, C.-Y.;Wang, W., Construction of Covalent Organic Framework for Catalysis: Pd/COF-LZU1 in Suzuki–Miyaura Coupling Reaction. *J. Am. Chem. Soc.* **2011**, *133*, 19816-19822.

61. Zhong, J. J.; Yang, C.; Chang, X. Y.; Zou, C.; Lu, W.;Che, C. M., Platinum(II) Photo-Catalysis for Highly Selective Difluoroalkylation Reactions. *Chem. Commun.* **2017**, *53*, 8948-8951.

62. Liang, Z.; Xu, S.; Tian, W.;Zhang, R., Eosin Y-Catalyzed Visible-Light-Mediated Aerobic Oxidative Cyclization of N,N-Dimethylanilines with Maleimides. *Beilstein J. Org. Chem.* **2015**, *11*, 425-430.

63. Yang, X.-L.; Guo, J.-D.; Lei, T.; Chen, B.; Tung, C.-H.;Wu, L.-Z., Oxidative Cyclization Synthesis of Tetrahydroquinolines and Reductive Hydrogenation of Maleimides under Redox-Neutral Conditions. *Org. Lett.* **2018**, *20*, 2916-2920.

64. Nicholls, T. P.; Constable, G. E.; Robertson, J. C.; Gardiner, M. G.;Bissember, A. C., Bronsted Acid Cocatalysis in Copper(I)-Photocatalyzed alpha-Amino C-H Bond Functionalization. *ACS Catal.* **2016**, *6*, 451-457.

65. Müller, K.; Faeh, C.;Diederich, F., Fluorine in Pharmaceuticals: Looking Beyond Intuition. *Science* **2007**, *317*, 1881-1886.

66. O'Hagan, D., Understanding Organofluorine Chemistry. An Introduction to the C–F Bond. *Chem. Soc. Rev.* **2008**, *37*, 308-319.

67. Chen, B.;Vicic, D. A., Transition-Metal-Catalyzed Difluoromethylation, Difluoromethylenation, and Polydifluoromethylenation Reactions. In *Organometallic Fluorine Chemistry*, Braun, T.; Hughes, R. P., Eds. Springer International Publishing: Cham, 2015; pp 113-141.

68. Wang, Z.; Guo, C.-Y.; Yang, C.;Chen, J.-P., Ag-Catalyzed Chemoselective Decarboxylative Mono- and gem-Difluorination of Malonic Acid Derivatives. *J. Am. Chem. Soc.* **2019**, *141*, 5617-5622.

69. Yang, Y.; Niu, H.; Xu, L.; Zhang, H.;Cai, Y., Triazine Functionalized Fully Conjugated Covalent Organic Framework for Efficient Photocatalysis. *Appl. Catal. B Environ.* **2020**, *269*, 118799.

70. Shen, J.-C.; Jiang, W.-L.; Guo, W.-D.; Qi, Q.-Y.; Ma, D.-L.; Lou, X.; Shen, M.; Hu, B.; Yang, H.-B.;Zhao, X., A Rings-in-Pores Net: Crown Ether-Based Covalent Organic Frameworks for Phase-Transfer Catalysis. *Chem. Commun.* **2020**, *56*, 595-598.

Supporting Information

2.6. **Materials and Methods**

NMR spectra were recorded on a 400 MHz NMR spectrometer. Chemical shifts δ are reported in ppm, and the abbreviations s, d, t, q, m and *J* are used for singlet, doublet, triplet, quartet, multiplet, and coupling constant, respectively. Infrared spectra were recorded on a Shimadzu IRAffinity-1S spectrophotometer. Solid-state NMR experiments were performed on a Bruker UltrashieldTM 400 MHz NMR spectrometer. The ^{13}C cross-polarization magic-angle spinning (CP/MAS) NMR spectra were recorded with a 4-mm triple-resonance MAS probe and a sample spinning rate of 10.0 kHz; a contact time of 3 ms (ramp 100) and pulse delay of 2 s were applied. The sample was packed in a zirconia rotor.

Powder X-ray diffraction (PXRD) data was collected with a Rigaku MiniFlex II desktop X-Ray diffractometer operated at 30 kV and 15 mA. Scanning electron microscopy (SEM) observations were performed on a FEI Nova 200 Nano Lab microscope. Transmission electron microscopy (TEM) images were obtained with a FEI Titan 80-300 transmission electron microscope. Gas adsorption isotherms were obtained by a volumetric method using a Quantachrome Autosorb iQ-MP/XR gas sorption analyzer. Surface area was calculated from the adsorption data using Brunauer-Emmett-Teller (BET) method. The pore-size-distribution curve was obtained from the adsorption branches using nonlocal density functional theory (NLDFT) method.

2.7. Synthesis and Experimental Procedures

2.7.1. Synthesis of COF linkers

2.7.1.1. Synthesis of 1,3,6,8-tetrakis(4-aminophenyl)pyrene (L1)[1]

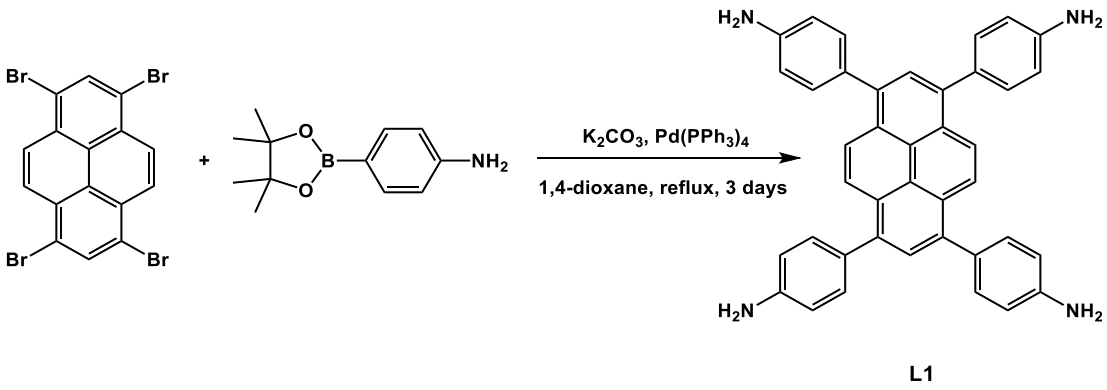

Scheme 2. 7. Synthetic route for lignad **L1**.

1,3,6,8-tetrabromopyrene (1.5 g, 2.9 mmol), 4-aminophenylboronic acid pinacol ester (3.0g, 13.7 mmol), K_2CO_3 (2.2 g, 15.7 mmol), and $Pd(PPh_3)_4$ (330 mg, 0.29 mmol) in were added to degassed dioxane:water (4:1, 40 mL). The mixture was heated at 115 °C for 3 days. After cooling to room temperature, H_2O (50 mL) was added. The resulting precipitate was collected *via* filtration and was washed with H_2O (50 mL) and MeOH (100 mL). Recrystallization from dioxane, followed by drying under high vacuum furnished the title compound, as a bright yellow powder (1.45 g, 89%).

^{1}H NMR (400 MHz, DMSO-d_6) δ 8.14 (s, 4H), 7.80 (s, 2H), 7.36 (d, J = 8.4 Hz, 8H), 6.78 (d, J = 8.4 Hz, 8H), 5.31 (s, 8H).

^{13}C NMR (101 MHz, DMSO-d_6) δ 148.6, 137.6, 131.5, 129.5, 128.0, 127.2, 126.6, 124.9, 114.4.

2.7.1.2. Synthesis of 2-(4-Formylphenyl)-5-formylpyridine (L2)[2]

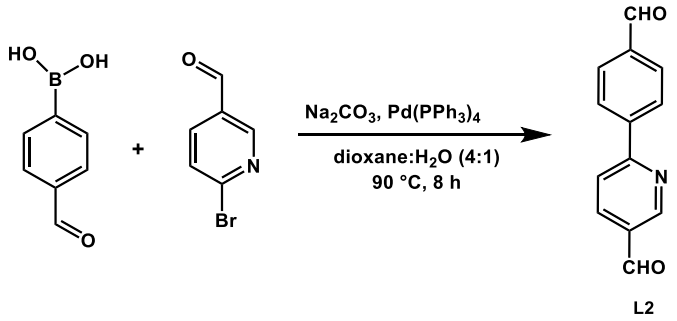

Scheme 2. 8. Synthetic route for lignad **L2**.

4-formylphenylboronic acid (1.0 g, 6.67 mmol), 6-bromo-3-pyridinecarboxaldehyde (1.2 g, 6.45 mmol), sodium carbonate (1.9 g, 17.9 mmol), and tetrakis(triphenylphosphine)-palladium (0.30 g, 0.26 mmol) were dissolved in a degassed mixture of dioxane:water (4:1, 30 mL). The mixture was heated under N_2 at 90 °C for 8 h. The reaction mixture was cooled to ambient temperature and extracted with dichloromethane. The organic layer was washed with saturated sodium hydrogen carbonate solution and brine, then dried with magnesium sulfate and concentrated to dryness. The crude material was recrystallizated from $CHCl_3$/hexane to give the pure product as an off-white solid (1.1 g, 81 %).

^{1}H NMR (400 MHz, $CDCl_3$) δ 10.18 (s, 1H), 10.11 (s, 1H), 9.18 (s, 1H), 8.28 (dd, *J* = 12.2, 5.2 Hz, 3H), 8.01 (dd, *J* = 16.2, 8.3 Hz, 3H).

^{13}C NMR (101 MHz, DMSO-d_6) δ 193.3, 192.5, 159.4, 152.0, 143.0, 137.9, 137.4, 130.9, 130.4, 128.4, 122.2.

2.7.2. Synthesis of COFs

2.7.2.1. Synthesis of COF-UARK-49

2-(4-Formylphenyl)-5-formylpyridine (8.4 mg, 0.04 mmol) and 1,3,6,8-tetrakis(4-aminophenyl)-pyrene (11.3 mg, 0.02 mmol) were placed in a glass ampule vessel (20 mL), followed by adding a solution of mesitylene:dioxane:acetic acid (3 M) (0.5:0.5:0.1 mL). The mixture was sonicated for 5 min and then flash frozen in liquid nitrogen. The vessel was evacuated to an inner pressure of ~20 Pa, flame-sealed, and heated at 120 °C for 3 days. The resulting precipitate was washed sequentially with DMF (3 times) and acetone (3 times) to give a powder, which was dried at 120 °C under vacuum for 12 h to give the desired product (11.6 mg, 64%).

2.7.2.2. Synthesis of COF-UARK-49-Pt

COF-UARK-49 COF (70 mg), *cis*-[$PtCl_2(DMSO)_2$] (30 mg, 0.071mmol), and NaOAc (7.2 mg, 0.088 mmol) were mixed in 4 mL toluene and the mixture was heated at 50 °C overnight. The resulting suspension was filtered and washed sequentially with DMF (3 times) and acetone (3 times) to give a brown powder, which was dried under vacuum for 12 h to give the Pt loaded COF (83 mg). The Pt loading was determined to be 9.1% by ICP-MS.

2.7.2.3. Synthesis of Py-2P COF

4,4’-biphenyldicarboxaldehyde (12.6 mg, μmol) and 1,3,6,8-tetrakis(4-aminophenyl)pyrene (21 mg, 0.02 mmol) were filled into a reaction tube, followed by the addition of mesitylene (1 mL), 1,4-dioxane (0.5 mL), and 6 M acetic acid (0.15 mL). The tube was sealed, and the reaction mixture was heated at 120 °C for 3 d. After cooling to room temperature, the precipitate was collected by filtration, yielding an orange powder. This framework was found to lose its crystallinity upon evaporation of the solvent.

2.7.2.4. Synthesis of Py-2P-Pt COF

Py-2P COF (20 mg) and *cis*-[$PtCl_2(DMSO)_2$] (10 mg, 0.024mmol) were mixed in 2 mL toluene and the mixture was heated at 50 °C overnight. The resulting suspension was filtered and washed sequentially with DMF (3 times) and acetone (3 times) to give a brown powder, which was dried under vacuum for 12 h to give the Pt loaded COF. The Pt loading was determined to be 12.5% by ICP-MS.

2.8. Structure Simulation

N_2 adsorption isotherms were calculated using grand canonical Monte Carlo (GCMC) simulations performed with the multi-purpose simulation package RASPA.[3] The framework atoms were kept fixed at the crystallographic positions for both COFs. We used the standard Lennard-Jones (LJ) potential to model the interactions between fluid/fluid and fluid/framework atoms. The LJ parameters for the framework atoms were obtained from the Dreiding force field.[4] N_2 was modeled using the TraPPE[5] potential with charges placed on each atom and at the center of mass. The Lorentz-Berthelot mixing rules were employed to calculate fluid/solid LJ parameters, and LJ interactions beyond 12.8 Å were neglected. The Ewald sum method was used to compute the electrostatic interactions. 104 Monte Carlo cycles were performed, the first 50% of which were used for equilibration, and the remaining cycles were used to calculate the ensemble averages.

2.9. Photocatalysis

2.9.1. General Procedure for Difluoroalkylation Reaction

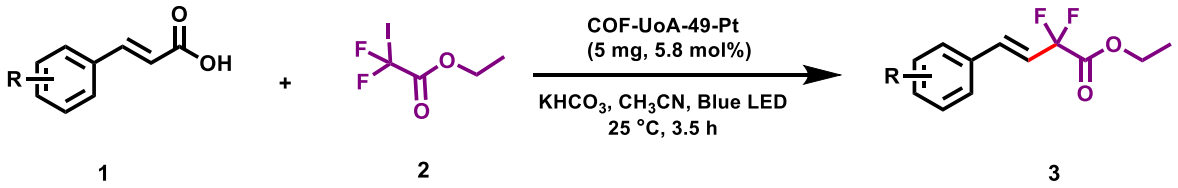

Scheme 2. 9. General method for the difluoroalkylation.

The cinnamic acid derivatives (0.04 mmol), ethyldifluoroiodoacetate (0.044 mmol), potassium dicarbonate (0.044 mmol) and COF-UARK-49-Pt (5 mg, 5.8 mol%) were dissolved in 1 mL CH_3CN in a 4 mL reaction tube equipped with magnetic stir bar. The reaction tube was deaerated with nitrogen for 15 min and then sealed. Then the reaction mixture was irradiated with a blue LED light for 3.5 h. After reaction, the product was isolated by TLC plate chromatography of silica gel using *n*-hexane:ethyl acetate (10:1) as the eluent.

2.9.2. Difluoroalkylation reaction with TEMPO

The cinnamic acid derivatives (0.04 mmol), ethyldifluoroiodoacetate (0.044 mmol), TEMPO (0.044 mmol), potassium dicarbonate (0.044 mmol), and COF-UARK-49-Pt (5 mg, 5.8 mol%) were mixed in 1 mL CH_3CN in a 4 mL reaction tube equipped with magnetic stir bar. The mixture was deaerated with nitrogen for 15 min before the reaction tube was sealed. The mixture was irradiated with a blue LED light for 3.5 h. The product was confirmed by ESI-MS. **HRMS** (ESI) (m/z): $[M+H]^+$calcd. for $C_{13}H_{24}F_2NO_3$: 280.1646, found:280.1718.

2.9.3. General Reaction Procedure for the Oxidative Cyclization Reaction

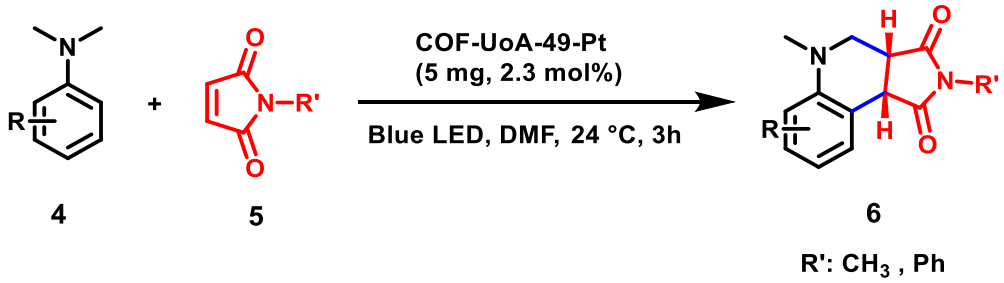

Scheme 2. 10. General method for the oxidative cyclization.

N,*N*-dimethylaniline derivatives (0.2 mmol), *N*-phenylmaleimide (0.1 mmol), and COF-UARK-49-Pt catalyst (5 mg, 2.3 mol%) were mixed in 1 mL DMF in a 4 mL glass vial containing a magnetic stir bar. This vial was then capped and irradiated with a blue LED light for 3 h.

2.10. Supporting Figures

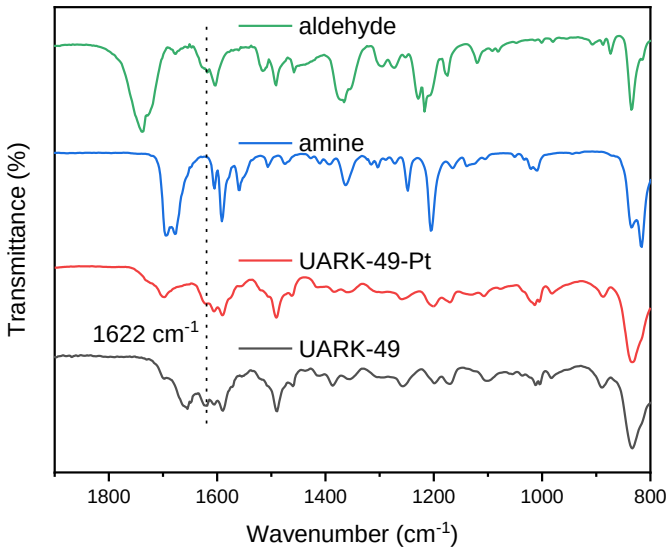

Figure 2. 5. FT-IR spectra of COF-UARK-49-Pt (red), COF-UARK-49 (grey), aldehyde linker (green), and amine linker (blue).

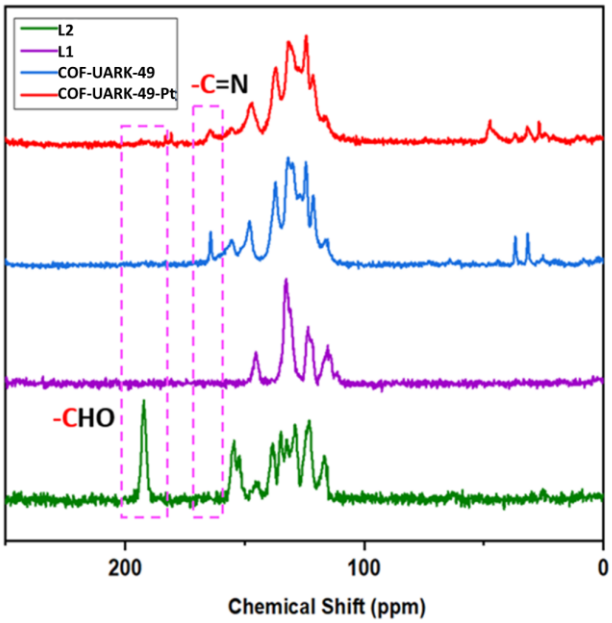

Figure 2. 6. ^{13}C CP/MAS spectra of L1, L2, COF-UARK-49, and COF-UARK-49-Pt.

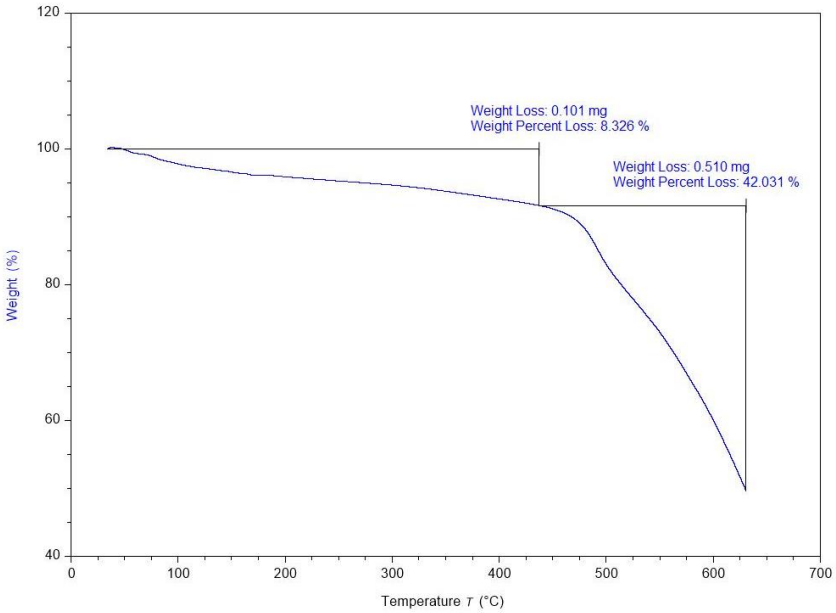

Figure 2. 7. TGA trace of COF-UARK-49 under N_2 atmosphere.

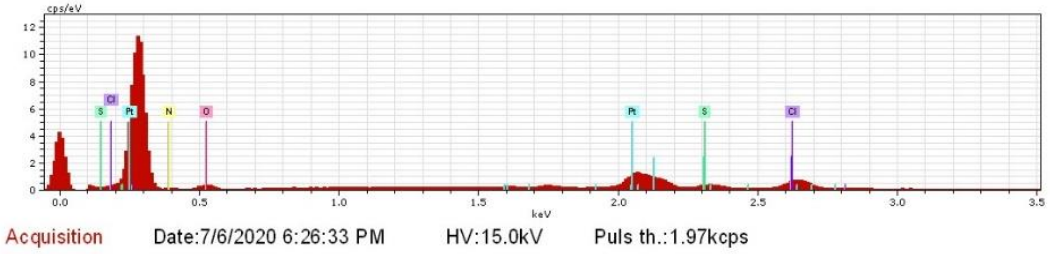

El	AN	Series	unn. C [wt.%]	norm. C [wt.%]	Atom. C [at.%]	Error (1 Sigma) [wt.%]
N	7	K-series	5.28	16.64	36.64	1.31
O	8	K-series	6.34	19.98	38.51	1.25
S	16	K-series	1.66	5.22	5.02	0.10
Cl	17	K-series	4.74	14.94	13.00	0.20
Pt	78	M-series	13.71	43.22	6.83	0.57
		Total:	31.73	100.00	100.00	

Figure 2. 8. EDX spectrum of COF-UARK-49-Pt.

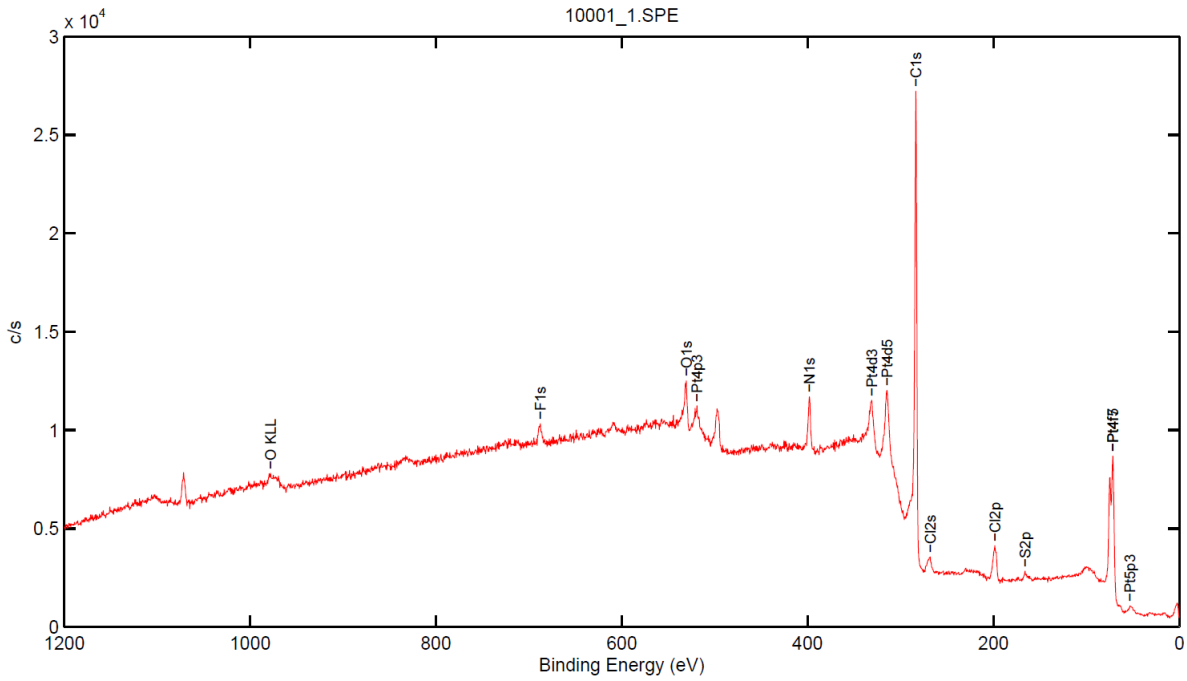

Figure 2. 9.XPS Survey spectrum of COF-UARK-49-Pt.

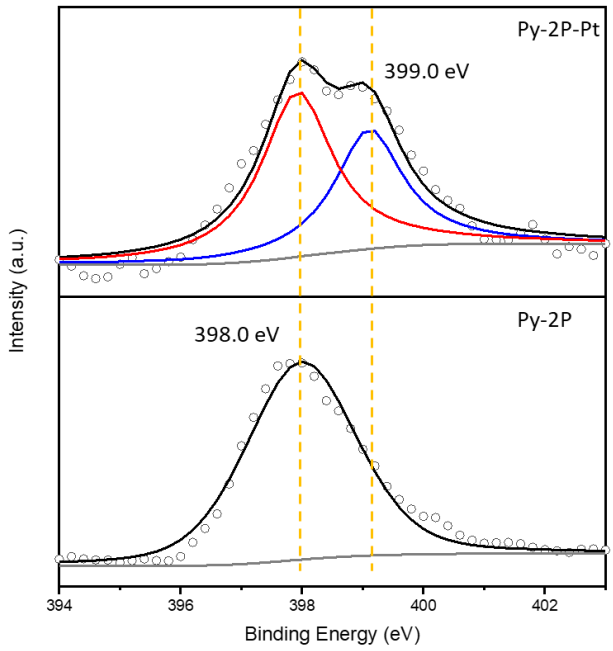

Figure 2. 10. N 1s XPS spectra of Py-2P and Py-2P-Pt.

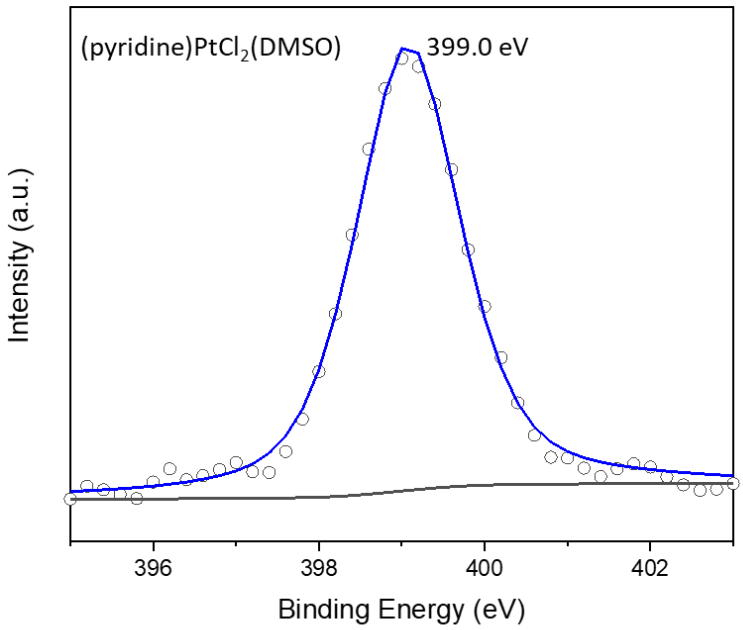

Figure 2. 11. N 1s XPS spectra of $PtCl_2$(DMSO)(pyridine) (cis and trans 1:1 mixture).

Table 2. 2. DFT calculated structure of different N coordinated Pt complex based on the model imine compound. [a]

Coordination mode	Optimized structure	Gibbs free energy / Hartrees	Relative energy to pyridine coordinated structure / kcal mol^{-1}
Pyridine N	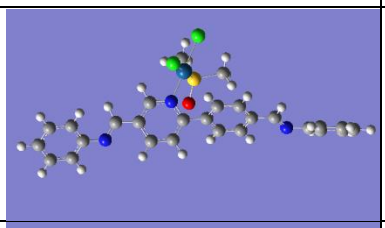	-2720.395809	0
Imine N	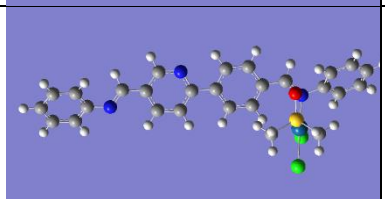	-2720.396953	-0.72
Imine N	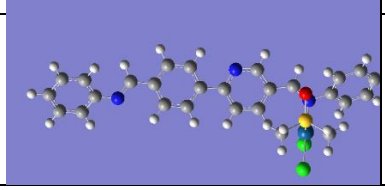	-2720.395518	0.90

[a] The geometry optimization was carried out by B3LYP hybrid functional with 6-31G(d,p) basis set for the main group atoms and the effective core potentials (ECPs) of Hay and Wadt with the LanL2DZ double-valence basis set for Pt.

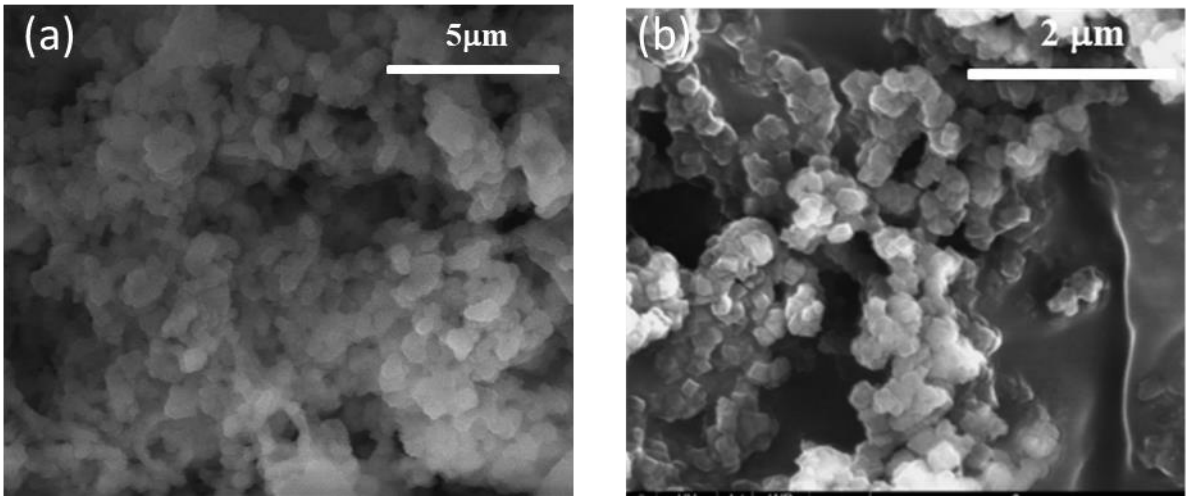

Figure 2. 12. SEM images of (a) COF-UARK-49 and (b) COF-UARK-49-Pt.

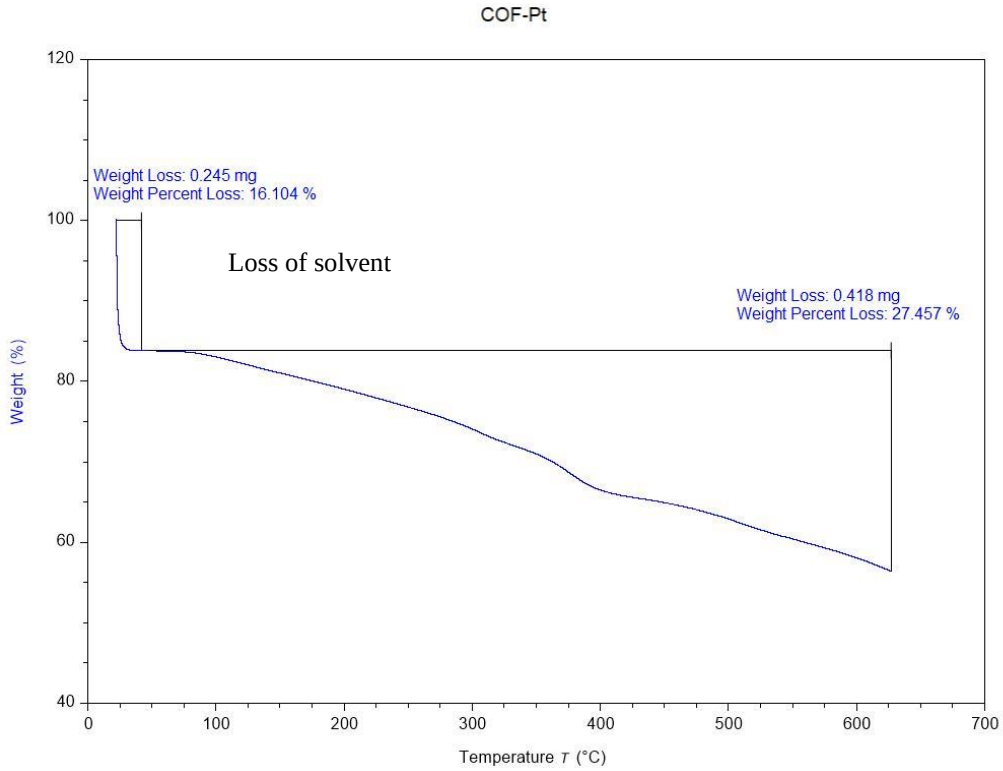

Figure 2. 13. TGA trace of COF-UARK-49-Pt under N_2 atmosphere.

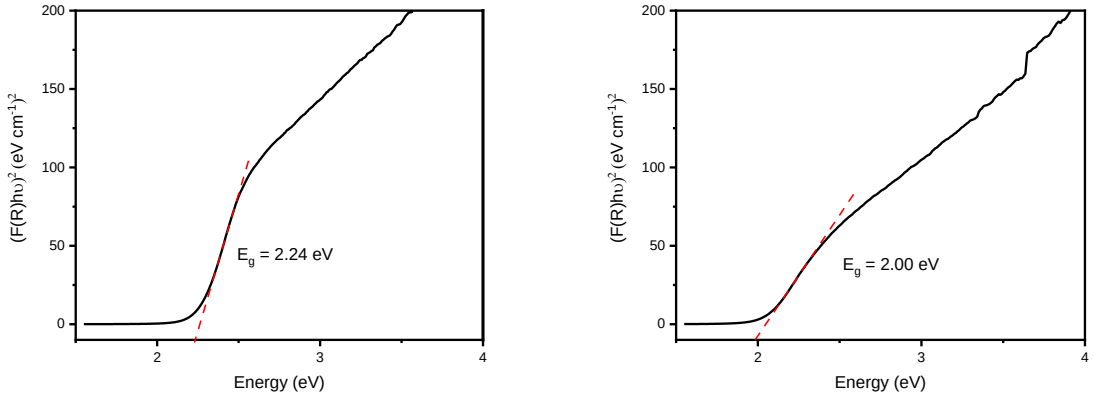

Figure 2. 14. Plot of Kubelka-Munk function used for band gap extraction of COF-UARK-49 (left) and COF-UARK-49-Pt (right).

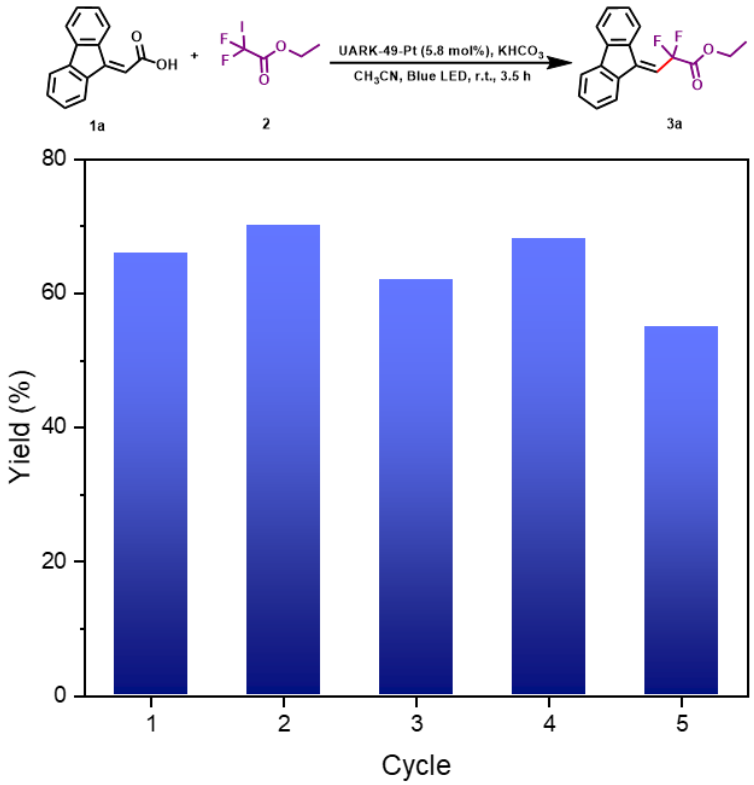

Figure 2. 15. Recyclability test of COF-UARK-49-Pt in decarboxylation-difluoroalkylation reaction.

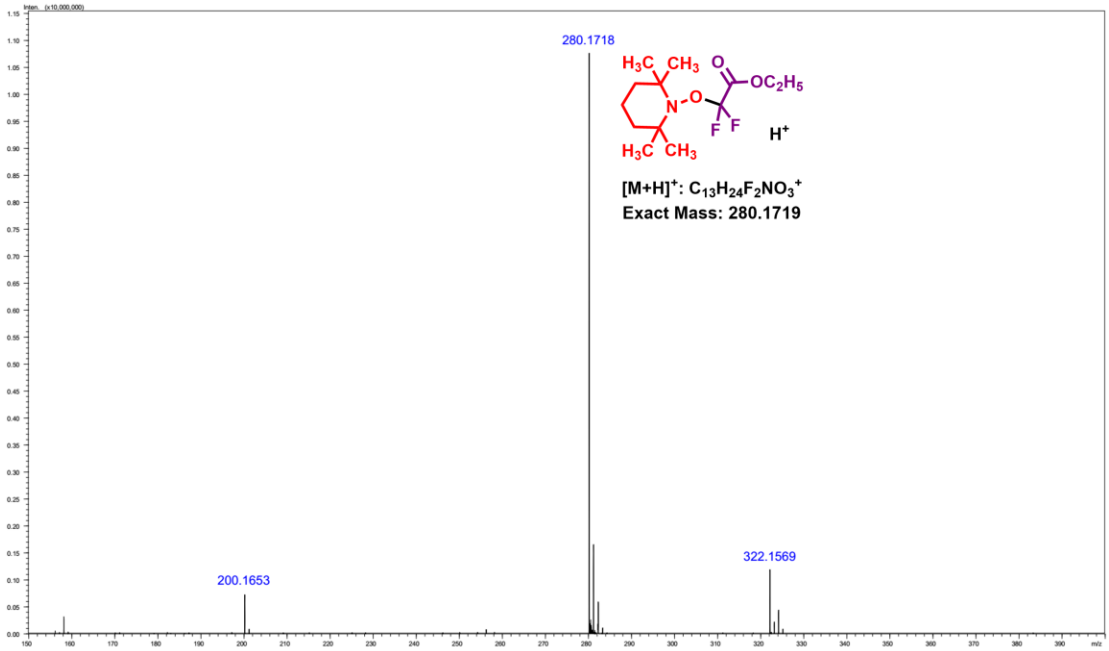

Figure 2. 16. HR ESI-MS of the adduct of TEMPO and difluoro radical.

Table 2. 3. Optimization Reaction Conditions for the Photocatalytic Oxidative Cyclization Reaction.[a]

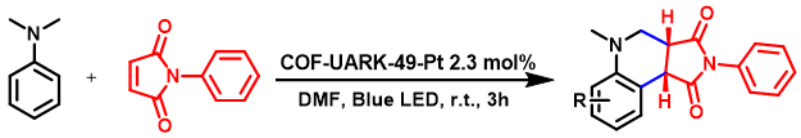

Entry	Difference from the Standard Condition	Yield (%)[b]
1	None	66
2	Without light	No reaction
3	Without catalyst	<4
4	COF-UARK-49 instead of COF-UARK-49-Pt	23
5	In the presence of 0.1 mmol $AgNO_3$	25
6	In the presence of 0.1 mmol KI	trace
7	In the presence of 0.1 mmol 1,4-benzoquinone	trace
8	Under N_2 atmosphere	7
9	$PtCl_2$(DMSO)(pyridine) instead of COF-UARK-49-Pt	46

[a]A mixture of **4a** (0.2 mol) and **5a** (0.1 mol) in 1 mL DMF in the presence of 5 mg (2.3 mol%) of the catalyst. [b]HPLC yield.

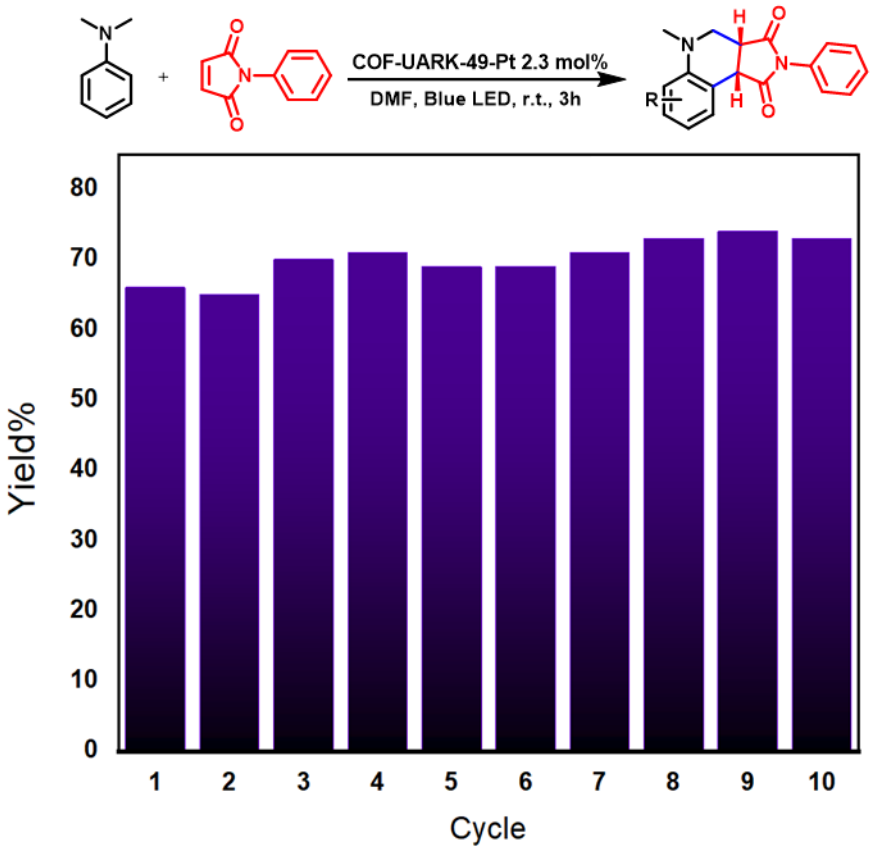

Figure 2. 17. Recyclability test of COF-UARK-49-Pt in oxidative cyclization reaction.

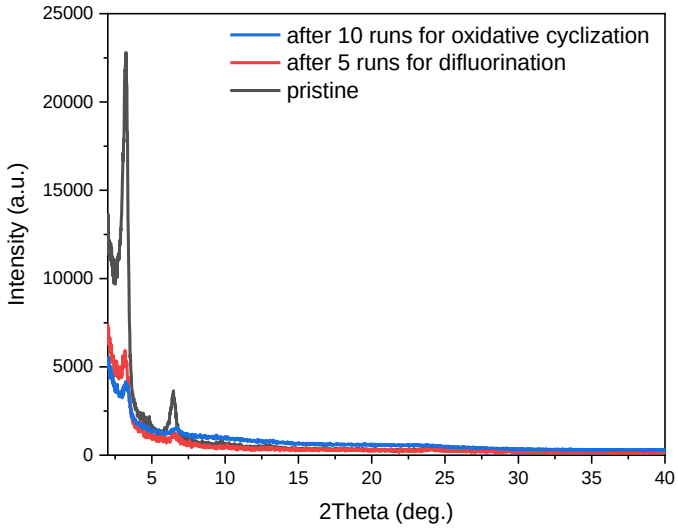

Figure 2. 18. PXRD spectra of recovered COF-UARK-49-Pt.

2.11. Spectroscopic Data of the Products

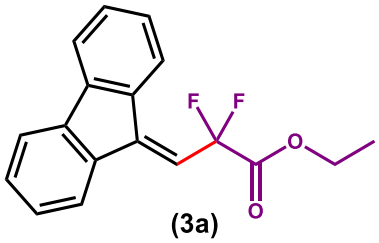

(3a)

Scheme 2. 11. The chemical structure of **3a**.

Ethyl 3-(9H-fluoren-9-ylidene)-2,2-difluoropropanoate (lit.[6]) (3a)

^{1}H NMR (400 MHz, $CDCl_3$) δ 8.11 (d, *J* = 7.8 Hz, 1H), 7.65 (t, *J* = 6.5 Hz, 3H), 7.48 – 7.35 (m, 2H), 7.35 – 7.24 (m, 2H), 6.65 (t, *J* = 15.8 Hz, 1H), 4.36 (q, *J* = 7.1 Hz, 2H), 1.32 (t, *J* = 7.1 Hz, 3H).

^{13}C NMR (101 MHz, $CDCl_3$) δ 163.5 (t, *J* = 34.8 Hz), 143.8 (t, *J* = 7.6 Hz), 142.2, 140.1, 138.1, 134.0 (t, *J* = 1.8 Hz), 130.4, 130.1, 127.7, 127.4, 127.2 (t, *J* = 7.5 Hz), 121.0, 119.8, 119.7 (d, *J* = 2.2 Hz), 115.1 (t, *J* = 29.4 Hz), 112.8 (t, 248.0 Hz), 63.4, 13.9.

^{19}F NMR (376 MHz, $CDCl_3$) δ -96.04 (2F).

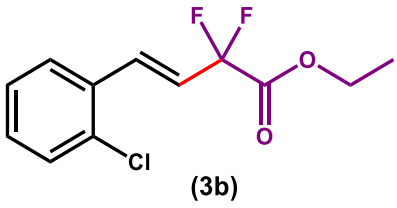

(3b)

Scheme 2. 12. The chemical structure of **3b**.

Ethyl (*E*)-4-(2-chlorophenyl)-2,2-difluorobut-3-enoate (lit.[6]) (3b)

^{1}H NMR (400 MHz, $CDCl_3$) δ 7.60 – 7.54 (m, 1H), 7.51 (dt, *J* = 16.2, 2.6 Hz, 1H), 7.45 – 7.37 (m, 1H), 7.39-7.21 (m, 2H), 6.33 (dt, *J* = 16.2, 11.1 Hz, 1H), 4.38 (q, *J* = 7.1 Hz, 2H), 1.39 (t, *J* = 7.1 Hz, 3H).

^{13}C NMR (101 MHz, $CDCl_3$) δ 163.7, 134.3, 133.2 (t, *J* = 9.8 Hz), 132.4, 130.5, 130.0, 127.3, 127.0, 121.5 (t, *J* = 25.3 Hz), 112.4 (t, *J* =245 Hz), 63.2, 13.9.

^{19}F NMR (376 MHz, $CDCl_3$) δ -103.15 (2F).

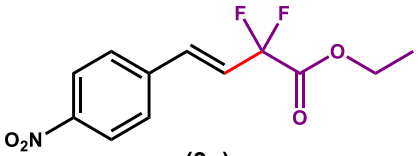

(3c)

Scheme 2. 13. The chemical structure of **3c**.

Ethyl (*E*)-2,2-difluoro-4-(4-nitrophenyl)but-3-enoate ((lit.[6]) (3c)

^{1}H NMR (400 MHz, $CDCl_3$) δ 8.27 (d, *J* = 8.7 Hz, 2H), 7.64 (d, *J* = 8.7 Hz, 2H), 7.17 (d, *J* = 14.1 Hz, 1H), 6.49 (dt, *J* = 16.2, 11.1 Hz, 1H), 4.40 (q, *J* = 7.1 Hz, 2H), 1.40 (t, *J* = 7.2 Hz, 3H).

^{13}C NMR (101 MHz, $CDCl_3$) δ 163.3 (t, *J* = 39.5 Hz), 148.2, 140.2, 134.5 (t, *J* = 9.2 Hz), 128.1, 124.1, 123.3 (t, *J* = 25.0 Hz), 112.0 (t, *J* = 249.6 Hz), 63.4, 13.9.

^{19}F NMR (376 MHz, $CDCl_3$) δ = -103.96 (2F).

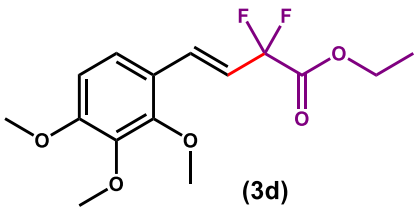

(3d)

Scheme 2. 14. The chemical structure of **3d**.

Ethyl (*E*)-2,2-difluoro-4-(2,3,4-trimethoxyphenyl)but-3-enoate(3d)

^{1}H NMR (400 MHz, $CDCl_3$) δ 7.23 (m,1H), 7.17 (d, *J* = 8.8 Hz, 1H), 6.68 (d, *J* = 8.8 Hz, 1H), 6.29 (dt, *J* = 16.3, 11.5 Hz, 1H), 4.35 (q, *J* = 7.1 Hz, 2H), 3.88 (d, *J* = 6.9 Hz, 9H), 1.36 (t, *J* = 7.2 Hz, 3H).

^{13}C NMR (101 MHz, $CDCl_3$) δ 164.5 – 163.7 (m), 154.9, 152.6, 142.3, 131.6 (t, *J* = 9.9 Hz), 122.4, 121.1, 117.8 (t, *J* = 24.9 Hz), 113.0 (t, *J* = 248.1 Hz), 62.9, 61.2, 60.8, 56.0, 13.9.

^{19}F NMR (376 MHz, CDCl3) δ = -102.90 (2F).

HRMS (ESI) (m/z): $[M+H]^+$ calcd. for $C_{15}H_{19}F_2O_5$: 317.11, found: 317.109

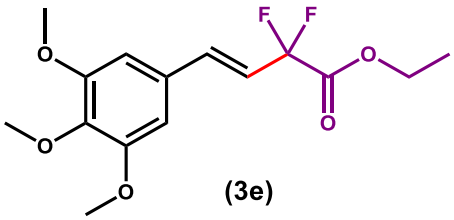

(3e)

Scheme 2. 15. The chemical structure of **3e**.

Ethyl (*E*)-2,2-difluoro-4-(3,4,5-trimethoxyphenyl)but-3-enoate(lit.[6]) (3e)

^{1}H NMR (400 MHz, $CDCl_3$) δ 7.01 (dt, *J* = 16.1, 2.3 Hz, 1H), 6.68 (s, 2H), 6.21 (dt, *J* = 16.1, 11.4 Hz, 1H), 4.37 (q, *J* = 7.1 Hz, 2H), 3.89 (d, *J* = 8.7 Hz, 9H), 1.38 (t, *J* = 7.1 Hz, 3H).

^{13}C NMR (101 MHz, $CDCl_3$) δ 163.9 (t, *J* = 34.9 Hz), 153.4, 139.5, 136.8 (t, *J* = 9.5 Hz), 129.6 (d, *J* = 1.3 Hz), 118.1 (t, *J* = 25.0 Hz), 112.7 (t, *J* = 248.8 Hz), 104.6, 63.1, 60.9, 56.1, 13.9.

^{19}F NMR (376 MHz, CDCl3) δ = -103.25(2F).

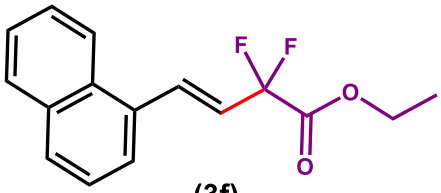

(3f)

Scheme 2. 16. The chemical structure of **3f**.

Ethyl (*E*)-2,2-difluoro-4-(naphthalen-1-yl)but-3-enoate (lit.[6]) (3f)

^{1}H NMR (400 MHz, $CDCl_3$) δ 8.09 (d, *J* = 8.3 Hz, 1H), 7.95 – 7.83 (m, 3H), 7.66 (d, *J* = 7.2 Hz, 1H), 7.54 (ddd, *J* = 19.3, 15.8, 7.3 Hz, 3H), 6.39 (dt, *J* = 15.9, 11.4 Hz, 1H), 4.40 (q, *J* = 7.1 Hz, 2H), 1.40 (t, *J* = 7.1 Hz, 3H).

^{13}C NMR (101 MHz, $CDCl_3$) δ 163.9 (t, *J* = 34.7 Hz), 134.3 (t, *J* = 9.3 Hz), 133.5, 131.7, 131.1, 129.8, 128.7, 126.7, 126.2, 125.4, 124.7 (t, *J* = 1.7 Hz), 123.3, 121.8 (t, *J* = 24.8 Hz), 112.6 (t, *J* = 248.7 Hz), 63.1, 14.0.

^{19}F NMR (376 MHz, CDCl3) δ = -103.09 (2F).

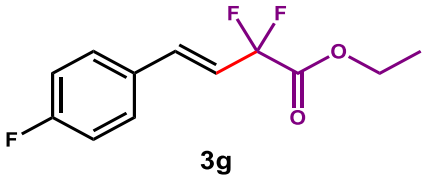

3g

Scheme 2. 17. The chemical structure of **3g**.

Ethyl (*E*)-2,2-difluoro-4-(4-fluorophenyl)but-3-enoate (lit.[6]) (3g)

^{1}H NMR (400 MHz, $CDCl_3$) δ 7.44 (dd, *J* = 8.4, 5.4 Hz, 2H), 7.14 – 6.99 (m, 3H), 6.24 (dt, *J* = 16.2, 11.3 Hz, 1H), 4.37 (q, *J* = 7.1 Hz, 2H), 1.38 (t, *J* = 7.1 Hz, 3H).

^{13}C NMR (101 MHz, $CDCl_3$) δ 164.8, 162.3, 136.3 (t, *J* = 9.5 Hz), 130.1, 129.3 (d, *J* = 8.4 Hz), , 117.9 (t, *J* = 24.9 Hz), 116.0 (d, *J* = 21.9 Hz), 112.4 (t, *J* = 248.7 Hz), 63.1, 13.9.

^{19}F NMR (377 MHz, $CDCl_3$) δ -103.46 (2F), -111.16 (1F).

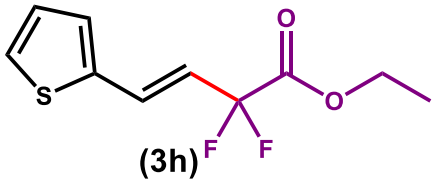

(3h)

Scheme 2. 18. The chemical structure of **3h**.

Ethyl (*E*)-2,2-difluoro-4-(thiophen-2-yl)but-3-enoate (lit.[7]) (3h)

^{1}H NMR (400 MHz, $CDCl_3$) δ 7.33 (d, *J* = 5.0 Hz, 1H), 7.24 – 7.14 (m, 2H), 7.03 (dd, *J* = 5.0, 3.7 Hz, 1H), 6.12 (dt, *J* = 15.9, 11.5 Hz, 1H), 4.36 (q, *J* = 7.1 Hz, 2H), 1.38 (t, *J* = 7.1 Hz, 3H).

^{13}C NMR (101 MHz, $CDCl_3$) δ 163.8 (t, *J* = 35.0 Hz), 138.9 (t, *J* = 1.5 Hz), 129.7 (t, *J* = 10.1 Hz), 129.3 (t, *J* = 1.4 Hz), 127.8, 127.2 (d, *J* = 0.9 Hz), 117.5 (t, *J* = 25.3 Hz), 112.4, 63.1, 13.9.

^{19}F NMR (376 MHz, $CDCl_3$) δ -102.97 (2F).

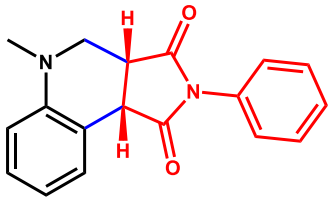

(6a)

Scheme 2. 19. The chemical structure of **6a**.

(3a*R,9b*S**)-5-Methyl-2-phenyl-3a,4,5,9b-tetrahydro-1H-pyrrolo[3,4-c]quinoline-1,3(2H)-dione (lit.[8]) (6a)**

^{1}H NMR (400 MHz, $CDCl_3$) δ 7.54 (d, *J* = 7.5 Hz, 1H), 7.44 (t, *J* = 7.5 Hz, 2H), 7.36 (t, *J* = 7.4 Hz, 1H), 7.26 (dd, *J* = 16.8, 8.0 Hz, 3H), 6.92 (t, *J* = 7.4 Hz, 1H), 6.76 (d, *J* = 8.2 Hz, 1H), 4.18 (d, *J* = 9.6 Hz, 1H), 3.63 (dd, *J* = 11.4, 2.7 Hz, 1H), 3.55 (ddd, *J* = 9.6, 4.2, 2.8 Hz, 1H), 3.14 (dd, *J* = 11.4, 4.4 Hz, 1H), 2.85 (s, 3H).

^{13}C NMR (101 MHz, $CDCl_3$) δ 177.6, 175.7, 148.4, 132.0, 130.3, 129.0, 128.7, 128.5, 126.3, 119.7, 118.5, 112.5, 50.6, 43.5, 42.1, 39.4.

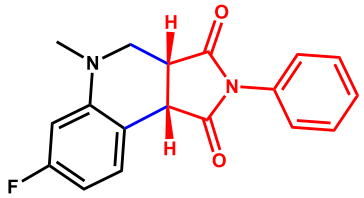

(6b-1)

Scheme 2. 20. The chemical structure of **6b-1**.

(3a*R,9b*S**)-7-Fluoro-5-methyl-2-phenyl-3a,4,5,9b-tetrahydro-1H-pyrrolo[3,4-c]quinoline-1,3(2H)-dione (6b-1):**

^{1}H NMR (400 MHz, $CDCl_3$) δ 7.53 – 7.41 (m, 3H), 7.37 (t, *J* = 7.4 Hz, 1H), 7.27 (dd, *J* = 6.1, 2.4 Hz, 2H), 6.60 (td, *J* = 8.3, 2.4 Hz, 1H), 6.50 – 6.38 (m, 1H), 4.14 (d, *J* = 9.6 Hz, 1H), 3.68 – 3.60 (m, 1H), 3.55 (ddd, *J* = 9.6, 4.3, 2.9 Hz, 1H), 3.16 (d, *J* = 15.9 Hz, 1H), 2.84 (s, 3H).

^{13}C NMR (101 MHz, $CDCl_3$) δ 177.3, 175.6 (d, *J* = 1.5 Hz), 164.6, 162.1, 149.9, 149.8, 131.8, 131.5 (d, *J* = 10.0 Hz), 129.0, 128.6, 126.3, 113.8 (d, *J* = 2.9 Hz), 106.1 (d, *J* = 21.9 Hz), 100.1 (d, *J* = 26.1 Hz), 50.1, 43.1, 41.4, 39.4.

^{19}F NMR (376 MHz, $CDCl_3$) δ -112.62 (1F).

HRMS (ESI) (m/z): $[M+H]^+$ calcd. for $C_{18}H_{16}FN_2O_2$: 311.1118, found: 311.1192.

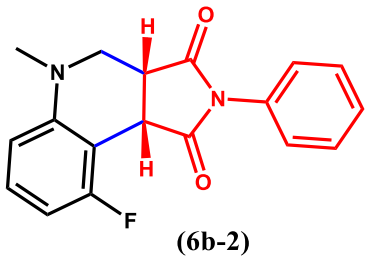

(6b-2)

Scheme 2. 21. The chemical structure of **6b-2**.

(3a*R,9b*S**)-9-Fluoro-5-methyl-2-phenyl-3a,4,5,9b-tetrahydro-1H-pyrrolo[3,4-c]quinoline-1,3(2H)-dione (6b-2)**

^{1}H NMR (400 MHz, $CDCl_3$) δ 7.45 (t, *J* = 7.5 Hz, 2H), 7.37 (t, *J* = 7.4 Hz, 1H), 7.34 – 7.27 (m, 2H), 7.19 (dd, *J* = 14.7, 8.2 Hz, 1H), 6.70 (t, *J* = 8.6 Hz, 1H), 6.55 (d, *J* = 8.3 Hz, 1H), 4.60 (d, *J* = 9.7 Hz, 1H), 3.67 – 3.60 (m, 1H), 3.55 (ddd, *J* = 9.8, 4.6, 2.0 Hz, 1H), 3.11 – 3.02 (m, 1H), 2.84 (s, 3H).

^{13}C NMR (101 MHz, $CDCl_3$) δ 177.6, 174.4, 163.1, 160.7, 150.8, 150.8, 131.9, 129.3 (d, *J* = 10.3 Hz), 129.0, 128.5, 126.3, 108.2 (d, *J* = 2.8 Hz), 107.0, 106.8, 51.7, 43.4, 39.7, 36.5.

^{19}F NMR (376 MHz, $CDCl_3$) δ -116.78 (1F).

HRMS (ESI) (m/z): $[M+H]^+$calcd. for $C_{18}H_{16}FN_2O_2$: 311.1118, found: 311.1192.

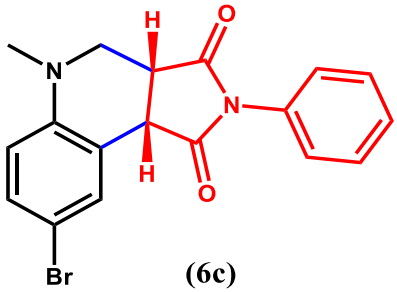

(6c)

Scheme 2. 22. The chemical structure of **6c**.

(3a*R,9b*S**)-8-Bromo-5-methyl-2-phenyl-3a,4,5,9b-tetrahydro-1H-pyrrolo[3,4-c]quinoline-1,3(2H)-dione (lit.[8]) (6c)**

^{1}H NMR (400 MHz, $CDCl_3$) δ 7.67 (d, *J* = 2.0 Hz, 1H), 7.46 (t, *J* = 7.5 Hz, 2H), 7.43 – 7.25 (m, 4H), 6.63 (d, *J* = 8.8 Hz, 1H), 4.13 (d, *J* = 9.6 Hz, 1H), 3.63 (dd, *J* = 11.5, 2.7 Hz, 1H), 3.56 (ddd, *J* = 9.5, 4.2, 2.9 Hz, 1H), 3.13 (dd, *J* = 11.5, 4.4 Hz, 1H), 2.84 (s, 3H).

^{13}C NMR (101 MHz, $CDCl_3$) δ 177.1, 175.1, 147.4, 132.7,131.8, 131.4, 129.1, 128.6, 126.1, 120.3, 114.2, 111.7, 50.3, 43.3, 41.8, 39.4.

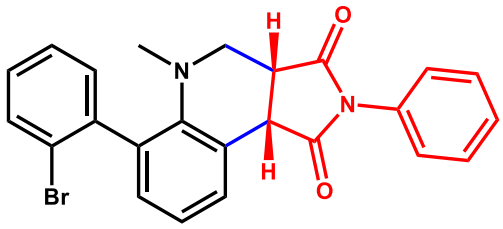

(6d)

Scheme 2. 23. The chemical structure of **6d**.

(3a*R,9b*S**)-6-(2-Bromophenyl)-5-methyl-2-phenyl-3a,4,5,9b-tetrahydro-1H-pyrrolo[3,4-c]quinoline -1,3(2H)-dione (6d)**

^{1}H NMR (400 MHz, $CDCl_3$) δ 7.84 – 7.63 (m, 2H), 7.54 – 7.45 (m, 2H), 7.45 – 7.27 (m, 5H), 7.27 – 7.08 (m, 3H), 4.25 (t, *J* = 9.4 Hz, 1H), 3.56 (tdd, *J* = 17.5, 12.8, 5.0 Hz, 2H), 3.49 – 3.38 (m, 1H), 2.43 (s, 3H).

^{13}C NMR (101 MHz, $CDCl_3$) δ 177.8, 175.8, 146.1, 141.4, 134.9, 134.2, 132.6, 132.0, 131.6, 131.1, 130.8, 130.5, 129.1, 128.6, 127.2, 126.2, 124.2, 122.8,122.6, 122.4, 50.8, 42.2, 41.0, 39.4.

HRMS (ESI) (m/z): $[M+H]^+$ calcd. for $C_{24}H_{20}BrN_2O_2$: 447.0630, found: 447.0705.

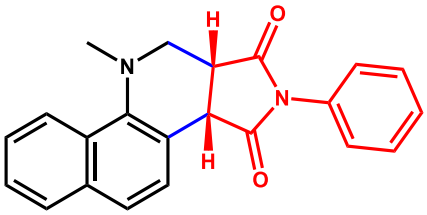

(6e)

Scheme 2. 24. The chemical structure of **6e**.

(3a*R,9b*S**)-10-methyl-2-phenyl-3a,10,11,11a-tetrahydro-1H-benzo[h]pyrrolo[3,4-c]quinoline-1,3(2H)-dione (6e)**

^{1}H NMR (400 MHz, $CDCl_3$) δ 8.19 (d, *J* = 8.3 Hz, 1H), 7.84 (dd, *J* = 8.0, 4.1 Hz, 2H), 7.65 (d, *J* = 8.6 Hz, 1H), 7.57 – 7.44 (m, 5H), 7.40 (t, *J* = 7.4 Hz, 1H), 7.29 (s, 1H), 4.32 (d, *J* = 8.5 Hz, 1H), 3.73 – 3.62 (m, 3H), 3.58 – 3.49 (m, 1H), 3.01 (s, 3H).

^{13}C NMR (101 MHz, $CDCl_3$) δ 177.6, 175.5, 144.5, 133.9, 131.9, 129.1, 128.6, 128.5, 128.3, 127.5, 126.3,126.2, 125.9, 124.2, 123.6, 119.3, 51.1, 43.9, 41.7, 38.3.

HRMS (ESI) (m/z): $[M+H]^+$ calcd. for $C_{22}H_{19}N_2O_2$: 343.1368, found: 343.1443

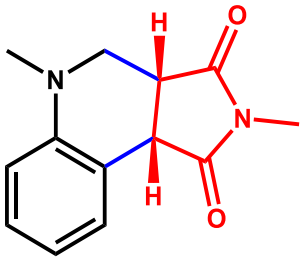

(6f)

Scheme 2. 25. The chemical structure of **6f**.

(3a*R,9b*S**)-2,5-Dimethyl-3a,4,5,9b-tetrahydro-1H-pyrrolo[3,4-c]quinoline-1,3(2H)-dione (lit.[8]) (6f)**

^{1}H NMR (400 MHz, $CDCl_3$) δ 7.49 (d, *J* = 7.5 Hz, 1H), 7.22 (t, *J* = 7.8 Hz, 1H), 6.90 (t, *J* = 7.2 Hz, 1H), 6.71 (d, *J* = 8.2 Hz, 1H), 4.01 (d, *J* = 9.5 Hz, 1H), 3.54 (dd, *J* = 11.5, 2.4 Hz, 1H), 3.37 (ddd, *J* = 9.4, 4.3, 2.4 Hz, 1H), 3.05 (dd, *J* = 11.5, 4.5 Hz, 1H), 3.00 (s, 3H), 2.80 (s, 3H).

^{13}C NMR (101 MHz, $CDCl_3$) δ 178.7, 176.8, 148.4, 130.1, 128.5, 119.6, 118.7, 112.4, 50.4, 43.6, 42.0, 39.4, 25.3.

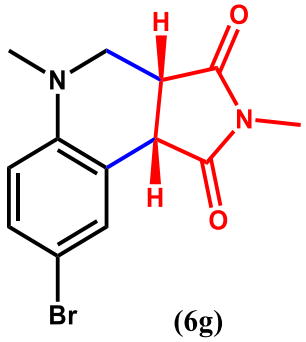

(6g)

Scheme 2. 26. The chemical structure of **6g**.

(3a*R,9b*S**)-8-bromo-2,5-dimethyl-3a,4,5,9b-tetrahydro-1H-pyrrolo[3,4-c]quinoline-1,3(2H)-dione (lit.[8]) (6g)**

^{1}H NMR (400 MHz, $CDCl_3$) δ 7.60 (d, *J* = 2.1 Hz, 1H), 7.29 (dd, *J* = 8.7, 2.3 Hz, 1H), 6.57 (d, *J* = 8.8 Hz, 1H), 3.95 (d, *J* = 9.5 Hz, 1H), 3.53 (dd, *J* = 11.5, 2.5 Hz, 1H), 3.37 (ddd, *J* = 9.3, 4.2, 2.6 Hz, 1H), 3.04 (d, *J* = 4.5 Hz, 1H), 3.00 (s, 3H), 2.78 (s, 3H).

^{13}C NMR (101 MHz, $CDCl_3$) δ 178.2, 176.1, 147.4, 132.6, 131.3, 120.5, 114.1, 111.6, 50.2, 43.3, 41.7, 39.4, 25.4.

2.12. NMR Spectra

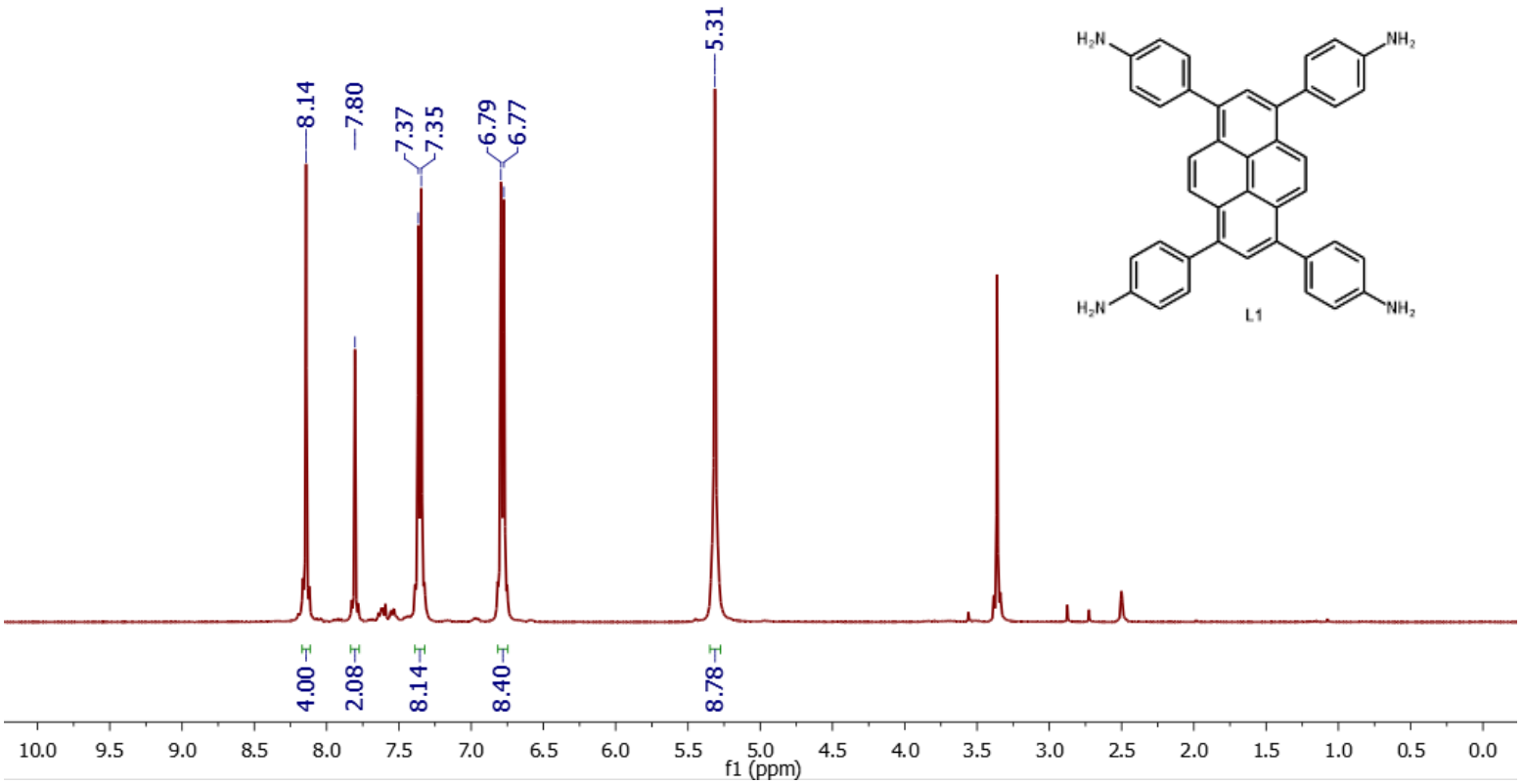

Figure 2. 19. ^{1}H NMR (400 MHz) of **L1** in DMSO-d_6.

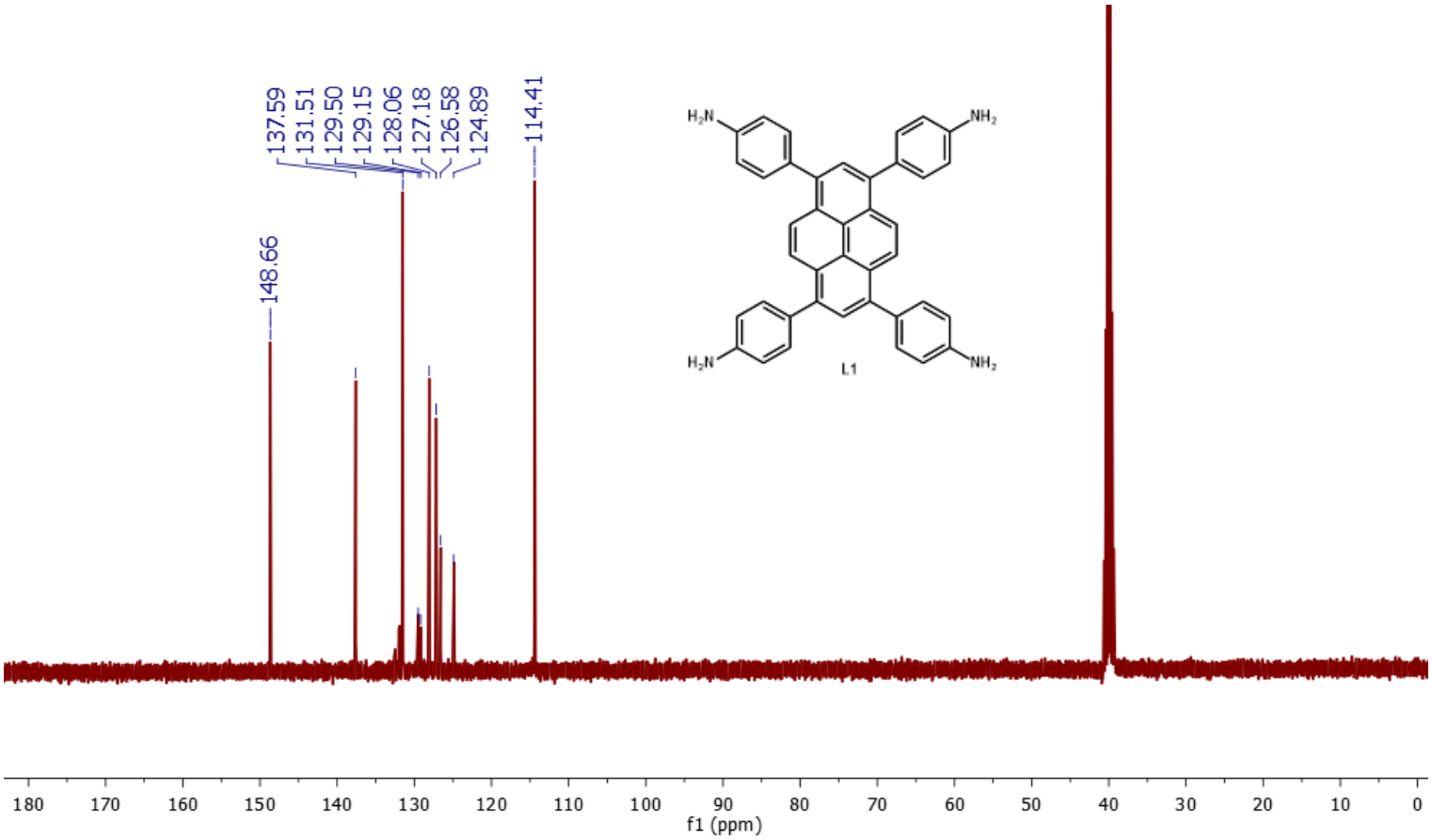

Figure 2. 20. ^{13}C NMR (101 MHz) of **L1** in DMSO-d_6.

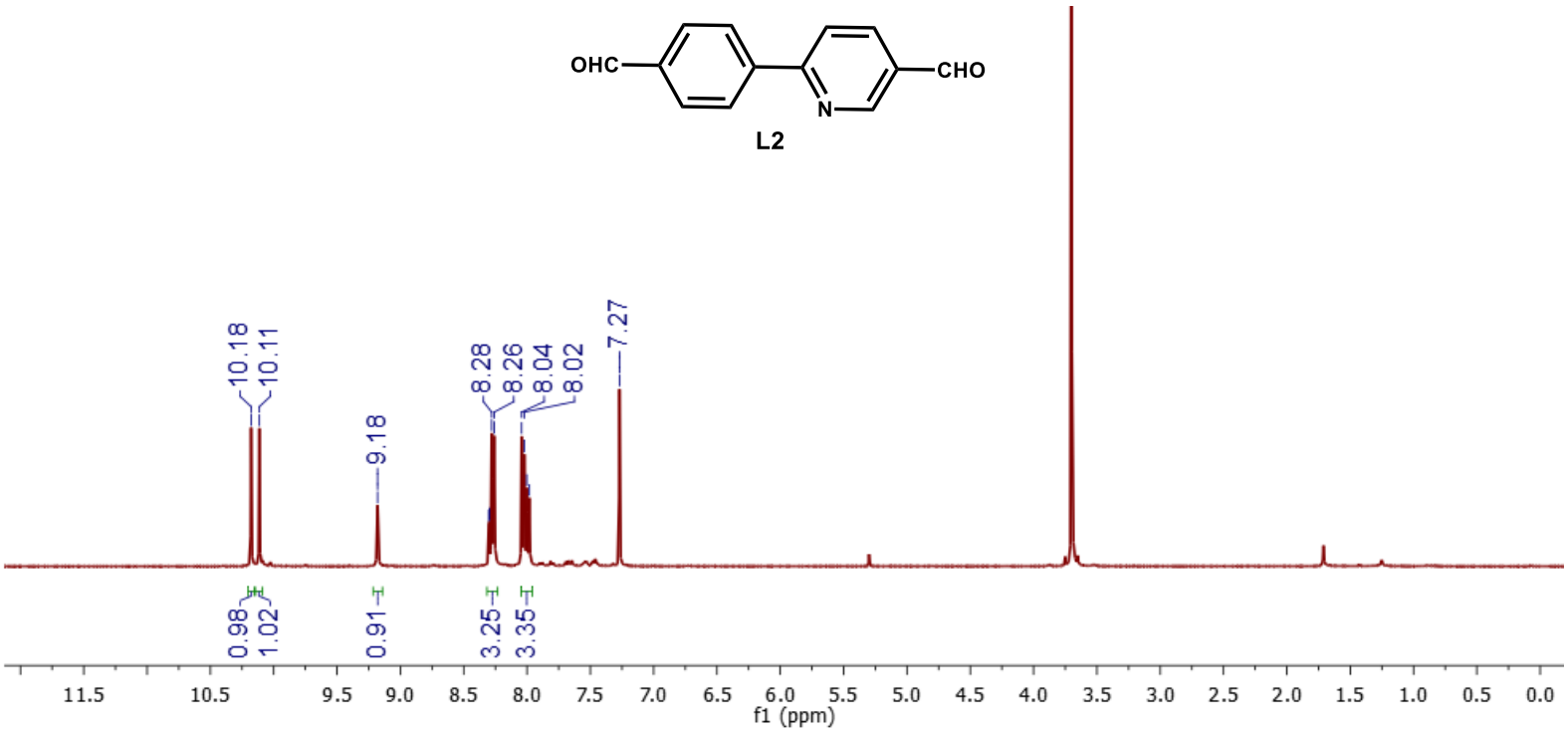

Figure 2. 21. ^{1}H NMR (400 MHz) of **L2** in $CDCl_3$.

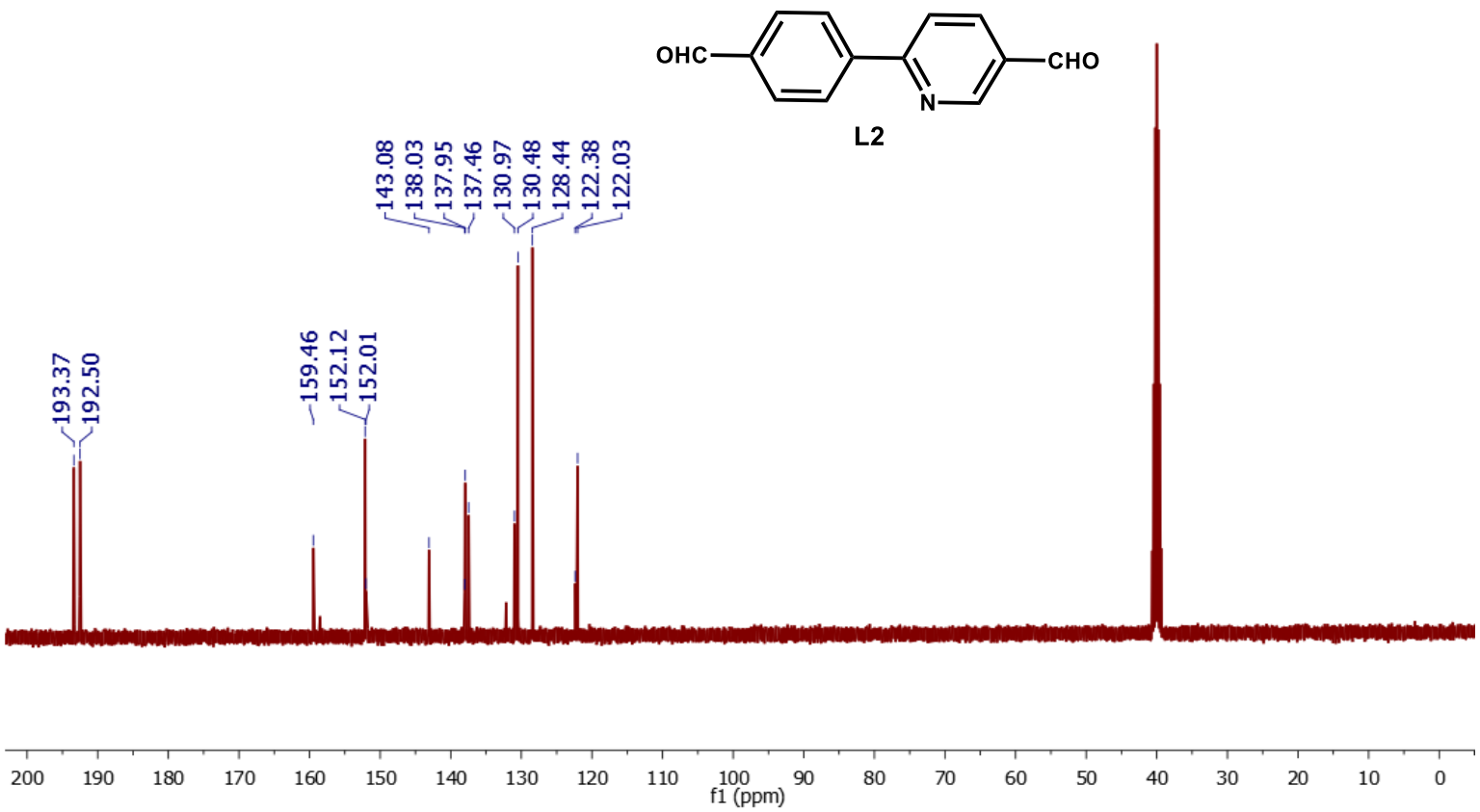

Figure 2. 22.^{13}C NMR (101 MHz) of **L2** in DMSO-d_6.

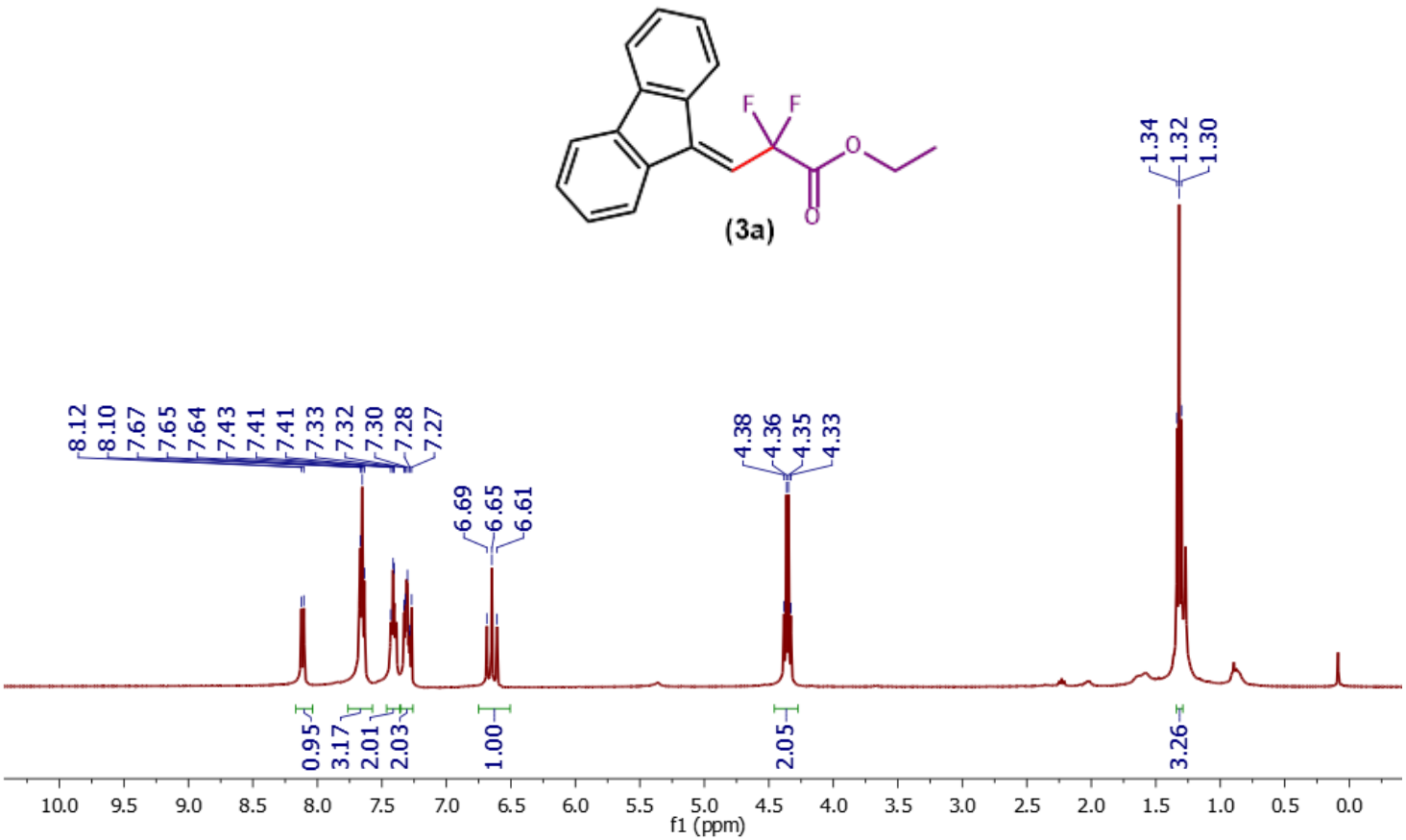

Figure 2. 23. ^{1}H NMR (400 MHz) of **3a** in $CDCl_3$.

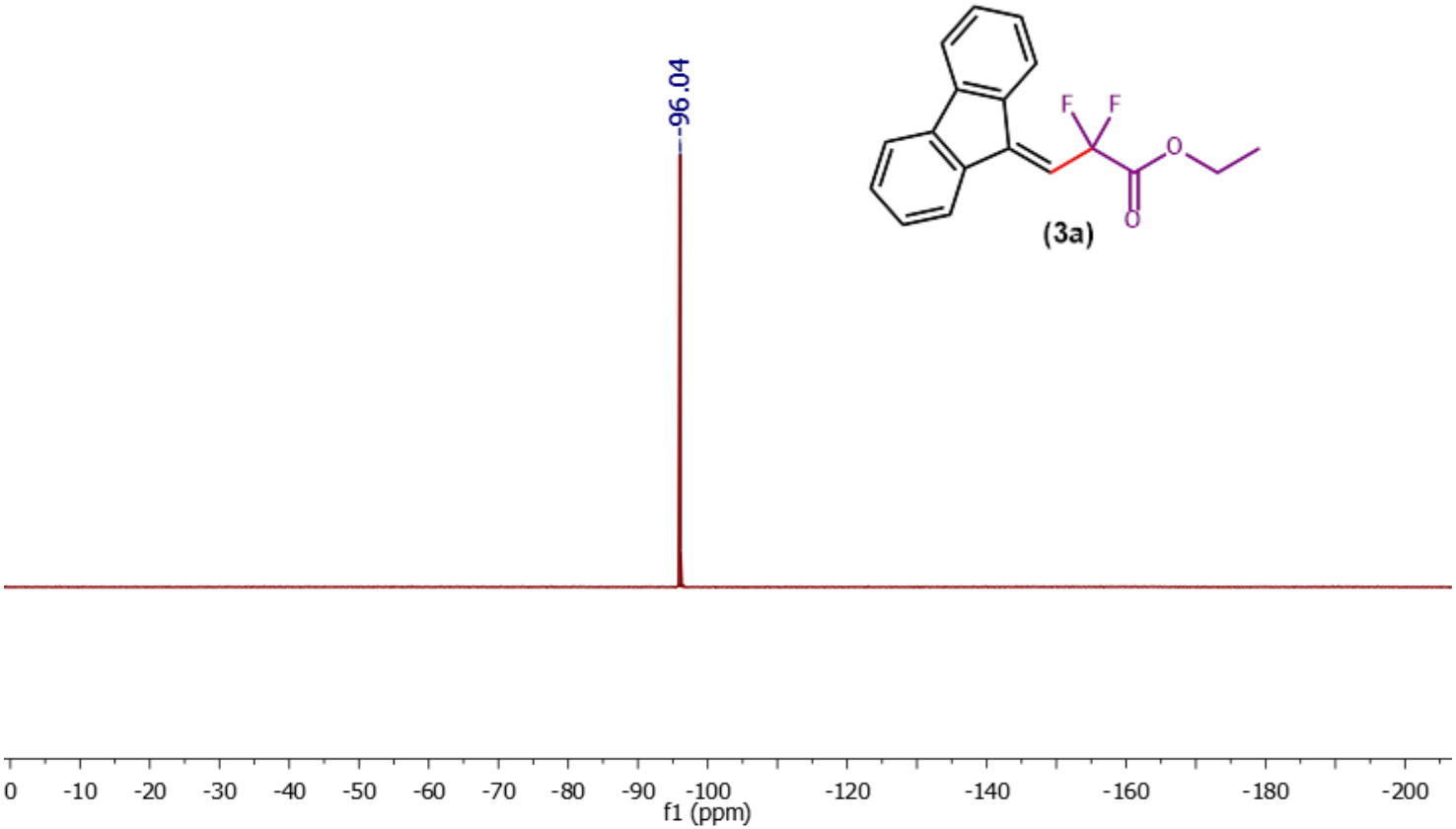

Figure 2. 24. ^{19}F NMR (376 MHz) of **3a** in $CDCl_3$.

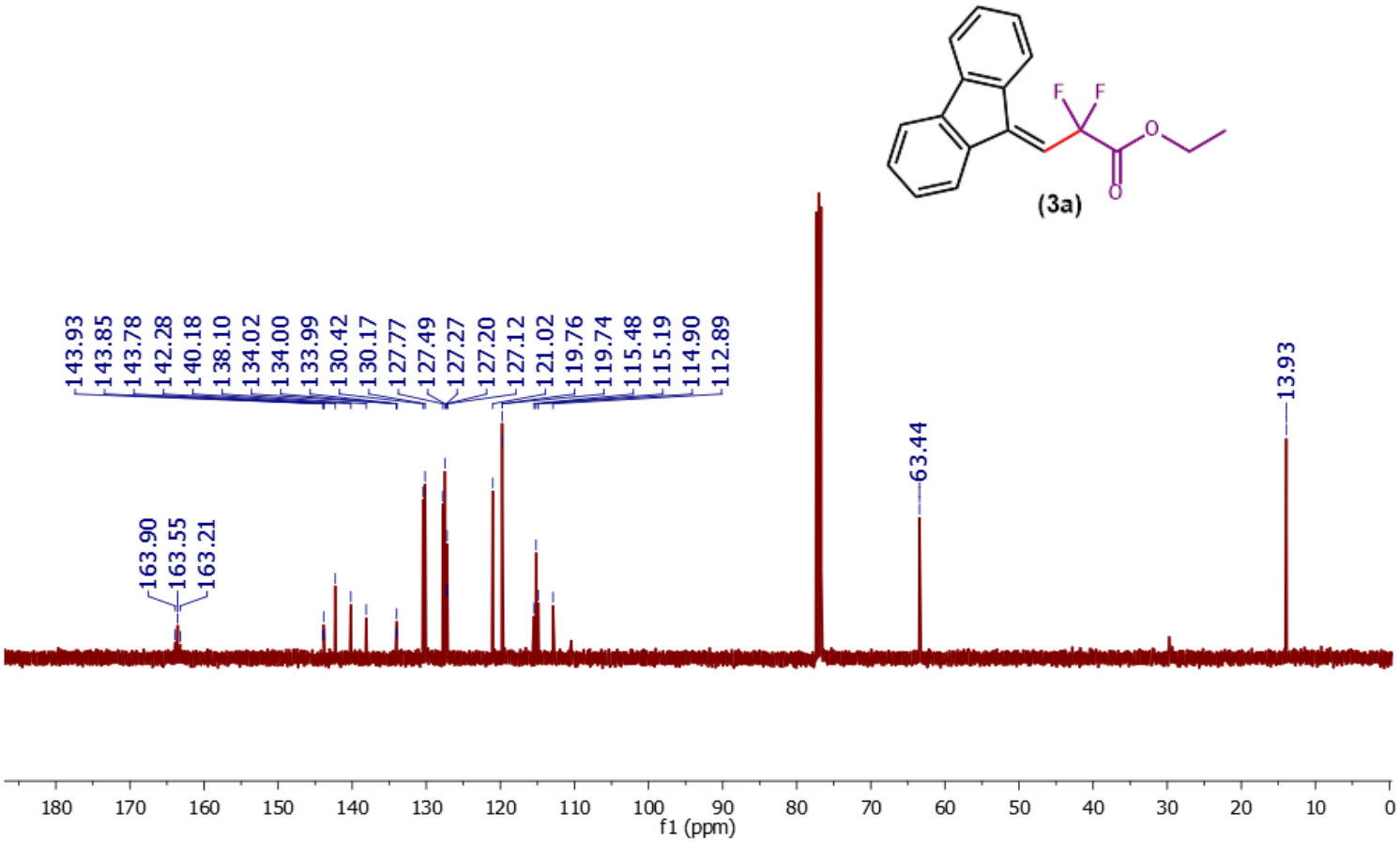

Figure 2. 25. ^{13}C NMR (101 MHz) of **3a** in $CDCl_3$.

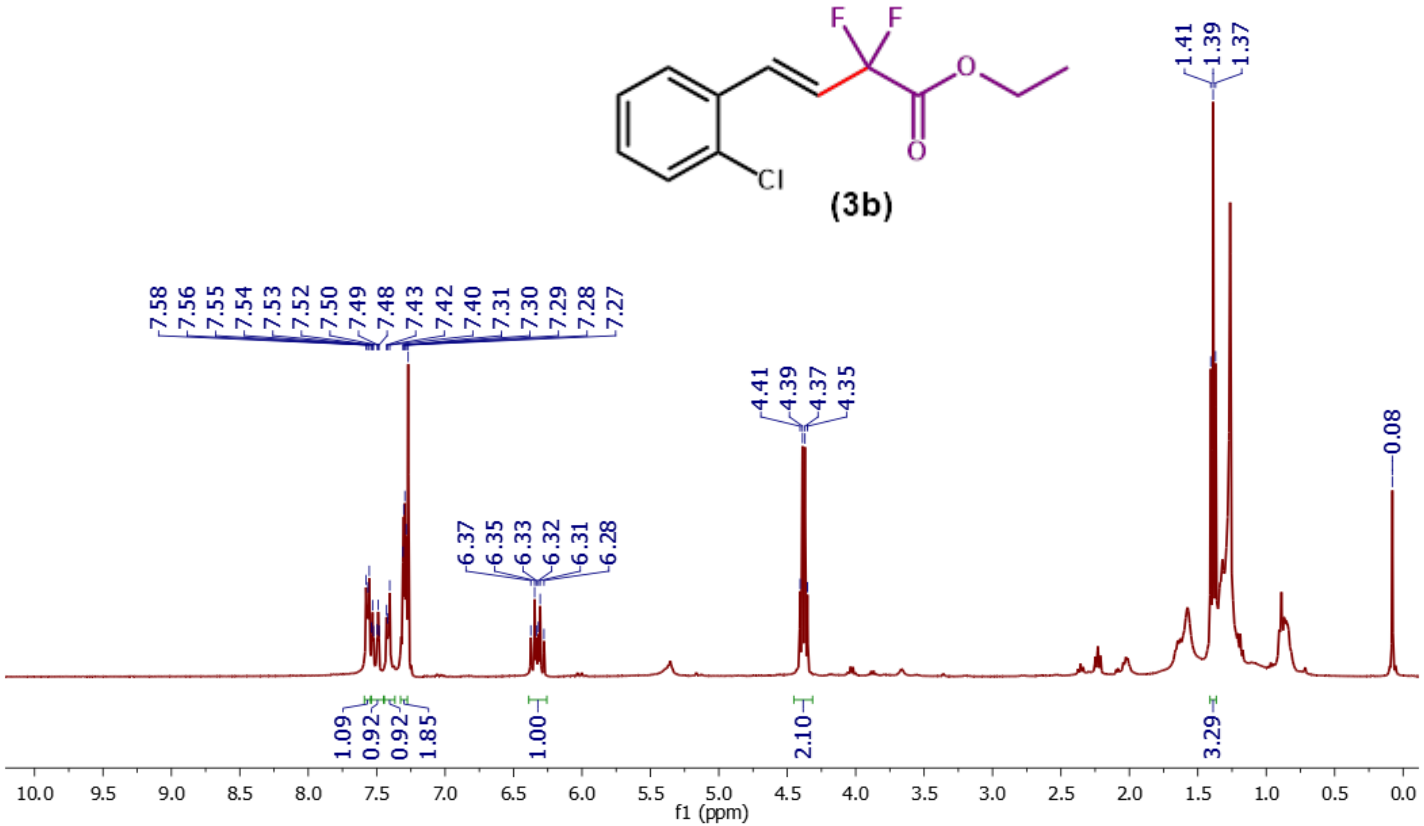

Figure 2. 26. ^{1}H NMR (400 MHz) of **3b** in $CDCl_3$.

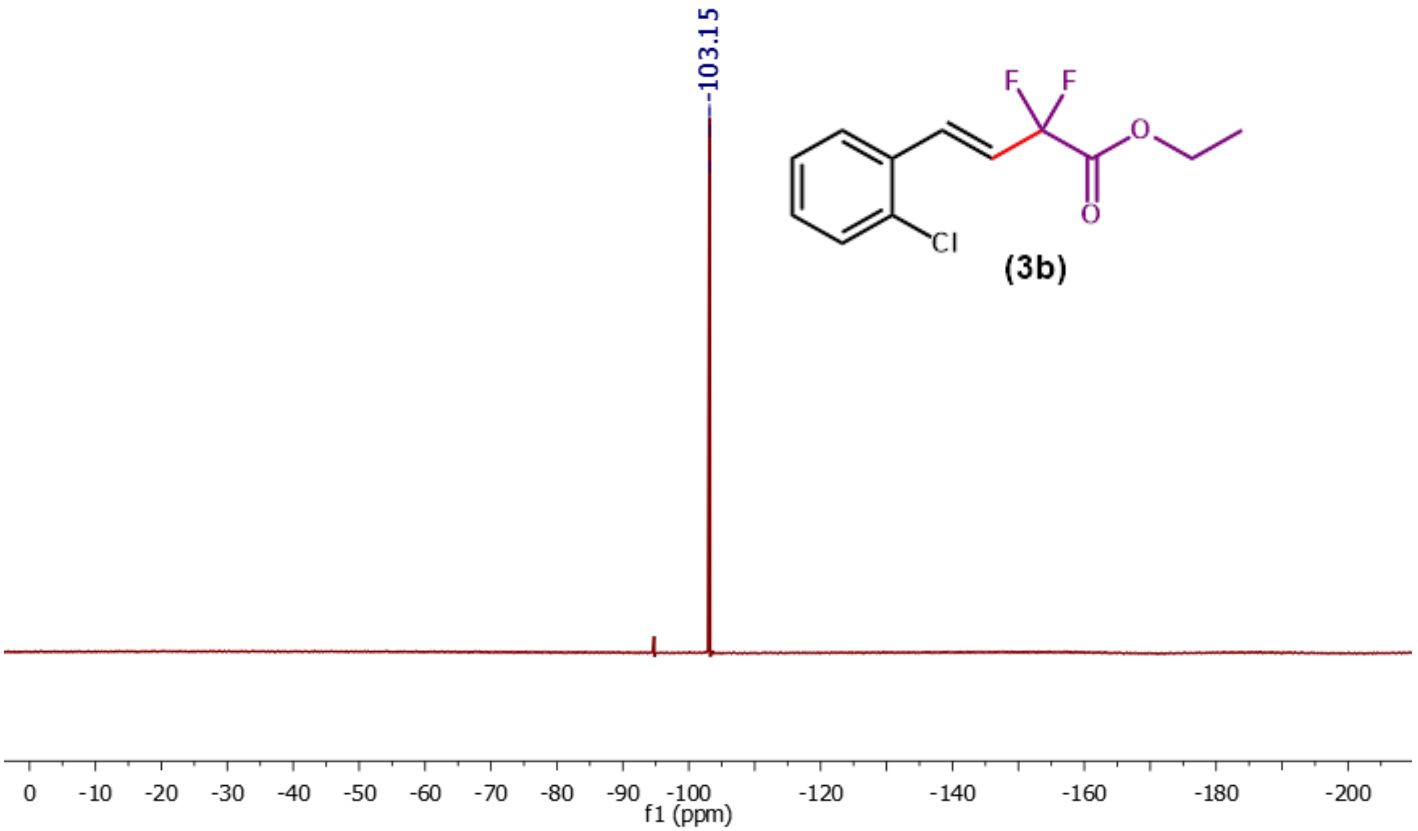

Figure 2. 27. ^{19}F NMR (376 MHz) of **3b** in $CDCl_3$.

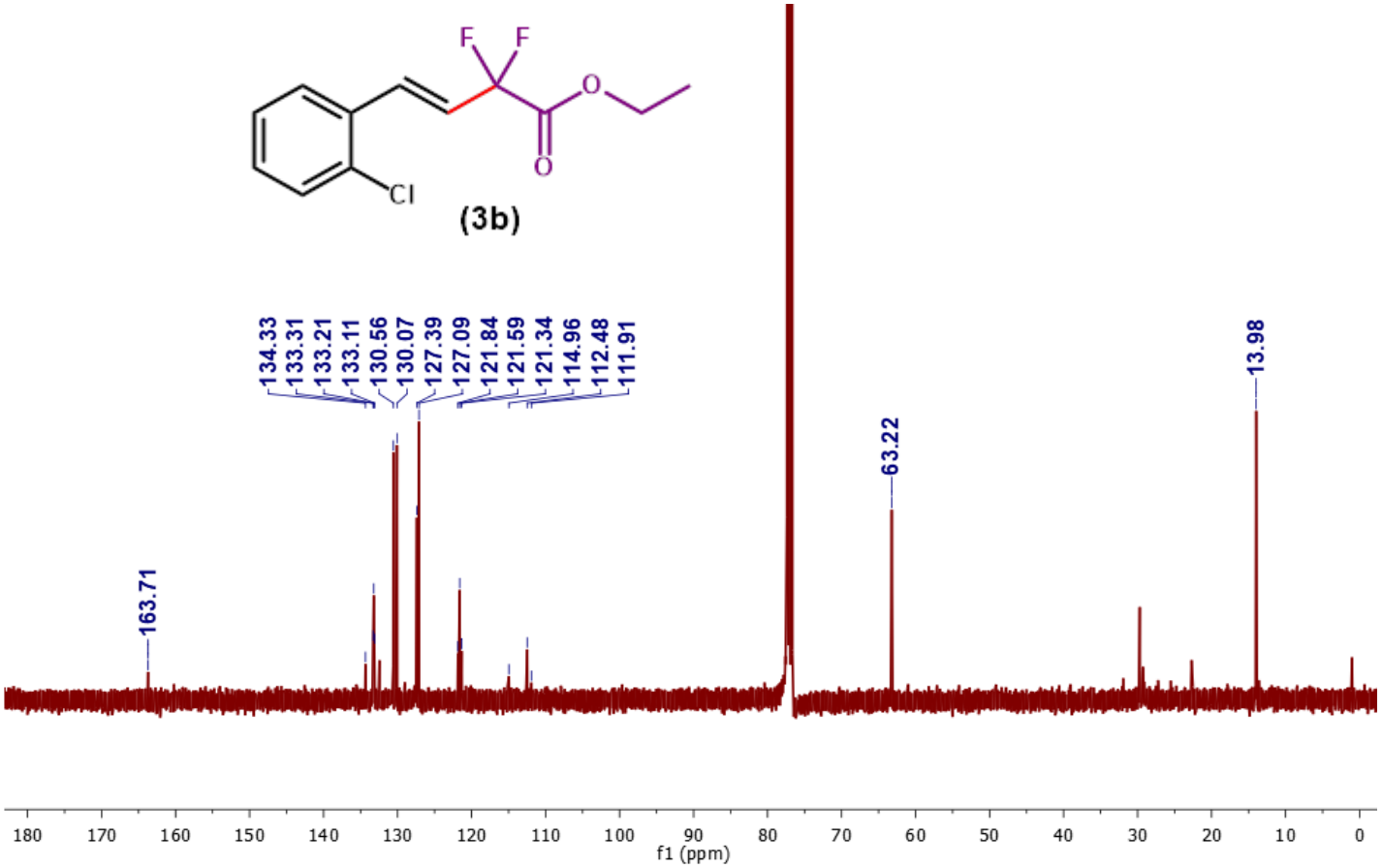

Figure 2. 28. ^{13}C NMR (101 MHz) of **3b** in $CDCl_3$.

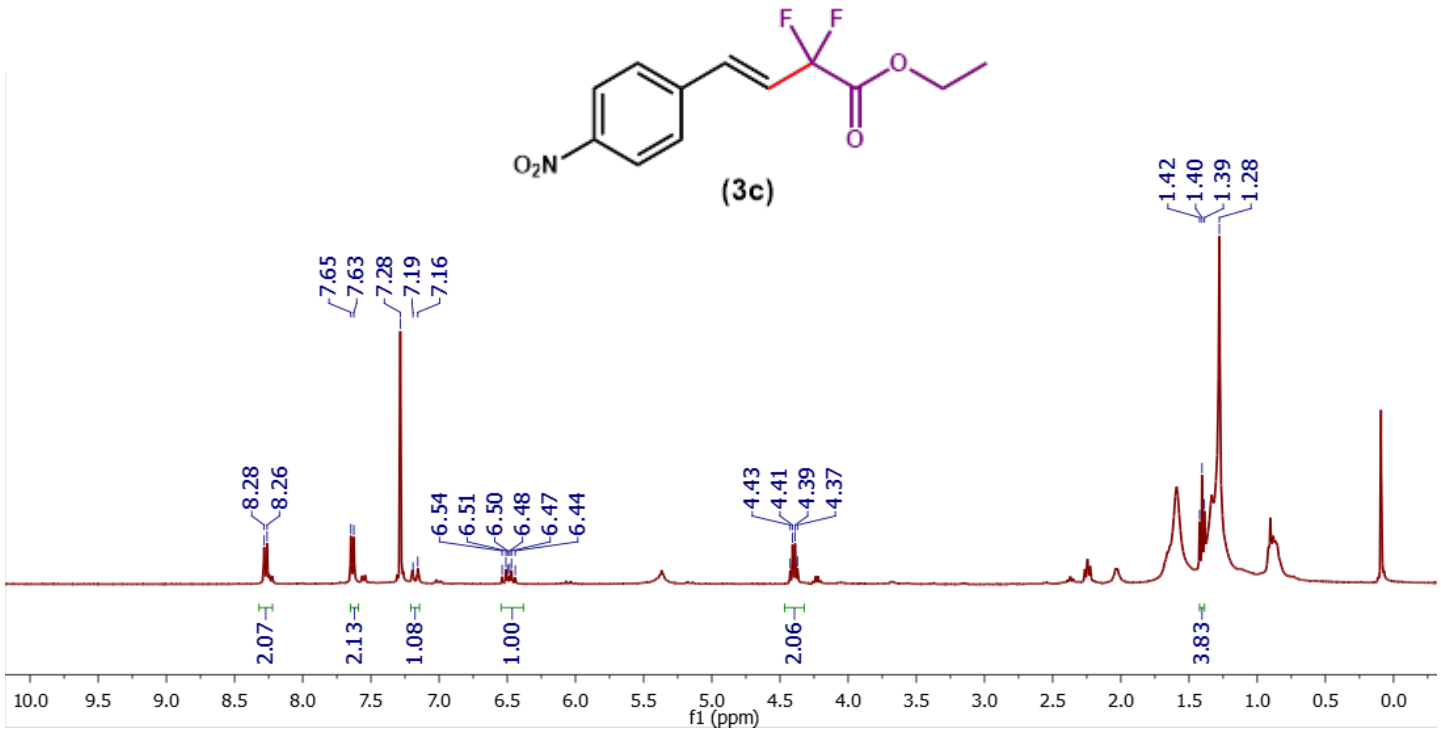

Figure 2. 29. ^{1}H NMR (400 MHz) of **3c** in $CDCl_3$.

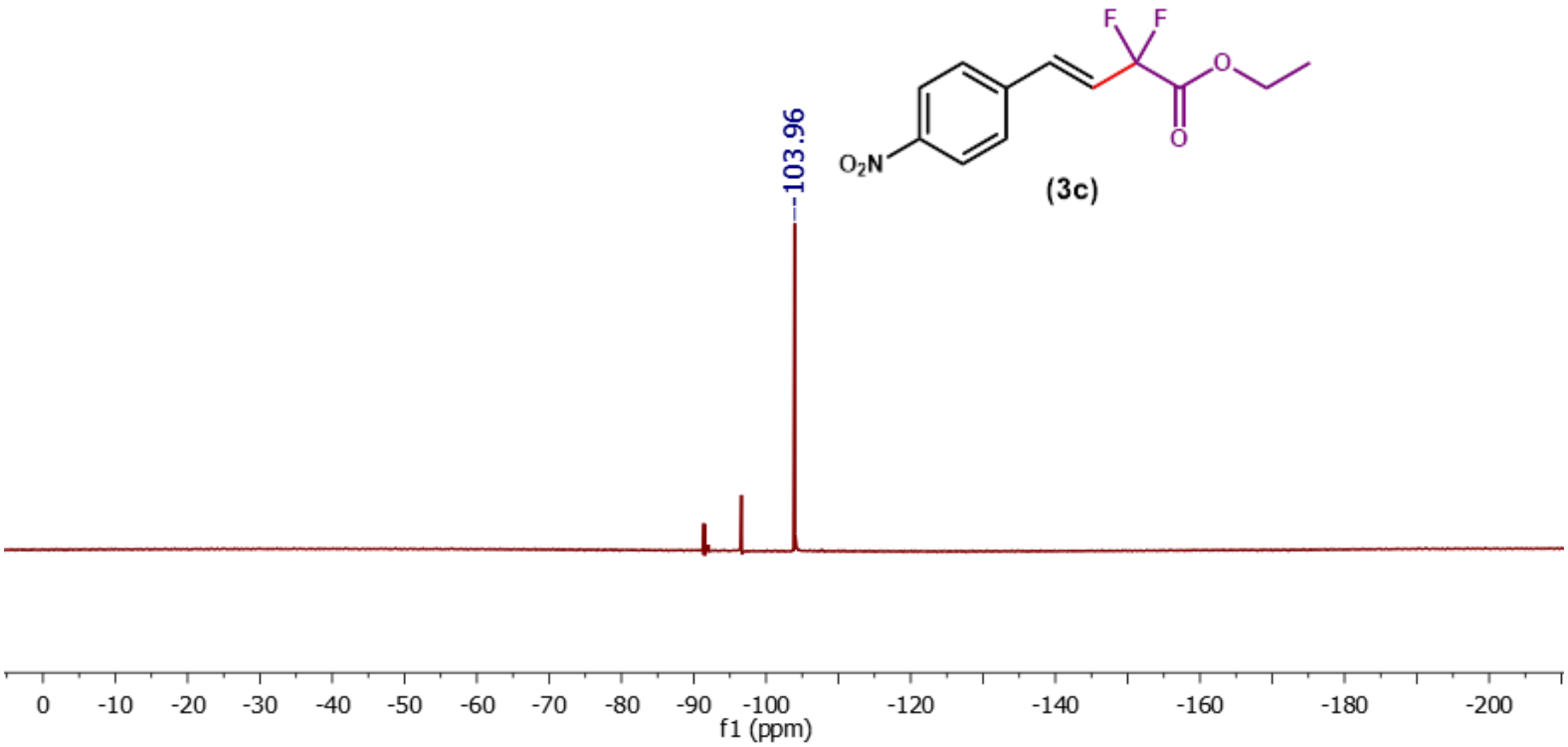

Figure 2. 30. ^{19}F NMR (376 MHz) of **3c** in $CDCl_3$.

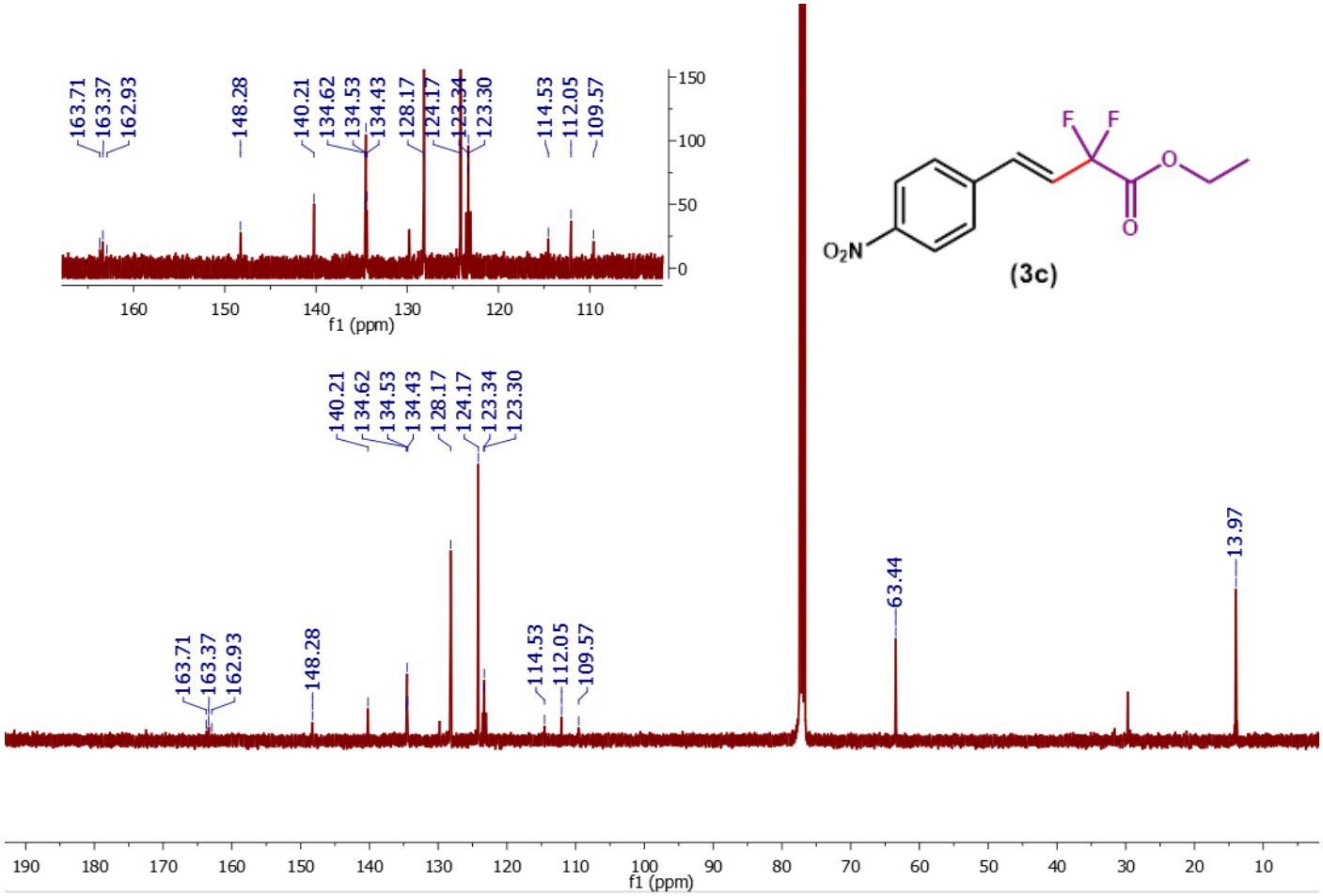

Figure 2. 31. ^{13}C NMR (101 MHz) of **3c** in $CDCl_3$.

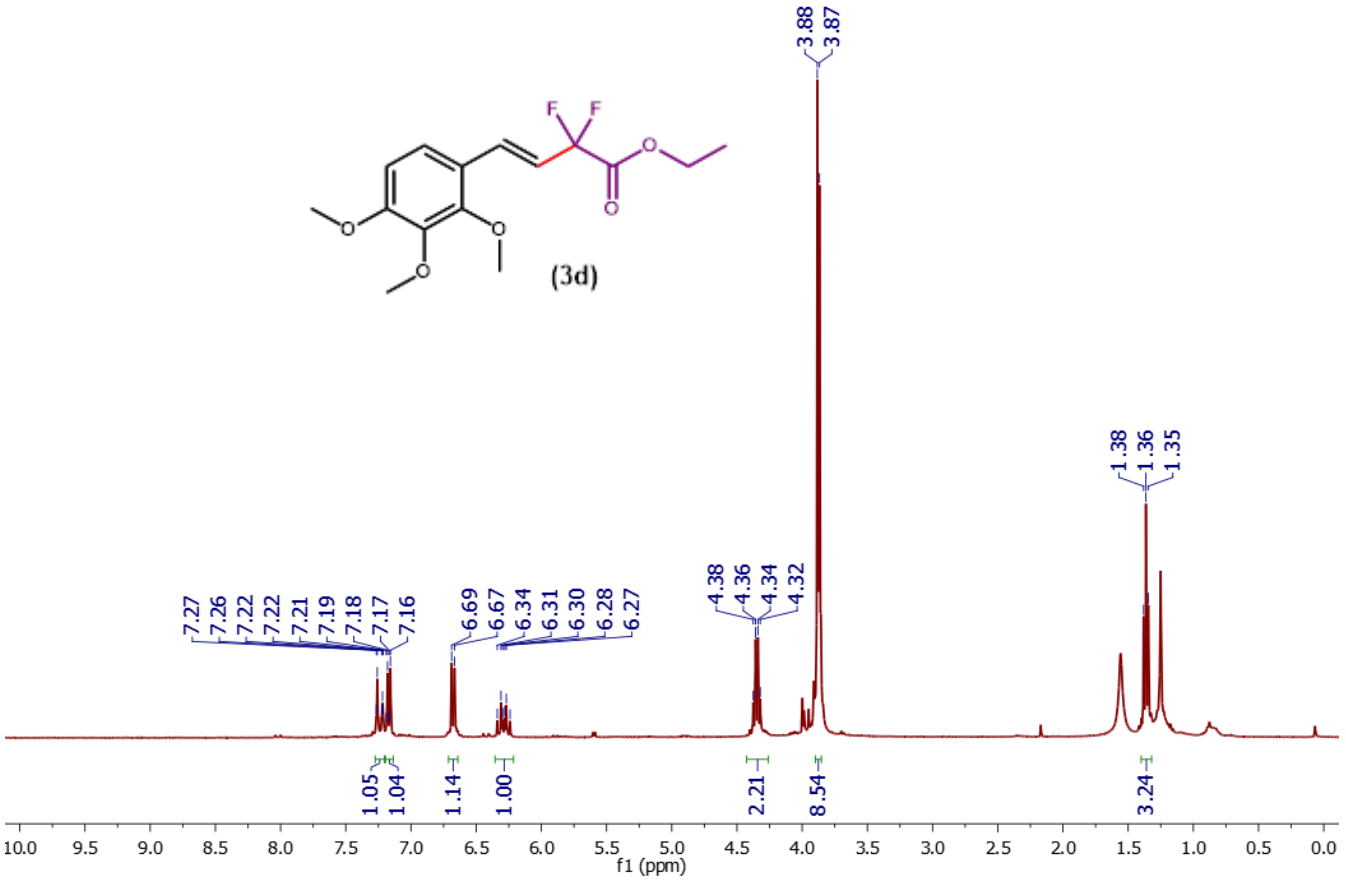

Figure 2. 32.[1]H NMR (400 MHz) of **3d** in $CDCl_3$.

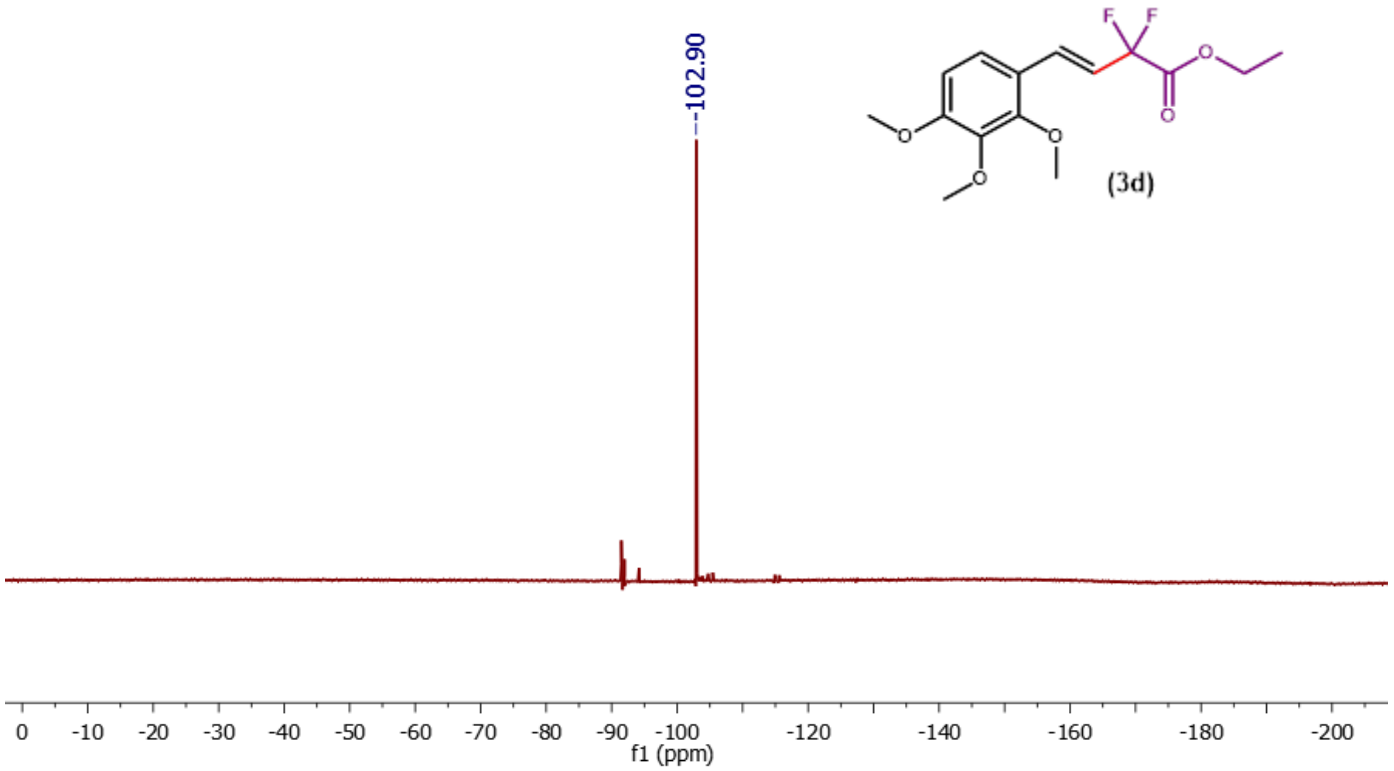

Figure 2. 33.^{19}F NMR (376 MHz) of **3d** in $CDCl_3$.

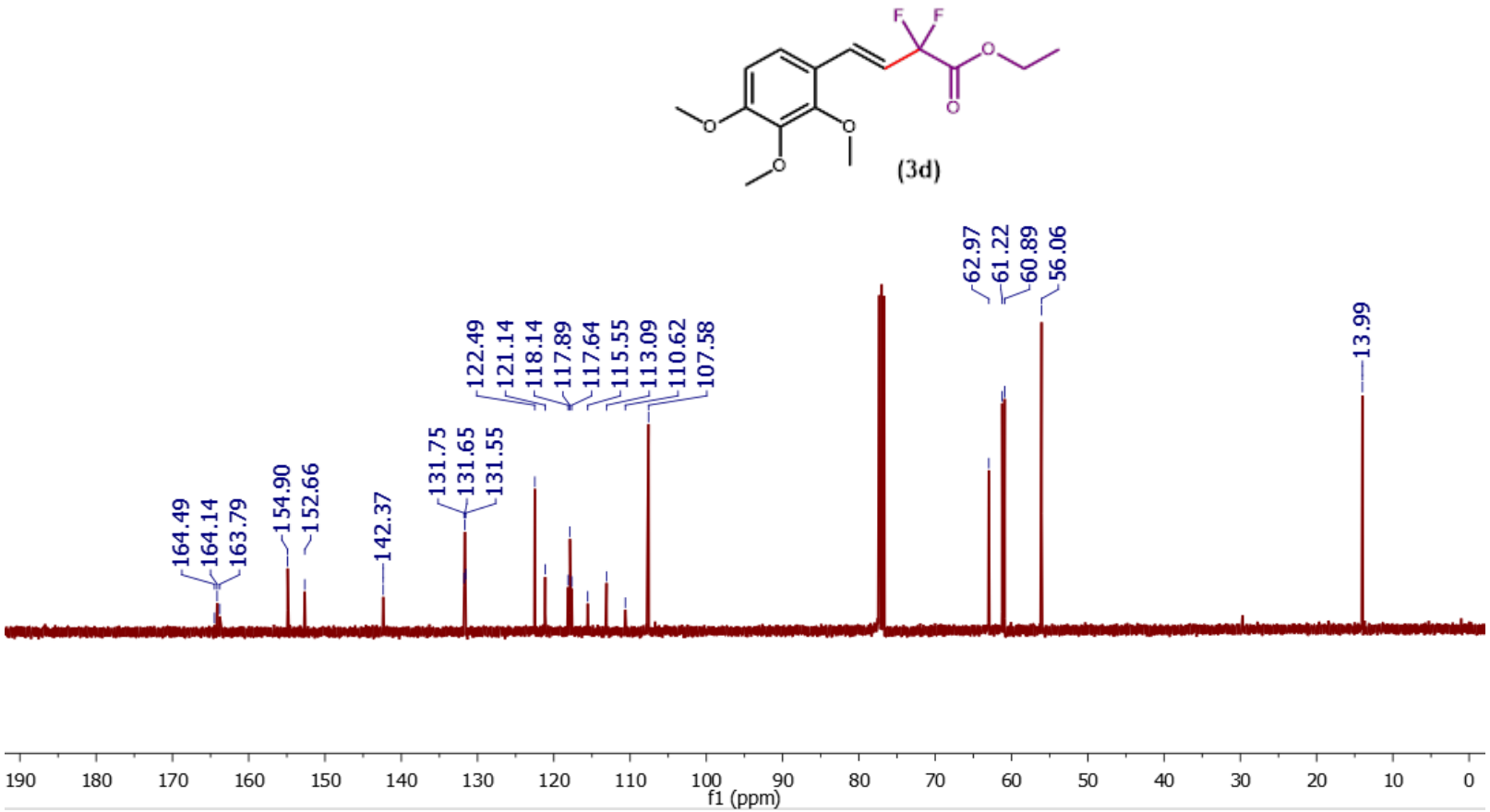

Figure 2. 34.^{13}C NMR (101 MHz) of **3d** in $CDCl_3$.

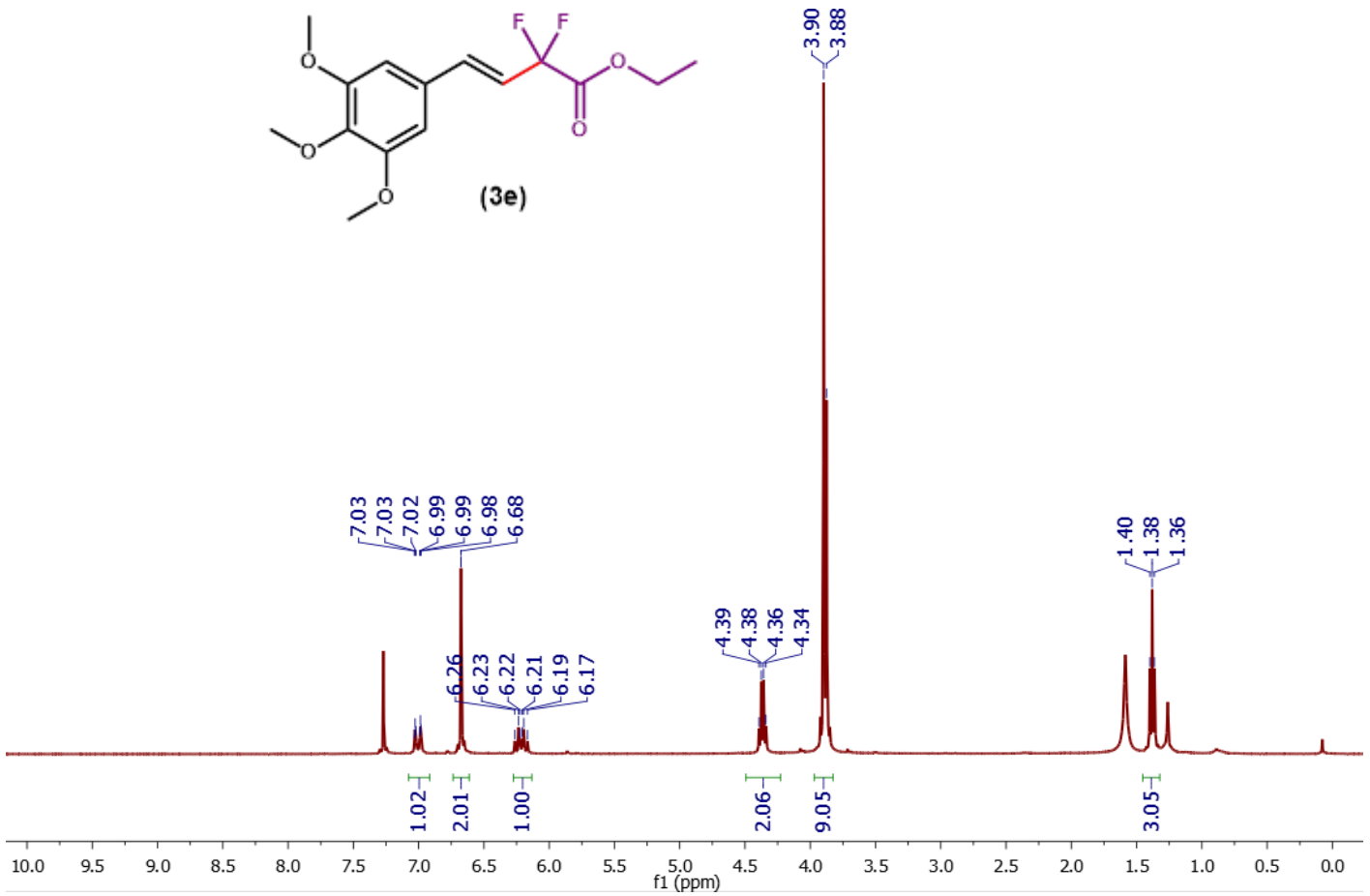

Figure 2. 35. ^{1}H NMR (400 MHz) of **3e** in $CDCl_3$.

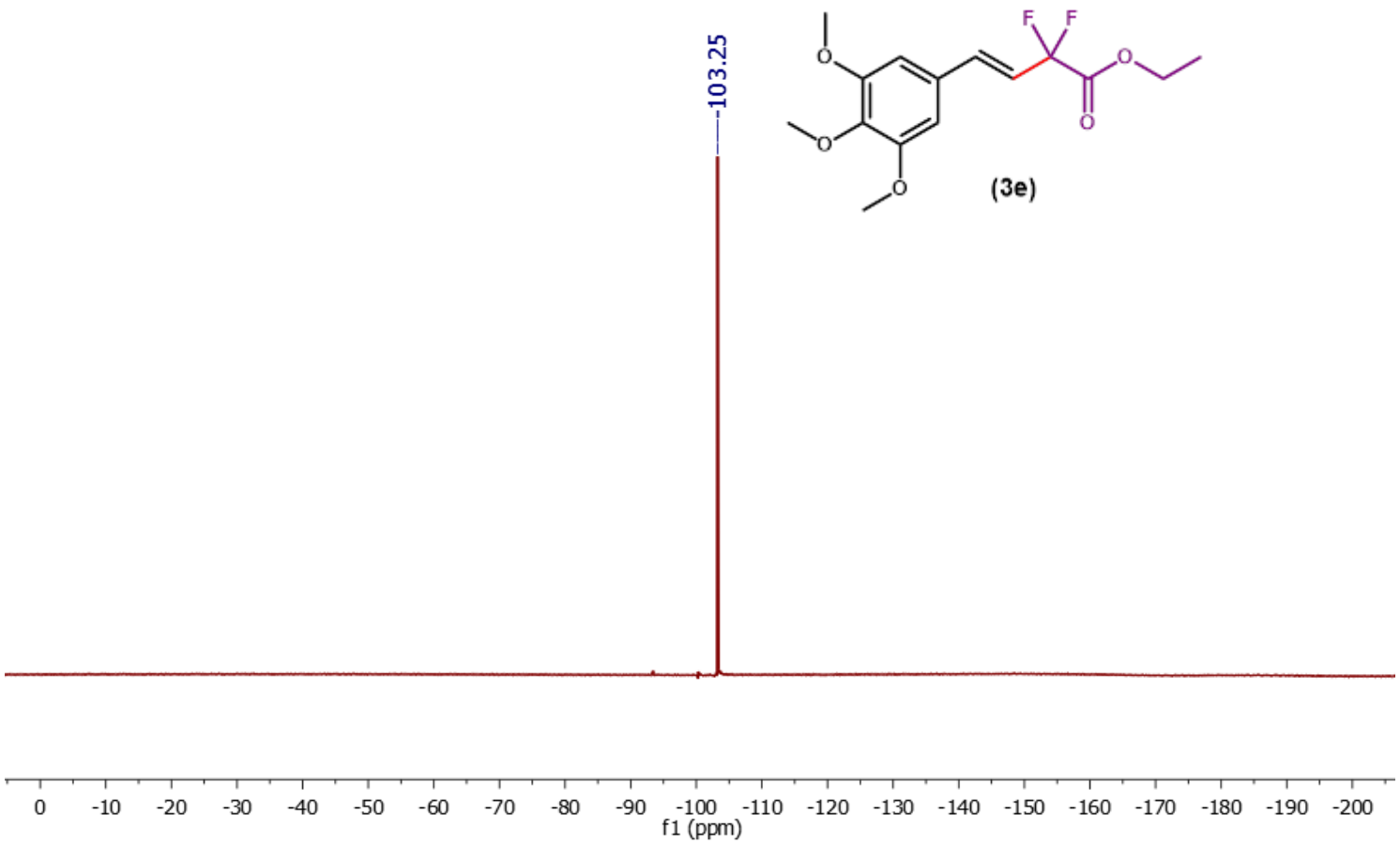

Figure 2. 36. ^{19}F NMR (376 MHz) of **3e** in $CDCl_3$.

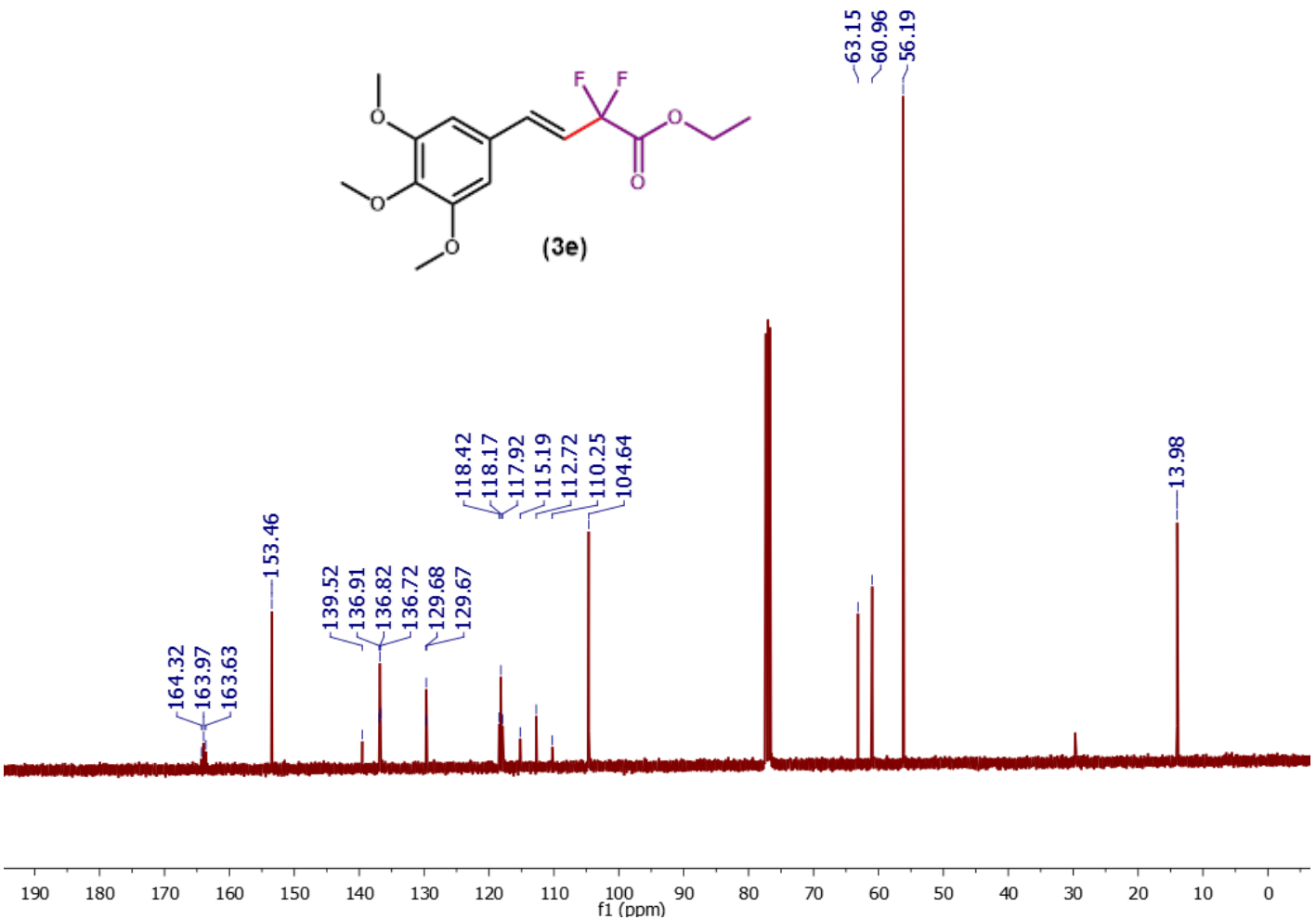

Figure 2. 37. ^{13}C NMR (101 MHz) of **3e** in $CDCl_3$.

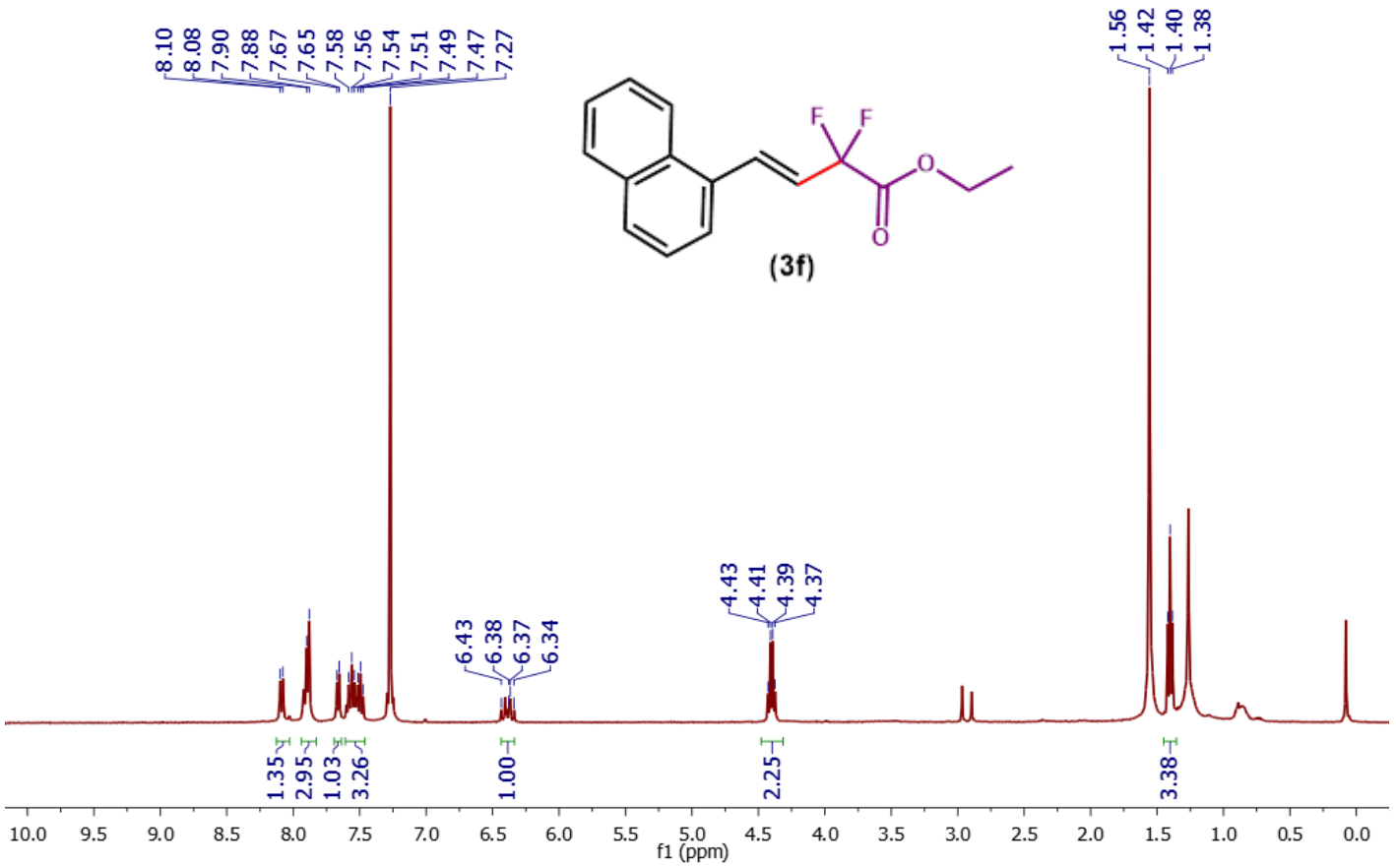

Figure 2. 38. ^{1}H NMR (400 MHz) of **3f** in $CDCl_3$.

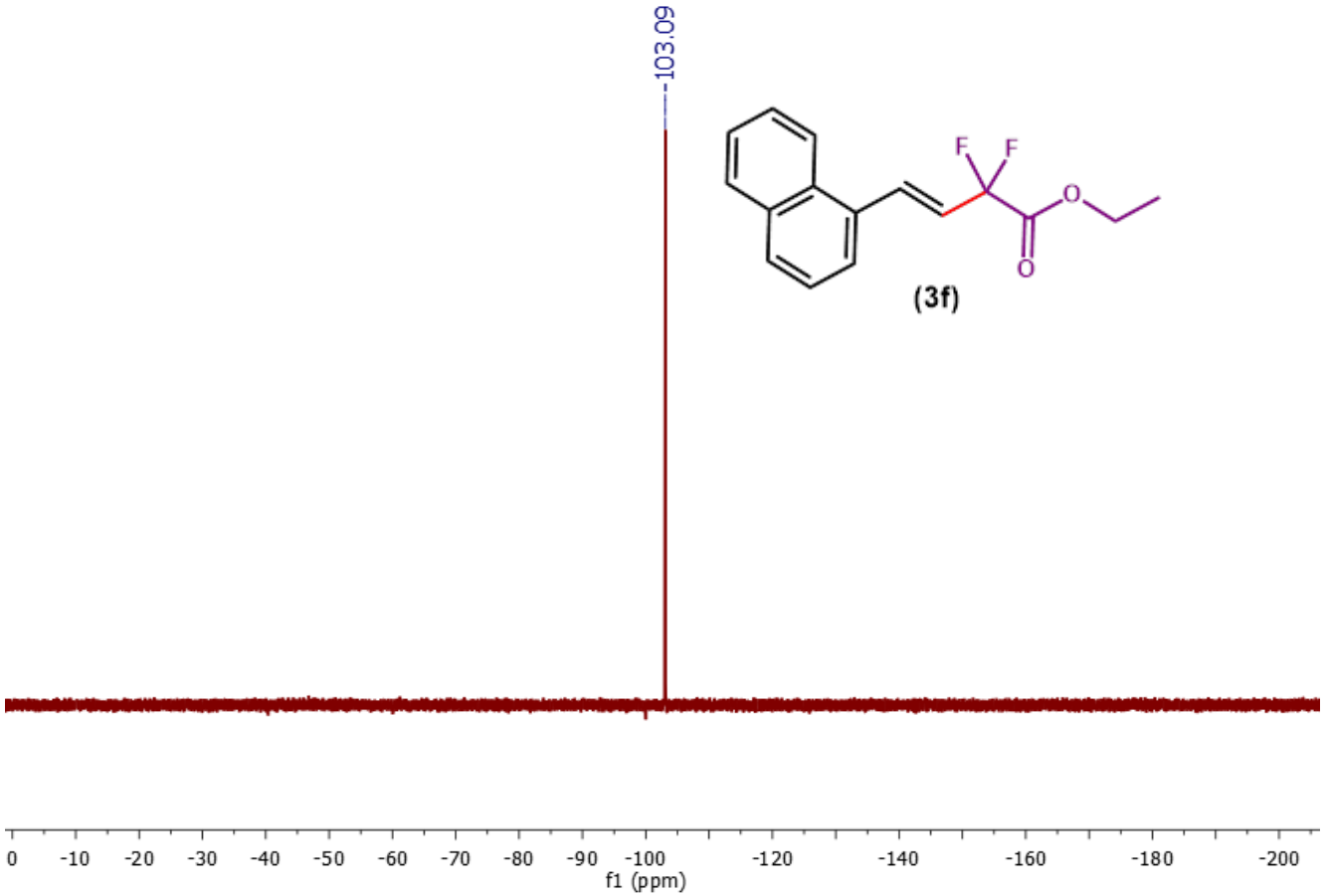

Figure 2. 39. ^{19}F NMR (376 MHz) of **3f** in $CDCl_3$.

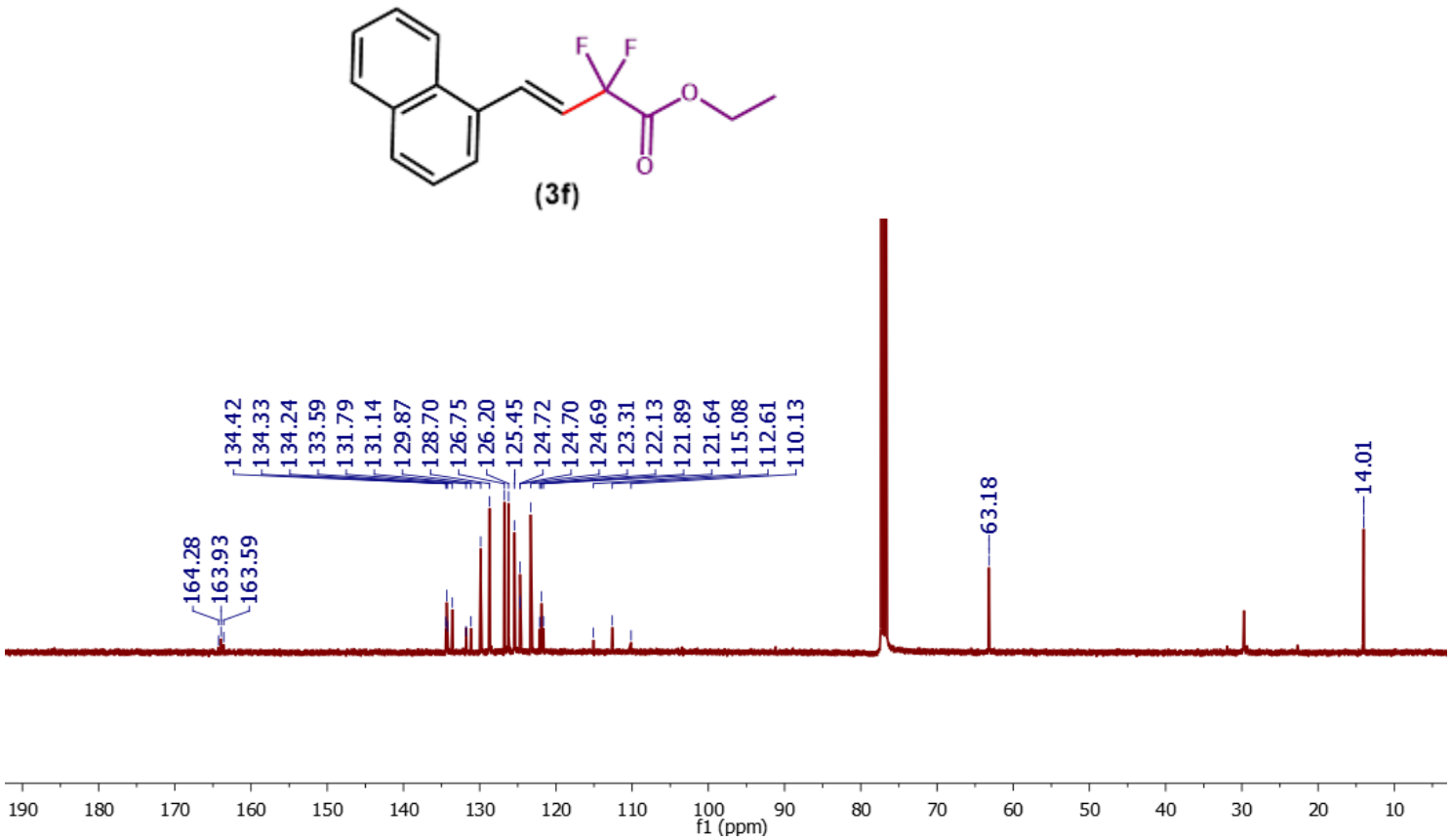

Figure 2. 40. ^{13}C NMR (101 MHz) of **3f** in $CDCl_3$.

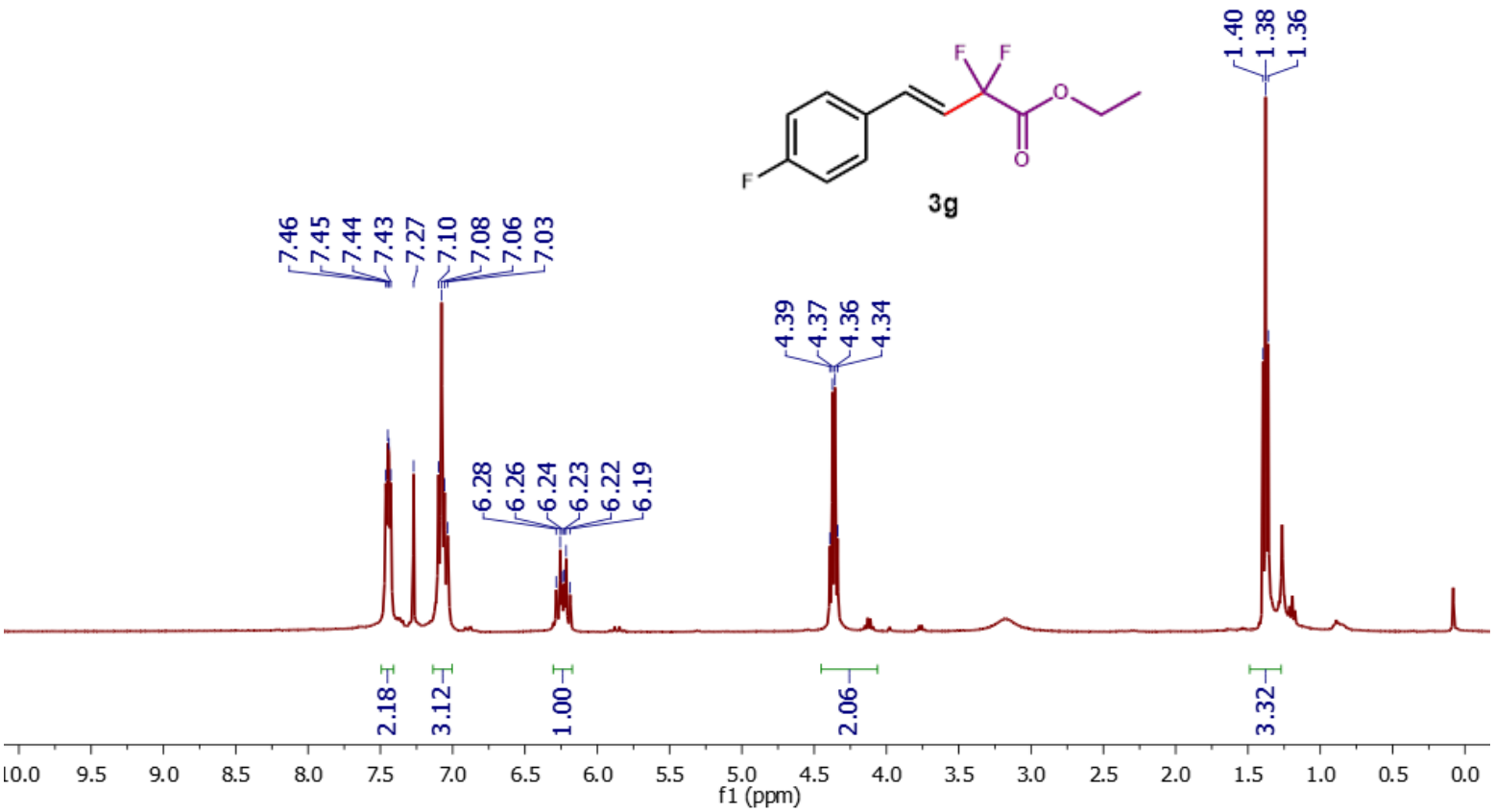

Figure 2. 41. ^{1}H NMR (400 MHz) of **3g** in $CDCl_3$.

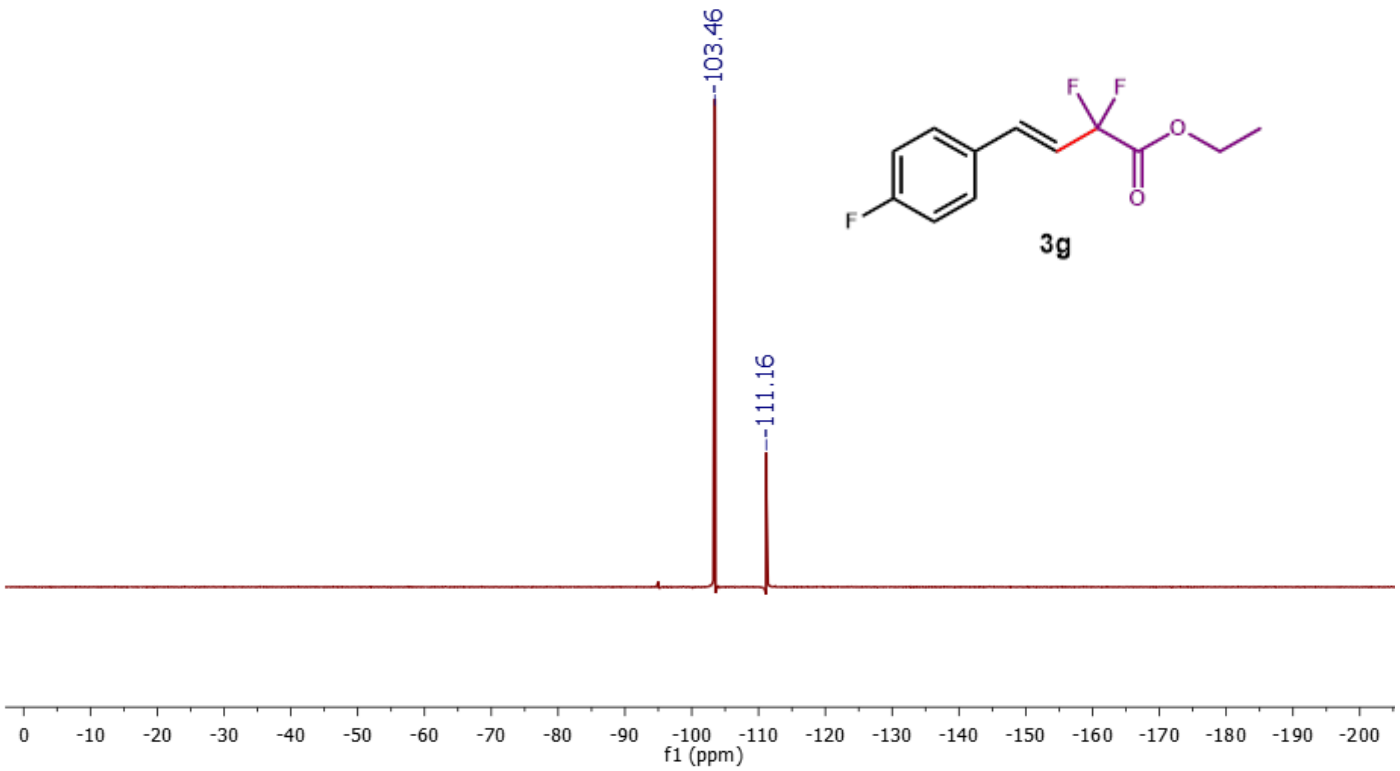

Figure 2. 42. ^{19}F NMR (376 MHz) of **3g** in $CDCl_3$.

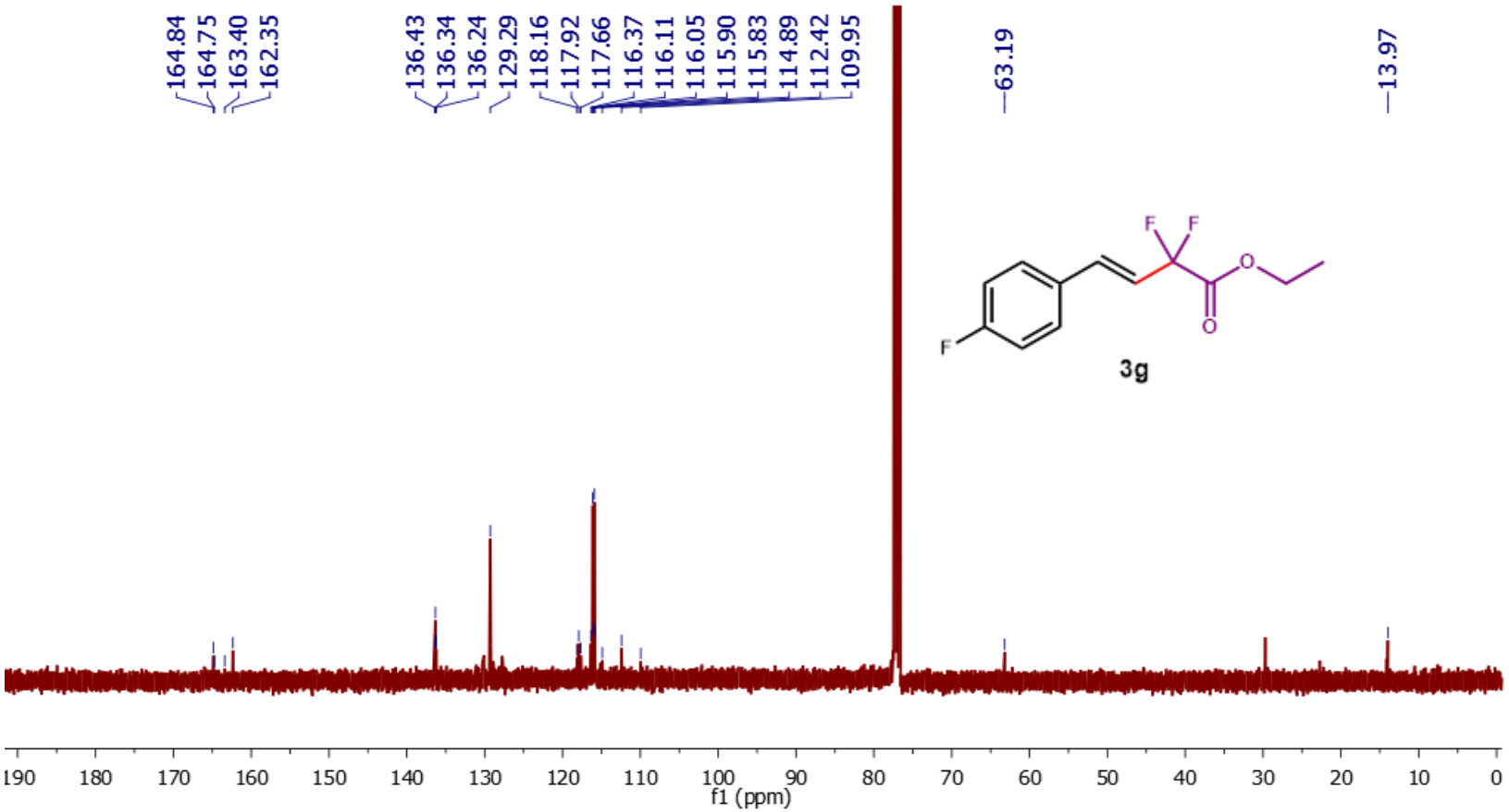

Figure 2. 43. ^{13}C NMR (101 MHz) of **3g** in $CDCl_3$.

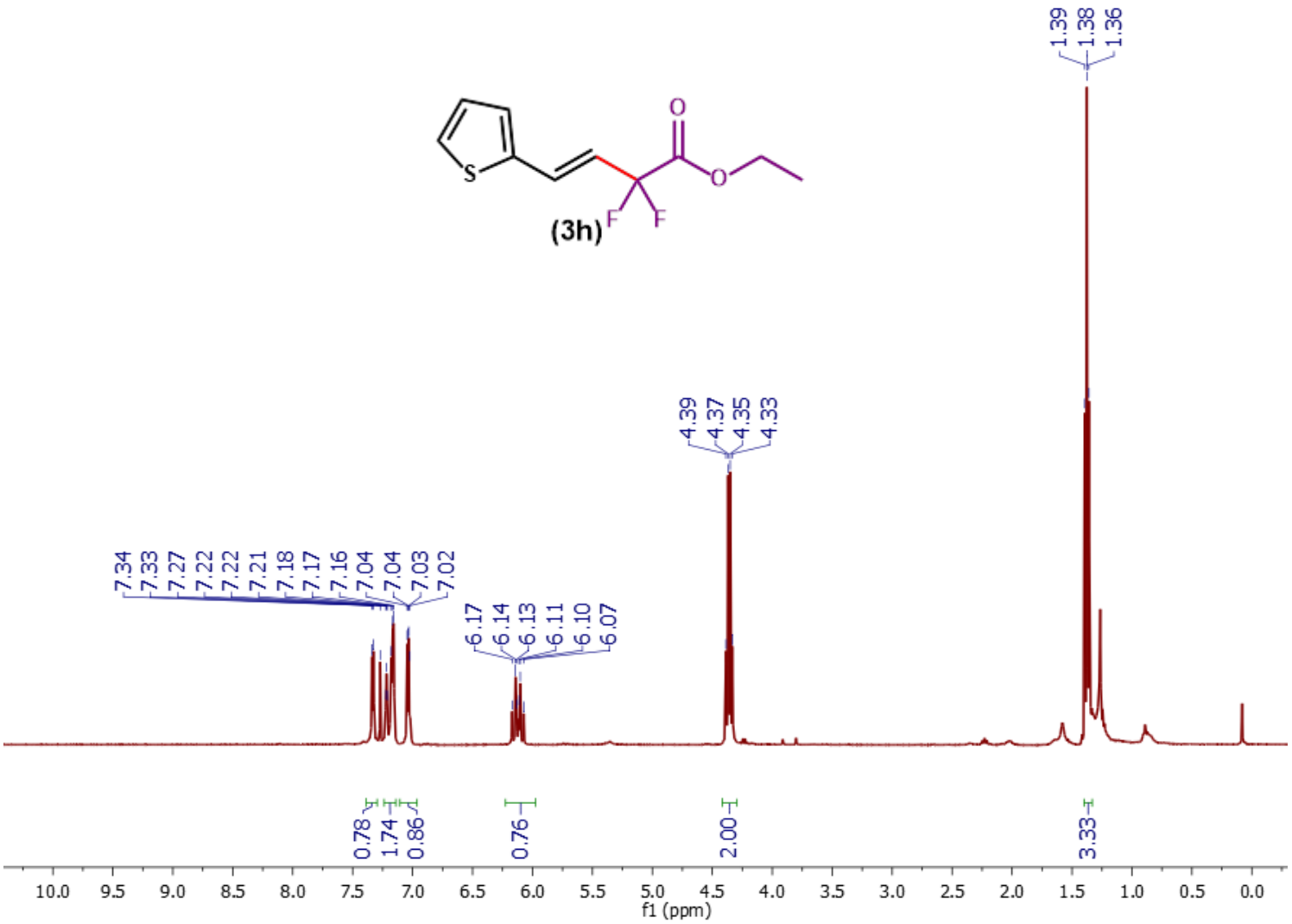

Figure 2. 44. ^{1}H NMR (400 MHz) of **3h** in $CDCl_3$.

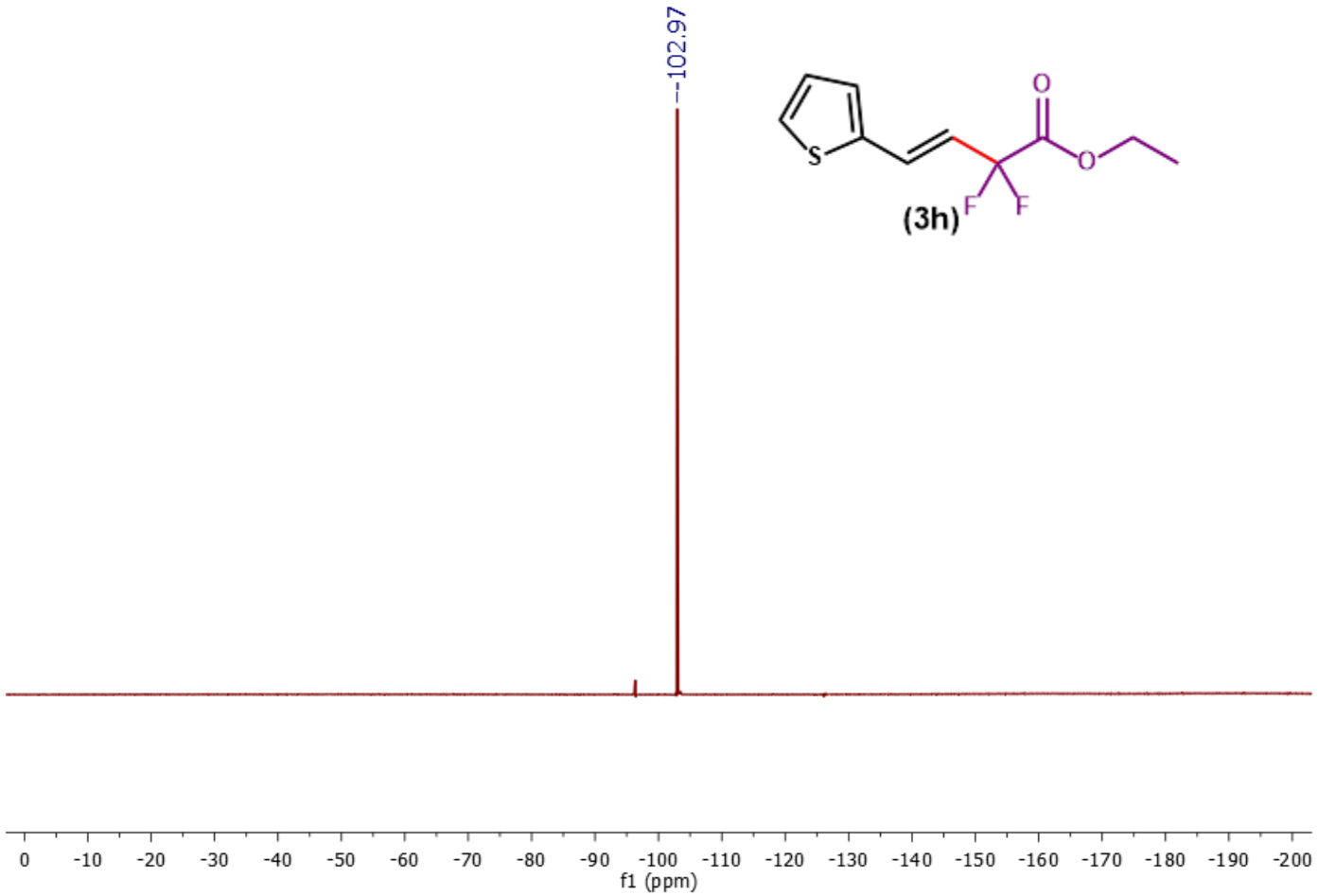

Figure 2. 45. ^{19}F NMR (376 MHz) of **3h** in $CDCl_3$.

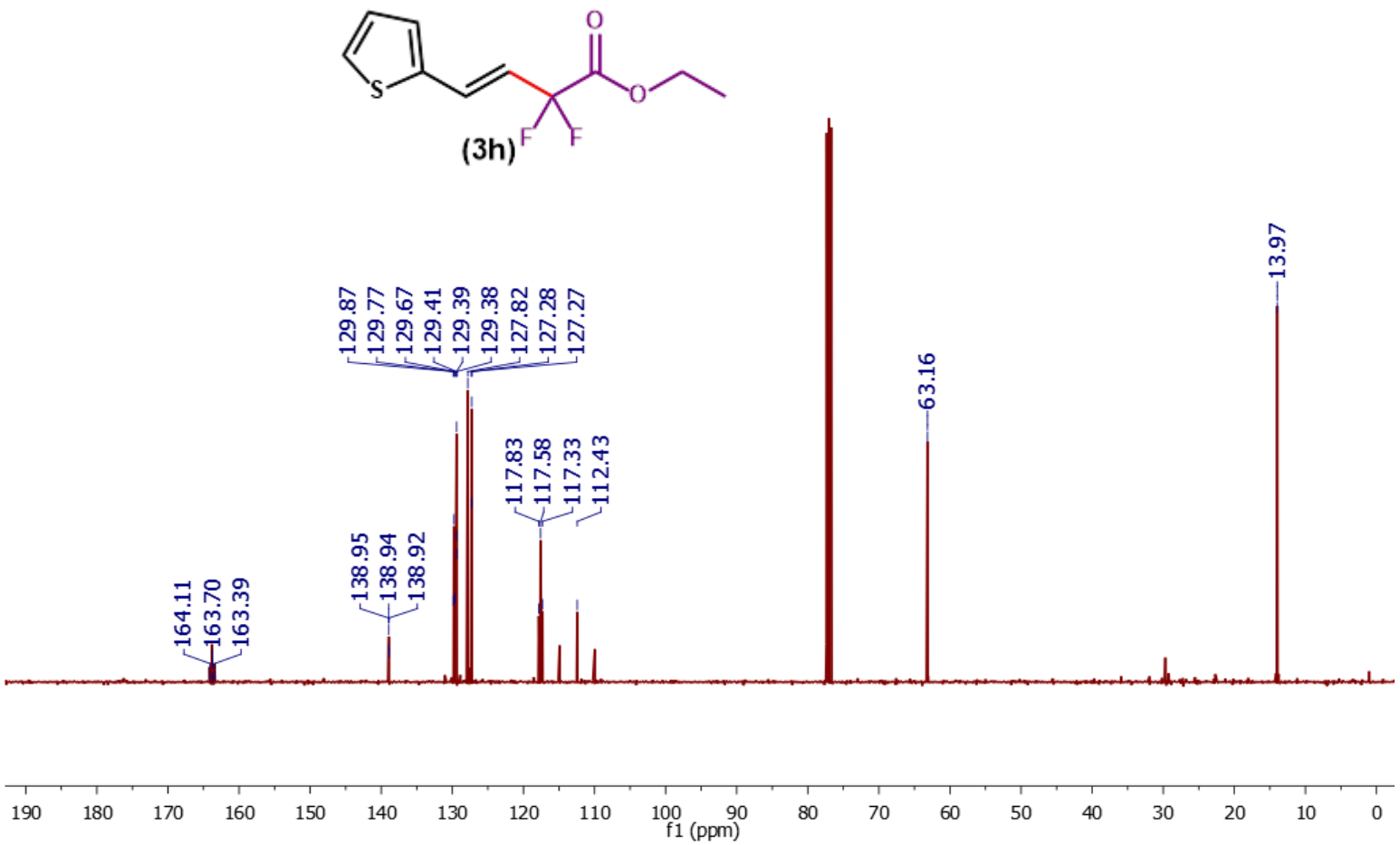

Figure 2. 46. ^{13}C NMR (101 MHz) of **3h** in $CDCl_3$.

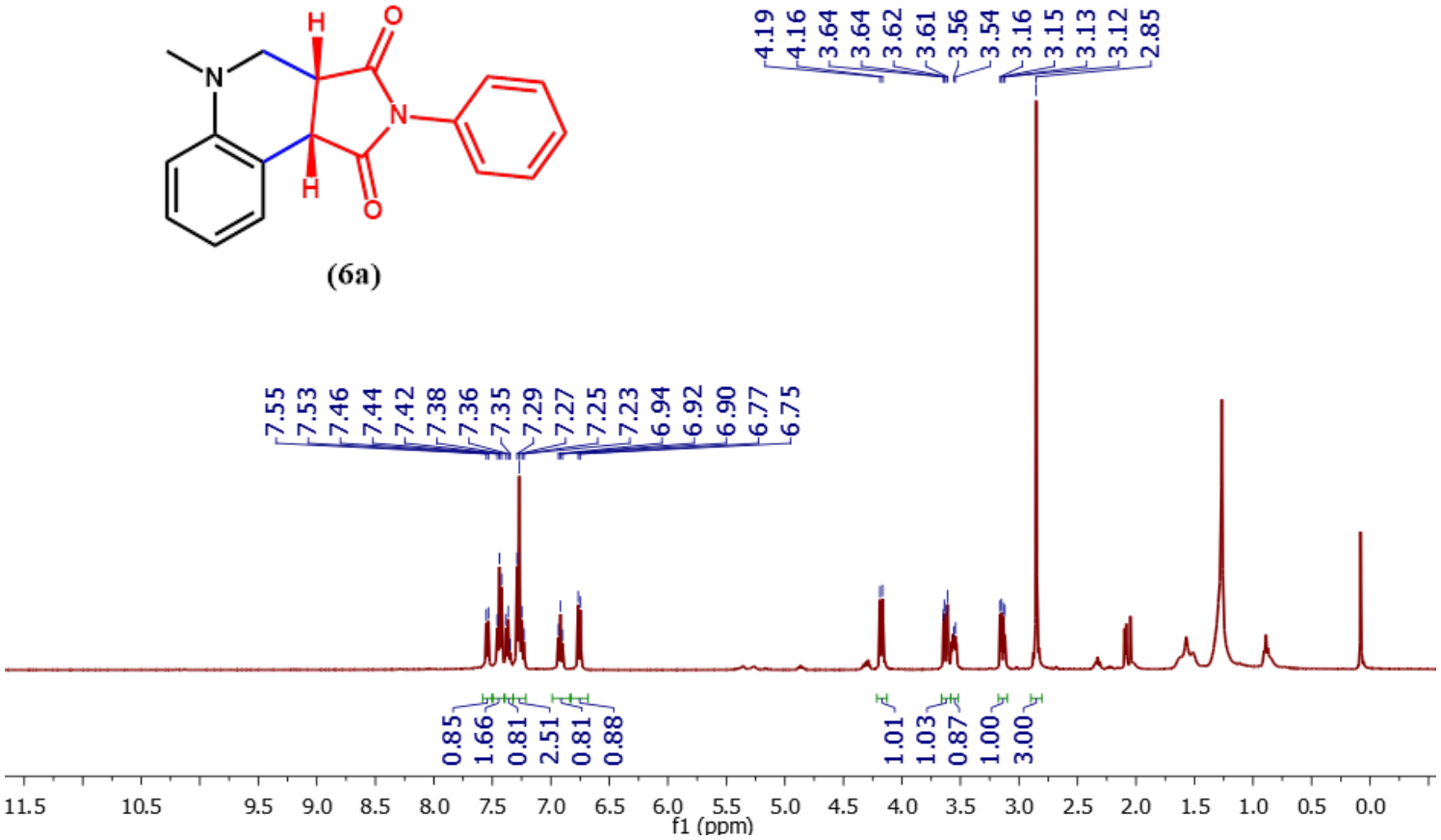

Figure 2. 47. ^{1}H NMR (400 MHz) of 6**a** in $CDCl_3$.

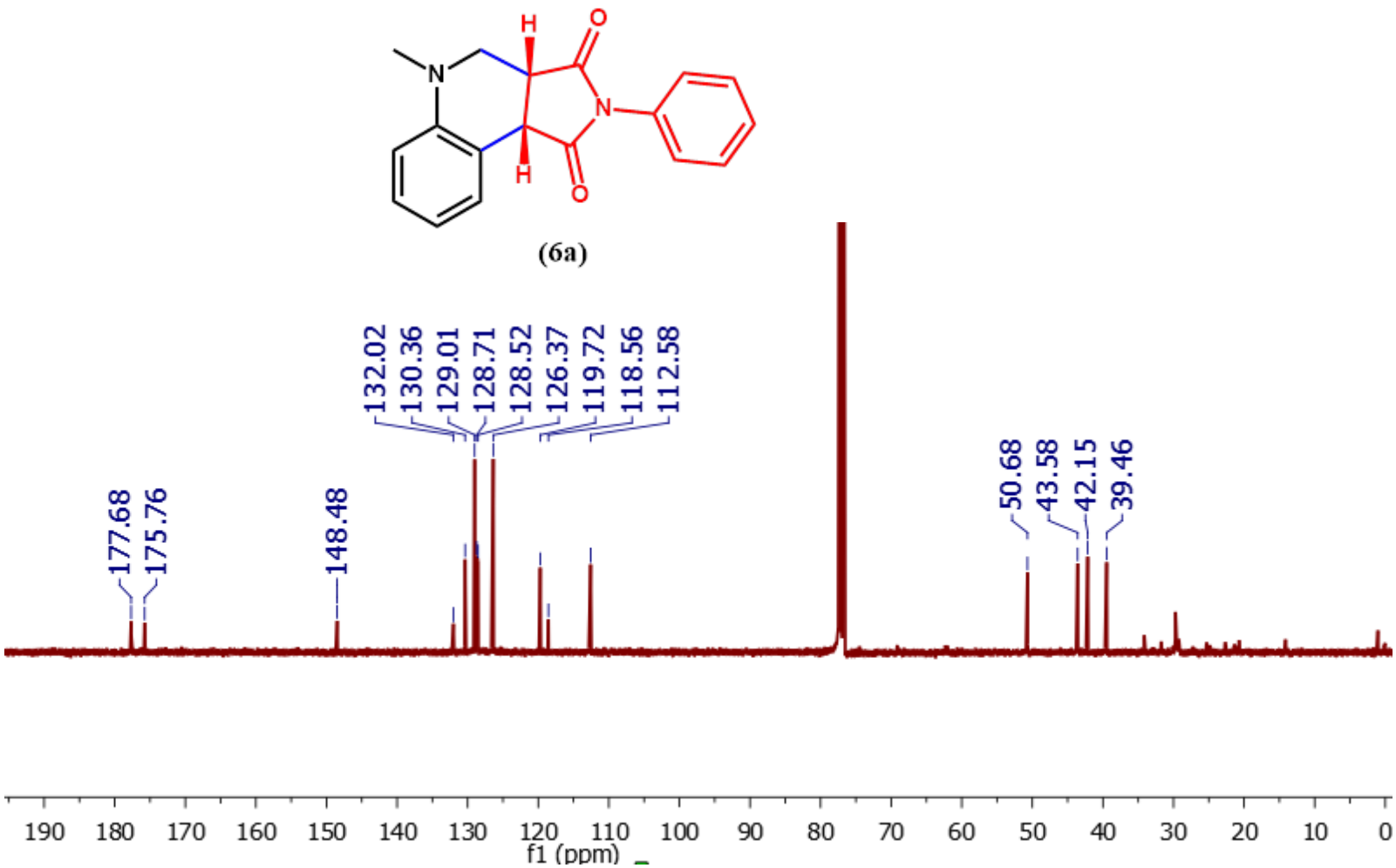

Figure 2. 48. ^{13}C NMR (101 MHz) of **6a** in $CDCl_3$.

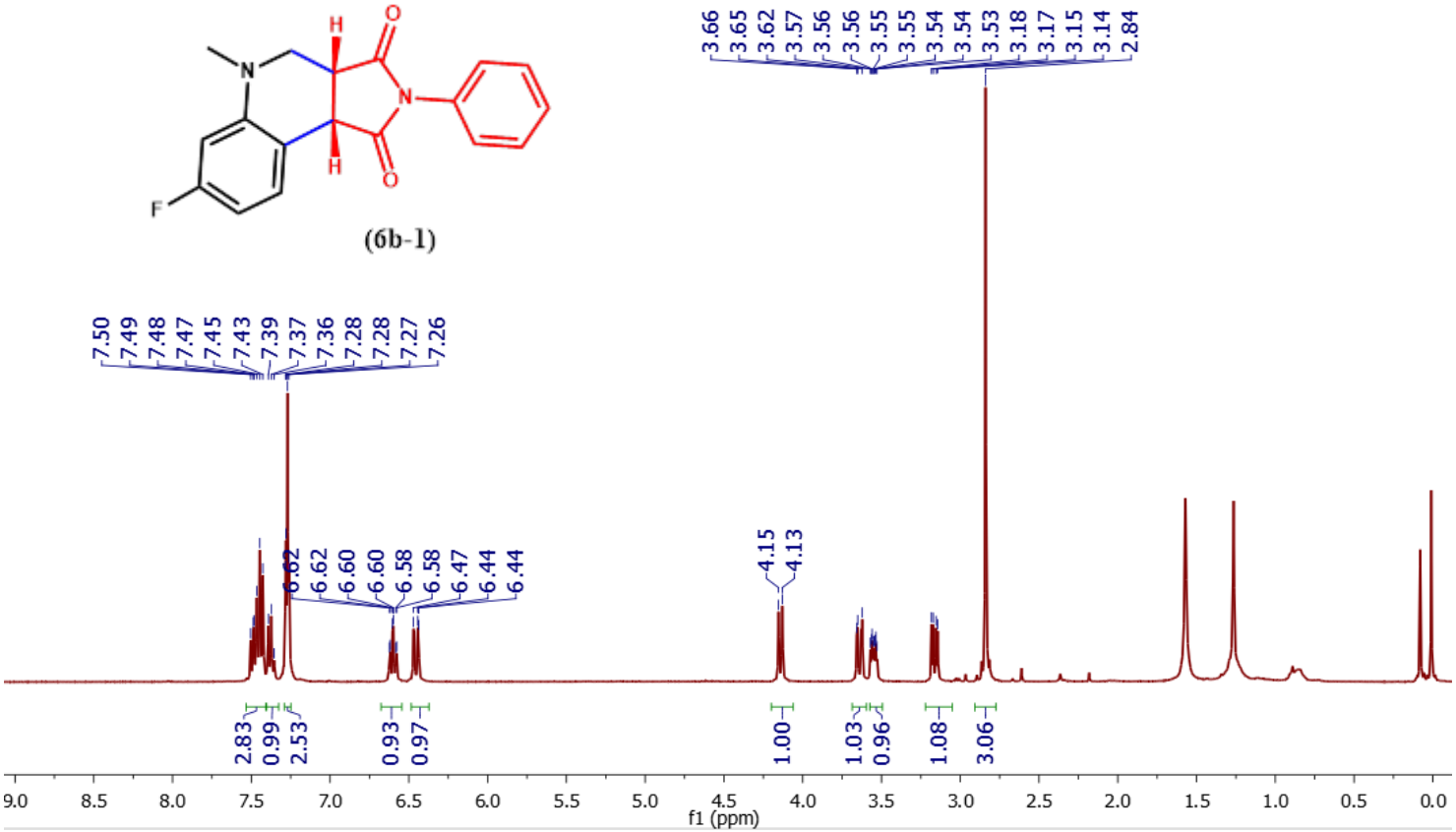

Figure 2. 49. ^{1}H NMR (400 MHz) of **6b-1** in $CDCl_3$.

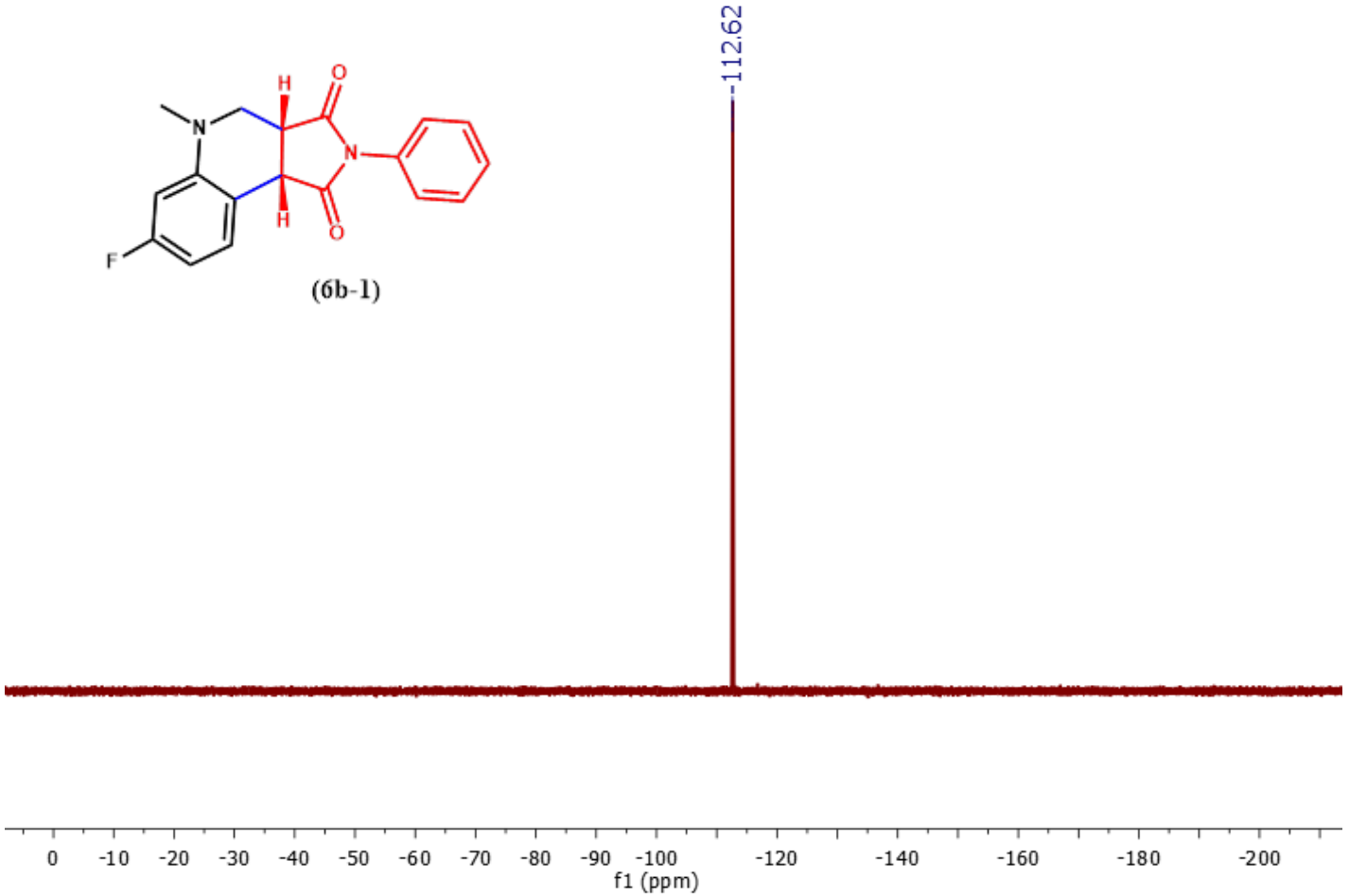

Figure 2. 50. ^{19}F NMR (376 MHz) of **6b-1** in $CDCl_3$.

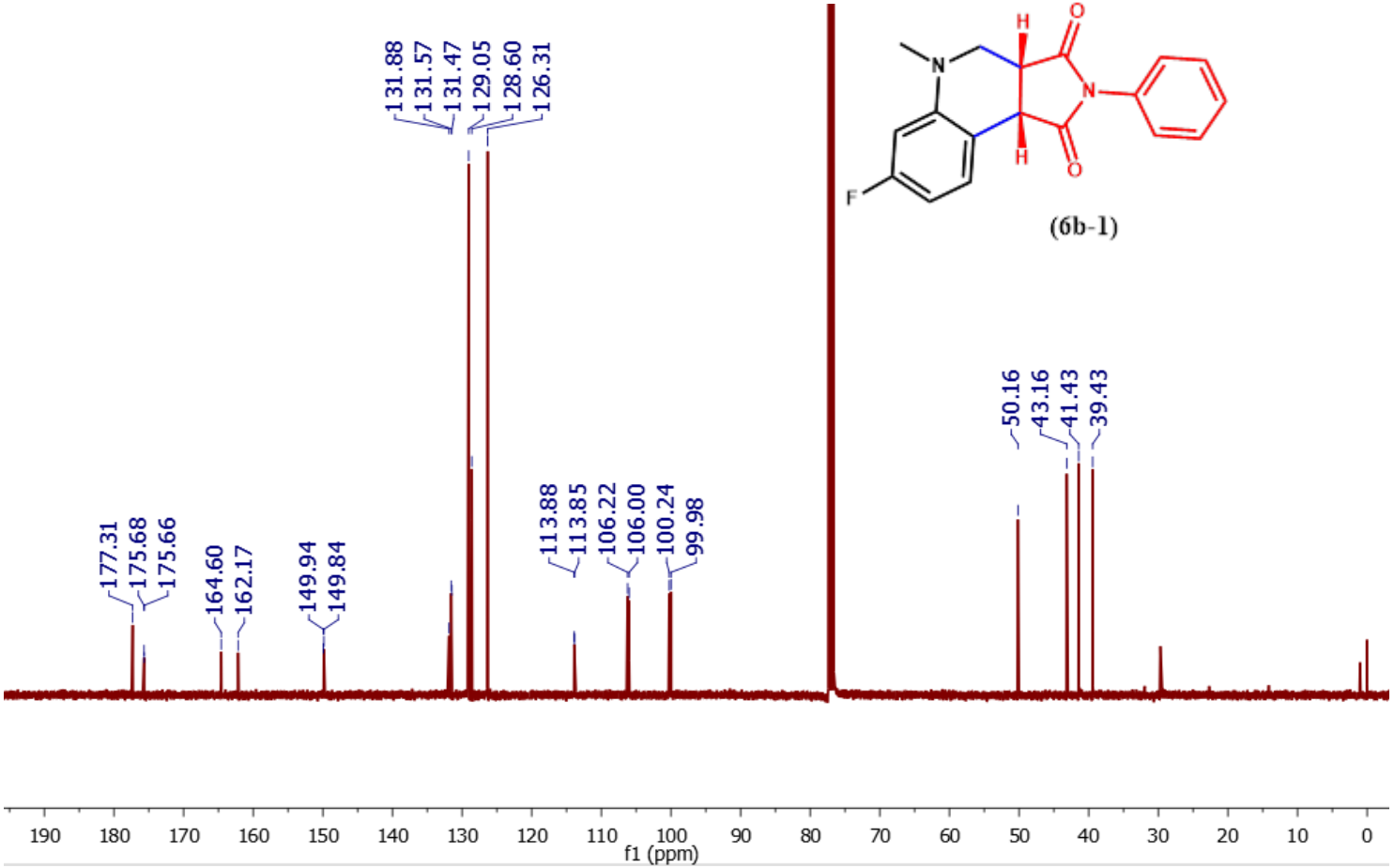

Figure 2. 51. ^{13}C NMR (101 MHz) of **6b-1** in $CDCl_3$.

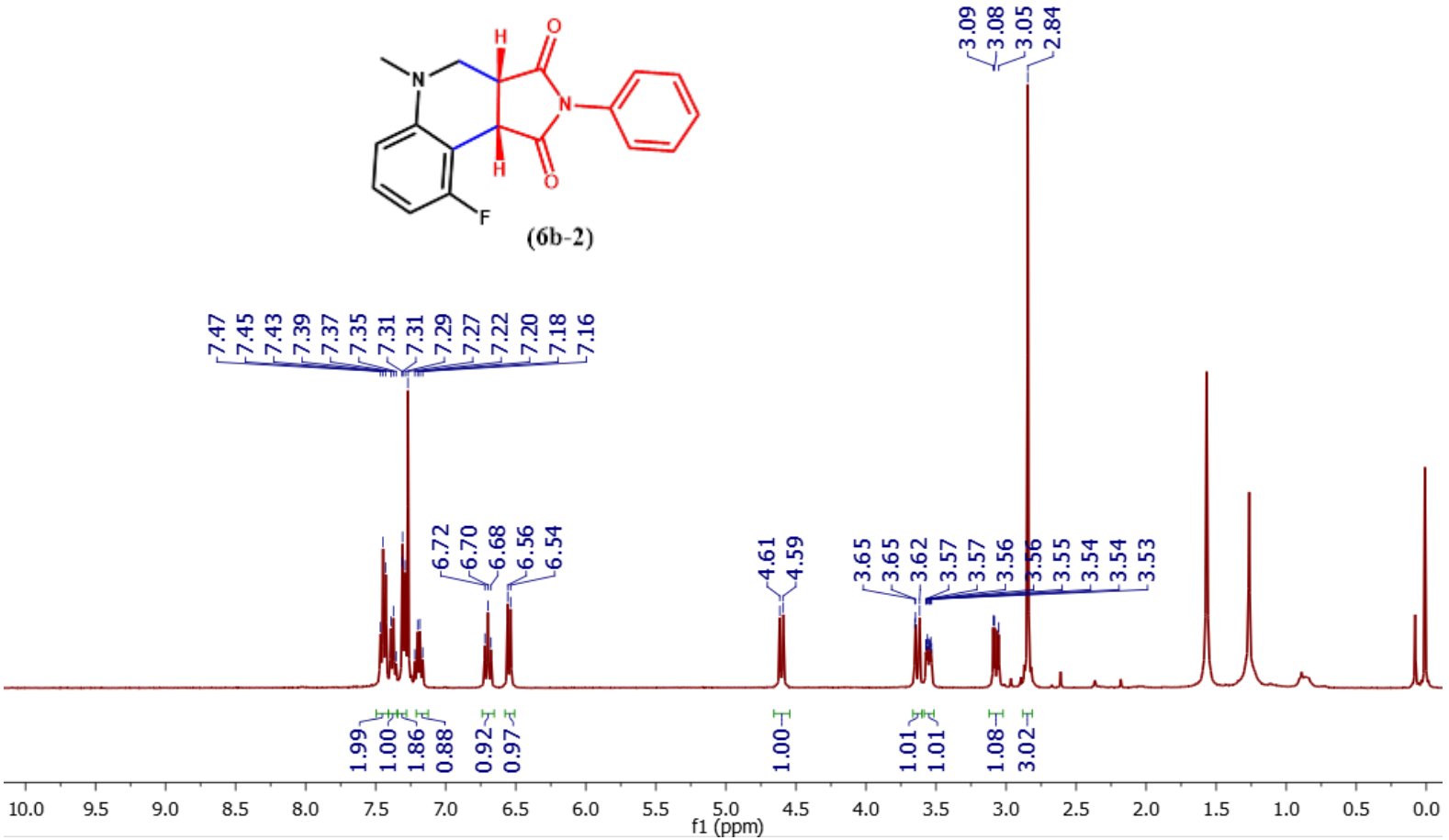

Figure 2. 52. ^{1}H NMR (400 MHz) of **6b-2** in $CDCl_3$.

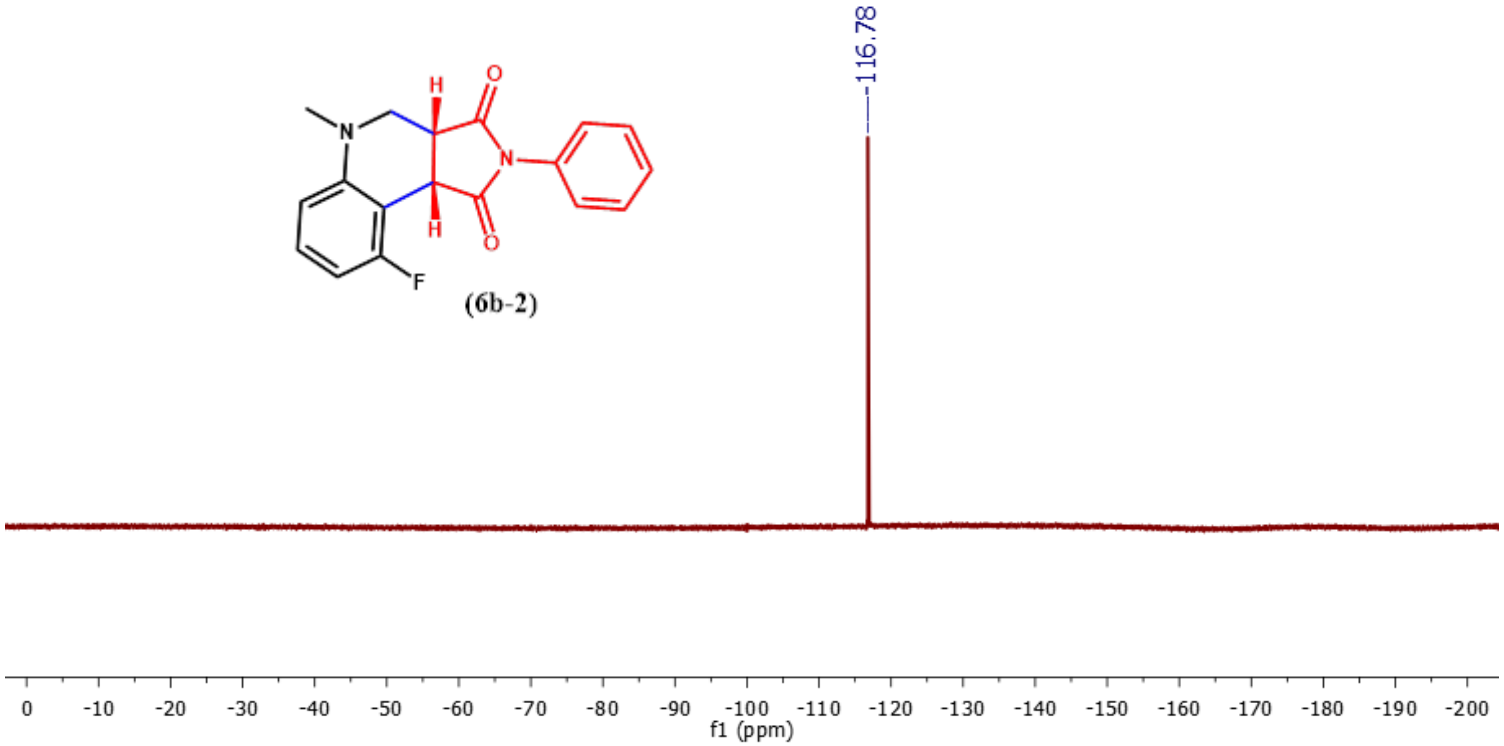

Figure 2. 53. ^{19}F NMR (376 MHz) of **6b-2** in $CDCl_3$.

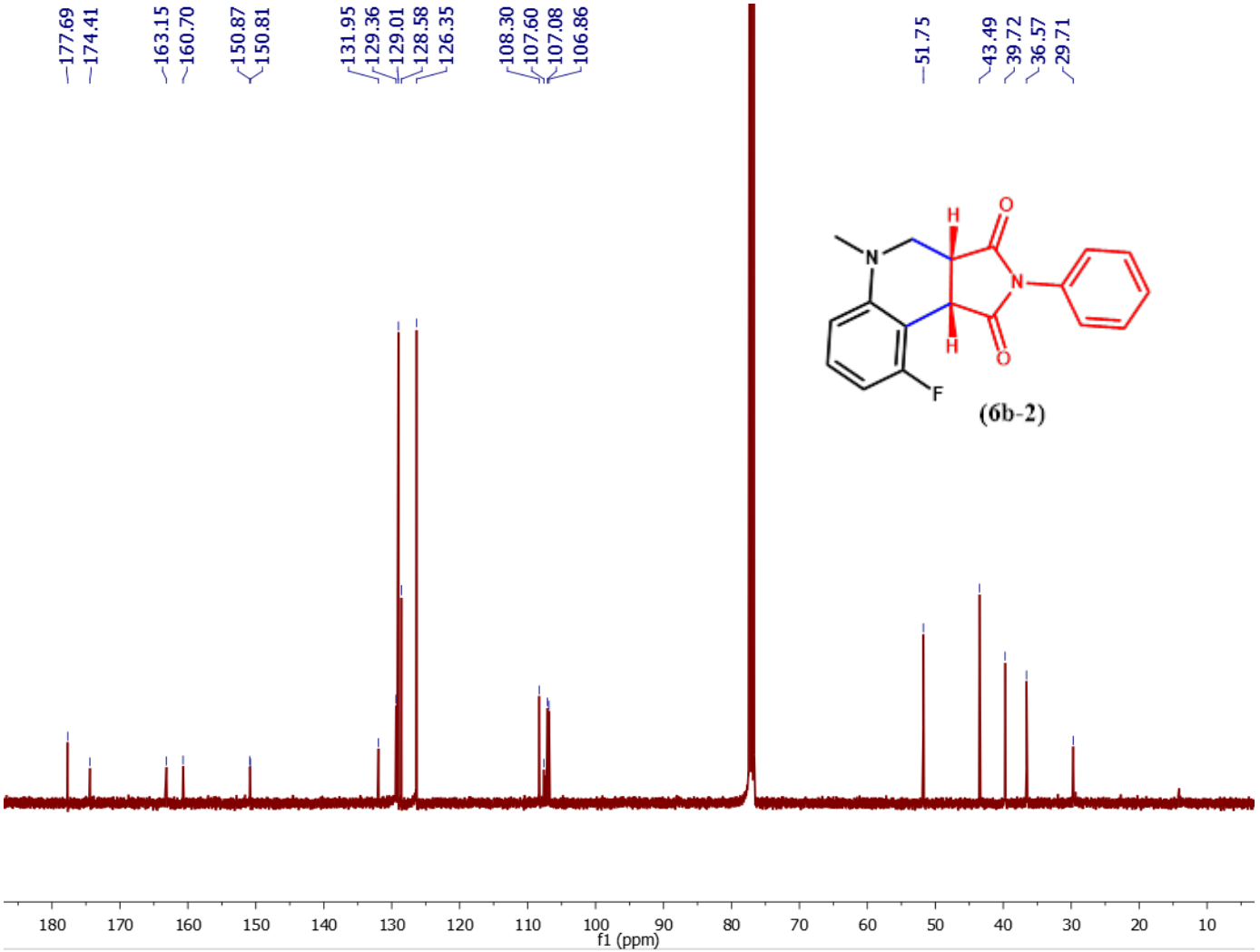

Figure 2. 54. ^{13}C NMR (101 MHz) of **6b-2** in $CDCl_3$.

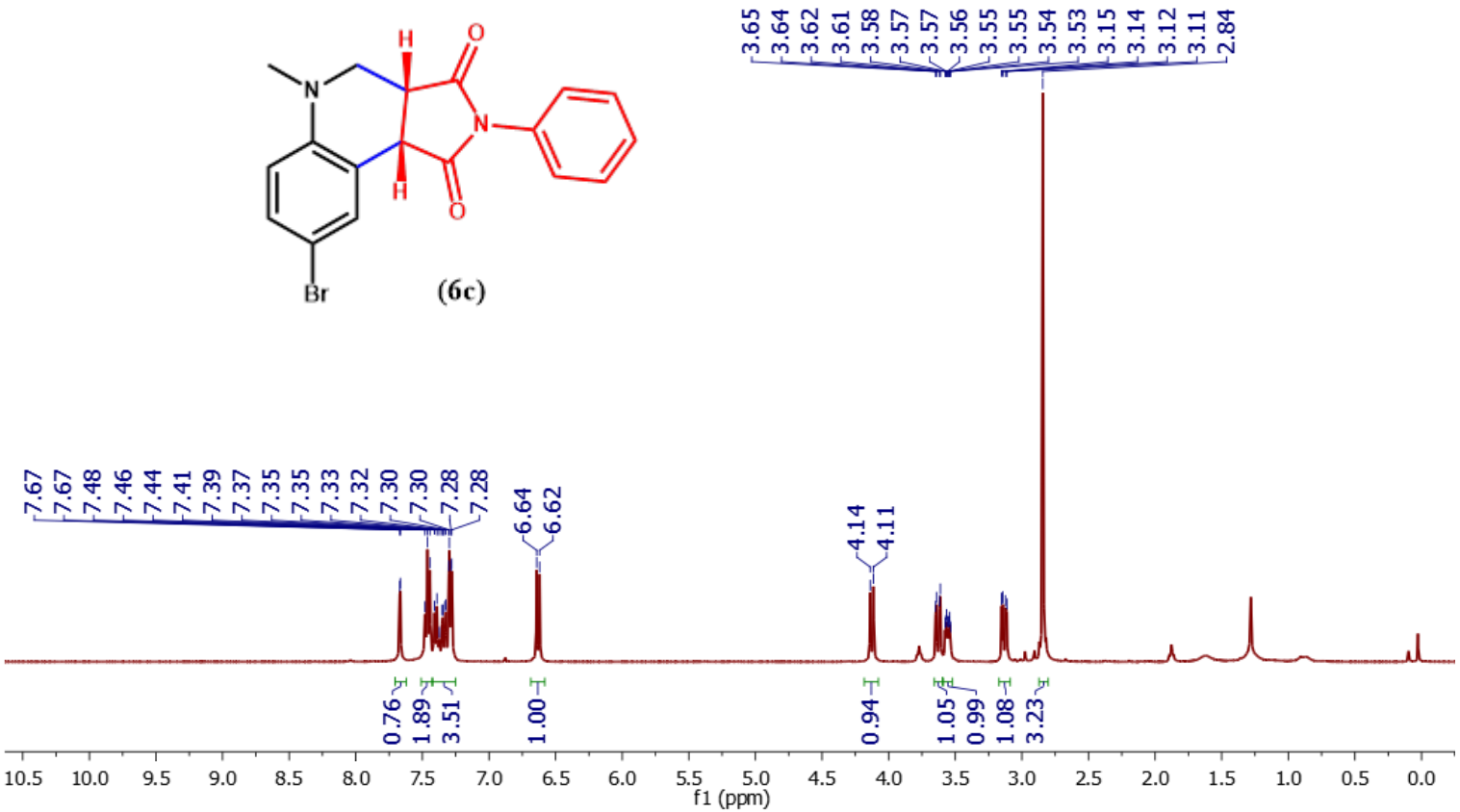

Figure 2. 55. ^{1}H NMR (400 MHz) of **6c** in $CDCl_3$.

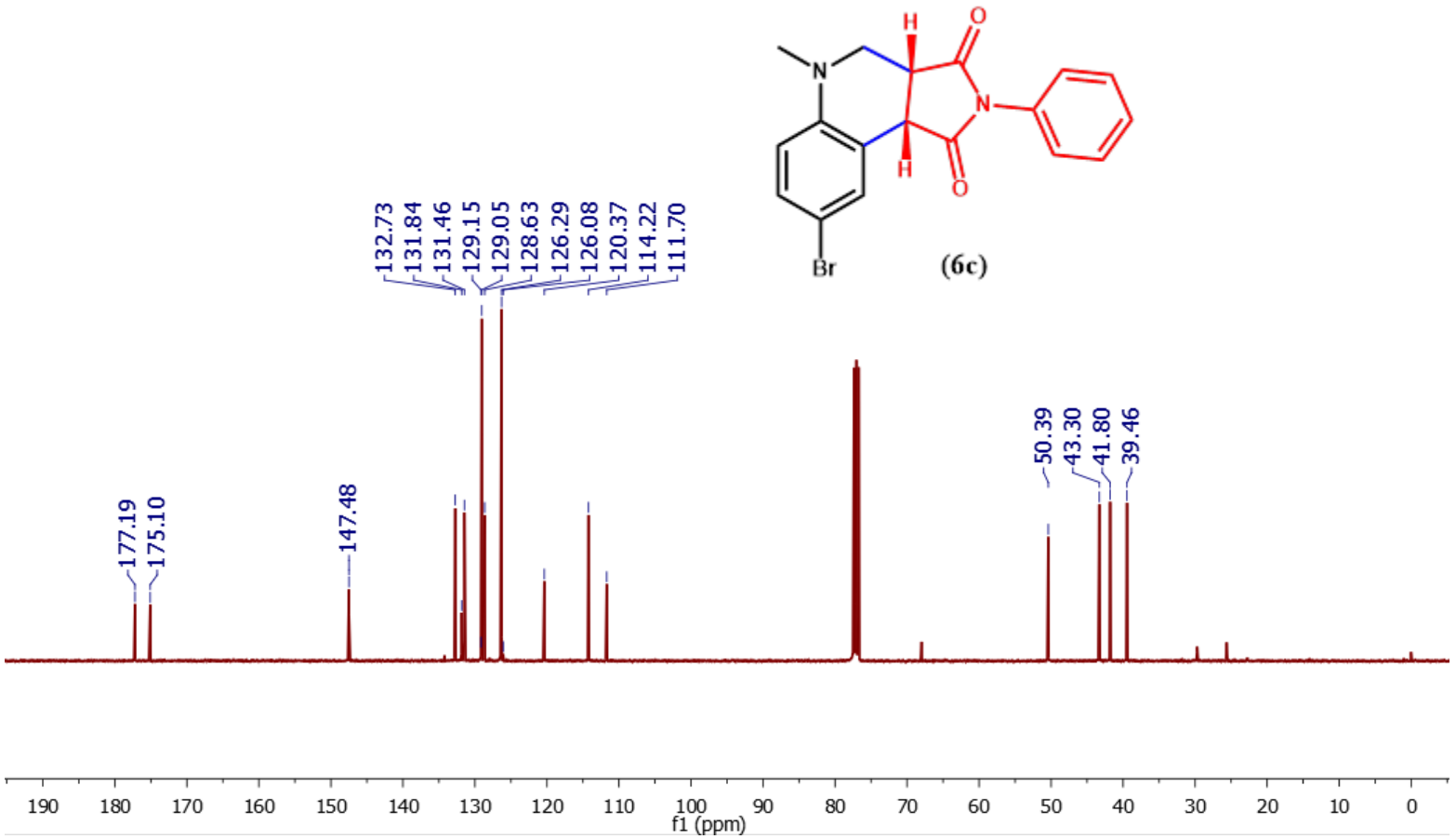

Figure 2. 56. ^{13}C NMR (101 MHz) of **6c** in $CDCl_3$.

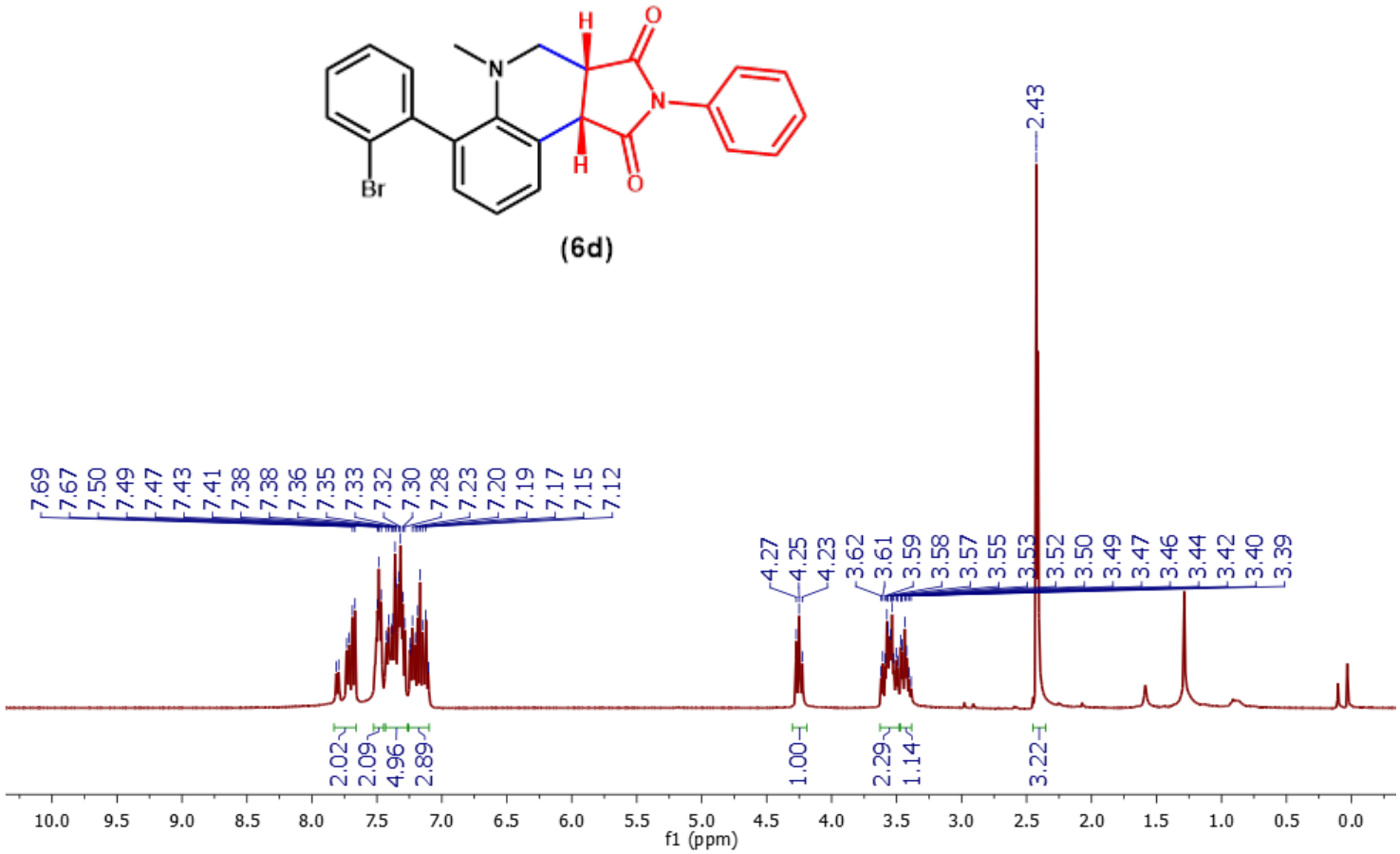

Figure 2. 57. ^{1}H NMR (400 MHz) of **6d** in $CDCl_3$.

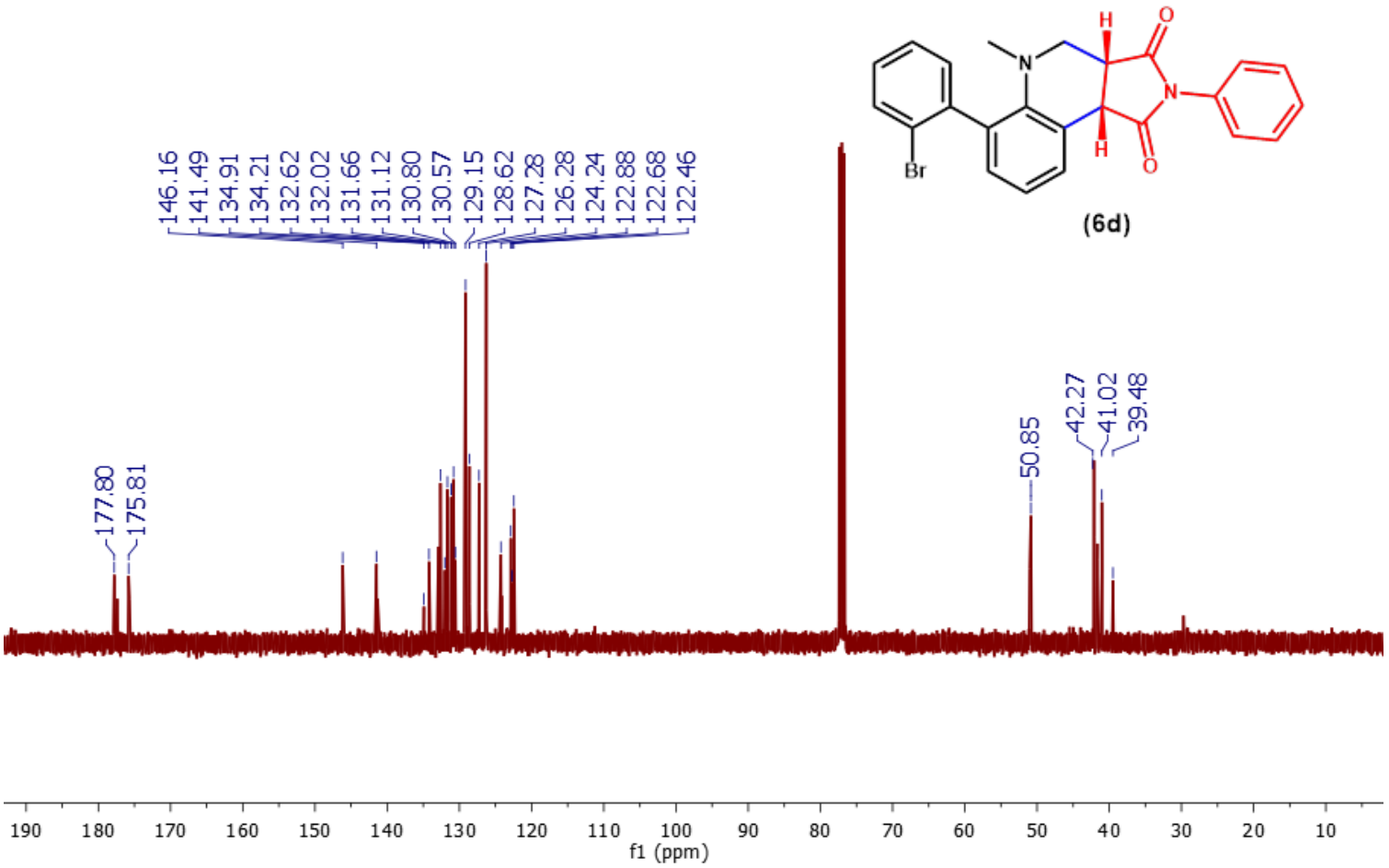

Figure 2. 58. ^{13}C NMR (101 MHz) of **6d** in $CDCl_3$.

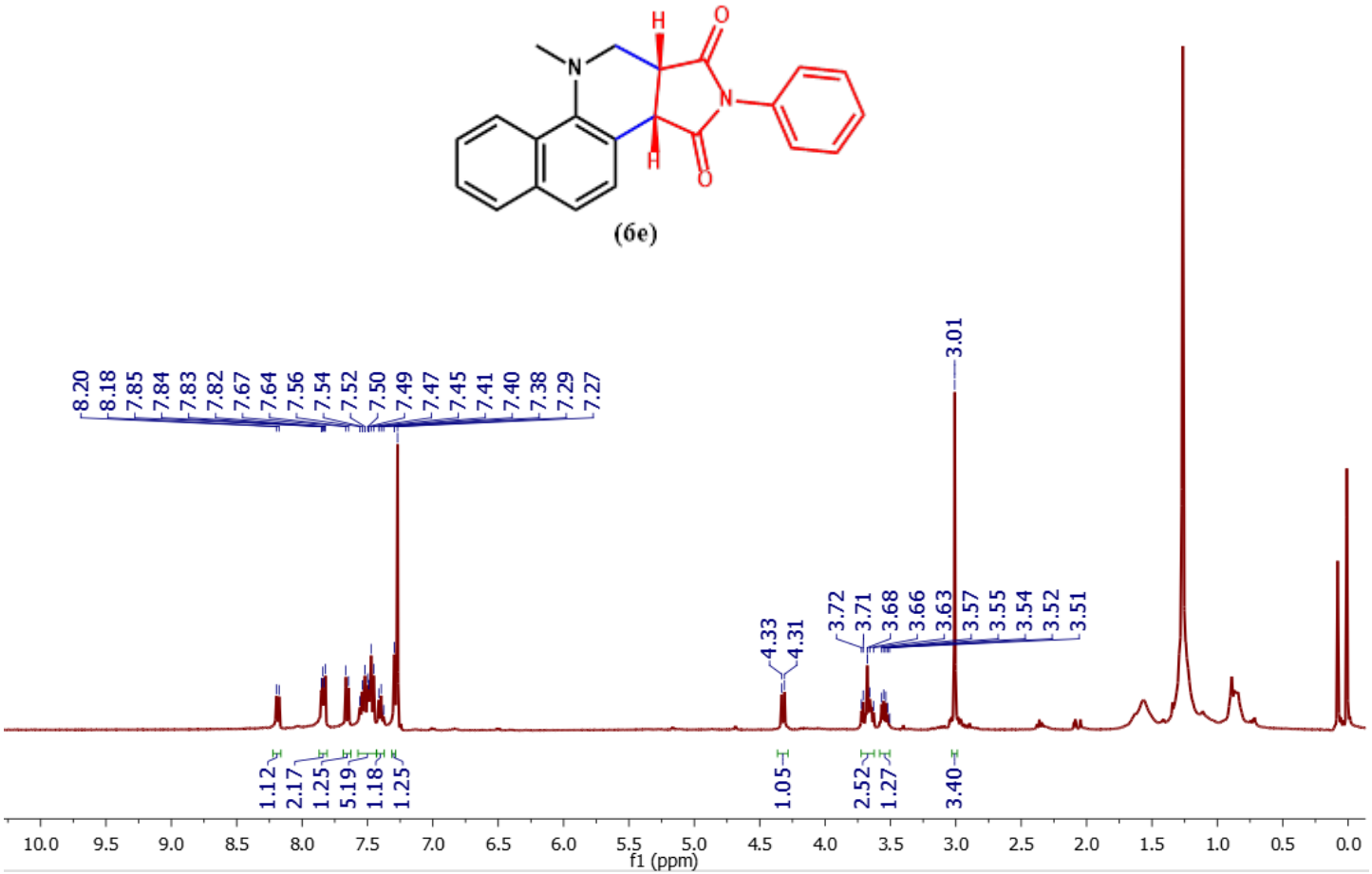

Figure 2. 59. ^{1}H NMR (400 MHz) of **6e** in $CDCl_3$.

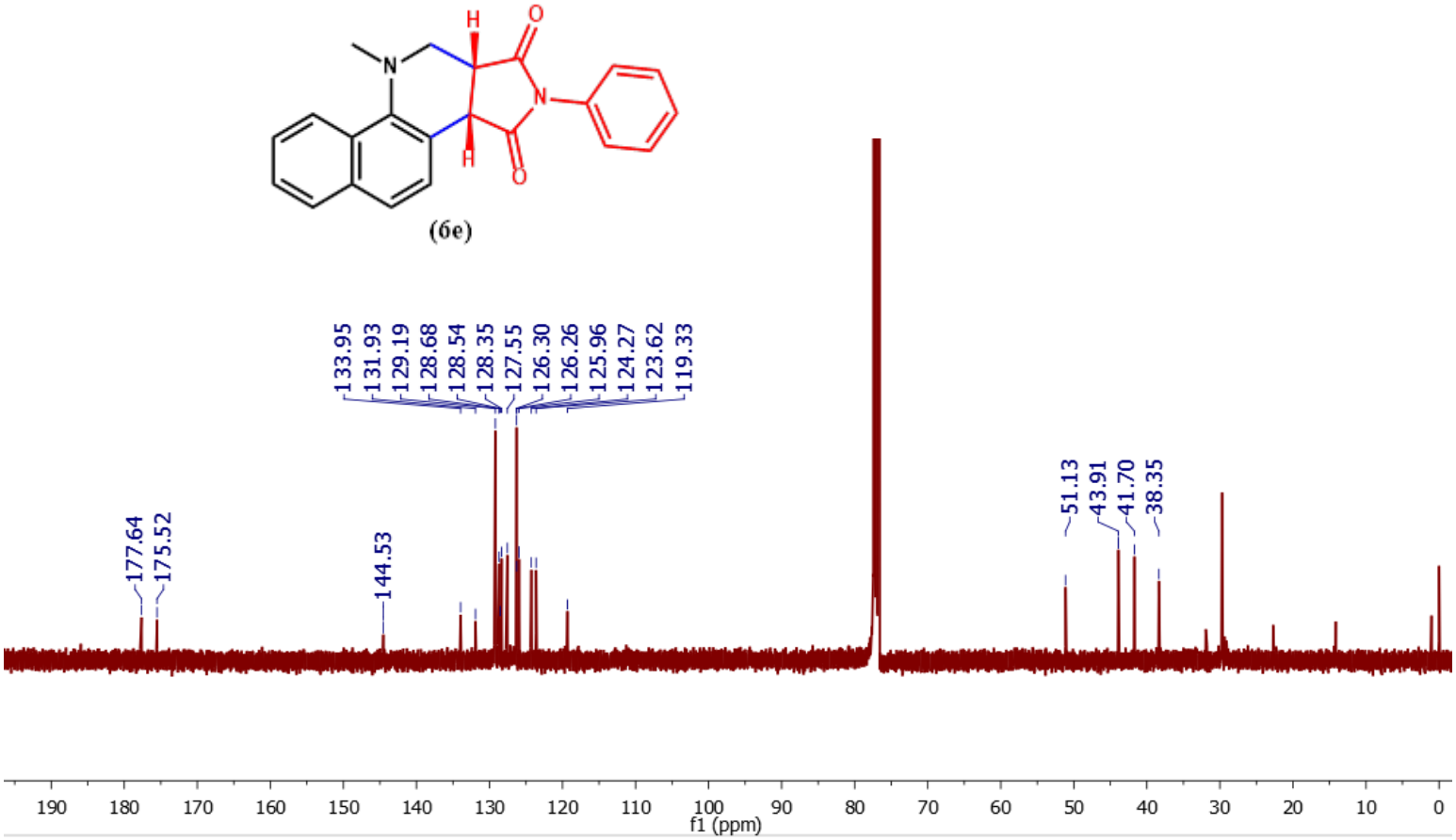

Figure 2. 60. ^{13}C NMR (101 MHz) of **6e** in $CDCl_3$.

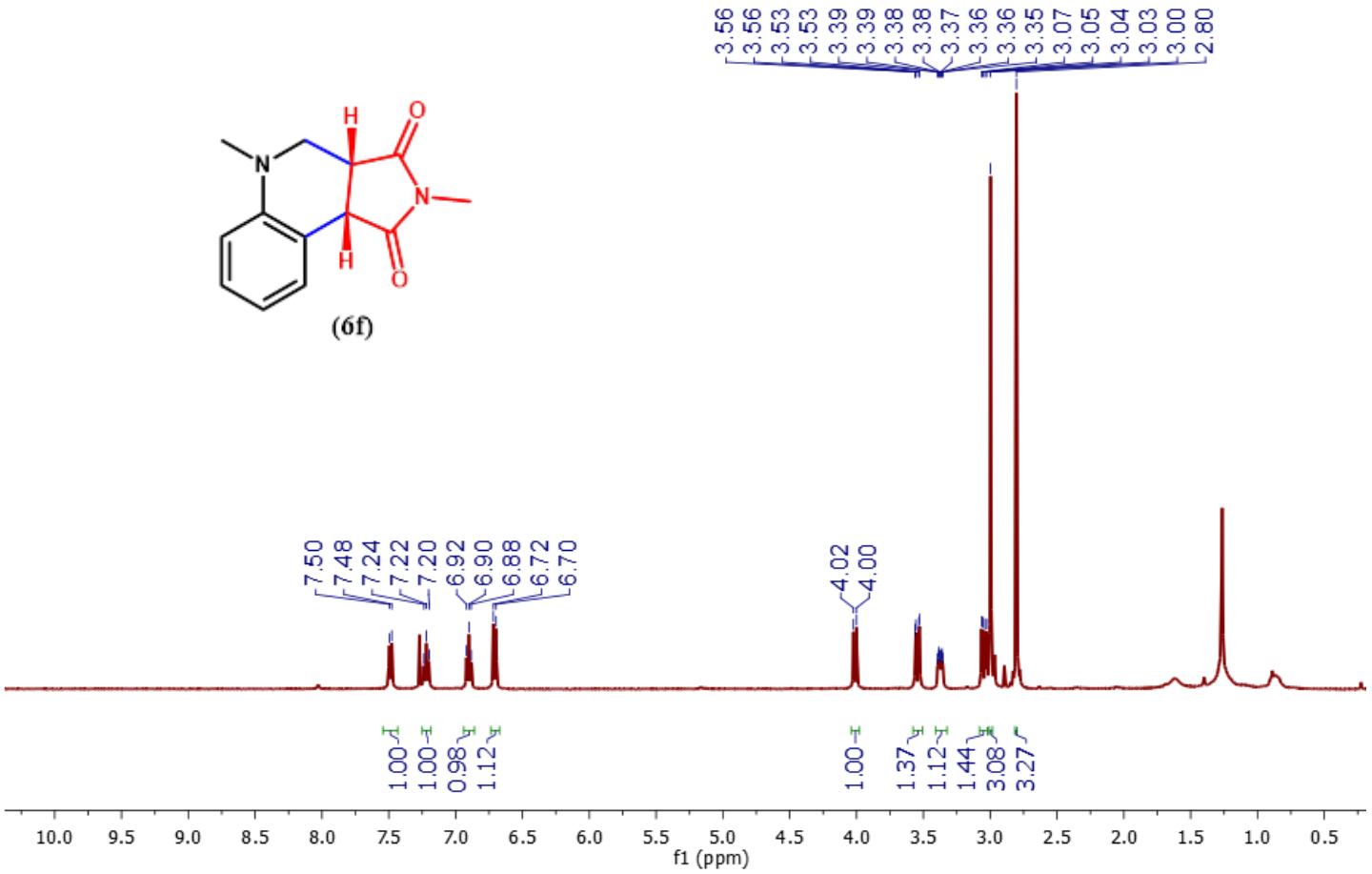

Figure 2. 61. ^{1}H NMR (400 MHz) of **6f** in $CDCl_3$.

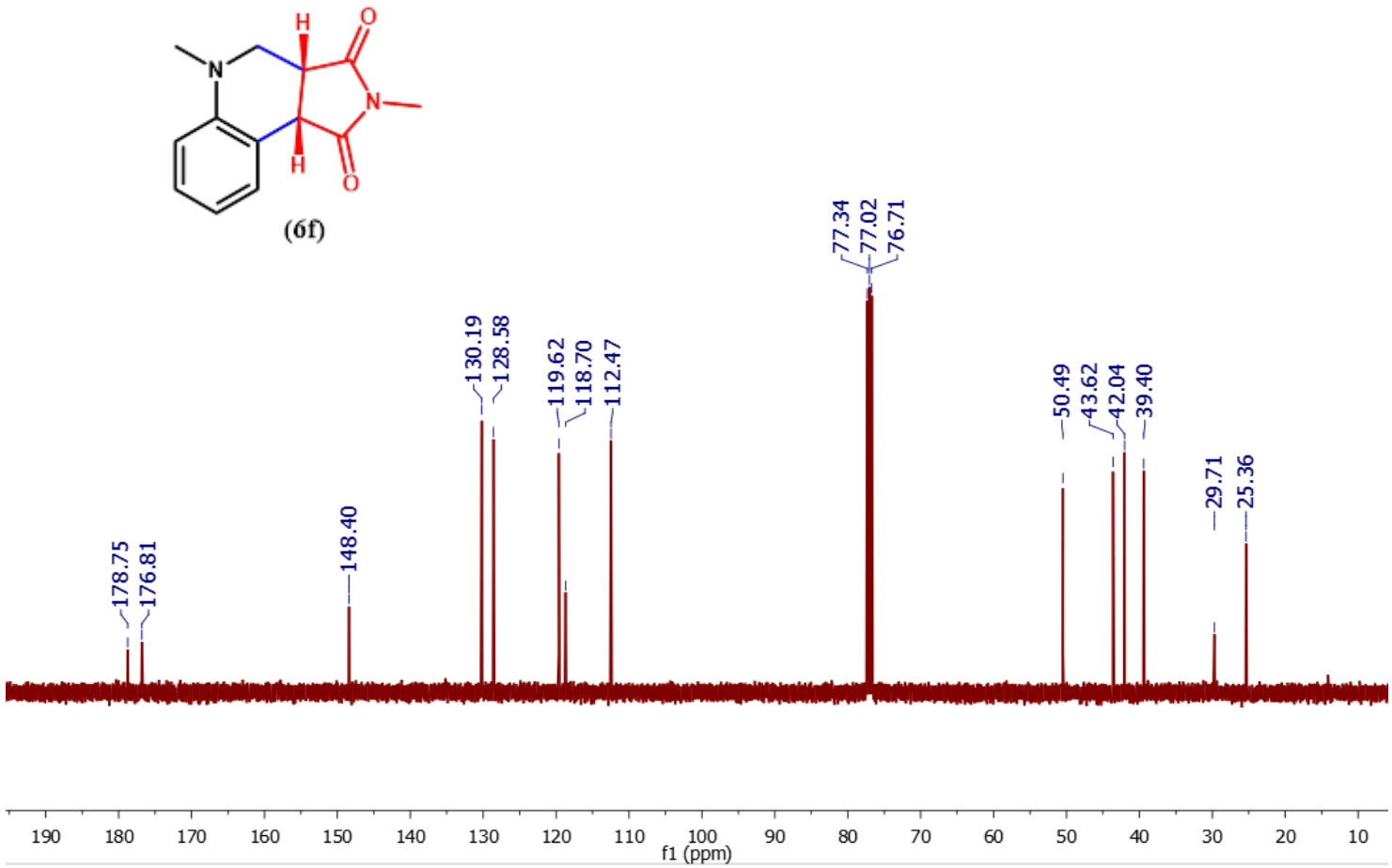

Figure 2. 62. ^{13}C NMR (101 MHz) of **6f** in $CDCl_3$.

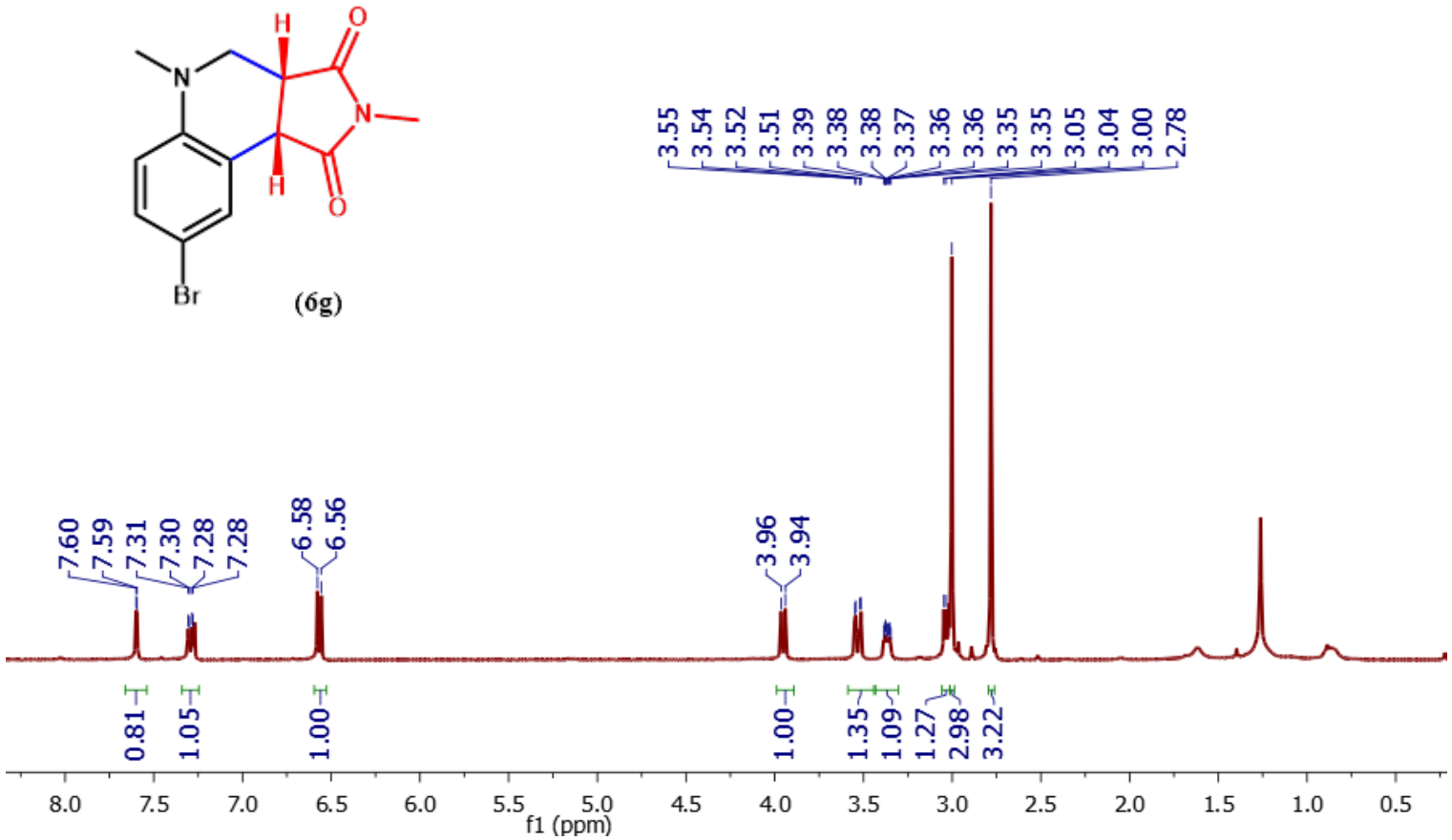

Figure 2. 63. ^{1}H NMR (400 MHz) of **6g** in $CDCl_3$.[9]

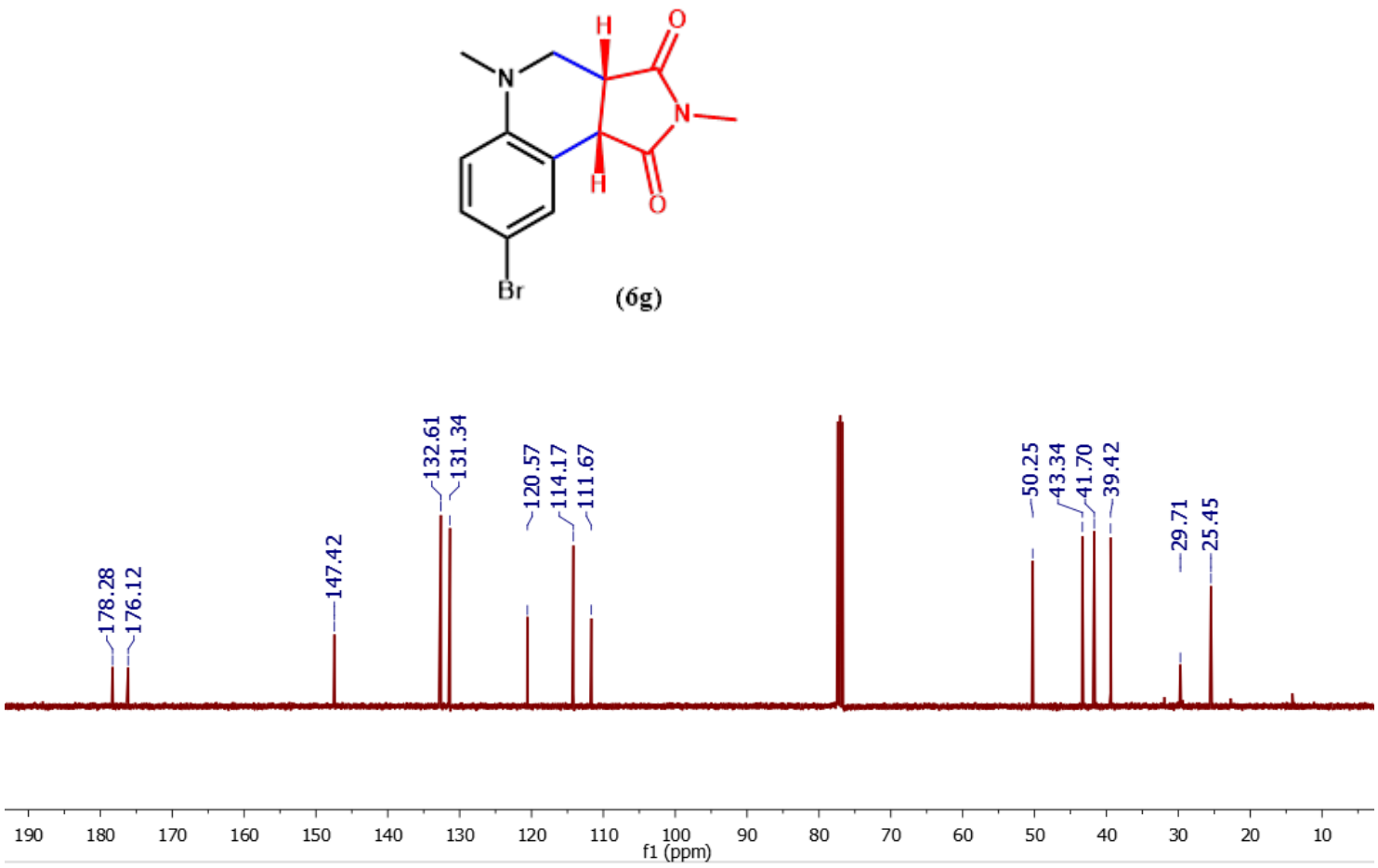

Figure 2. 64. ^{13}C NMR (101 MHz) of **6g** in $CDCl_3$.

2.13. Reference

1. Jin, S.; Sakurai, T.; Kowalczyk, T.; Dalapati, S.; Xu, F.; Wei, H.; Chen, X.; Gao, J.; Seki, S.;Irle, S., Two-Dimensional Tetrathiafulvalene Covalent Organic Frameworks: Towards Latticed Conductive Organic Salts. *Chem. Eur. J.* **2014**, *20*, 14608-14613.

2. Wong, M. Y.; Xie, G.; Tourbillon, C.; Sandroni, M.; Cordes, D. B.; Slawin, A. M. Z.; Samuel, I. D. W.;Zysman-Colman, E., Formylated Chloro-Bridged Iridium(III) Dimers as OLED Materials: Opening up New Possibilities. *Dalton Trans.* **2015**, *44*, 8419-8432.

3. Dubbeldam, D.; Calero, S.; Ellis, D. E.;Snurr, R. Q., RASPA: Molecular Simulation Software for Adsorption and Diffusion in Flexible Nanoporous Materials. *Mol. Simulat.* **2016**, *42*, 81-101.

4. Mayo, S. L.; Olafson, B. D.;Goddard, W. A., DREIDING: A Generic Force Field for Molecular Simulations. *J. Phys. Chem.* **1990**, *94*, 8897-8909.

5. Zhang, L.;Siepmann, J. I., Direct Calculation of Henry's Law Constants from Gibbs Ensemble Monte Carlo Simulations: Nitrogen, Oxygen, Carbon Dioxide and Methane in Ethanol. *Theor. Chem. Acc.* **2006**, *115*, 391-397.

6. Zhong, J.-J.; Yang, C.; Chang, X.-Y.; Zou, C.; Lu, W.;Che, C.-M., Platinum(II) Photo-Catalysis for Highly Selective Difluoroalkylation Reactions. *Chem. Commun.* **2017**, *53*, 8948-8951.

7. Feng, X.; Wang, X.; Chen, H.; Tang, X.; Guo, M.; Zhao, W.;Wang, G., Copper-Mediated Regioselective Hydrodifluoroalkylation of Alkynes. *Org. Biomol. Chem.* **2018**, *16*, 2841-2845.

8. Liang, Z.; Xu, S.; Tian, W.;Zhang, R., Eosin Y-Catalyzed Visible-Light-Mediated Aerobic Oxidative Cyclization of N,N-Dimethylanilines with Maleimides. *Beilstein J. Org. Chem.* **2015**, *11*, 425-430.

9. Yue, J.-Y.; Wang, L.; Ma, Y.; Yang, P.; Zhang, Y.-Q.; Jiang, Y.;Tang, B., Metal ion-assisted carboxyl-containing covalent organic frameworks for the efficient removal of Congo red. *Dalton Trans.* **2019**, *48*, 17763-17769.

Chapter 3. The Synthesis of new COFs via Nucleophilic Aromatic Substitution at Porphyrinoids

3.1. Abstract

We describe the design and synthesis of highly stable and irreversible amine-linked COFs. The proposed amine linkage is prepared via irreversible nucleophilic aromatic substitution reactions (S_NAr) of 5,10,15,20-tetrakis(perfluorophenyl)porphyrin (**$TPPF_{20}$**) **L1** with ethane-1,2-diamine **L2**, 1,4-phenylenedimethanamine **L3,** or cta(3-aminopropyl) silsesquioxanehydrochloride (OAS-POSS) **L4** to form **COF-21**, **XYCOF**, and **SiCOF**, respectively. Post-metalation of COF-21 with iron led to FeClCOF-21, in which its model **K**1 displayed excellent catalytic performance towards a tandem catalytic synthesis of 2-phenyl-1H-benzo[d]imidazole.

3.2. Introduction

COFs are crystalline porous materials linked by reversible covalent bonds such as boronate ester, boroxine, azine, hydrazone, and imine. They have a wide range of applications in gas storage, catalysis, sensing, and separation.[1-4] The relatively stable imine-linked COFs show remarkable promise in a variety of applications when compared to the easily hydrolyzed boronate esters or boroxine-linked COFs, indicating that stability is important in COF applications.[5-7] The reversible covalent linkage is the base of crystal formation as well as the inherent limitation of COF stability. The construction of COFs with irreversible bonds, on the other hand, is critical in the development of stable COFs. However, it remains challenging because irreversible reactions can lead to the formation of poor or non-crystalline polymers.[8] Few efforts have been made to investigate this possibility. Polyarylether-based COFs (also known as dioxin-linked COFs) were synthesized using an irreversible nucleophilic aromatic substitution reaction.[5] The irreversible benzoxazole- and amide-linked COFs were prepared under high-temperature and high-pressure conditions or

through chemical conversion.[4, 9] However, the available synthetic methods and the number of irreversible COFs are insufficient for widespread applications.

In this chapter, we describe the design and synthesis of highly stable and irreversible amine-linked COFs. The proposed amine linkage is prepared via irreversible nucleophilic aromatic substitution reactions (S_NAr) of fluorinated porphyrinoids with amine nucleophiles.

Fluorinated porphyrinoids, such as porphyrins (Pors), phthalocyanines (Pcs), corroles (Cors) and etc., are large aromatic and robust heterocyclic dyes that have been extensively studied for their wide array of applications in diverse fields, such as solar energy conversion, electronic devices, optical sensors, medicine, etc. (**Scheme 3.1**).[10] Porphyrinoids are favored for their diverse applications due to their ability to chelate most transition metals and their capable photophysical properties.[10]

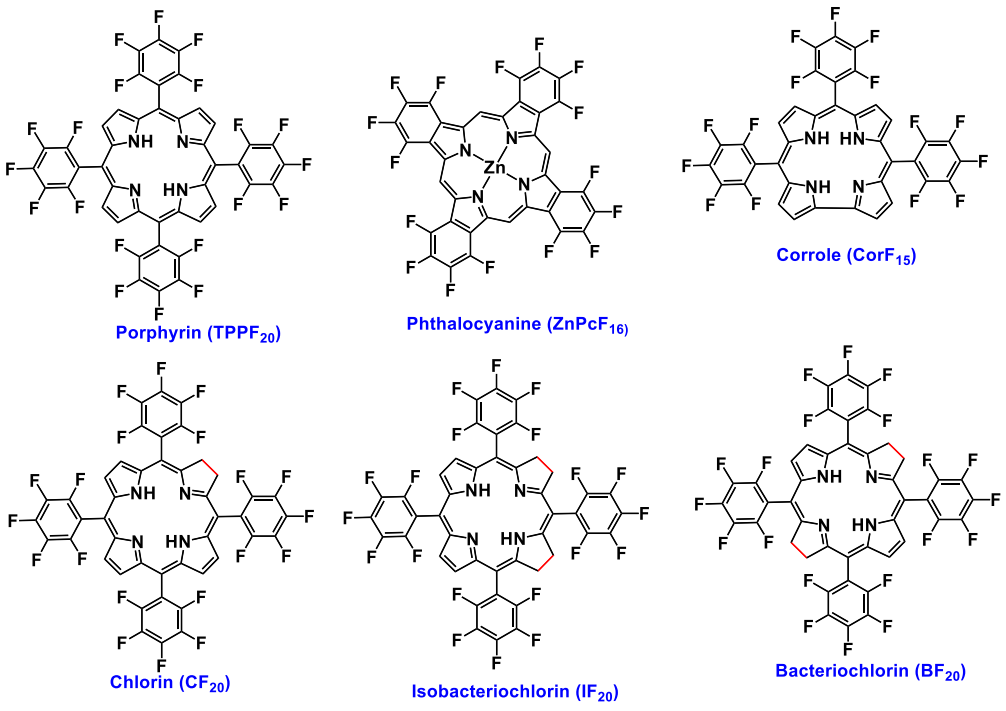

Scheme 3. 1. Diversity of Fluorinated porphyrinoids , adapted from ref 10, Copyright 2016 Organic and Biomolecular Chemistry.

In this report, we have selected 5,10,15,20-tetrakis(perfluorophenyl)porphyrin (**$TPPF_{20}$**) **L2** as a C_4 knot to construct tetragonal COFs because the pentafluorophenyl group in porphyrinoids can easily undergo nucleophilic substitution of fluorine with O-, S- or N-nucleophiles. Furthermore, the significant regioselectivity of the nucleophilic aromatic substitution at the para-position only leads to tetra-substituted products, avoiding undesirable by-products (**Scheme 3.2)**.[11]The reactivity of the para fluoro group on the pentafluorophenyl moiety depends on the type of nucleophile used, where the softer nucleophiles are more reactive than harder nucleophiles, $HS–CH_2R > H_2N–CH_2R$. $HO–CH_2R$. Studies also found that the secondary nucleophiles are being much less reactive in comparison to primary nucleophiles. With this knowledge, we decided to test various aromatic and aliphatic primary amines as a linker for COF synthesis.[12, 13]

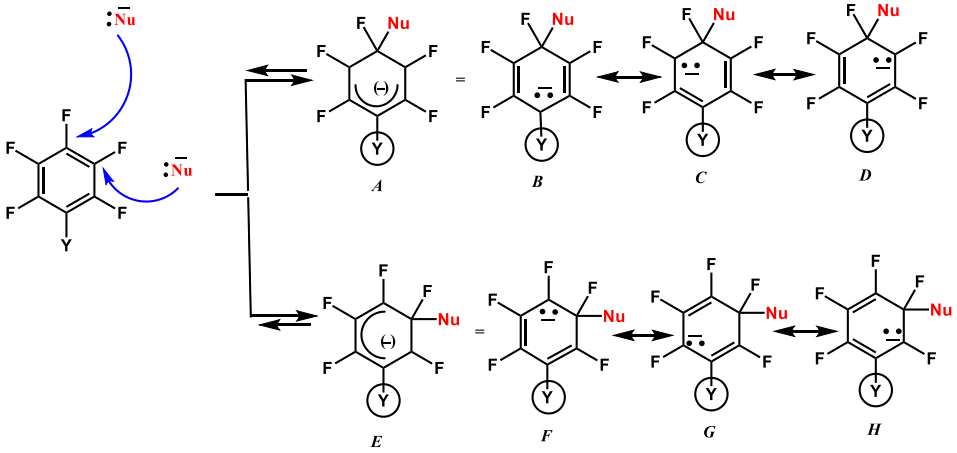

Scheme 3. 2. Regioselectivity of the nucleophilic aromatic substitution at the para-position in pentafluorophenyl group, adapted from ref 11, Copyright 2010 Fluorine Chemistry.

Herein, we show how 5,10,15,20-tetrakis(perfluorophenyl)porphyrin (**$TPPF_{20}$**) **L1** can react with ethane-1,2-diamine **L2** and 1,4-phenylenedimethanamine **L3** in the presence of a base to produce two crystalline, porous, amine-linked frameworks, **COF-21** and **XYCOF,** respectively (**Figure 3.1B**). Although five fluorine atoms are present in the pentafluorophenyl group, under optimal

reaction conditions, the substitution occurs with high regioselectivity in the para-position, which makes **L1** a directional building unit for a square net growth with an amine linker **L2** or **L3**.

3.3. Methods

Design and preparation of amine-linked COFs

We initiated our study with the synthesis of amine-linked molecular analogs **M1** and **M2**. They were successfully synthesized with a microwave reactor using DMSO as a solvent at 90°C for 30 and 75 min, respectively (**Figure 3.1A**). Their structures were then analyzed by ^{1}H and ^{13}C NMR spectroscopy and high-resolution ESI mass spectroscopy (**Figure 3.23 and 3.24**). The results show that all fluorine in the para positions on **L1** were selectively substituted by the amine nucleophile.

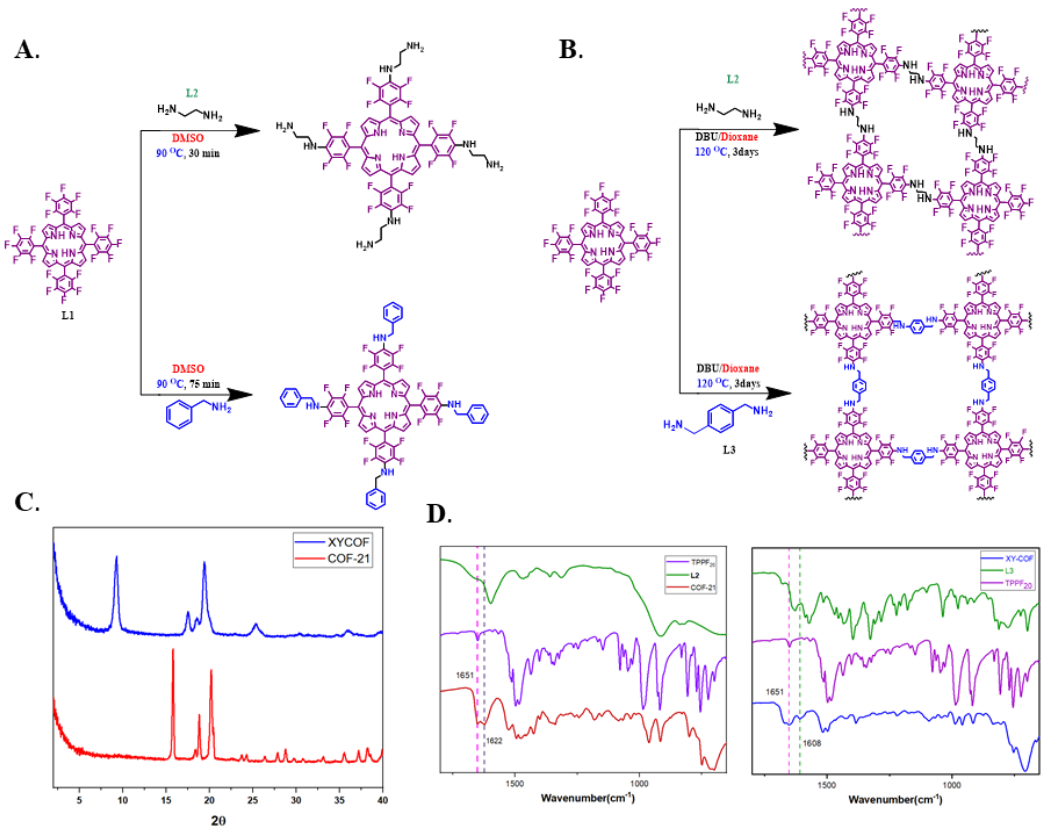

Figure 3. 1. (A**).** The synthesis of molecular analog M1and M2; (B). The synthesis of COF-21 and XYCOF; **(**C). PXRD patterns of COF-21 and XYCOF; (D). FT-IR spectra of COF-21 and XYCOF.

With this knowledge in mind, we attempted the synthesis of COFs by reacting **L1** with **L2** and **L3**. Extensive efforts were applied to screen different synthetic conditions including amine linkers, bases, temperatures, solvent mixtures, and reaction time. A crystalline framework termed COF-21 was successfully synthesized in the presence of stoichiometric DBU as a base at 120 °C for 3 d with high yield (60%). We further extended the reaction scope by crystallizing **XYCOF** by linking **L1** and **L3** under similar conditions. We should point out that the conditions under which these COFs were synthesized are different from those used in making amine-linked molecular analogs **M1** and **M2**.

After the successful synthesis of COF- linked amines, FeClCOF-21 was obtained by refluxing COF-21 with $FeCl_2.4H_2O$ in DMF for 4h.(See the supporting information for details).

3.4. Result and discussion

Characterization of amine-linked COFs

The crystallinity of **COF-21** and **XYCOF** was confirmed by powder X-ray diffraction (PXRD), with no diffraction peaks corresponding to the starting materials (**Figure 3.1C**). Both eclipsed and staggered stacking modes were considered but have not been confirmed yet by computational simulation using Material Studio. The scanning electron microscopy shows only one morphology observed for each COF (**Figure 3.3** and **3.4**).

The successful formation of the amine linkage was confirmed by FT-IR spectroscopy (**Figure 3.1D and 3.7**). In COF-21, the spectra show new peaks at 1,182 cm^{-1} and 1,622 cm^{-1} correspond to C–N vibration stretch and C–N–H bending stretch in the secondary amine linkage. The disappearance of the 3289 and 3357 cm^{-1} peaks, corresponding to the N-H vibration stretch of primary amine in **L2**, demonstrated the complete conversion of a primary amine. In **XYCOF**, on

the other hand, the new peaks at 1,221 cm^{-1} and 1,608 cm^{-1} confirmed the formation of C–N vibration stretch and C–N–H bending stretch in the secondary amine linkage. The disappearance of the 1,036 cm^{-1}peak, corresponding to the C-N vibration stretch of a primary amine in **L3**, demonstrated the complete conversion of primary amines (**Figure 3.1D, 3.8**).

In addition, the quantitative formation of amine linkages was verified by ^{13}C cross-polarization magic angle spinning (CP/MAS) NMR spectroscopy (**Figure 3.11 and 3.12).** It was observed that the primary amine carbon peak of **L2,** at 45 ppm, shifted to 37 ppm in the ^{13}C -NMR spectrum of **COF-21**. Similarly, the primary amine carbon peak belonging to **L3** at 47 ppm shifted to 45 ppm in the ^{13}C -NMR spectrum of **XYCOF**, indicating the formation of secondary amine linkages.

Inspired by our results, we expanded our study to synthesize 3D COFs instead of 2DCOFs. 3D COFs can characteristically possess numerous open sites and show promising applications in different areas.[6] Moreover, the incorporation of porphyrins into 3D provides accessibility in all porphyrin units within the framework, thus making them extremely attractive for catalysis. Considering their interesting properties and promising applications, the design and synthesis of porphyrin-functionalized 3D COFs are highly demanded. Thus, we designed and synthesized **SiCOF** via connecting **L1** and **L4** (See SI for more details about the synthesis). The crystallinity was confirmed by powder X-ray diffraction PXRD and the formation of amine linkage by FT-IR (**Figure 3.2B 3.9**).

Porphyrins are favored for their diverse applications such as their ability to chelate most transition metals and their capable photophysical properties. [10] For example, zinc porphyrins have shown excellent PDT/PTT efficacy, making them promising photothermogenic photosensitizers for cancer treatment. For this reason, we designed and synthesized **ZnCOF** by binding (**$ZnTPPF_{20}$**)

N and **L2,** which is its crystallinity confirmed by PXRD (**Figure 3.2B**). However, according to the FT-IR spectra (**Figure 3.10**), the 3289 and 3357 cm^{-1} peaks corresponding to the N-H vibration stretch of primary amines in **L2** did not change after the formation of the porous material. That indicates the possibility of Zn coordination to the primary amines rather than a reaction with the pentafluorophynel group in the porphyrin or both.

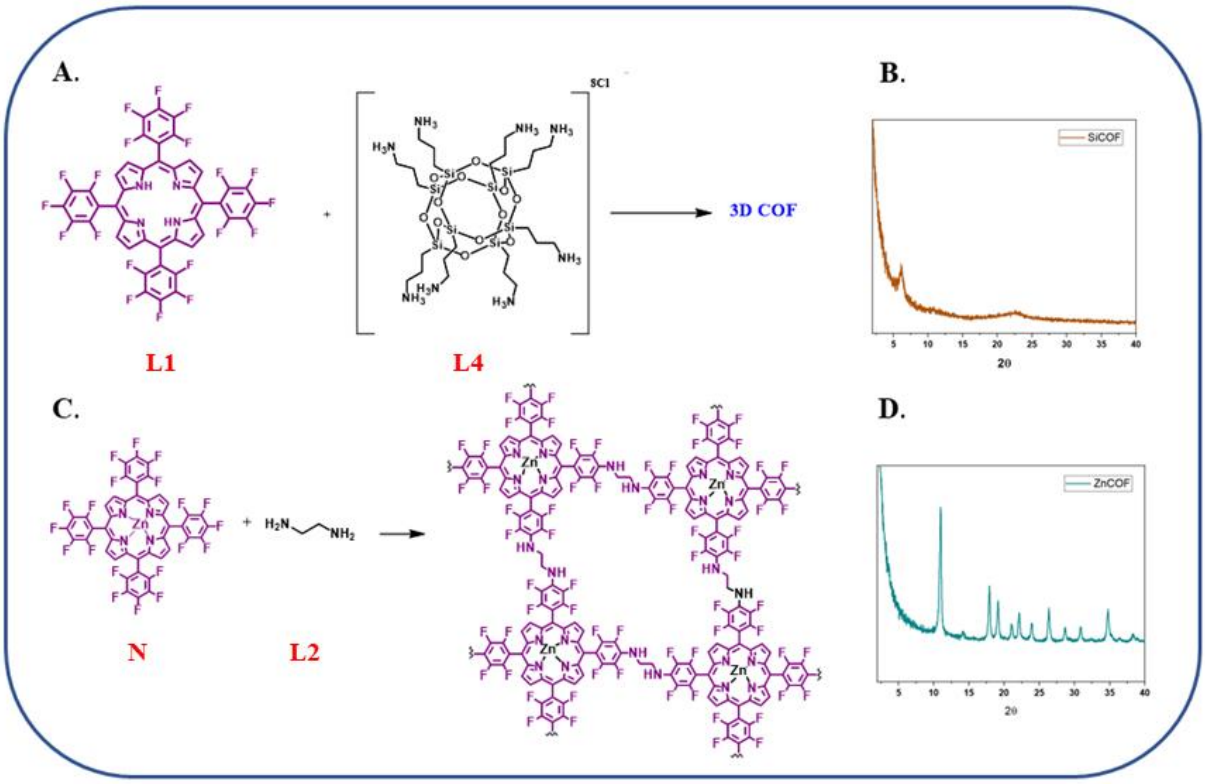

Figure 3. 2. (A). and (C). The synthesis of SICOF and ZnCOF, (B) and (D). PXRD patterns of SICOF and ZnCOF, respectively.

Tandem catalytic synthesis of 2-phenyl-1H-benzo[d]imidazole catalyzed by FeClCOF-21

In our study, we are aiming to synthesize a variety of benzimidazole derivatives through a tandem catalytic process: an in-situ oxidation-cyclic aminal formation-oxidation sequence catalyzed by (**FeClCOF-21**). The benzimidazole ring is known as an essential pharmacophore in modern drug research. Its derivatives have shown significant activity against several viruses such as HIV,[14]

herpes (HSV-1), influenza, and human cytomegalovirus (HCMV). Furthermore, they are significant intermediates in organic reactions [15] and can serve as ligands to transition metals for modeling biological systems.[16] Therefore, benzimidazole preparations have received a lot of attention in recent years.

We initiated our investigation by evaluating the catalytic activity of **FeClTTPF$_{20}$** on the tandem reaction. Screening experiments in various solvents, including acetonitrile, ethanol, or a mixture of ethanol and acetonitrile, pointed to acetonitrile as the most suitable reaction medium (**Table 3.1**). The optimized condition facilitated the synthesis of the corresponding oxidation products, 2-phenyl-1H-benzo[d]imidazole **D**. The results indicated that the reaction occurs through sequential addition of benzene-1,2-diamine **C** to benzaldehyde **B**, after complete conversion of benzyl alcohol, to produce **D**, with FeClTTPF$_{20}$ **K1** functioning as both an oxidation catalyst and Lewis acid (**Table 3.1, entry 8**).

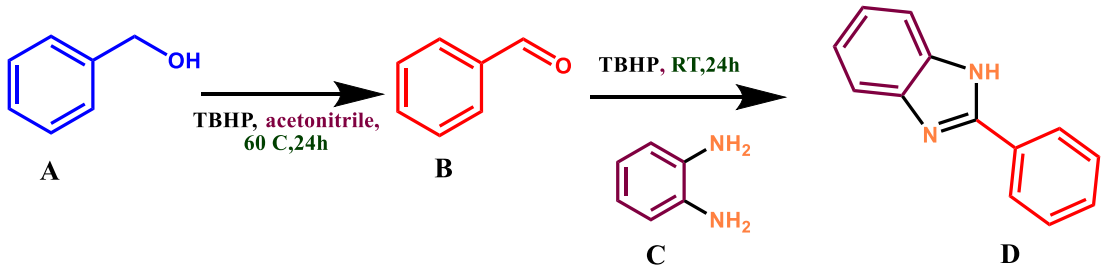

Scheme 3. 3. Tandem catalytic synthesis of 2-phenyl-1H-benzo[d]imidazole.

Table 3. 1. Optimaizaion of the tandem reaction coditions.

Entry	Solvent	Temperature	**A**	**B %**	**C%**	**D %**
1	EtOH	rt	-	96	-	-
2	acetonitrile	rt	-	✓	✓	~80
3	acetonitrile	60	✓	✓	✓	~80
4	EtOH	rt	✓	~90	✓	0
5	EtOH	60	✓	~90	✓	0
6	EtOH:acetonitrile,	rt	✓	~50	✓	0
7	EtOH:acetonitrile,	60	✓	~50	✓	0
8[a]	acetonitrile	1. 60 2. rt	✓	~99%	✓	~95

[a] the sequential addition of benzene-1,2-diamine **C** to benzaldehyde **B**, after a complete conversion of benzyl alcohol, to form **D**, with $FeClTTPF_{20}$ **K1** functioning as both an oxidation catalyst and Lewis acid.

3.5.Conclusion and Future Work

In this study, we have successfully designed and synthesized several COFs with amine linkages via nucleophilic aromatic substitution on $TTPF_{20}$. However, future characterizations such as BET and computational simulation of PXRD are required to confirm the porosity and crystallinity of all obtained COFs. The catalytic activity of **FeClCOF-21** will then be evaluated on a tandem catalytic process: an in-situ oxidation-cyclic aminal formation-oxidation sequence for the formation of benzimidazole derivatives. XYCOF will be used for the removal of perfluorinated alkyl substances PFAS such as perfluorooctanoic acid (PFOA) from water. **SiCOF** will be tested for the efficient

capture and storage of radioactive iodine (^{129}I or ^{131}I). Finally, **ZnCOF** will be used as a photothermogenic photosensitizer for cancer treatment

3.6. References

1. Côté, A. P.; Benin, A. I.; Ockwig, N. W.; Keeffe, M.; Matzger, A. J.;Yaghi, O. M., Porous, Crystalline, Covalent Organic Frameworks. *Science* **2005**, *310*, 1166.

2. Feng, X.; Ding, X.;Jiang, D., Covalent organic frameworks. *Chem. Soc. Rev.* **2012**, *41*, 6010-6022.

3. Ding, S.-Y.;Wang, W., Covalent organic frameworks (COFs): from design to applications. *Chem. Soc. Rev.* **2013**, *42*, 548-568.

4. Waller, P. J.; Gándara, F.;Yaghi, O. M., Chemistry of Covalent Organic Frameworks. *Acc. Chem. Res.* **2015**, *48*, 3053-3063.

5. Guan, X.; Li, H.; Ma, Y.; Xue, M.; Fang, Q.; Yan, Y.; Valtchev, V.;Qiu, S., Chemically stable polyarylether-based covalent organic frameworks. *Nat Chem* **2019**, *11*, 587-594.

6. Lu, Q.; Ma, Y.; Li, H.; Guan, X.; Yusran, Y.; Xue, M.; Fang, Q.; Yan, Y.; Qiu, S.;Valtchev, V., Postsynthetic Functionalization of Three-Dimensional Covalent Organic Frameworks for Selective Extraction of Lanthanide Ions. *Angewandte Chemie (International ed. in English)* **2018**, *57*, 6042-6048.

7. Ding, S.-Y.; Wang, P.-L.; Yin, G.-L.; Zhang, X.;Lu, G., Energy transfer in covalent organic frameworks for visible-light-induced hydrogen evolution. *International Journal of Hydrogen Energy* **2019**, *44*, 11872-11876.

8. Qian, H.-L.; Meng, F.-L.; Yang, C.-X.;Yan, X.-P., Irreversible Amide-Linked Covalent Organic Framework for Selective and Ultrafast Gold Recovery. *Angew. Chem. Int. Ed.* **2020**, *59*, 17607-17613.

9. Waller, P. J.; Lyle, S. J.; Osborn Popp, T. M.; Diercks, C. S.; Reimer, J. A.;Yaghi, O. M., Chemical Conversion of Linkages in Covalent Organic Frameworks. *J. Am. Chem. Soc.* **2016**, *138*, 15519-15522.

10. Bhupathiraju, N.; Rizvi, W.; Batteas, J. D.;Drain, C. M., Fluorinated porphyrinoids as efficient platforms for new photonic materials, sensors, and therapeutics. *Org Biomol Chem* **2016**, *14*, 389-408.

11. Kvíčala, J.; Beneš, M.; Paleta, O.;Král, V., Regiospecific nucleophilic substitution in 2,3,4,5,6-pentafluorobiphenyl as model compound for supramolecular systems. Theoretical study of transition states and energy profiles, evidence for tetrahedral SN2 mechanism. *Journal of Fluorine Chemistry* **2010**, *131*, 1327-1337.

12. Kvíčala, J.; Beneš, M.; Paleta, O.;Kral, V., ChemInform Abstract: Regiospecific Nucleophilic Substitution in 2,3,4,5,6-Pentafluorobiphenyl as Model Compound for

Supramolecular Systems. Theoretical Study of Transition States and Energy Profiles, Evidence for Tetrahedral SN2 Mechanism. *Journal of Fluorine Chemistry - J FLUORINE CHEM* **2010**, *131*.

13. Golf, H. R. A.; Reissig, H.-U.;Wiehe, A., Nucleophilic Substitution on (Pentafluorophenyl)dipyrromethane: A New Route to Building Blocks for Functionalized BODIPYs and Tetrapyrroles. *Organic Letters* **2015**, *17*, 982-985.

14. Porcari, A. R.; Devivar, R. V.; Kucera, L. S.; Drach, J. C.;Townsend, L. B., Design, synthesis, and antiviral evaluations of 1-(substituted benzyl)-2-substituted-5,6-dichlorobenzimidazoles as nonnucleoside analogues of 2,5,6-trichloro-1-(beta-D-ribofuranosyl)benzimidazole. *Journal of medicinal chemistry* **1998**, *41*, 1252-62.

15. Karimi-Jaberi, Z.;Amiri, M., An Efficient and Inexpensive Synthesis of 2-Substituted Benzimidazoles in Water Using Boric Acid at Room Temperature. *E-Journal of Chemistry* **2012**, *9*, 793978.

16. Fekner, T.; Gallucci, J.;Chan, M. K., Synthesis and Metalation of a Chiral, Pyridine-Strapped, Cyclic Bis(benzimidazole) Ligand. *Organic Letters* **2004**, *6*, 989-992.

3.7. Synthesis and General Procedures

3.7.1. Synthesis of Starting Materials

3.7.1.1. The Synthesis of *meso*- tetrakis(pentafluorophenyl) porphyrin L1[1]

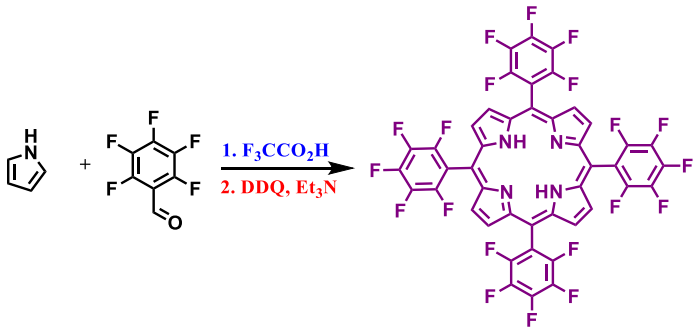

Scheme 3. 4. Synthetic route for ligand **L1**.

This reaction condition was performed four times with two different samples of trifluoromethanesulfonic acid. To a 2 L round-bottom flask containing a stir bar, CH_2Cl_2 (1.0 L), pyrrole (0.5ml,0.007, 1.0eq), and pentafluorobenzaldehyde (0.9ml,0.007, 1.0eq) were added. After stirring briefly, the reaction was initiated by the addition of trifluoromethanesulfonic acid (65 µL, 0.1eq). The flask was tightly capped, and the reaction mixture was stirred at room temperature overnight. At a reaction time of 24 h, the reaction mixture was oxidized by the addition of 1,4-Cyclohexadiene-1,2-dicarbonitrile, 4,5-dichloro-3,6-dioxo DDQ (1.8g, 1.8eq) at room temperature. After ~1 min, triethylamine (0.4ml, 4.00 eq relative to the acid) was added, and the mixture was stirred at room temperature. At an oxidation reaction time of 30 min, an aliquot (1.2 mL) of the reaction mixture was removed for TLC. At 1 h, the reaction mixture was filtered through a pad of activity silica and eluted with CH_2Cl_2 (300 mL) until porphyrin was no longer detected in the eluent by TLC (silica, 1:1 CH_2Cl_2/hexanes). The filtrate was concentrated to a dark, purple/brown film. The product was then separated by chromatography using silica gel (1:3, 1:2,

and 1:1 CH_2Cl_2/hexanes). Fractions containing (**TPPF$_{20}$**) **L1** (0.601 g, 35.4%) were obtained with a solvent composition of 1:3 CH_2Cl_2/hexanes. Elution with 1:3 CH_2Cl_2/hexanes was continued until porphyrin was no longer detected in the eluent by TLC (1:1 CH_2Cl_2/hexanes). 1H NMR ($CDCl_3$) δ 8.925 (s, 8 H), -2.909 (s, 2 H).

3.7.1.2. Synthesis of (Pentafluorophenyl)dipyrromethene) [2]

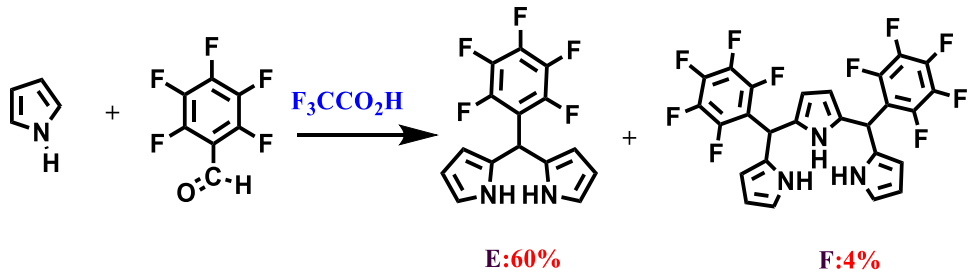

Scheme 3. 5. Synthetic route for **E** and **F**.

A solution of pentafluorobenzaldehyde (3.6ml, 0.029,1eq) in freshly distilled pyrrole (75ml, 1.08, 44.4eq) was degassed with a stream of nitrogen for 20 min before adding trifluoroacetic acid (180 µL, 0.1eq). The mixture was stirred for 30min to one hour at room temperature. After the completion of the reaction, it was diluted with CH_2Cl_2 (800 mL), and then washed with 0.1M NaOH (400 mL). The organic phase was washed with water (400 mL) and dried over Na_2SO_4. Evaporation of the solvent at reduced pressure gave brown oil. Unreacted pyrrole was removed under high vacuum, yielding a tacky solid that was flashed on a column of silica using a mixture of hexanes: DCM (4:1, 3:1, and 2:1) as the eluent. The products, in TLC plate (pink A and purple B), were obtained (5.50g) of 5-(pentafluorophenyl) dipyrromethane as black to gray powder (60% yield).[2]1H NMR (400 MHz, CDCl3): δ 5.90 (1H, s, CH), 6.02 (2H, s, ArH), 6.161 – 6.168(2H, m, ArH), 6.735 – 6.739 (2H, m, ArH), 8.14 (2H, brs, NH); 19F NMR (400 MHz, CDCl3): δ -160.98 – -161.40 (2F, m, ArF), -155.71 (1F, t, J = 21.0 Hz, ArF) -141.43 (2F, brd, J = 20.7 Hz, ArF). and

(0.6g) of pentafluorophenyl)tripyrromethane as dark purple(4%).: 1H NMR 400 MHz, CDCl3) δ = 8.12 (bs, 2H, NH), 8.01(bs, 1H, NH), 6.74 (m, 2H, βH), 6.16 (m, 2H, βH), 5.99 (s, 2H, αH), 5.93 (d, J = 1.6 Hz, 2H, βH), 5.83 (s, 2H, meso-H).

3.7.1.3. The synthesis of 5,15-bis(pentafluorophenyl)-10,20-diphenylporphyrin [3]

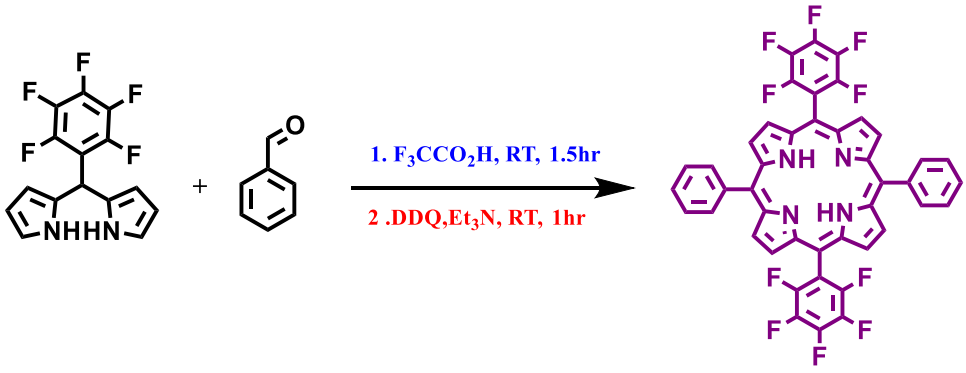

G

Scheme 3. 6. Synthetic route for **G**.

To a flask equipped with a magnetic stir bar, 5-(pentafluorophenyl)dipyrromethane (1.5g, 0.0048, 1.0eq) and benzaldehyde(0.53ml, .0051) were dissolved in CH_2Cl_2 , followed by addition of trifluoroacetic acid (1.49ml, 0.0086, 1.8eq). After stirring for 1.5 h at room temperature, 2,3-dichloro-5,6-dicyano-1,4-benzoquinone DDQ (1.6g, 0.0070, 1.5eq) was added. The mixture was stirred for another 1 h and then was neutralized by triethylamine. The reaction mixture was then filtered through a pad of silica gel with CH_2Cl_2 until the eluting solution was pale brown. The resulting solution was evaporated to dryness, and the resulting residue was purified by silica-gel column chromatography (hexanes/CH_2Cl_2 = 3:1, v/v) to afford pure 5,15-bis(pentafluorophenyl)-10,20-diphenylporphyrin as a purple solid (0.280 g, 14%).[3] 1H NMR (400 MHz, $CDCl_3$): δ = 8.95(d, J = 4.9 Hz, 4H), 8.81 (d, J = 4.8 Hz, 4H), 8.25 (d, J = 6.4 Hz, 4H), 7.83-7.77 (m, 6H), −2.83 (s, 2H).

3.7.1.4. The Synthesis of 5-(4-nitro phenyl) dipyrromethene [4]

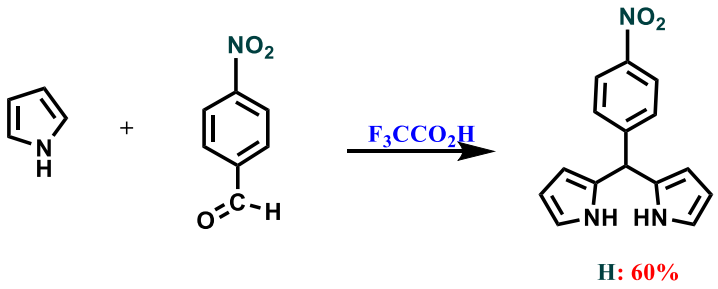

Scheme 3. 7. Synthetic route for **H.**

A solution of nitrobenzaldehyde (3g, 0.0198, 1.0eq) in freshly distilled pyrrole (75ml, 1.08,44.4 eq) was degassed with a stream of argon for 15 min before adding trifluoroacetic acid (15µL, 0.1eq). The mixture was stirred for 1.5 min at room temperature. After the completion of the reaction, it was quenched with NaOH and stirred for 30min. Then, the salt was filtered from the mixture. After unreacted pyrrole was removed under high vacuum, the solid was washed with DCM, hexane and diethylether and filtered, yielding a tacky solid (2.266g, 48%).[4]1H NMR ($CDCl_3$) δ 5.59 (s, 1 H), 5.88 (s, 2 H), 6.187 (q, J= 3.2 Hz, 2 H), 6.75-6.77 (m, 2 H), 7.37 (AA′BB′m, 2 H), 7.99 (br s, 2 H), 8.18 (AA′BB′m, 2 H).

3.7.1.5 The Synthesis of 5,15-bis(4-nitrophenyl)-10,20-diphenylporphyrin [5]

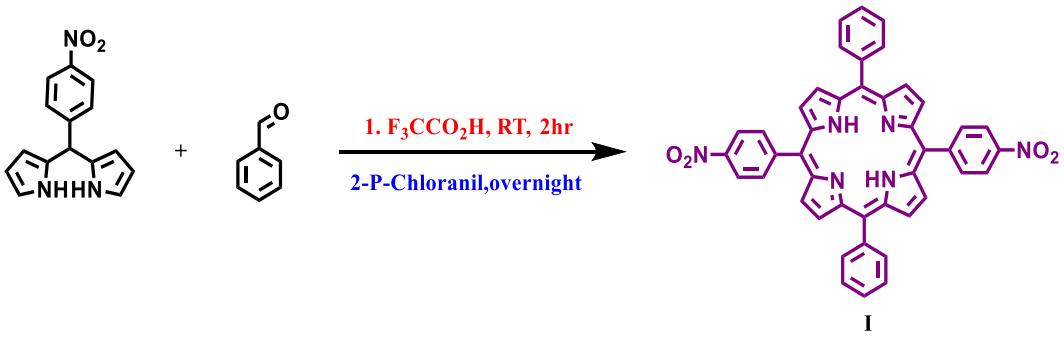

I

Scheme 3. 8. Synthetic route for **I.**.

A solution of dipyrromethane (1.00g, 0.0032,1eq) and benzaldehyde (0.382 ml, .0037) in chloroform (325 mL) was degassed by bubbling with nitrogen for 1 h. The reaction vessel was shielded from ambient light. Trifluoroacetic acid (0.52ml, 0.0067) was then added to one portion. The solution was stirred for 2 h at room temperature under a nitrogen atmosphere. To the reddish-black reaction mixture, p-chloranil was added with overnight stirring. Triethylamine was added and then the reaction mixture was concentrated. Flash column chromatography on silica gel (30:1) (DCM/Ethyl acetate) yielded the desired porphyrin from the mixture as the third major band. Reprecipitation with chloroform and methanol afforded a vivid reddish-purple solid (368mg, 33%).[5] 1H NMR (400 MHz, $CDCl_3$) -2.79 (br s, 2H), 7.78 (m, 6H), 8.21 (d, J ¼ 8 Hz, 4H), 8.84 (d, J ¼ 8 Hz, 4H), 8.65 (d, J ¼ 8 Hz, 4H), 8.75 (d, J ¼ 4 Hz, 4H), 8.90(d, J ¼ 4 Hz, 4H).

3.7.1.6 The Synthesis of 4,4'-(10,20-diphenylporphyrin-5,15-diyl)dianiline [6]

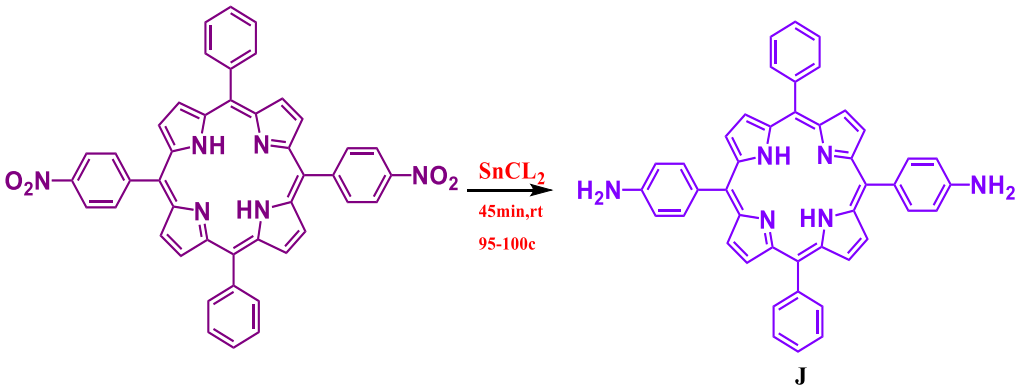

J

Scheme 3. 9. Synthetic route for **J**.

$SnCl_2$(0.192ml, 15eq) was added to a suspension of 4,4'-(10,20-diphenylporphyrin-5,15-diyl)dianiline (40mg, 0.056mM)in concentrated HCl (8.4ml) solution. The reaction mixture was stirred for 45 min at room temperature and maintained at 85°C for an additional 24 h. After cooling, the reaction was quenched by the slow addition of 6M of NaOH(100ml). The organic layer was extracted with CH_2Cl_2 and washed with water. After standing over anhydrous Na_2SO_4, the organic extract was concentrated to dryness. Flash column chromatography on silica gel with Hexane: ethyl acetate (2:1) as the eluent and subsequent reprecipitation from $CHCl_3$&CH_3OH gave 4,4'-(10,20-diphenylporphyrin-5,15-diyl)dianiline as a deep violet solid (24 mg, 66%).[6] 1 H NMR (400 MHz, $CDCl_3$) -2.73 (br s, 2H), 4.13 (br s, 4H), 7.08 (d, J ¼ 8.3 Hz, 4H), 7.74 (m, 6H), 8.00(d, J ¼ 8.3 Hz, 4H), 8.22 (d, J ¼ 4 Hz, 4H), 8.82 (d, J ¼ 4.8 Hz, 4H), 8.93 (d, J ¼ 4.8 Hz, 4H).

3.7.1.7. The Synthesis of N1,N1',N1'',N1'''-(porphyrin-5,10,15,20-tetrayltetrakis(2,3,5,6-tetrafluorobenzene-4,1-diyl))tetrakis(ethane-1,2-diamine) [7]

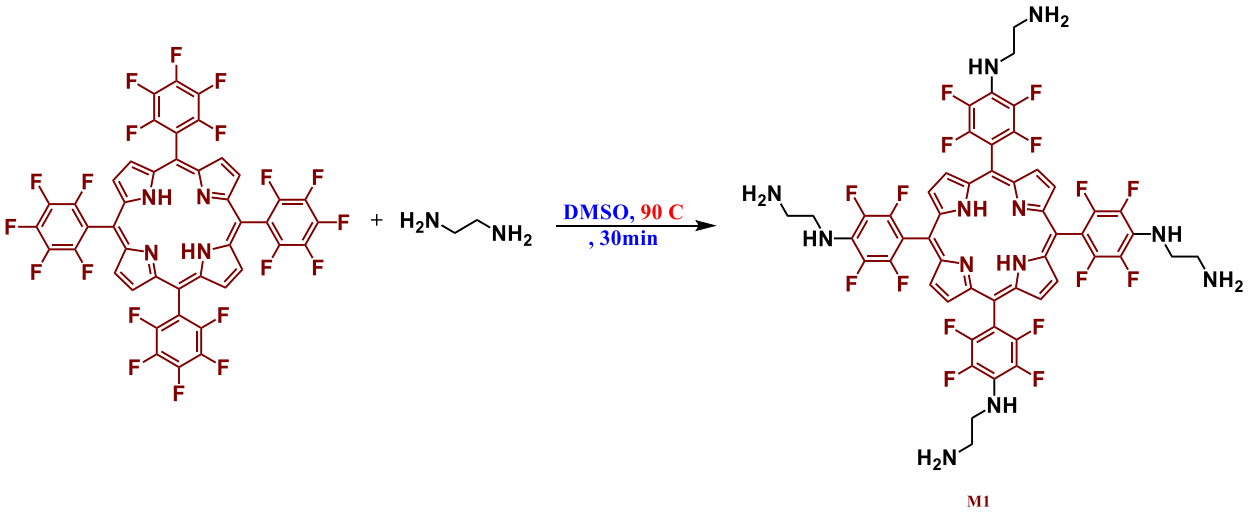

Scheme 3. 10. Synthetic route for **M1**.

The following is a general technique for preparing $TPPF_{20}$ amino derivatives using microwave irradiation: 50 mg of 5,10,15,20-tetrakispentafluorophenylporphyrin (51.3 mol) and 20 equiv. of the selected amine derivative were added to a small vial (DMSO, 0.5 mL).The closed vial was irradiated in a microwave reactor (200 W, 300 PIS, 90 ºC) for 30 min. The reaction was monitored by TLC and by ^{19}F NMR, usually between 4 to 6 times (9 to 15 min). After the completion of the reaction, the solvent was evaporated under reduced pressure. The crude mixture was redissolved in CH_2Cl_2 Or EtOAc and washed water. The extracted organic layer was dried (Na_2SO_4) and the solvent evaporated under reduced pressure. The desired products were then directly crystalized with DCM: n-Hexane. Typical yields were over 60%. ^1H NMR (400 MHz, DMSO) δ 9.23 (s, 8H), 6.44 (s, 4H), 3.65 – 3.58 (m, 8H), 3.56 (s, 4H), 2.97 (t, *J* = 6.2 Hz, 8H), -3.11 (s, 2H).^{13}C NMR (101 MHz, DMSO) δ 148.12, 145.81, 138.26, 135.90, 130.60, 105.29, 104.64, 66.82, 48.39, 42.58.^{19}F NMR (376 MHz, DMSO) δ -143.11, -160.80.

3.7.1.8. The Synthesis of 4,4',4'',4'''-(porphyrin-5,10,15,20-tetrayl)tetrakis(N-benzyl-2,3,5,6-tetrafluoroaniline) [7]

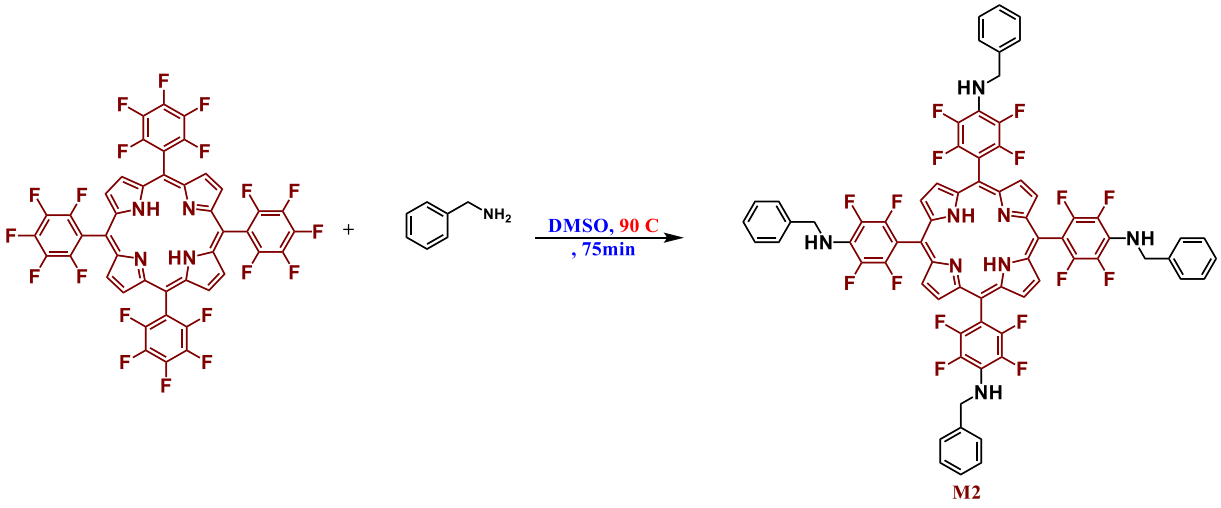

Scheme 3. 11. Synthetic route for **M2**.

50 mg of 5,10,15,20-tetrakispentafluorophenylporphyrin (51.3 mol) and 20 equiv. of phenylmethanamine were added to a small vial (DMSO, 0.5 mL). The closed vial was irradiated in a microwave reactor (200 W, 300 PIS, 90 ºC) for 75 min. The reaction was monitored by TLC and by ^{19}F NMR, usually between 4 to 6 times (9 to 15 min). After the completion of the reaction, the solvent was evaporated under reduced pressure. The crude mixture was redissolved in CH_2Cl_2 Or EtOAc and washed water. The extracted organic layer was dried (Na_2SO_4) and the solvent evaporated under reduced pressure. The desired products were then directly crystalized with DCM: n-Hexane. Typical yields were over 75%.^{1}H NMR (400 MHz, DMSO) δ 9.12 (s, 8H), 7.56 (d, *J* = 7.3 Hz, 8H), 7.47 (t, *J* = 7.6 Hz, 8H), 7.35 (t, *J* = 7.3 Hz, 4H), 7.23 (s, 4H), 4.78 (s, 9H), -3.18 (s, 2H). ^{13}C NMR (101 MHz, DMSO) δ 147.81, 145.53, 140.91, 137.82, 136.05 – 135.70 (m), 129.98, 128.97, 127.51, 105.19, 48.50.^{19}F NMR (376 MHz, DMSO) δ -142.91, -159.94.

3.7.1.9. The Synthesis of $FeTPPF_{20}$ [8, 9]

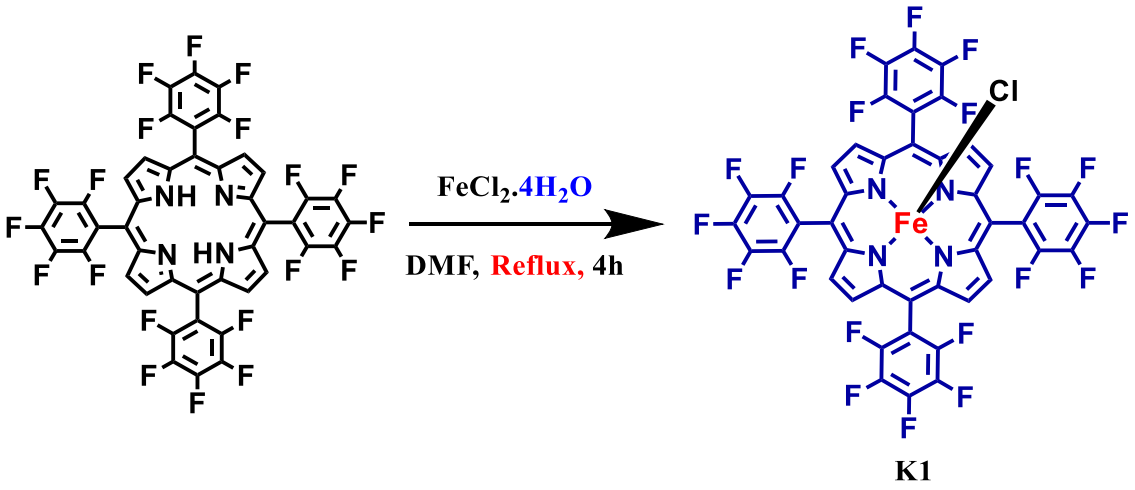

Scheme 3. 12. Synthetic route for **K1**.

A three-necked round-bottomed flask equipped with a thermometer, reflux condenser, and magnetic force stirrer was charged with DMF (5 mL), 5,10,15,20-tetrakispentafluorophenylporphyrin (50mg, 51.3 mol) $FeCl_2.4H_2O$ (0.32 mmol). The reaction mixture was stirred under reflux for 4 h at 150 °C. TLC revealed the complete disappearance of the starting material. Deionized water (20 mL) and 6M HCl (30 mL) were added to the cooled mixture, and a crystalline product was formed. After overnight deposition, followed by filtration washed with water several times and drying in a vacuum, the crude product was obtained. This was dissolved in CH_2Cl_2 and washed with water. The extracted organic layer was dried over Na_2SO_4 and the solvent evaporated under reduced pressure, yielding to the desired product as a powder (90%).

3.7.1.10. The Synthesis of $FeTTPF_{20}$ [8]

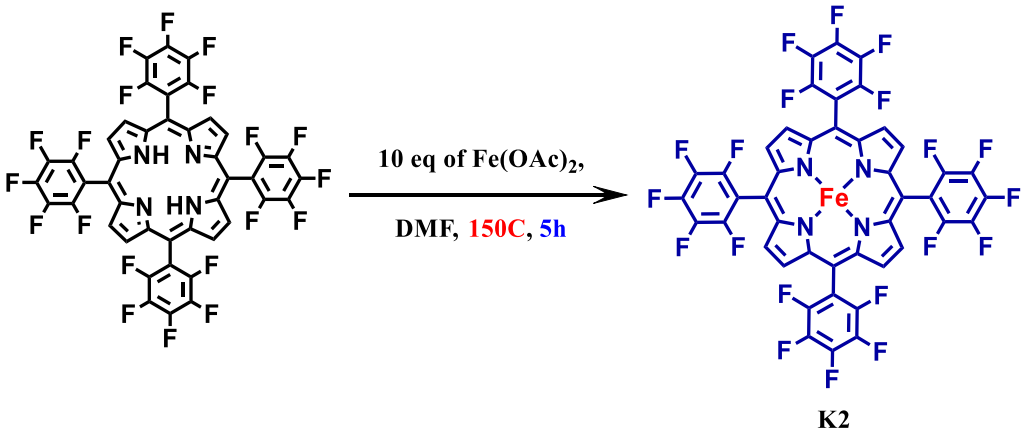

K2

Scheme 3. 13. Synthetic route for **K2**.

A three-necked round-bottomed flask equipped with a thermometer, reflux condenser, and magnetic force stirrer was charged with DMF (5 mL), 5,10,15,20-tetrakispentafluorophenylporphyrin (50mg, 51.3 mol) FeOAc (0.32 mmol). The reaction mixture was stirred under reflux for 5 h at 150 °C. TLC revealed the complete disappearance of the starting material. After the completion of the reaction, the solvent was evaporated under reduced pressure. The crude mixture was redissolved in CH_2Cl_2 and washed with water. The extracted organic layer was dried over Na_2SO_4 and the solvent evaporated under reduced pressure, yielding to the desired product as a powder (~80%).[10]

3.7.1.11. The Synthesis of ZnTTPF$_{20}$

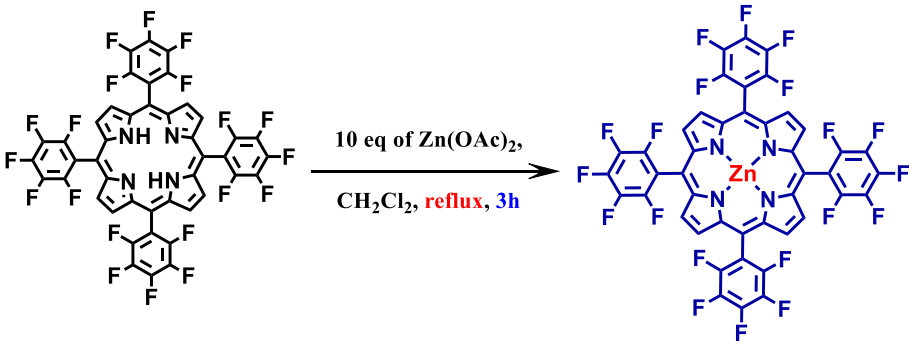

N

Scheme 3. 14. Synthetic route for **N**.

To a solution of **TPPF$_{20}$** (50 mg, 0.06 mmol) in a mixture of CH_2Cl_2 (10 mL) and methanol (2 mL) $Zn(OAc)_2$ (94 mg, 0.6 mmol) was added, and the mixture was refluxed for 3 h. Then the reaction mixture was washed with water (200 mL), the organic layer was dried over $NaSO_4$, and the solvent was removed under reduced pressure. Yield ~99% UVevis ($CHCl_3$): lmax, nm (ε 10^{-3}): 413 (5.83), 542 (4.46). 1 H NMR (400.13 MHz, $CDCl_3$), d: 9.01(s, 8H).

3.7.2. Synthesis of COF

3.7.2.1. COF-21 Synthesis

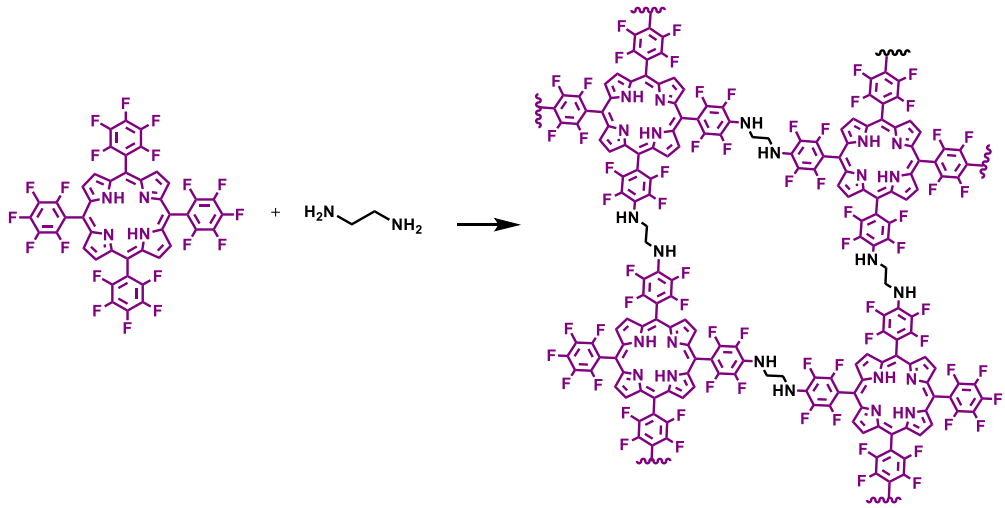

Scheme 3. 15. Synthetic route for COF-21.

Tetrakis(pentafluorophenyl)- Porphyrin (22.1 mg, 0.023mM) and ethylene diamine (3.9 µl, 0.046 mM) were placed in a glass ampule vessel (20 mL), followed by adding a solution of dioxane/ DBU (1ml; 2eq based on the amine). The mixture was sonicated for 5 min and then flash-frozen in liquid nitrogen. The vessel was evacuated to an inner pressure of ~20 Pa, flame-sealed, and heated at 120 °C for 3 days. The resulting precipitate was washed sequentially with DMF (3 times) and acetone (3 times) to give a powder, which was dried at 120 °C under vacuum for 12 h to give the desired product in 75% yield.

Table 3. 2. Modifying the reaction condition by changing the base, concentration and temperature.

Entry	**L1 (eq/mg)**	**L2 (eq/ µl)**	**Solvent (ml/mM)**	**T (°C)**	**Time (days)**	**Base(eq/mg)**	**product**
1	1.0/25mg	2/3.9	Dioxane (1.2/0.06)	120	3	t- ButOK/2eq (11.65mg)	~ 13 mg
2	1.0/25mg	2/3.9	Dioxane (1.2/0.06)	120	3	DIPEA/2eq (18.6 µl)	~1 mg
3	**1.0/22.1mg**	**2/3.5**	**Dioxane (1/0.06)**	**120**	**3**	**DBU/2eq (15.4µl)**	**~24 mg**
4	1.0/25mg	2/3.9	Dioxane (1.2/0.06)	120	3	Et3N/2eq (13.9 µl l)	~3mg
5	1.0/25mg	2/3.9	Dioxane (1.2/0.06)	110	3	Et3N/2eq (13.9µl)	~ 3mg
6	1.0/25mg	2/3.9	Dioxane (1.2/0.06)	90	3	Et3N/2eq (13.9 µl)	~2mg
7	1.0/25mg	2/3.9	Dioxane (1.2/0.06)	65	3	Et3N/2eq (13.9ul)	~2mg
8	1.0/22mg	2/3.5	Dioxane (1/0.06)	90	3	DBU/2eq (13.4µl)	~20 mg
9	1.0/22mg	2/3.5	Dioxane (1/0.06)	75	3	DBU/2eq (13.4µl)	~18 mg

3.7.2.2. XY-COF Synthesis

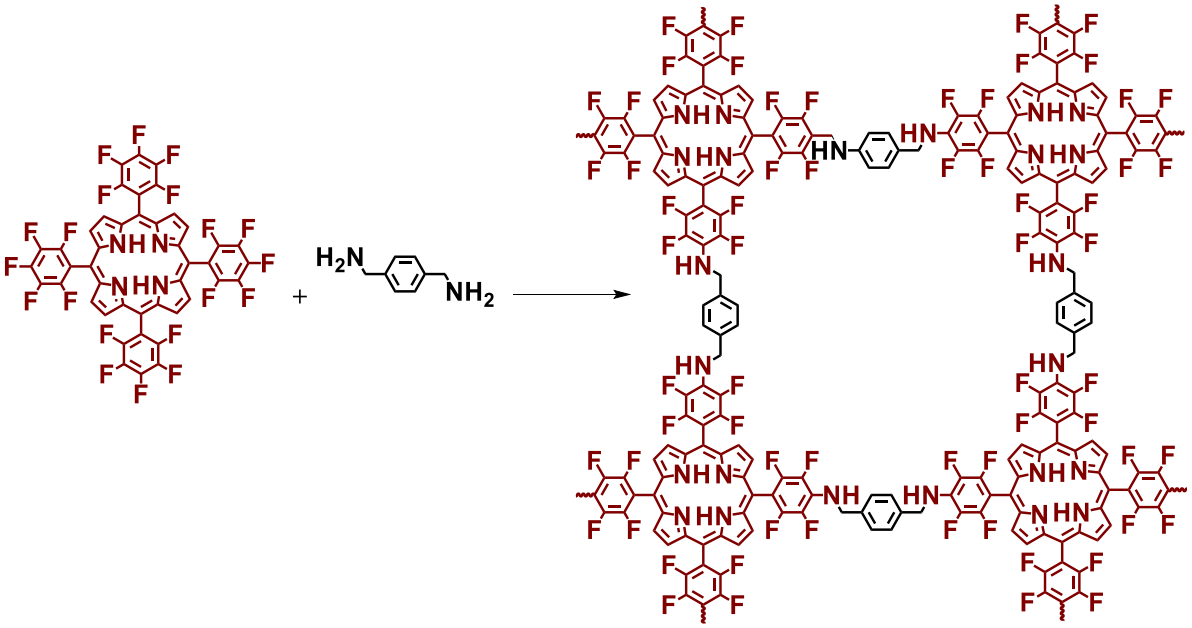

Scheme 3. 16. Synthetic route for XYCOF.

Tetrakis(pentafluorophenyl)- Porphyrin (25 mg) and xylene diamine (3.9 mg) were placed in a glass ampule vessel (20 mL), followed by adding a solution of dioxane/ DBU (1.2 ml; 2eq based on the amine). The mixture was sonicated for 5 min and then flash-frozen in liquid nitrogen. The vessel was evacuated to an inner pressure of ~20 Pa, flame-sealed, and heated at 120 °C for 3 days. The resulting precipitate was washed sequentially with DMF (3 times) and acetone (3 times) to give a powder, which was dried at 120 °C under vacuum for 12 h to give the desired product in 50% yield.

3.7.2.3. Si-COF Synthesis

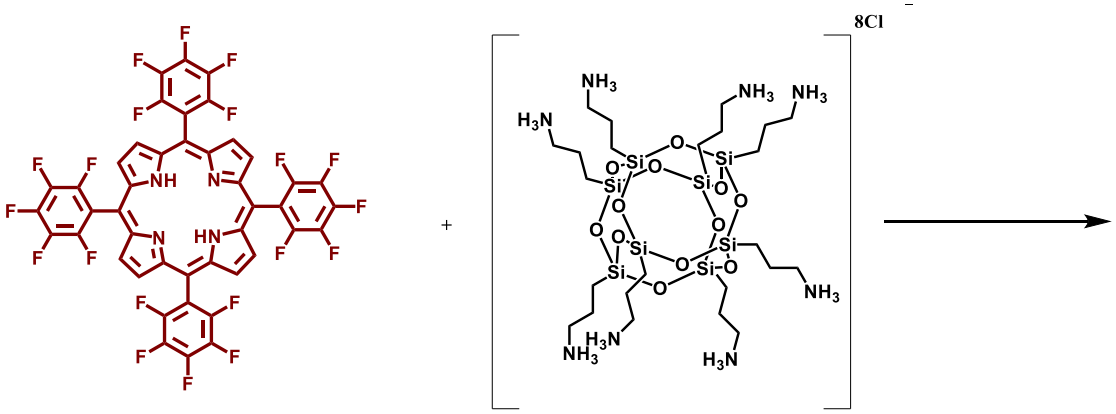

Scheme 3. 17. Synthetic route for SiCOF.

Tetrakis(pentafluorophenyl)-Porphyrin (25 mg, 0.026mM) and (7.4 mg,) were placed in a glass ampule vessel (20 mL), followed by adding a solution of dioxane/ triethylamine(0.7ml; 16eq based on the amine). The mixture was sonicated for 5 min and then flash-frozen in liquid nitrogen. The vessel was evacuated to an inner pressure of ~20 Pa, flame-sealed, and heated at 120 °C for 3 days. The resulting precipitate was washed sequentially with DMF (3 times) and acetone (3 times) to give a powder, which was dried at 120 °C under vacuum for 12 h to give the desired product in 40% yield.

Table 3. 3. Modifying the reaction condition by changing the base.

Entry	**L1(eq/mg)**	**L4 (eq/ µl)**	**Solvent (ml/mM)**	**T (°C)**	**Time (days)**	**Base(eq/mg)**	**product**
1	**1.0/22.1mg**	**2/3.5**	**Dioxane (1/0.06)**	**120**	**3**	**DBU/2eq (15.4µl)**	**~18 mg**
2	1.0/25mg	2/3.9	Dioxane(1.2/0.06)	120	3	Et3N/2eq (13.9 µl l)	~4mg

3.7.2.4. ZnCOF Synthesis

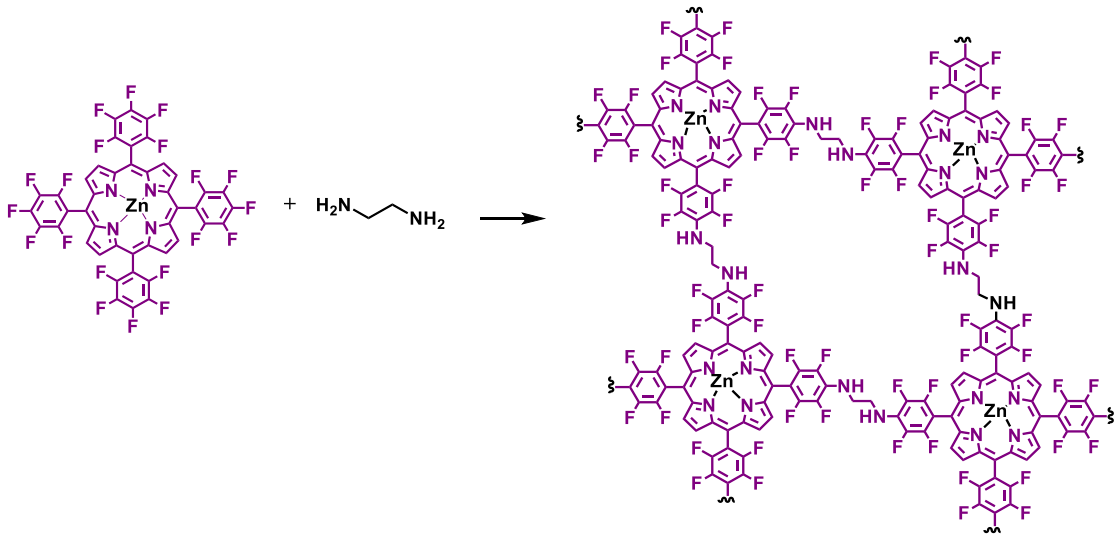

Scheme 3. 18. Synthetic route for COF-21.

Tetrakis(pentafluorophenyl)- Zinc Porphyrin (23.6 mg, 0.023mM) and ethylene diamine (3.9 µl, 0.046 mM) were placed in a glass ampule vessel (20 mL), followed by adding a solution of dioxane/ DBU (1ml; 2eq based on the amine). The mixture was sonicated for 5 min and then flash-frozen in liquid nitrogen. The vessel was evacuated to an inner pressure of ~20 Pa, flame-sealed, and heated at 120 °C for 3 days. The resulting precipitate was washed sequentially with DMF (3 times) and acetone (3 times) to give a powder, which was dried at 120 °C under vacuum for 12 h to give the desired product in 75% yield.

3.7.2.5. FeClCOF-21 Synthesis[9]

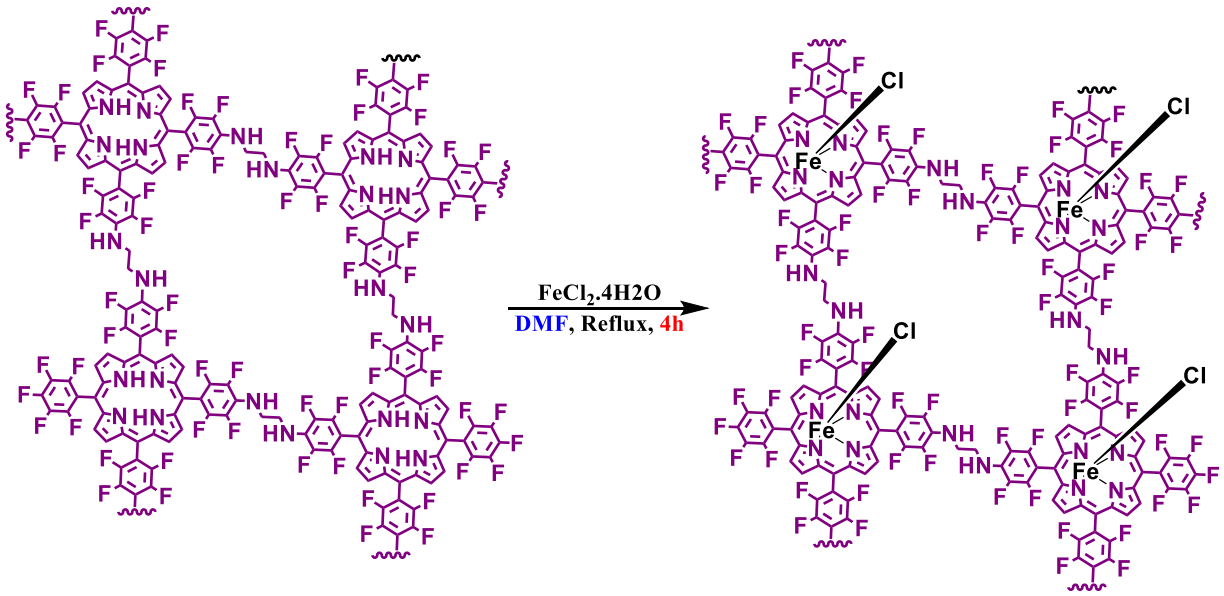

Scheme 3. 19. Synthetic route for FeClCOF-21.

A three-necked round-bottomed flask equipped with a thermometer, reflux condenser, and magnetic force stirrer was charged with DMF (5 mL), COF-21 (50mg, 51.3 mol) $FeCl_2.4H_2O$ (0.32 mmol). The reaction mixture was stirred under reflux for 4 h at 150 °C. TLC revealed the complete disappearance of the starting material. Deionized water (20 mL) and 6M HCl (30 mL) were added to the cooled mixture, and a crystalline product was filtrated and washed with water and acetone several times and drying under a vacuum, yielding to the desired product as a black powder (90%).

3.7.3. General Procedure for The Tandem Catalytic Conversion of Benzyl Alcohol [9, 11]

3.7.3.1. The synthesis of 2-phenyl-1H-benzo[d]imidazole

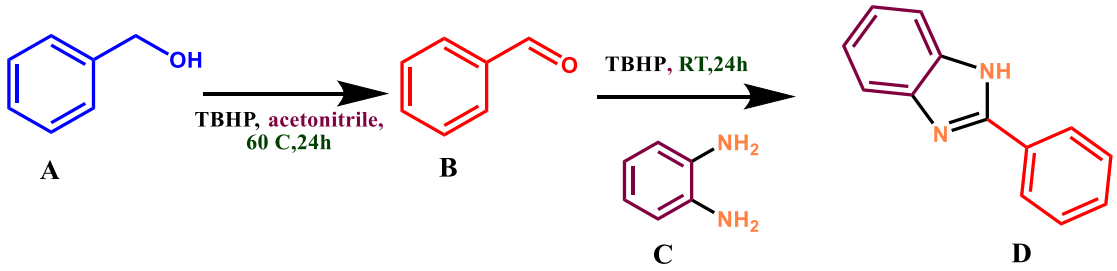

Scheme 3. 20. The synthesis of **D.**

Tandem catalytic synthesis of 2-phenyl-quinazolin-4(3H)-one through the reaction of benzyl alcohol and o-aminobenzamide using of $FeClTPPF_{20}$: to a mixture of benzyl alcohol (1.5mmol), $FeClTPPF_{20}$ (12.5mg, equivalent to 0.012mmol of Fe) in deuterated acetonitrile (3ml), TBHP (70% in water) (2.5mmol: 1.5mmol, 0.5mmol) was added into three portions, the first was added after 10min, second after 18 h and the third after 20h. The reaction mixture was stirred at 60 °C for 24h. After the complete conversion of benzyl alcohol to benzaldehyde (monitored by TLC), the mixture was cooled down to room temperature. Then, o-aminobenzamide (0.5mmol) was added to the reaction mixture and stirred overnight. The desired product was then confirmed by ^{1}H NMR.

3.8. Scanning Electron Microscopy (SEM) Studies

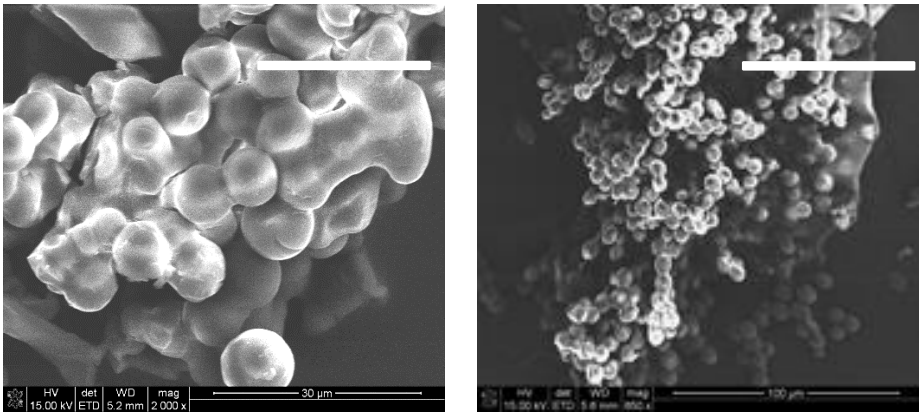

Figure 3. 3. SEM images showing oblong spherical particles of COF-21.

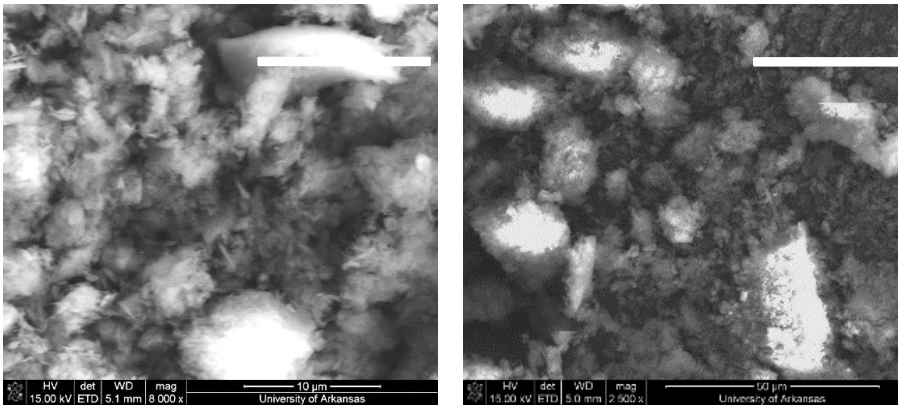

Figure 3. 4. SEM images showing oblong particles of XYCOF.

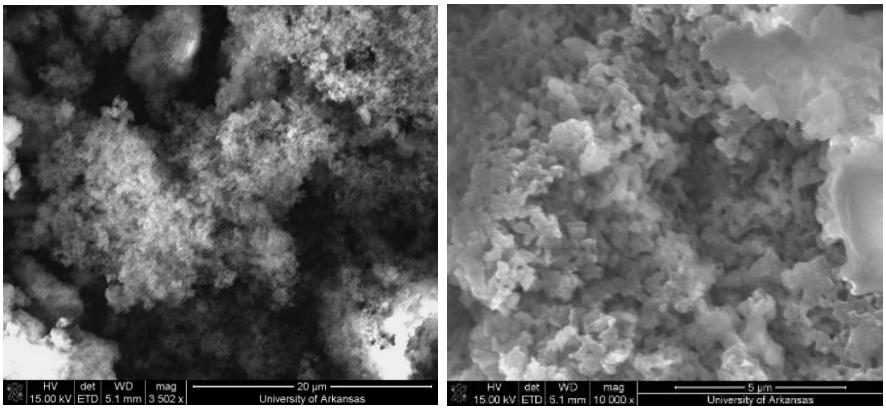

Figure 3. 5. SEM images showing oblong particles of SiCOF.

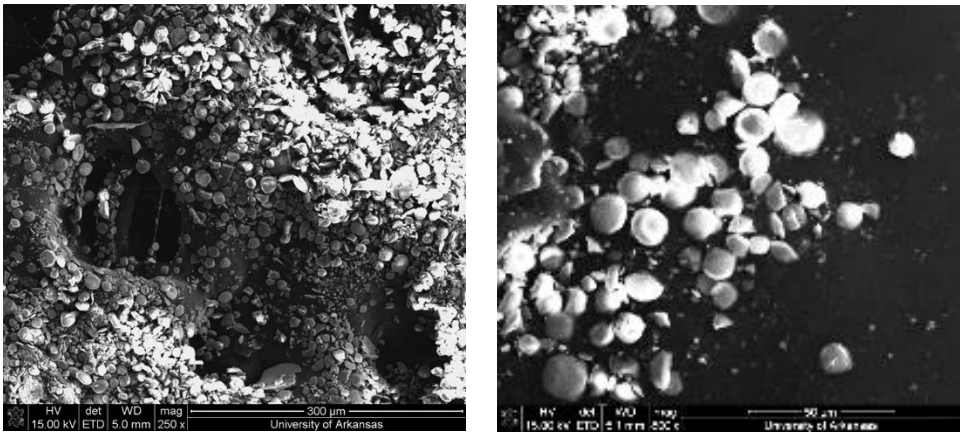

Figure 3. 6. SEM images showing oblong spherical particles of ZnCOF.

3.9. FT-IR Spectroscopy Studies

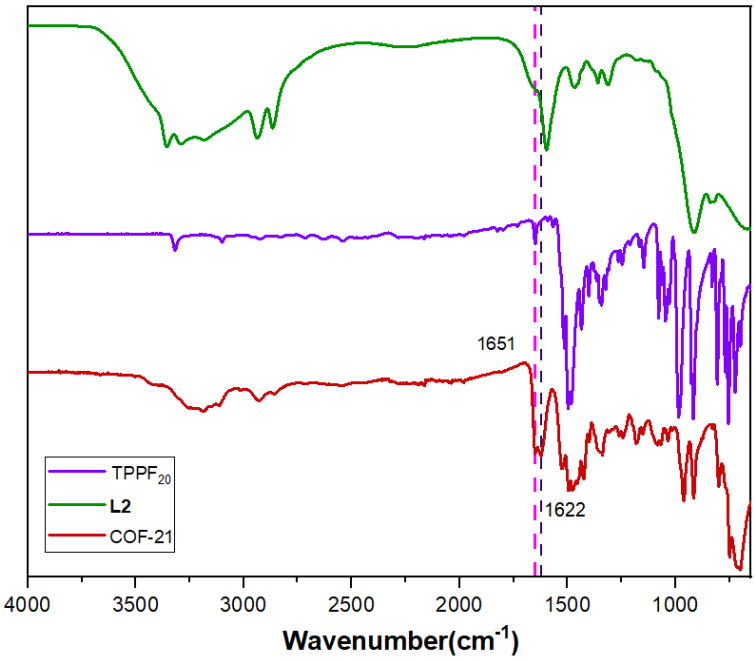

Figure 3. 7. FT-IR spectra of COF-21.

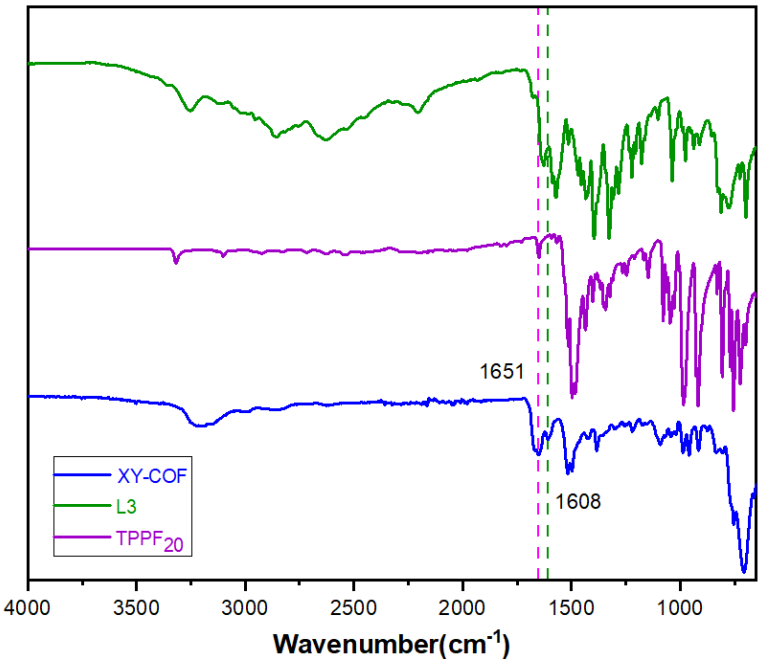

Figure 3. 8. FT-IR spectra of XYCOF.

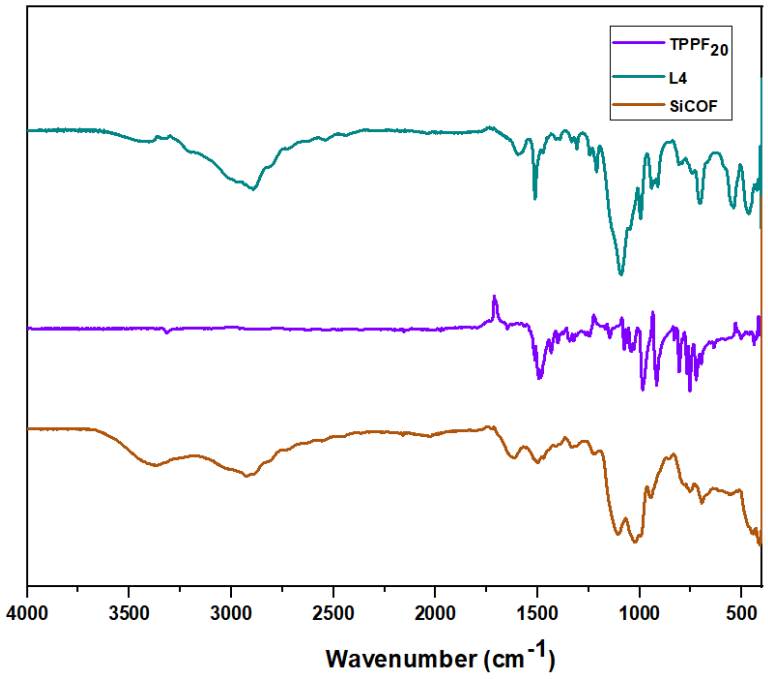

Figure 3. 9. FT-IR spectra of SiCOF.

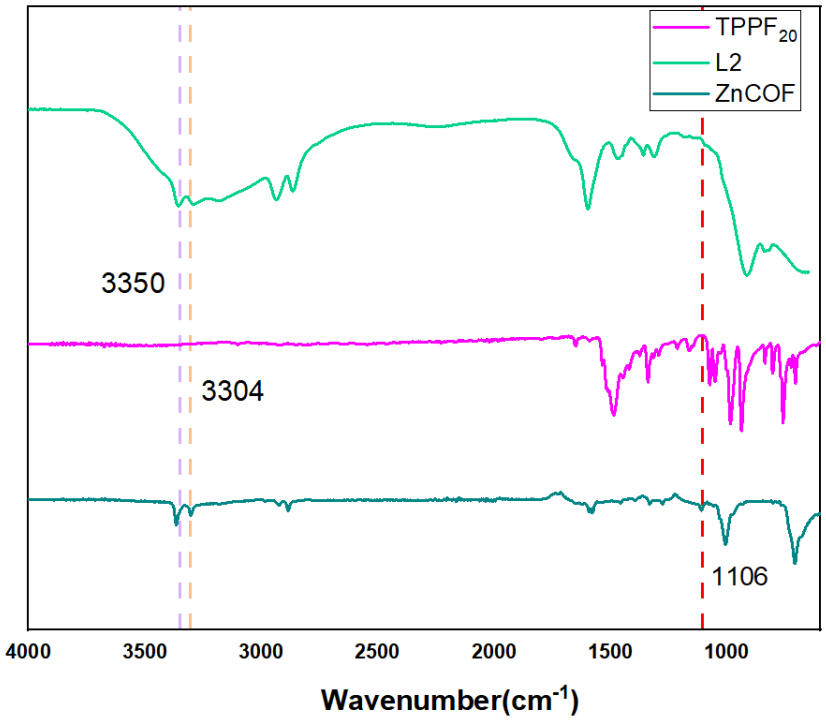

Figure 3. 10. FT-IR spectra ZnCOF.

3.10. Solid State ^{13}C NMR Spectra

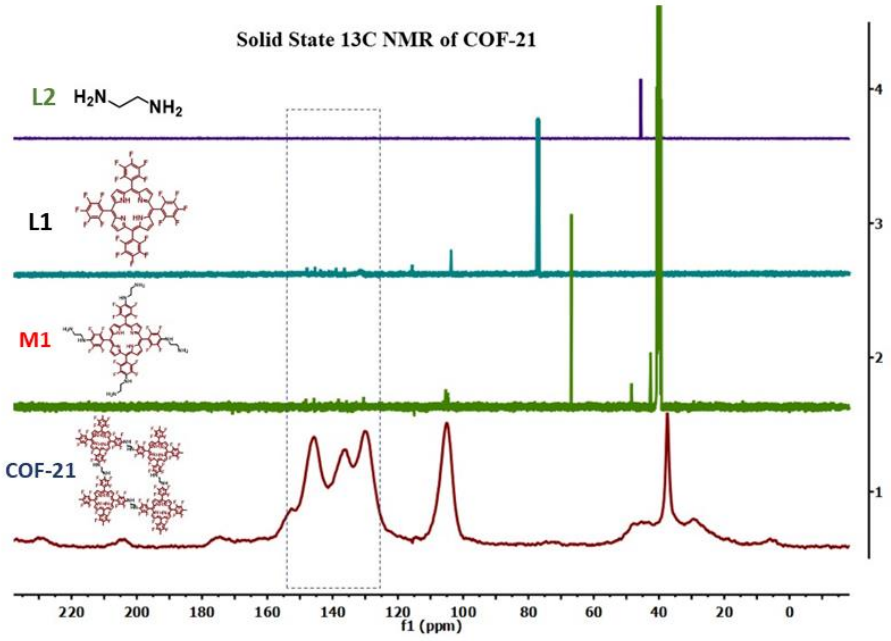

Figure 3. 11. ^{13}C CP/MAS of COF-21.

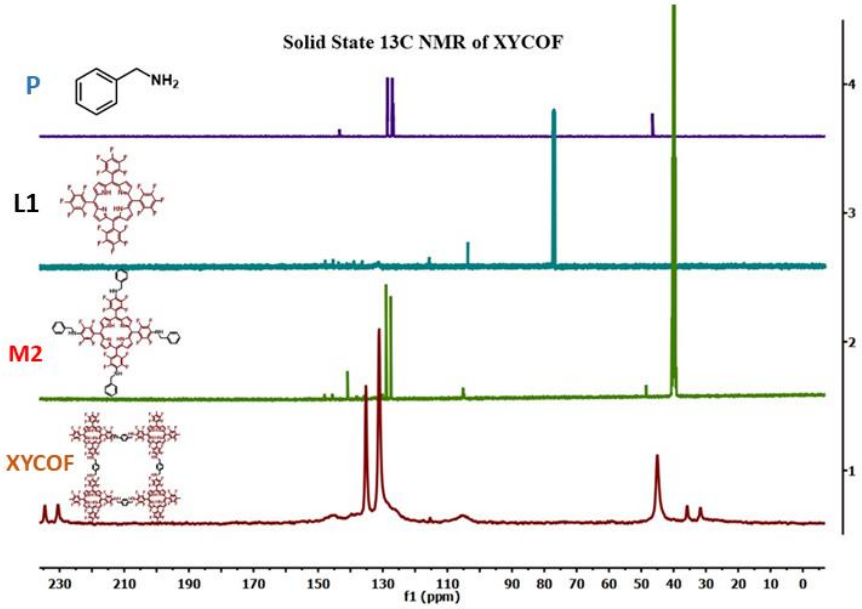

Figure 3. 12. ^{13}C CP/MAS of XYCOF.

3.11. Energy Dispersive X-ray (EDX)Analysis

A).

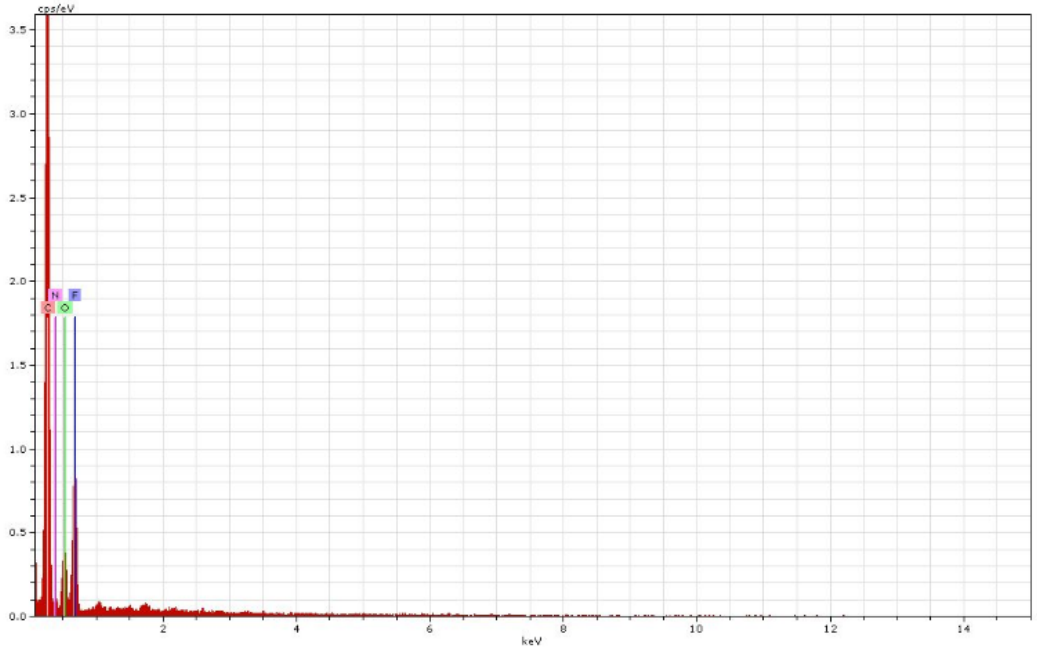

Spectrum: Acquisition

El	AN	Series	unn. C [wt.%]	norm. C [wt.%]	Atom. C [at.%]	Error [wt.%]
C	6	K-series	63.69	63.69	70.45	8.8
N	7	K-series	10.33	10.33	9.80	3.1
O	8	K-series	12.10	12.10	10.05	2.5
F	9	K-series	13.87	13.87	9.70	2.4
		Total:	100.00	100.00	100.00	

Figure 3. 13. EDX of COF-21.

B).

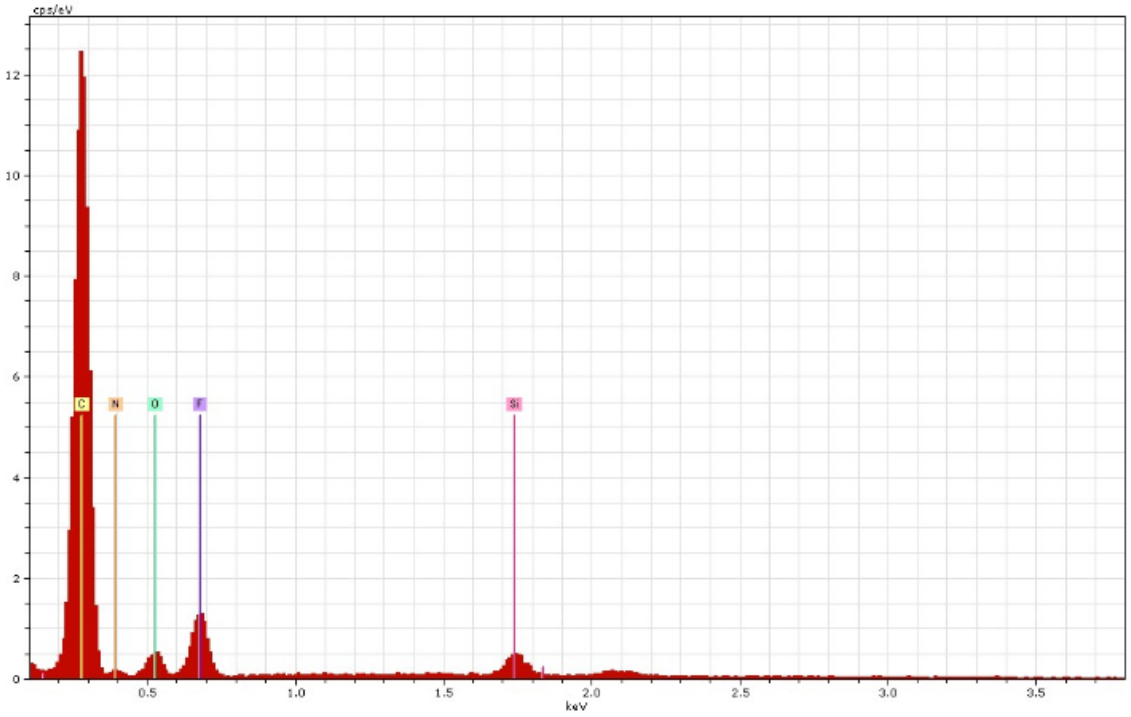

Spectrum: Acquisition

El	AN	Series	unn. C [wt.%]	norm. C [wt.%]	Atom. C [at.%]	Error (1 Sigma) [wt.%]
C	6	K-series	76.46	76.46	81.64	9.18
N	7	K-series	7.51	7.51	6.87	1.92
O	8	K-series	6.83	6.83	5.47	1.33
F	9	K-series	8.30	8.30	5.60	1.33
Si	14	K-series	0.91	0.91	0.41	0.07
		Total:	100.00	100.00	100.00	

Figure 3. 14. EDX of **XYCOF**.

C).

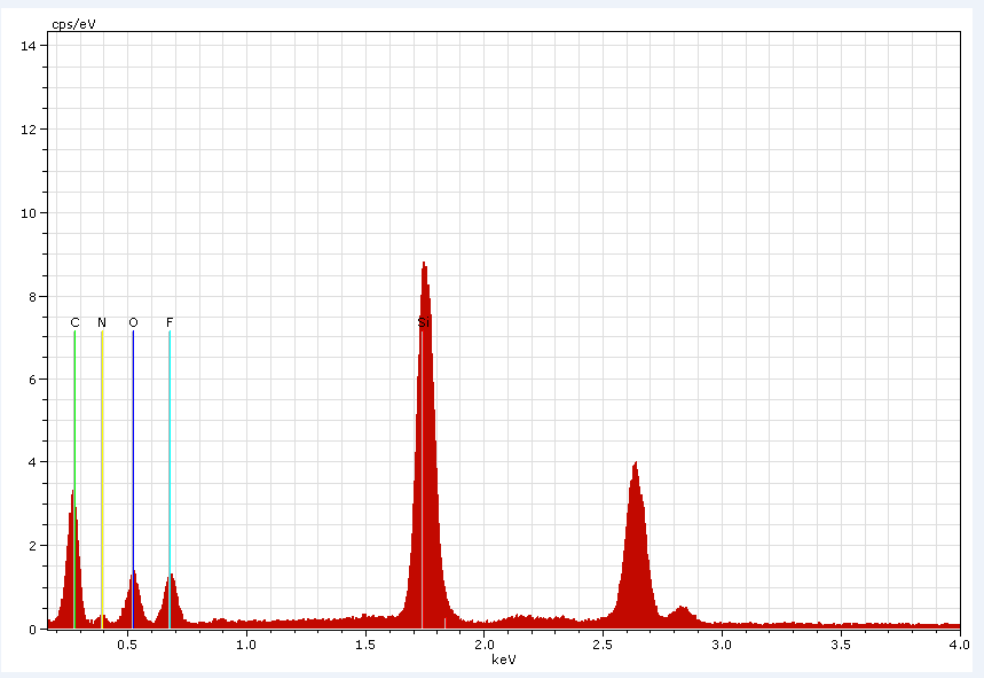

Figure 3. 15. EDX of **SiCOF**.

D).

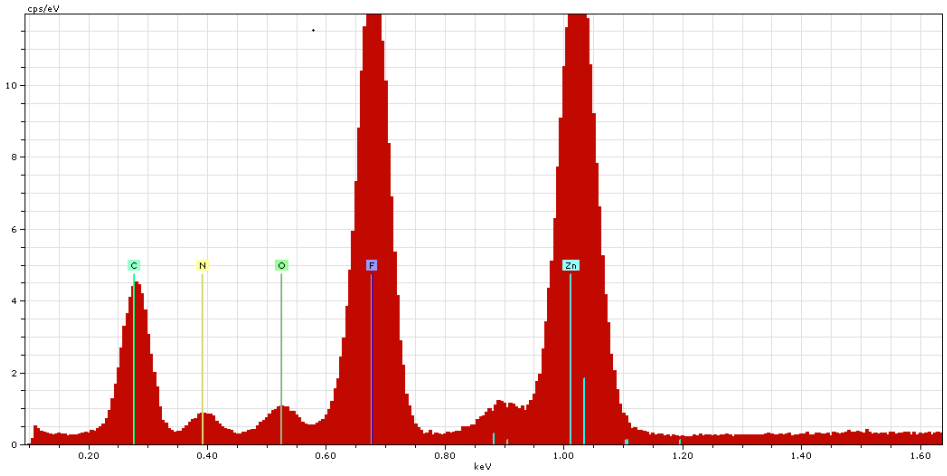

Figure 3. 16. EDX of **ZnCOF**.

E).

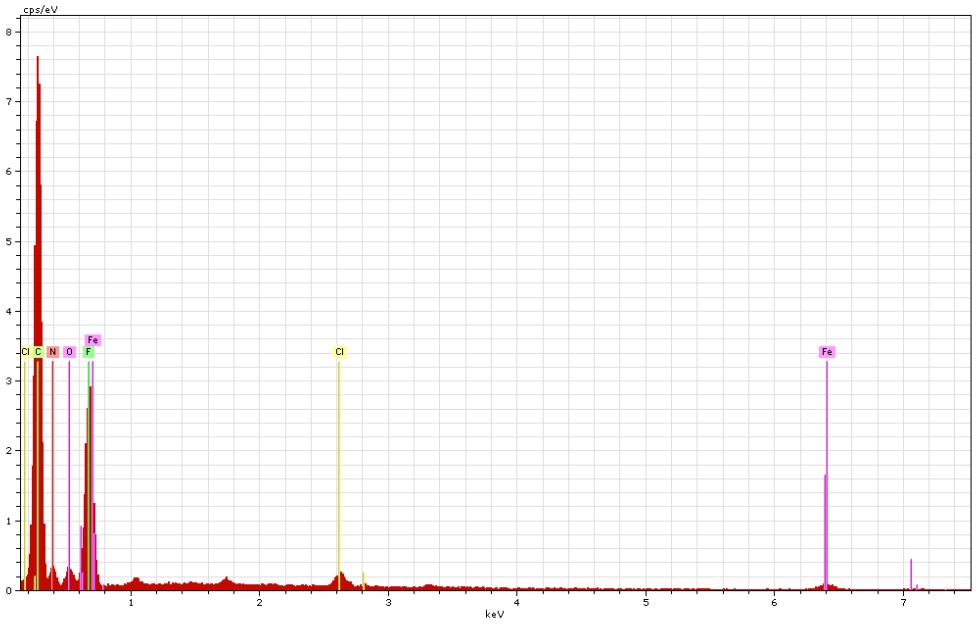

Spectrum: Acquisition

El	AN	Series	unn. C [wt.%]	norm. C [wt.%]	Atom. C [at.%]	Error (1 Sigma) [wt.%]
C	6	K-series	62.22	62.22	70.21	7.82
N	7	K-series	12.40	12.40	12.00	2.68
O	8	K-series	4.47	4.47	3.78	0.99
F	9	K-series	18.75	18.75	13.38	2.62
Cl	17	K-series	0.69	0.69	0.26	0.06
Fe	26	K-series	1.48	1.48	0.36	0.10
		Total:	100.00	100.00	100.00	

Figure 3. 17. EDX of **FeClCOF-21**.

3.12. X-ray Photoelectron Spectroscopy (XPS) Analysis

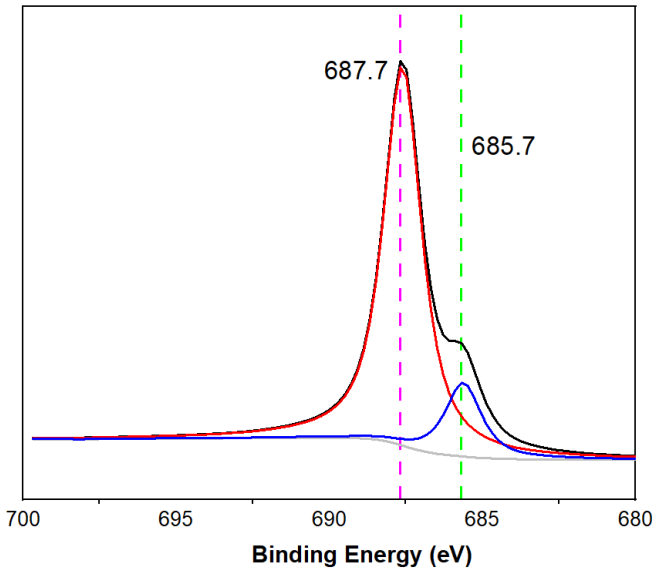

Figure 3. 18. XPS spectra of the F1s binding energy of COF-21.

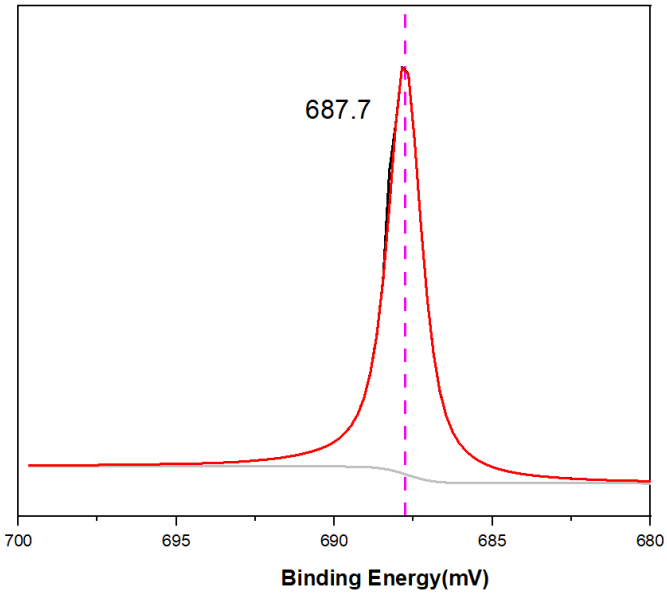

Figure 3. 19. XPS spectra of the F1s binding energy of $TPPF_{20}$ (**L1**).

3.13. UV-vis

A).

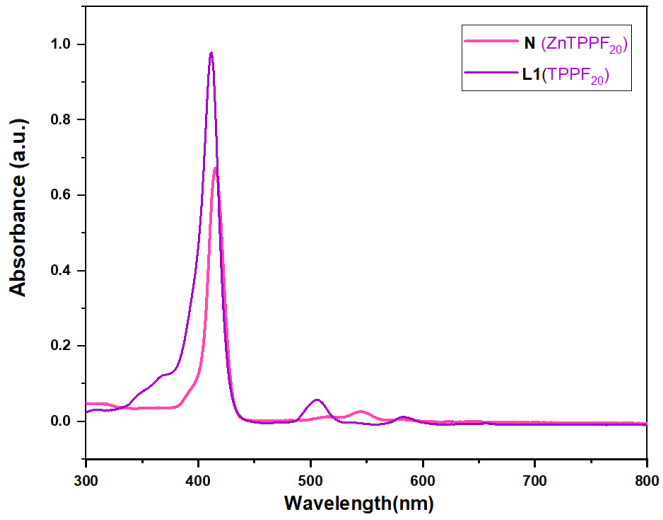

Figure 3. 20. UV-vis absorption **N (**$ZnTPPF_{20}$**)**in DCM.

B).

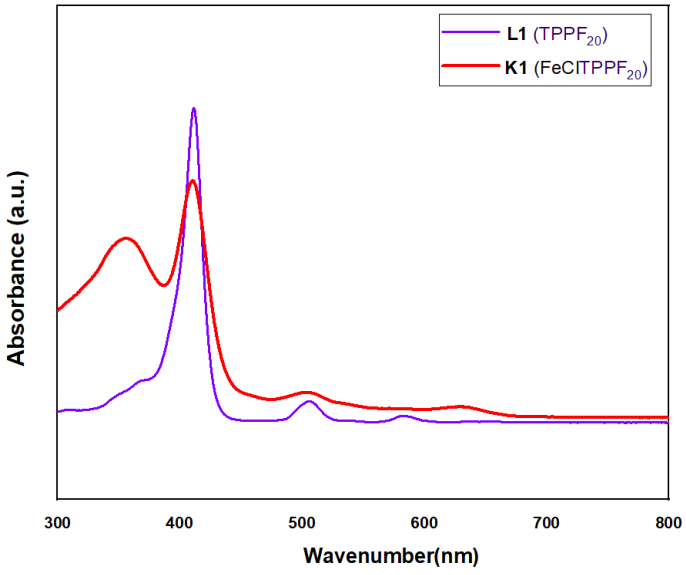

Figure 3. 21. UV-vis absorption **K1** in DCM.

C).

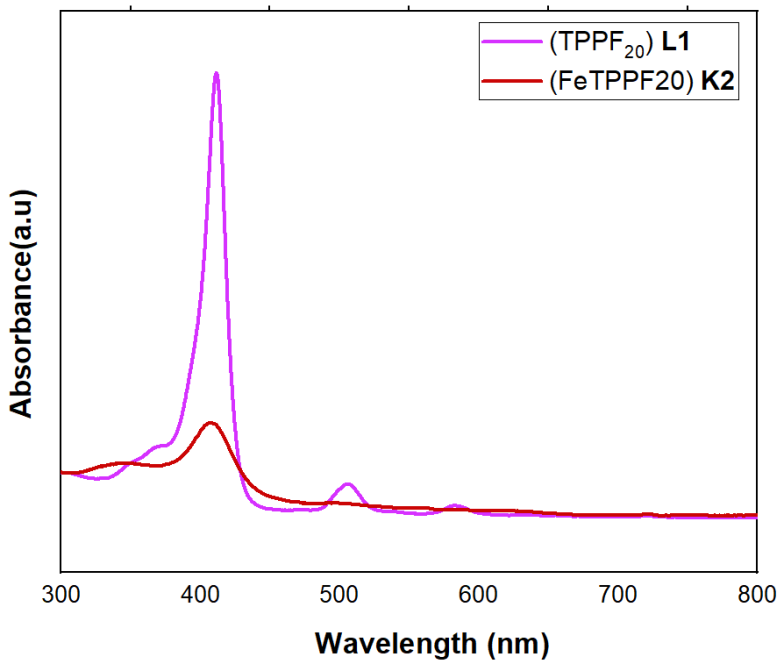

Figure 3. 22. UV-vis absorption **K2** in DCM.

3.14. Mass Spectroscopy

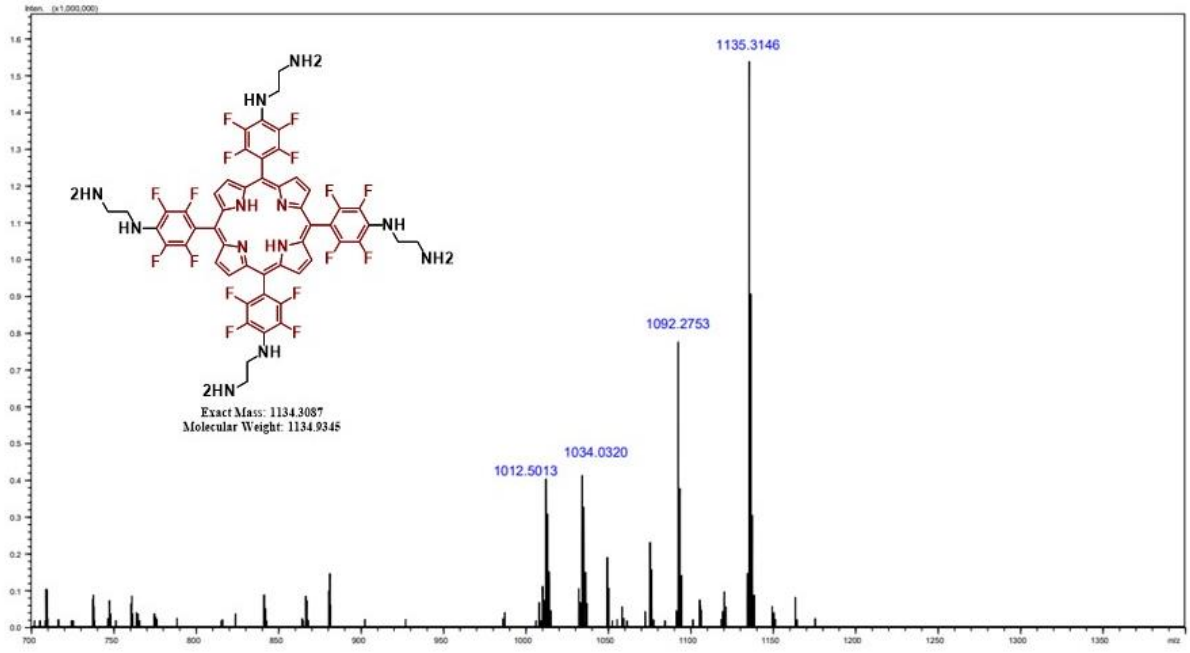

Figure 3. 23. High resolution mass of **M1**.

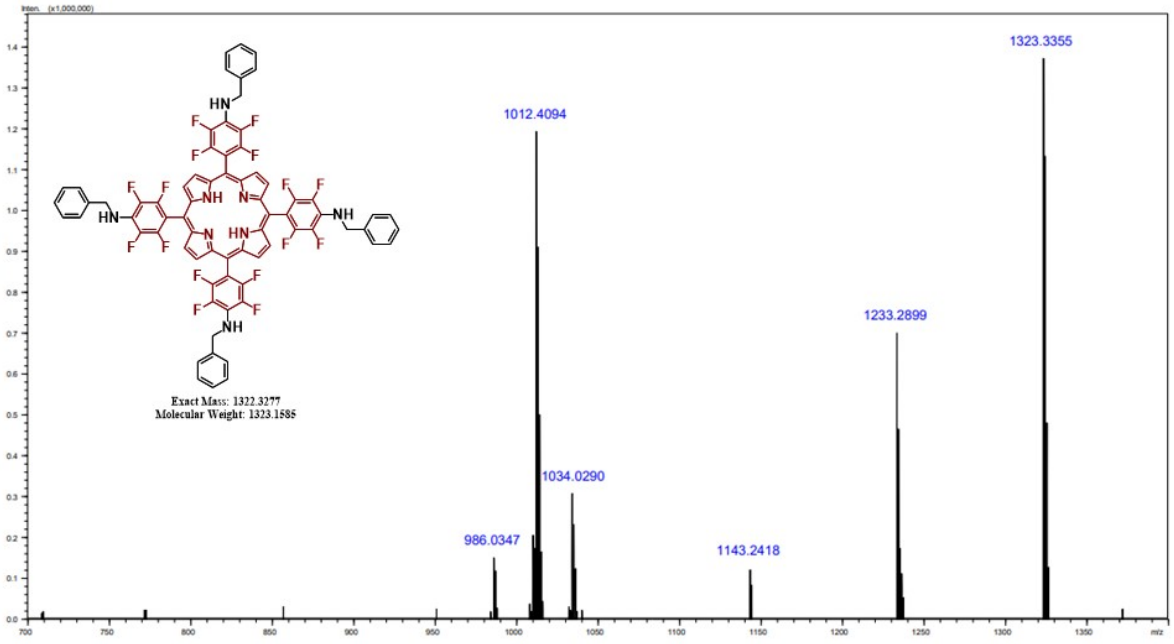

Figure 3. 24. High resolution mass of **M2**.

3.15. NMR Spectra

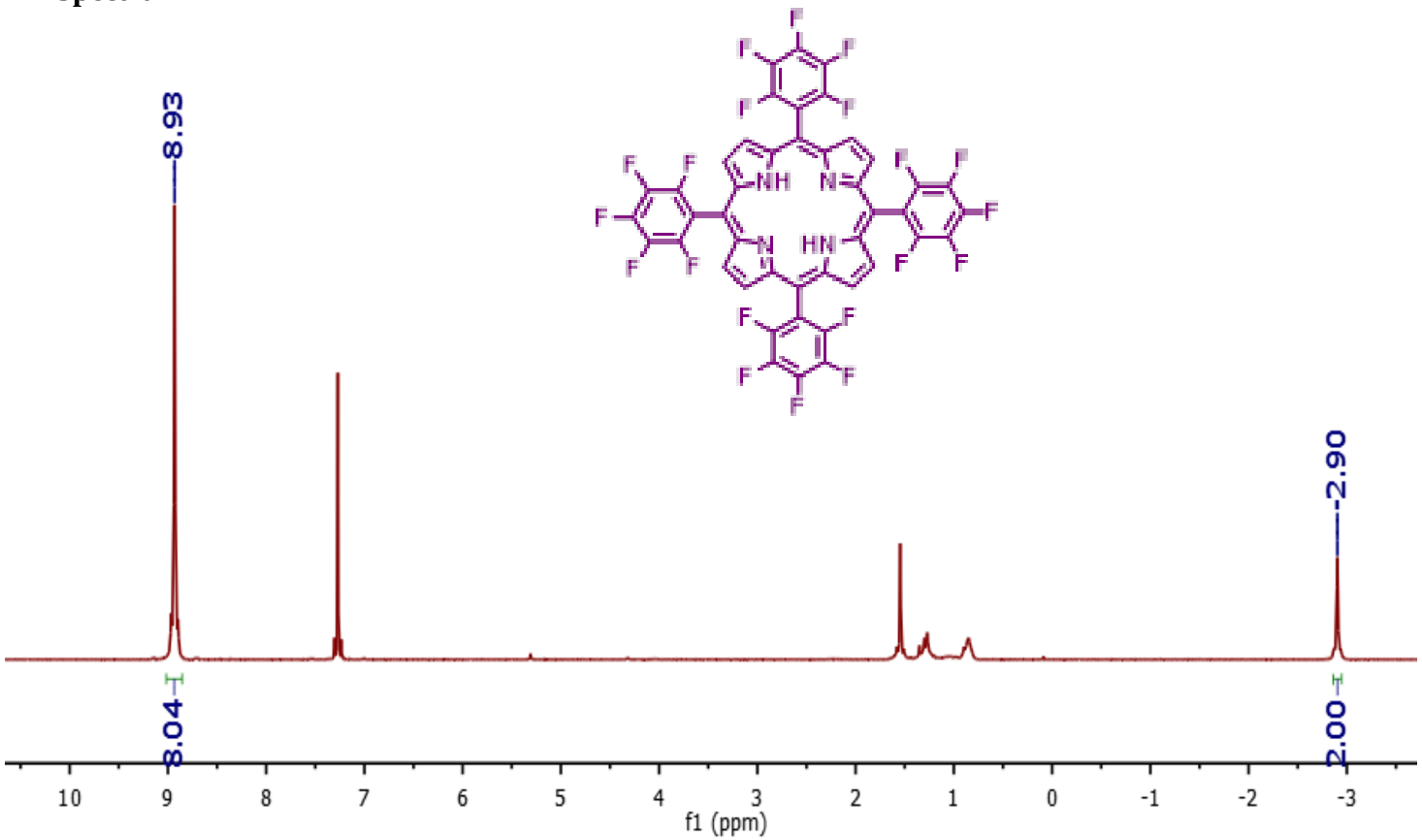

Figure 3. 25. ^{1}H NMR (400 MHz) of **L1** in $CDCl_3$.

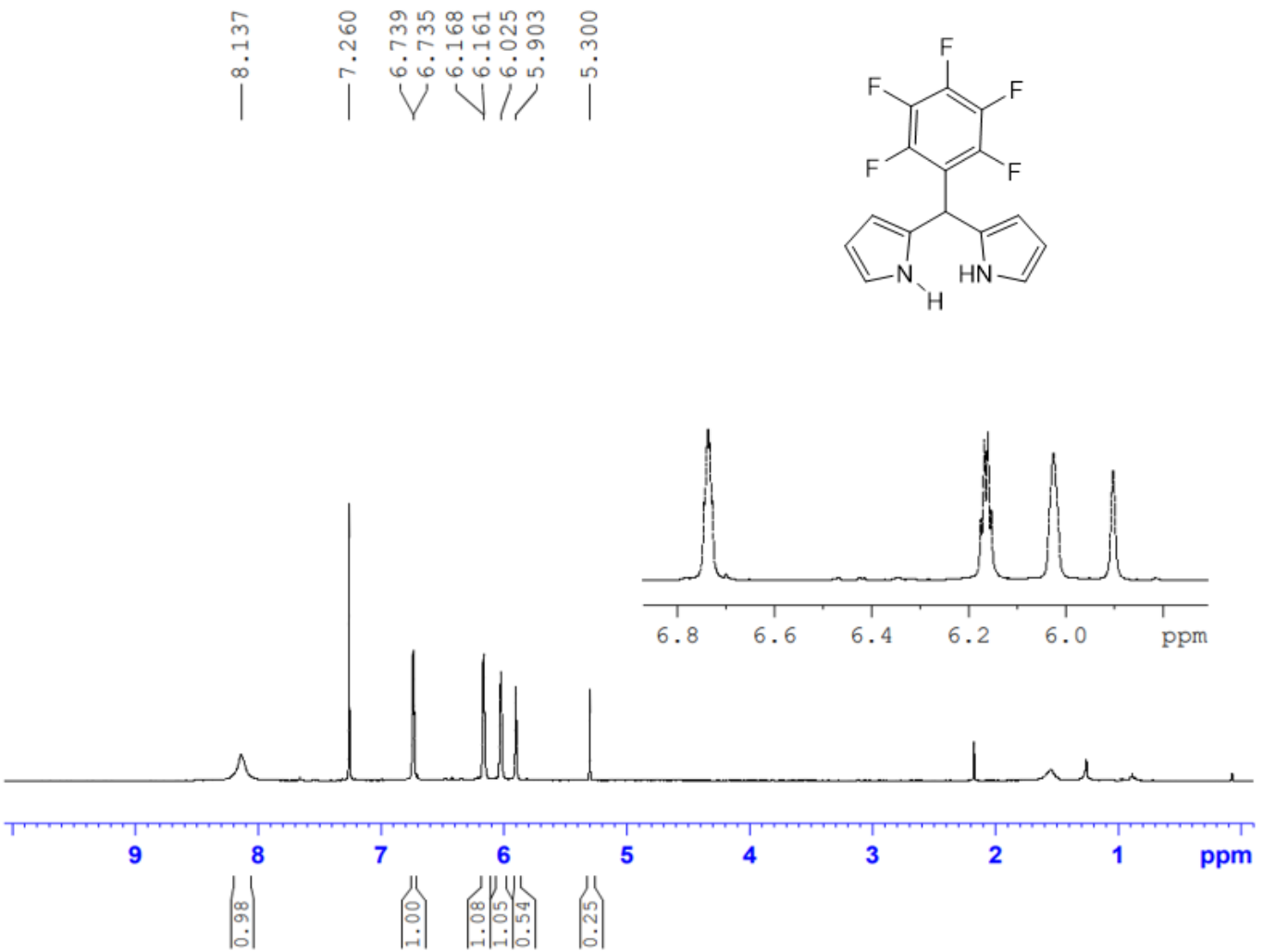

Figure 3. 26. ^{1}H NMR (400 MHz) of **E** in $CDCl_3$.

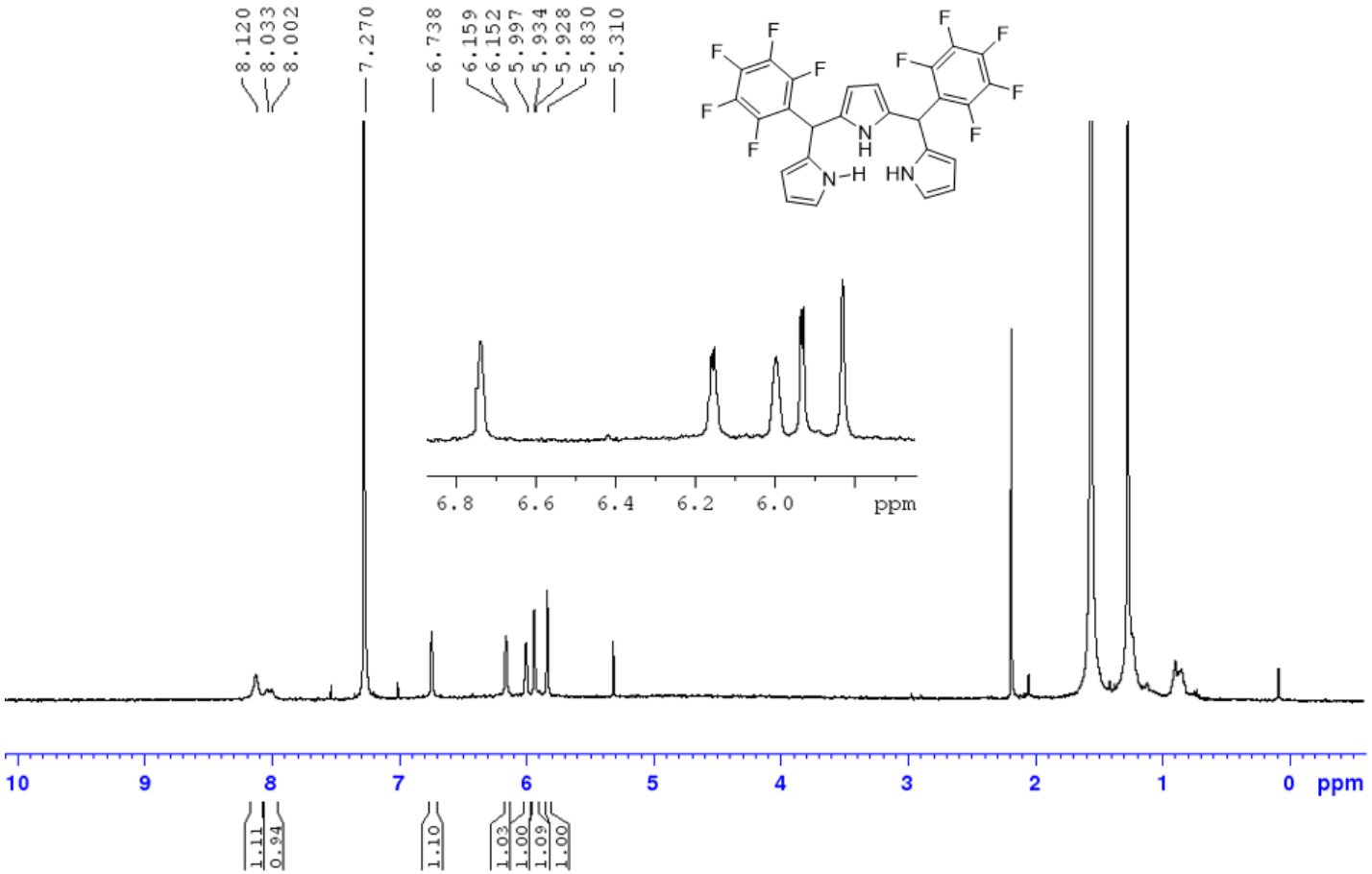

Figure 3. 27. ^{1}H NMR (400 MHz) of **F** in $CDCl_3$.

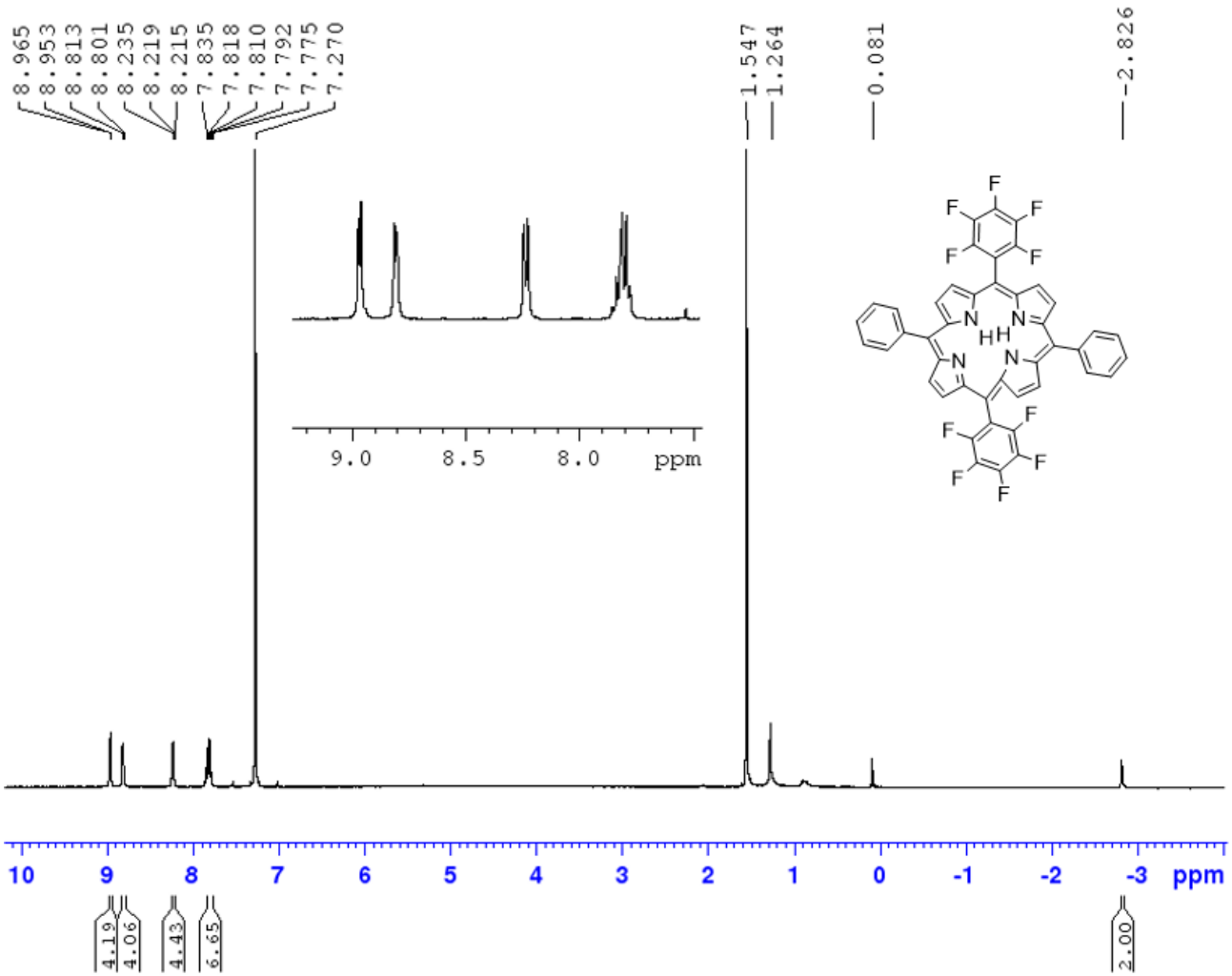

Figure 3. 28. ^{1}H NMR (400 MHz) of **G** in $CDCl_3$.

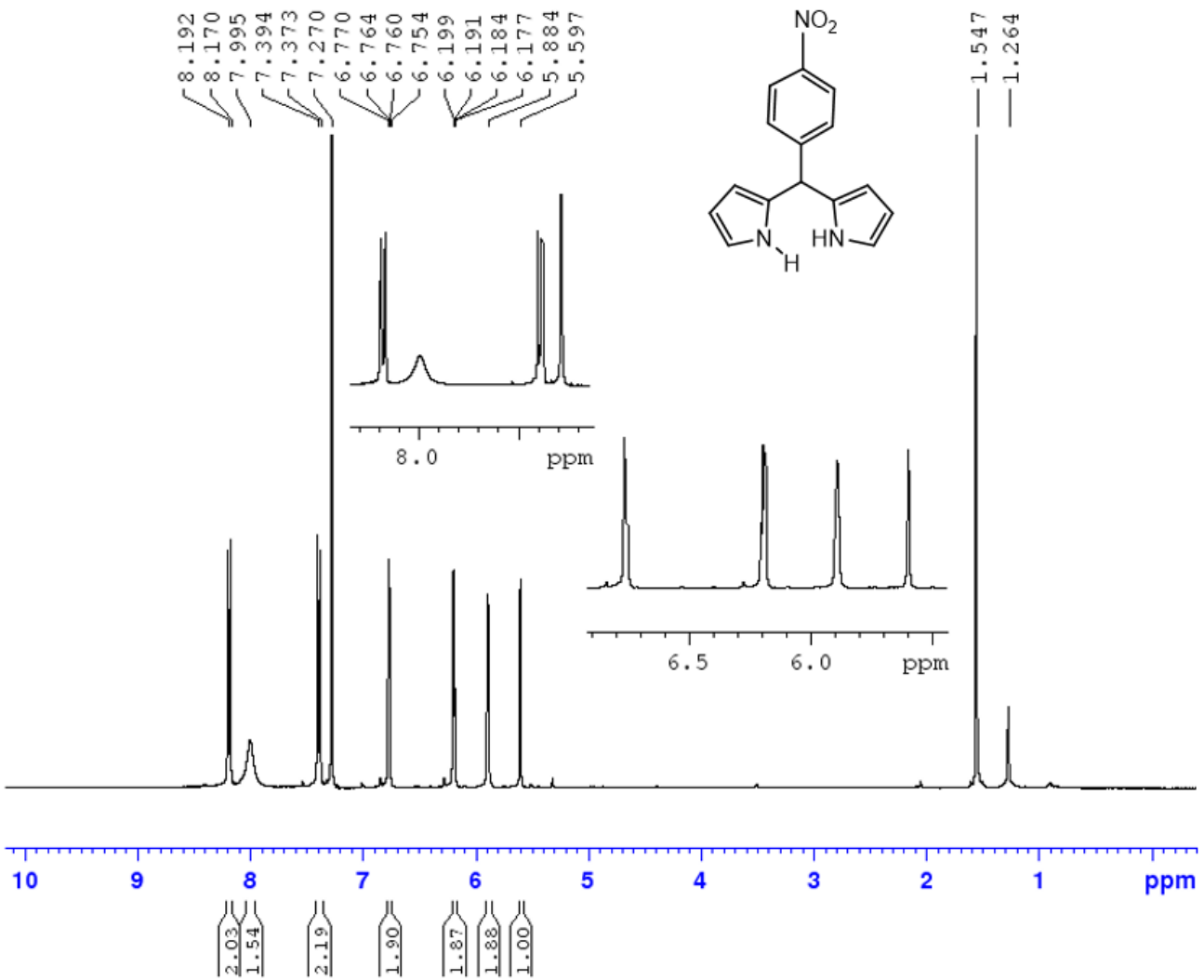

Figure 3. 29. ^{1}H NMR (400 MHz) of **H** in $CDCl_3$.

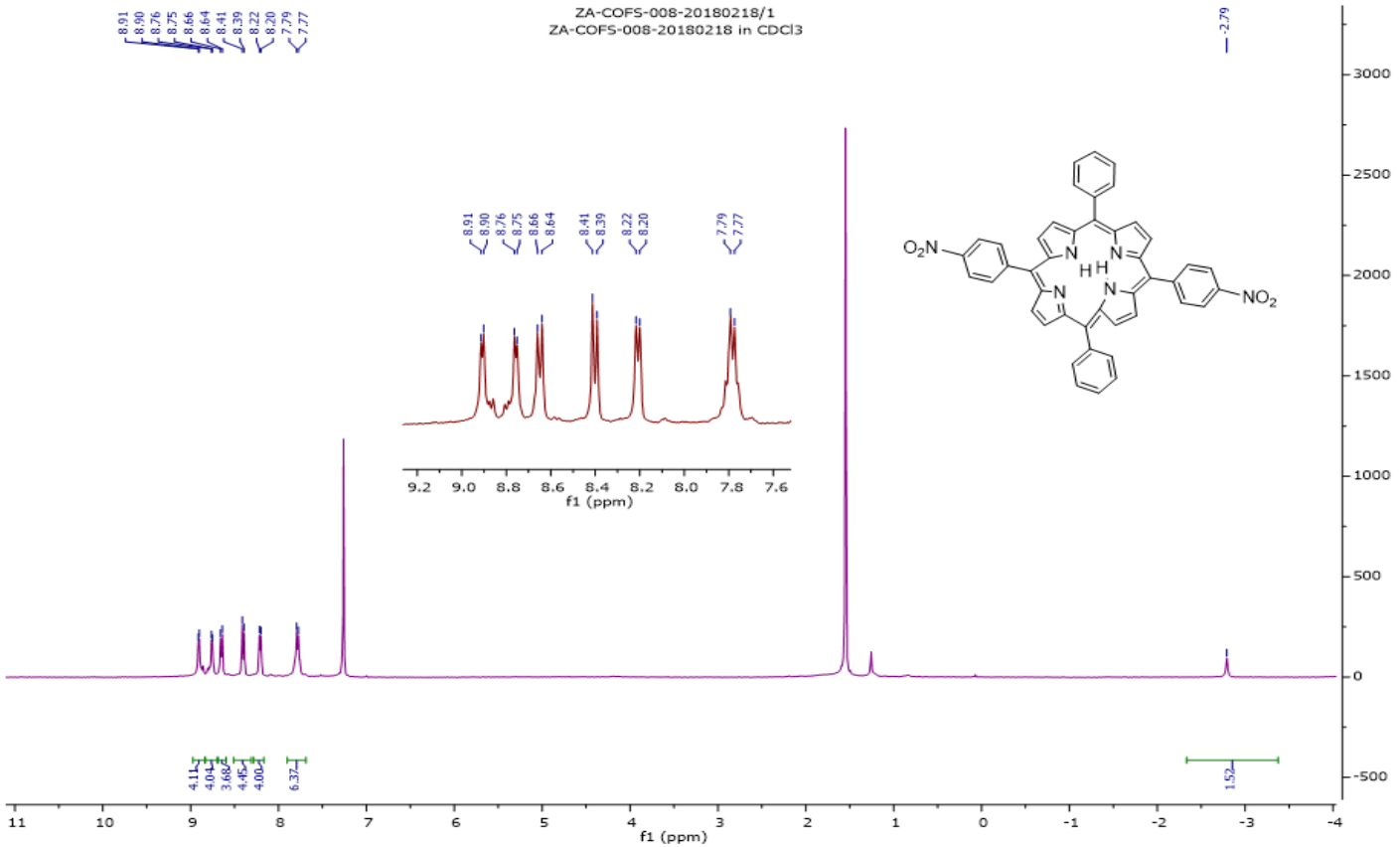

Figure 3. 30. ^{1}H NMR (400 MHz) of **I** in $CDCl_3$.

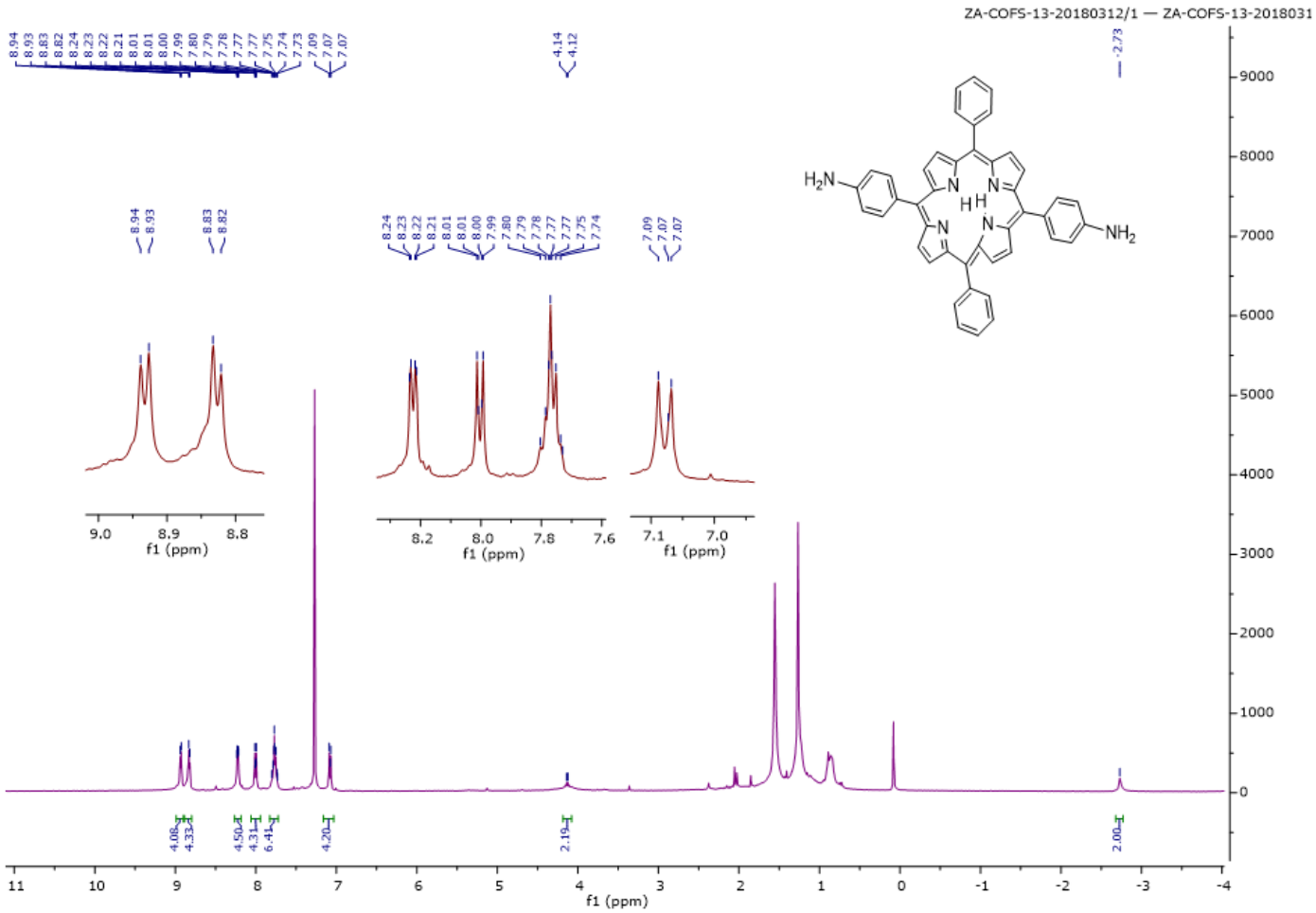

Figure 3. 31. ^{1}H NMR (400 MHz) of **J** in $CDCl_3$.

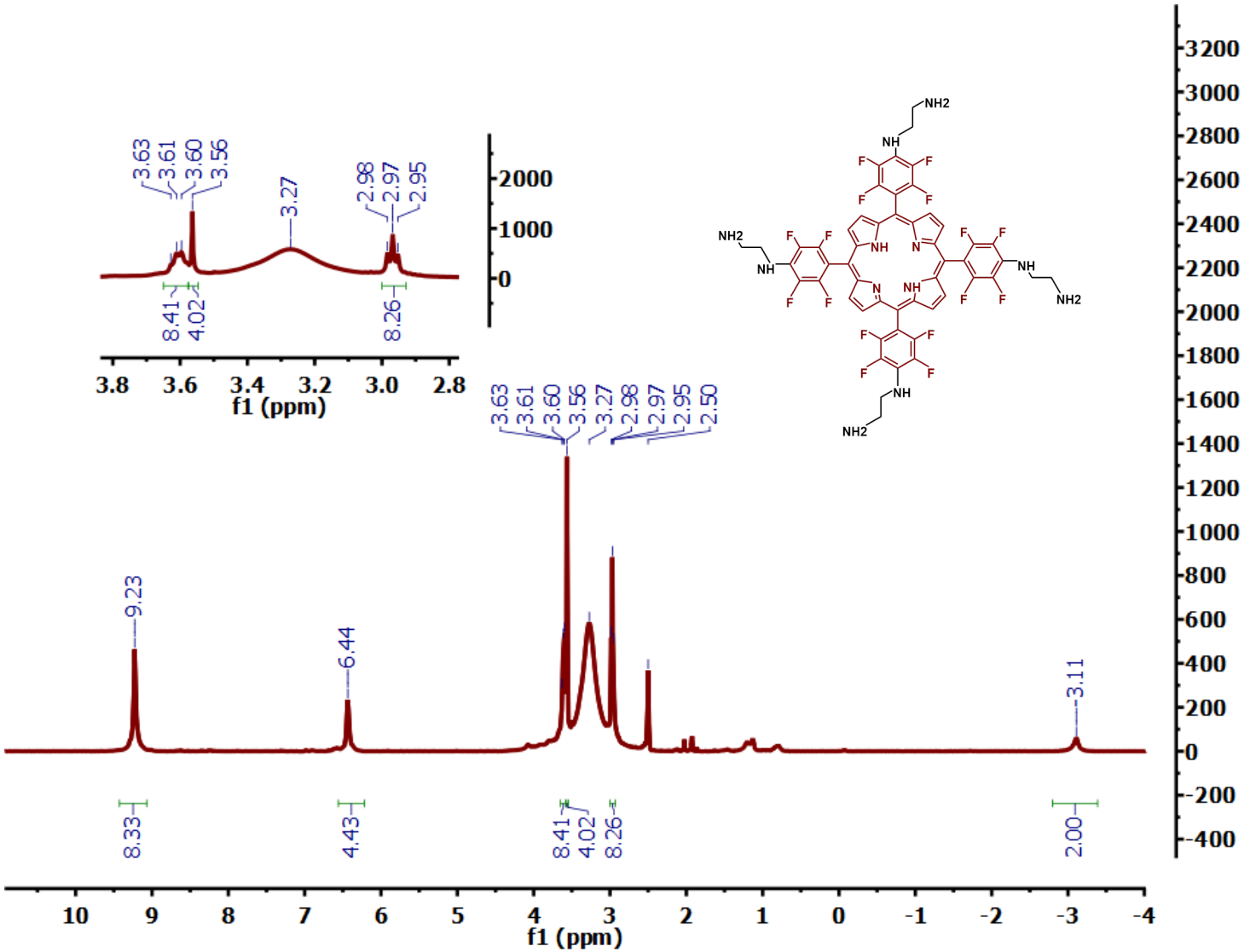

Figure 3. 32. ^{1}H NMR (400 MHz) of **M1**in DMSO-d_6).

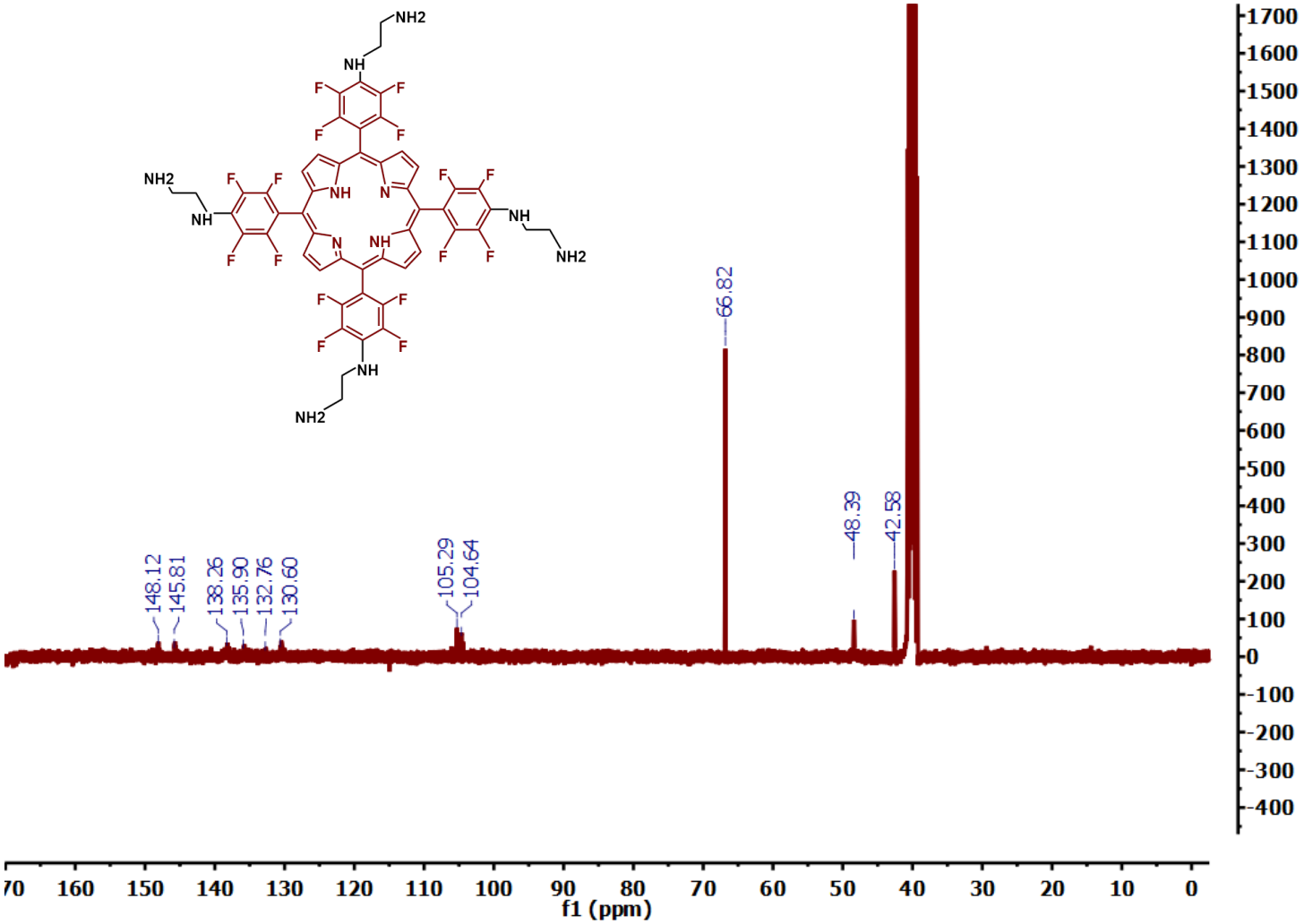

Figure 3. 33.[13]C NMR (101 MHz) of **M1** in DMSO-d_6.

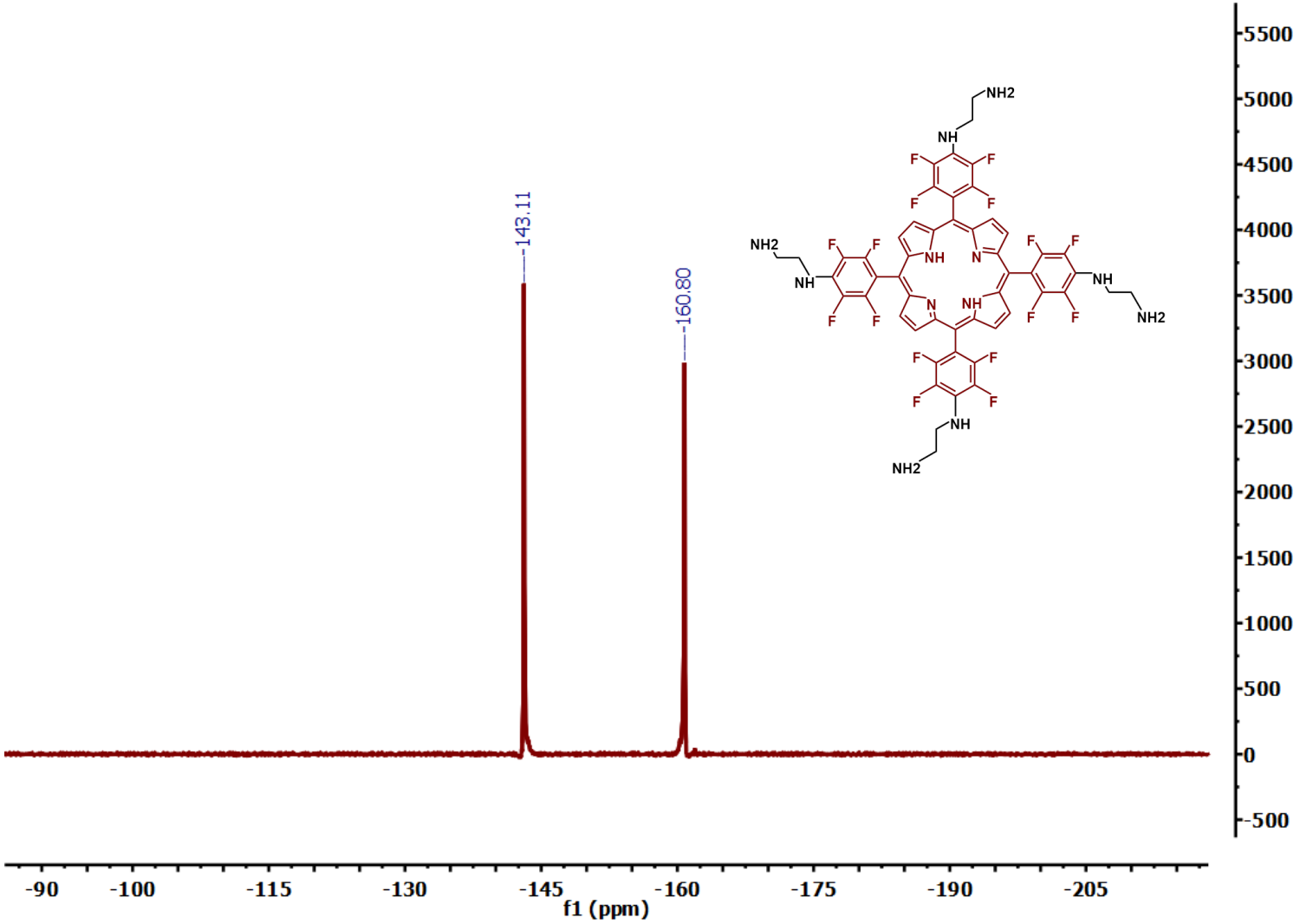

Figure 3. 34. ^{19}F NMR of **M1** (376 MHz, DMSO-d_6).

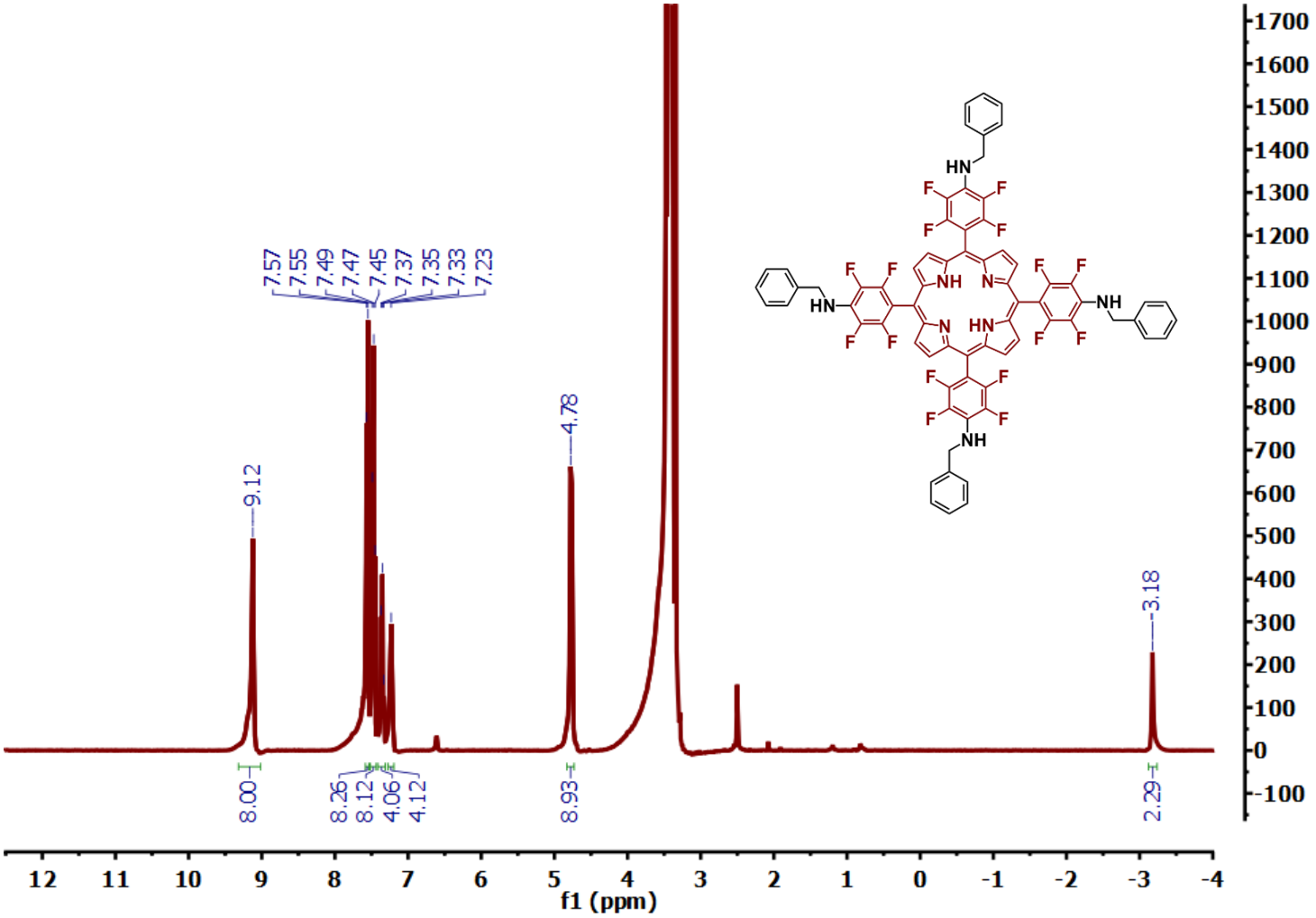

Figure 3. 35. ^{1}H NMR (400 MHz) of **M2** in DMSO-d_6.

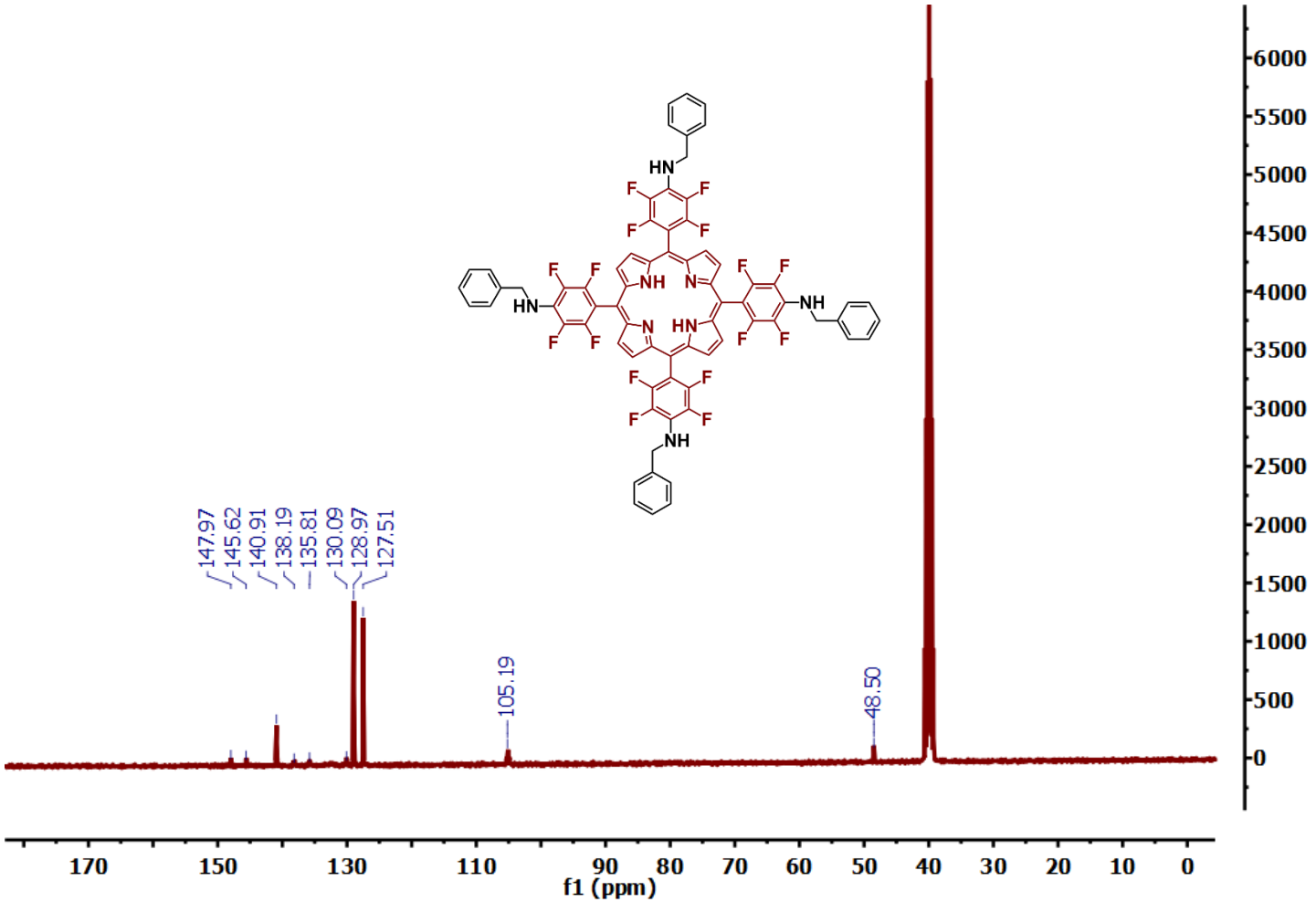

Figure 3. 36. ^{13}C NMR (101 MHz) of **M2** in DMSO-d_6.

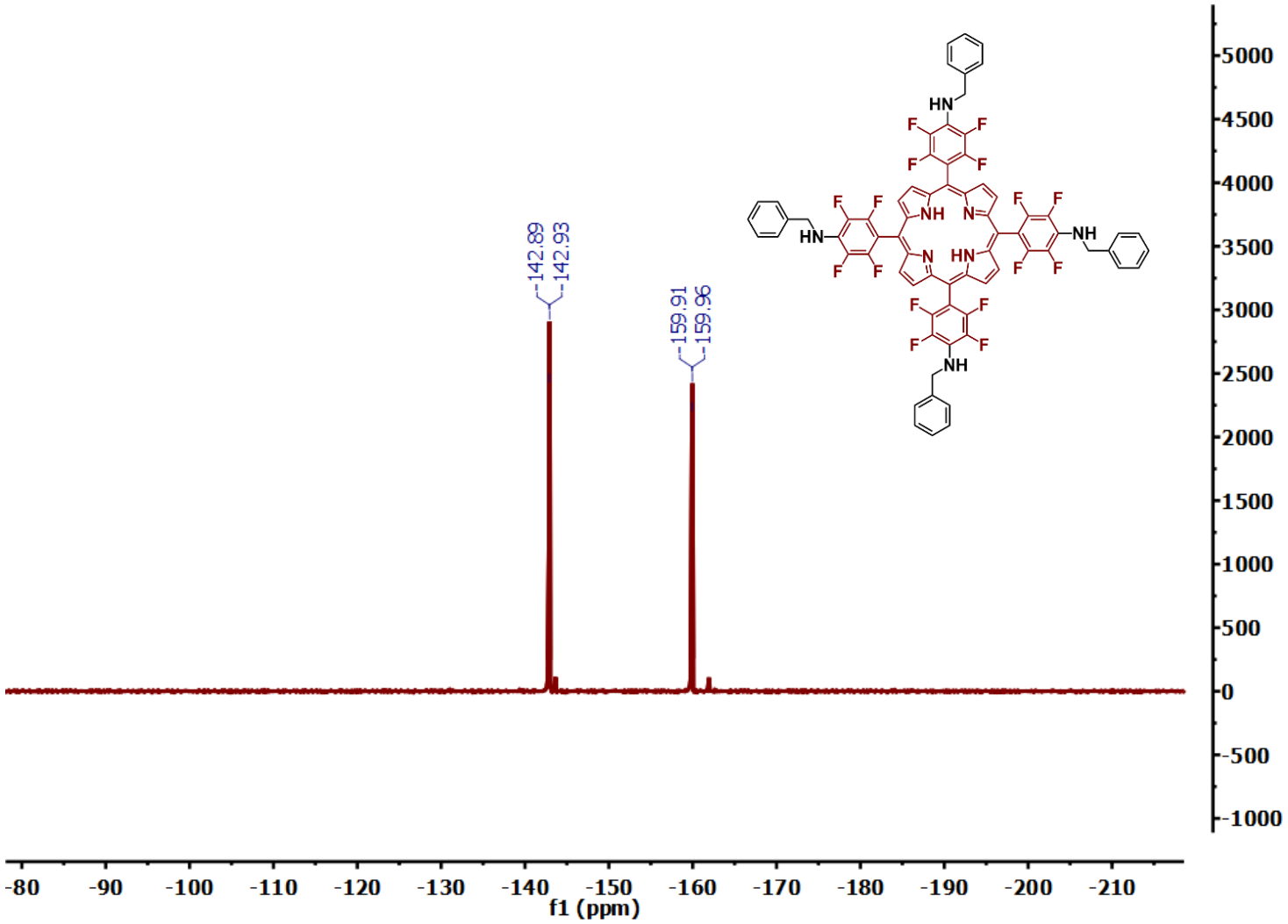

Figure 3. 37. ^{19}F NMR of **M2** (376 MHz, DMSO-d_6).

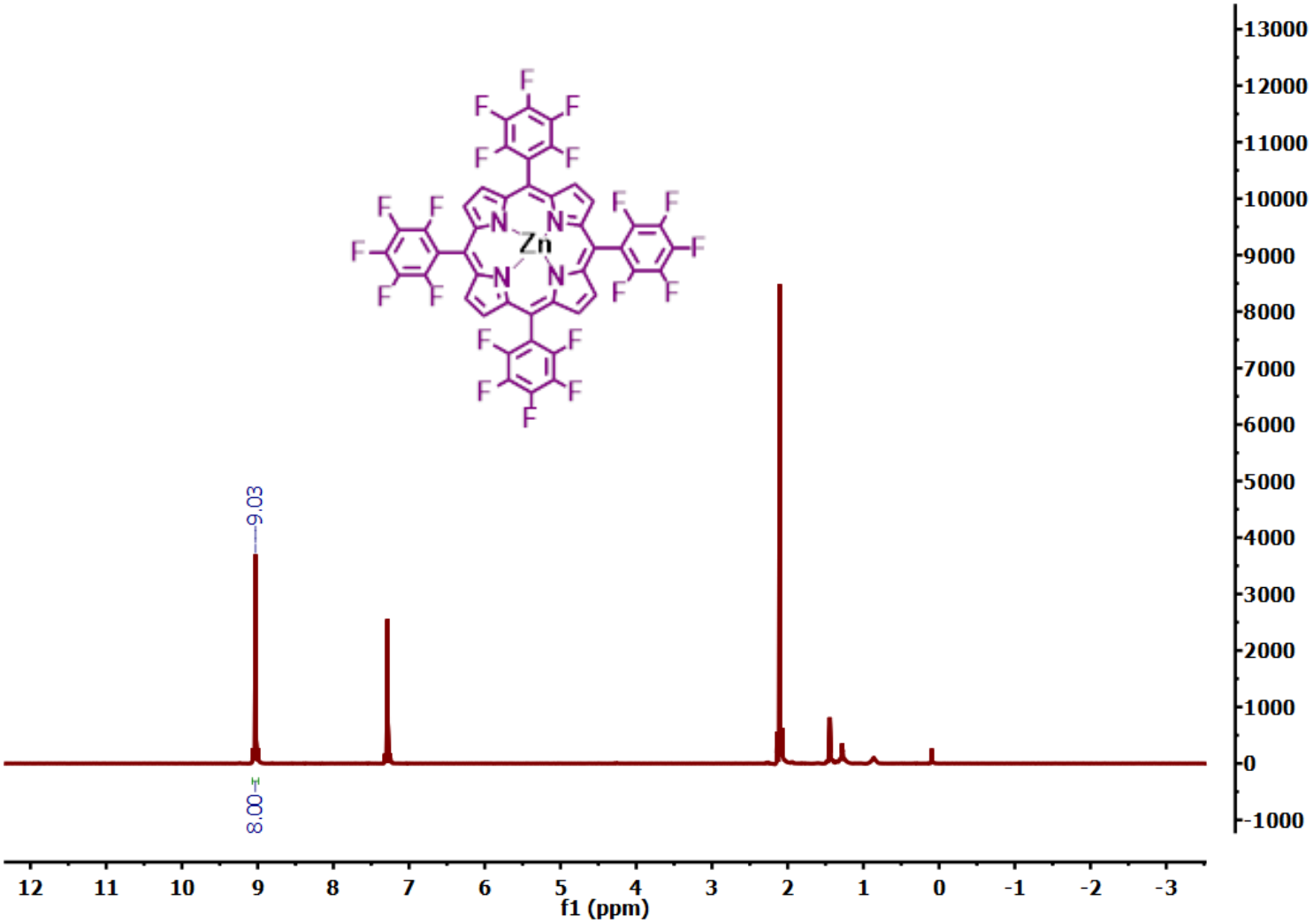

Figure 3. 38. ^{1}H NMR (400 MHz) of **N** in $CDCl_3$.

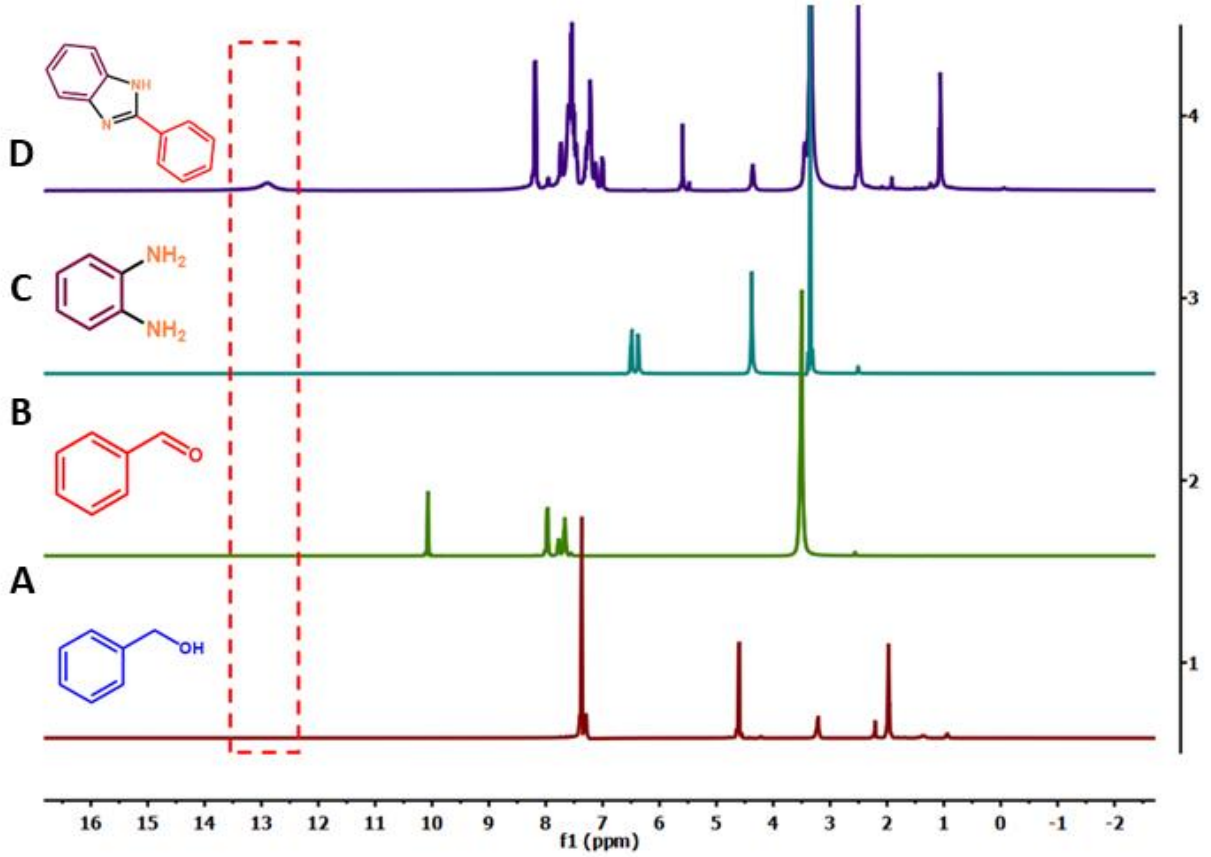

Figure 3. 39. ^{1}H NMR (400 MHz, DMSO-d_6) of **A**, **B**, **C**, and **D**.

3.16. Reference

1. Fisher, J. M.; Kensy, V. K.;Geier, G. R., 3rd, Two-Step, One-Flask Synthesis of an N-Confused Porphyrin Bearing Pentafluorophenyl Substituents. *J Org Chem* **2017**, *82*, 4429-4434.

2. Golf, H. R. A.; Reissig, H.-U.;Wiehe, A., Nucleophilic Substitution on (Pentafluorophenyl)dipyrromethane: A New Route to Building Blocks for Functionalized BODIPYs and Tetrapyrroles. *Organic Letters* **2015**, *17*, 982-985.

3. Han, Y.; Fang, H.; Jing, H.; Sun, H.; Lei, H.; Lai, W.;Cao, R., Singly versus Doubly Reduced Nickel Porphyrins for Proton Reduction: Experimental and Theoretical Evidence for a Homolytic Hydrogen-Evolution Reaction. *Angewandte Chemie (International ed. in English)* **2016**, *55*, 5457-5462.

4. Littler, B. J.; Miller, M. A.; Hung, C.-H.; Wagner, R. W.; O'Shea, D. F.; Boyle, P. D.;Lindsey, J. S., Refined Synthesis of 5-Substituted Dipyrromethanes. *The Journal of Organic Chemistry* **1999**, *64*, 1391-1396.

5. She, Y.; Fu, H.; Zhang, Z.; Song, X.-F.;Sun, Z. J. H., An improved synthesis of di-nitro-functionalized trans-a2b2-tetraphenylporphyrins. **2014**, *89*, 503-514.

6. Najeeb-Uz-Zaman Haider, S.; Zhu, W.;Liang, X., Methyl red-porphyrin chiral hybrids: Expansion of chiral-optical response in the visible region. *Dyes and Pigments* **2020**, *181*, 108565.

7. Rodrigues, J.; Farinha, A.; Muteto, P.; Woranovicz-Barreira, S.; Paz, F.; Neves, M.; Cavaleiro, J.; Tomé, A.; Gomes, M. T.; Sessler, J.;Tomé, J., New porphyrin derivatives for phosphate anion sensing in both organic and aqueous media. *Chemical communications (Cambridge, England)* **2013**, *50*.

8. Rebelo, S. L.; Silva, A. M.; Medforth, C. J.;Freire, C., Iron(III) Fluorinated Porphyrins: Greener Chemistry from Synthesis to Oxidative Catalysis Reactions. *Molecules* **2016**, *21*, 481.

9. Sharghi, H.; Beyzavi, M. H.;Doroodmand, M. M., Reusable Porphyrinatoiron(III) Complex Supported on Activated Silica as an Efficient Heterogeneous Catalyst for a Facile, One-Pot, Selective Synthesis of 2-Arylbenzimidazole Derivatives in the Presence of Atmospheric Air as a “Green” Oxidant at Ambient Temperature. *Eur J Org Chem* **2008**, *2008*, 4126-4138.

10. Ab Ghani, M. H.; Salleh, M. N.; Chen, R. S.; Ahmad, S.; Hanafi, I.; Royan, N. R. R.;Idris, M. N., Mechanical Properties Study of Epoxy Nanocomposite Reinforced Hybrid Fibre Carbon Nanotubes and Nano Clay. *Sains Malays* **2016**, *45*, 1259-1263.

11. Oveisi, A. R.; Zhang, K.; Khorramabadi-zad, A.; Farha, O. K.;Hupp, J. T., Stable and catalytically active iron porphyrin-based porous organic polymer: Activity as both a redox and Lewis acid catalyst. *Sci Rep-Uk* **2015**, *5*, 10621.

Chapter 4. Conclusion and Future Works

In chapter 2, we reported a pyrene-based imine COF with the incorporation of 2-phenylpyridine as a new metal binding group on the pore wall. The COF-UARK-49 adopted an unprecedented hetero-pore structure that results from the cis orientation of the C=N linkages. It also showed selective metalation (Pt) of the larger pores and enhanced photocatalytic performance in decarboxylative difluoroalkylation and oxidative cyclization reactions after Pt loading. Although imine and pyridyl *N* had similar stabilization effects for Pt in this work, the well-known cyclometallation chemistry of 2-phenylpyridine derivatives could introduce interesting metallacycles decorated COFs if other metals are used (e.g. Ir).

In chapter 3, we have successfully designed and synthesized several COFs with amine linkages via nucleophilic aromatic substitution on 5,10,15,20-tetrakis(perfluorophenyl)porphyrin (**$TPPF_{20}$**) **L1**. The synthesized COFs were characterized by several techniques such as X-ray diffraction (XRD), scanning electron microscope (SEM), Fourier transform infrared (FTIR) spectroscopy and nitrogen sorption isotherm analysis. However, additional characterizations such as BET and computational simulation of PXRD are required to confirm the porosity and crystallinity of all obtained COFs. Post-metalation of COF-21with iron resulted in **FeClCOF-21**, whose catalytic activity will then be evaluated on a tandem catalytic process: an in situ oxidation-cyclic aminal formation-oxidation sequence for the formation of benzimidazole derivatives. **XYCOF** will be used for the removal of perfluorinated alkyl substances PFAS such as perfluorooctanoic acid (PFOA) from water, whereas **SiCOF** will be tested for the efficient capture and storage of radioactive iodine (^{129}I or ^{131}I). Finally, **ZnCOF** will be used as a photothermogenic photosensitizer for cancer treatment.